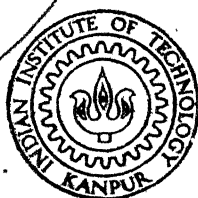


SPECTRA STRUCTURE CORRELATION IN CERTAIN POLYATOMIC SYSTEMS

By
YATENDRA SINGH JAIN

PH.D.
TH.
A-42513
PHY
1974
D
JAI
SPE
TH
PHY
1995.



DEPARTMENT OF PHYSICS
INDIAN INSTITUTE OF TECHNOLOGY KANPUR

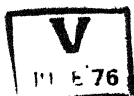
JULY 1974

SPECTRA STRUCTURE CORRELATION IN CERTAIN POLYATOMIC SYSTEMS

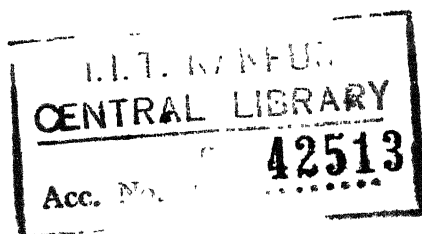
**A Thesis Submitted
In Partial Fulfilment of the Requirements
for the Degree of
DOCTOR OF PHILOSOPHY**

**By
YATENDRA SINGH JAIN**

**to the
DEPARTMENT OF PHYSICS
INDIAN INSTITUTE OF TECHNOLOGY KANPUR
JULY 1974**



PHY-1974-D-DAL-SPE



10 JUN 1975

परम पूज्य

पिताजी

स्व० श्री महावीर प्रसाद जैन

की

पावन स्मृति

को

सादर समर्पित

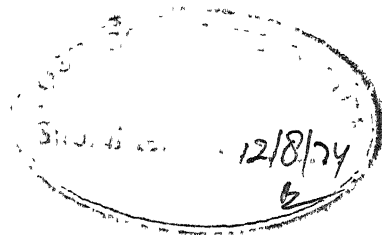
प्रेरणा—श्रोत सहृदय पिताजी जीवन पर्यंत मेरी उच्च शिक्षा के लिये

शुभकामनायें करते रहे । इस उद्देश्य को पूर्ण करने में

पूज्यनीया माँ का स्नेह—सिक्त आशीर्वाद


सदैव अविस्मरणीय

रहेगा ।



CERTIFICATE

This is to certify that the work presented in this thesis entitled 'Spectra Structure Correlation in Certain Polyatomic Systems' has been carried out by Shri Yatendra Singh Jain under my supervision and has not been submitted elsewhere for a degree.


(H.D. BIST)

Department of Physics
Indian Institute of Technology
Kanpur, India

<p>POST GRADUATE OFFICE</p> <p>This thesis has been approved for the award of the degree of Master of Technology (M.Tech.) in accordance with the regulations of the Institute of Technology, Kanpur Dated. 25-3-75 Jmay</p>
--

ACKNOWLEDGEMENTS

I do not find words to express my feelings of gratitude to Dr. H.D. Bist for his keen interest, invaluable suggestions and inspiring guidance during the course of this work.

I am very much grateful to Professor P. Venkateswarlu for useful discussions as well ^{as} intellectual and moral support at all stages of the work. I am indebted to Professor T.M. Srinivasan for his interest in the progress of this project and also to Professors J. Mahanty, A.S. Parasnis and D.R. Rao for their encouragement.

I am also grateful to Professor D.P. Khandelwal (HBTI, Kanpur) for inspiring me to work as a research scholar and for his unfailing interest in the successful completion of the project.

I gratefully thank Professor H.J. Bernstein (NRC, Canada) for his kind courtesy and Dr. A.L. Verma (presently at University of Amsterdam, Holand) for his constant help extended to me. I also thank Professor C.J.H. Schutte (Pretoria, South Africa) for his helpful communications.

Thanks are due to Drs. R.K. Ray, T. Das, U.C. Agarwal (Chemistry), G.C. Upreti, V.N. Sarin, A. Ojha (University of Jodhpur), K. Kumar (presently at NRC, Canada) and V.S. Tomar (presently at Zurich, Switzerland) and also to Mr. S.P. Srivastava for their help at various stages of this work.

It gives me a great pleasure to thankfully acknowledge the timely help from M/s. B.K. Srivastava, V.M. Malhotra, N.L. Pathak, J.S. Parihar,

V.K. Kapoor, G.S. Pande, V.P. Tayal and R.K. Jain. I also wish to express my appreciation for the helpful cooperation of the staff members of different laboratories and workshops.

Once again I thank Professor P. Venkateswarlu for providing Raman spectra of $(\text{NH}_4)_2\text{SO}_4$ recorded at University of California Santa Barbara, Dr. H.D. Bist for providing far IR spectra of solid halogens recorded at University of Florida, Gainesville and vibronic spectra of chlorobenzene recorded at Vanderbilt University, Nashville and Dr. A.L. Verma for recording Raman spectra of $(\text{NH}_4)_2\text{BeF}_4$ and $\alpha\text{-NiSO}_4 \cdot 6\text{H}_2\text{O}$ during his stay at NRC, Canada. Experimental facilities provided for these records by Professors H.J. Bernstein, H.P. Broida (Santa Barbara), J.C.D. Brand (presently at London, Canada) and W.B. Person (Gainesville, U.S.A.) are gratefully acknowledged.

I take this opportunity to express my esteemed regards to my teachers from whom I learnt a lot during my studies and also to my mother, sisters and brothers who have boundless affection for me and have contributed a lot to my progress. Here I do not know what is so worth in my dissertation to owe to my wife Smt. Ajai Jain 'Neeru' and my lovely daughter Km. Shuchi who shared my valuable time but gave me some peaceful and pleasant moments by extending their love and affection.

Finally, I thank Mr. R.D. Tripathi for undertaking the typing of this thesis with patience and interest and Mr. H.K. Panda for running the stencils.

YATENDRA SINGH JAIN

CONTENTS

Synopsis	i
List of Publications	iv
CHAPTER I	
INTRODUCTION	
1.1 General	1
1.2 Dynamics of a molecule	2
1.3 Normal mode	2
1.4 Infrared absorption	3
1.5 Raman scattering	3
1.6 Transition probability	5
1.7 IR band intensity	5
1.8 Raman band intensity	8
1.9 Band shapes	9
1.10 Selection rules	10
1.11 Classification of normal modes	11
1.12 Phonons	13
1.13 Conservation laws for phonons	14
1.14 Vibrational spectra	15
1.15 Hydrogen bond	19
1.16 Ferroelectrics	20
1.17 Attenuated total reflection (ATR) spectroscopy	26
REFERENCES	30
FIGURES	34

CHAPTER II

EXPERIMENTAL DETAILS

2.1	Purification of samples	39
2.2	Growth of large single crystals	39
2.3	Crystal cutting and polishing	40
2.4	Infrared instrument and accessories	41
2.5	Scan of IR spectra	42
2.6	Calibration in IR region	45
2.7	Raman instruments and accessories	45
2.8	Scan of Raman spectra	46
2.9	Calibration of Raman spectra	48
2.10	Deuteration of the hydrated compounds	48
	REFERENCES	49
	FIGURES	50

CHAPTER III

OPTICAL PHONONS AND FERROELECTRIC PHASE TRANSITION IN $(\text{NH}_4)_2\text{SO}_4$ CRYSTAL

ABSTRACT	57	
3.1	Introduction	59
3.2	Crystal structure	61
3.3	Phonon branches in the crystal	63
3.4	Classification of phonons	63
3.	The forms of Raman tensor components	65
3.6	Experimental	65
3.7	Results and discussion	
	I. Raman phonons in single crystal	67
	II. IR (ATR) spectra of single crystal	76

III. Raman and IR spectra of microcrystalline $(\text{NH}_4)_2\text{SO}_4$	78
IV Ferroelectric phase transition	85
3.8 Conclusion	95
REFERENCES	97
TABLES	103
FIGURES	115
APPENDICES	127

CHAPTER IV

OPTICAL PHONONS AND FERROELECTRIC PHASE TRANSITION IN $(\text{NH}_4)_2\text{BeF}_4$

ABSTRACT	133
4.1 Introduction	134
4.2 Crystal structure	135
4.3 Phonon branches in the crystal	136
4.4 Classification of phonons	136
4.5 Forms of Raman tensor components	137
4.6 Experimental	137
4.7 Results and discussion	
I. Raman phonons in single crystal	138
II. IR spectra of microcrystalline $(\text{NH}_4)_2\text{BeF}_4$	146
III. Spectra of SO_4^{2-} ion in $(\text{NH}_4)_2\text{BeF}_4$	149
IV. Ferroelectric phase transition	151
4.8 Conclusion	156
REFERENCES	158
TABLES	160
FIGURES	162
APPENDICES	168

CHAPTER V

OPTICAL PHONONS IN α -NiSO₄·6H₂O CRYSTAL

ABSTRACT	171
5.1 Introduction	173
5.2 Crystal structure	176
5.3 Phonon branches in the crystal	177
5.4 Classification of Phonons	179
5.5 Form of Raman tensor components	181
5.6 Experimental	183
5.7 Results and discussion	
I. Raman phonons in single crystal	185
II. IR (ATR) spectra of single crystal of NSH	195
III. IR spectra of microcrystalline NSH	197
IV. Force field constants for librations of H ₂ O molecules	203
5.8 Conclusion	209
REFERENCES	211
TABLES	216
FIGURES	229
APPENDICES	239

CHAPTER VI

SUMMARY	247
LIST OF ATTACHED PUBLICATIONS	253

SYNOPSIS

SPECTRA STRUCTURE CORRELATION IN CERTAIN POLYATOMIC SYSTEMS

Spectroscopic investigations dealing with absorption and inelastic scattering of photons have a major role in unravelling the complex structure and dynamical behaviour of many particle systems: molecules and crystals. In order to get an insight into the methodology of such investigations infrared and vibronic spectra of chlorobenzene were analysed in vapour phase. Similar attempts were made to understand the Raman and infrared spectra of simple molecular crystals of halogens. These two aspects are presented only as published papers at the end of the thesis.

The study of ferroelectrics has got stimulated interest in recent years because of their wide applications in electrical devices. Similar interest in the study of crystal hydrates may be observed as they provide adequate informations about interactions like H-bonding and metal-oxygen coordination. The understanding of these interactions is very useful in the study of several bio-chemical and bio-physical phenomena. As such investigations on ferroelectric $(\text{NH}_4)_2\text{SO}_4$ and $(\text{NH}_4)_2\text{BeF}_4$ and the transition metal hydrate $\alpha\text{-NiSO}_4 \cdot 6\text{H}_2\text{O}$ have been presented in the main thesis. The thesis has been divided in six chapters.

Various aspects of IR and Raman spectroscopy relevant to the present investigations have been briefly reviewed in Chapter I. A brief discussion has also been made on hydrogen bonding, important aspects of ferroelectrics and attenuated total reflection (ATR) spectroscopy. The treatment given is, however, general and independent of the specific systems studied. The application of these discussions is the concern of Chapters III, IV, V and VI.

branches have been classified into different symmetry species of D_4 point group to which the crystal symmetry belongs; both unit cell and site symmetry approaches have been used. It has been shown that under the T_h symmetry, the positions of oxygen atoms in $[\text{Ni}(\text{OH}_2)_6]^{2+}$ complex are not compatible with site symmetry (C_2) of Ni atom. O_h symmetry behaviour has consistently been proposed for the complex. Laser Raman spectra of single crystal have been recorded at room temperature in different geometries corresponding to different polarizations. ATR spectra have also been investigated and discussed. IR spectra of microcrystalline $\alpha\text{-NiSO}_4 \cdot 6\text{H}_2\text{O}$ and its deuterated analogue have been recorded to investigate particularly the librational modes of H_2O molecules which, however, appear as very weak and diffuse bands at room temperature in Raman spectra. The force field constants for librational modes of H_2O molecule have been computed using a simple model defining the molecule as a rigid harmonic liblator. All spectra have been observed to be consistent with known crystal structural data.

A summary of the thesis is presented in the last chapter (Chapter VI).

LIST OF PUBLICATIONS

1. The Planar Vibrations of Chlorobenzene in its Ground State from an Analysis of 2699Å Electronic Band System: H.D. Bist, V.N. Sarin, A. Ojha and Y.S. Jain, Spectrochim. Acta 26A, 841 (1970).
2. The 2699Å Electronic Band System of Chlorobenzene - The In-Plane Vibrational Modes in Excited State: H.D. Bist, V.N. Sarin, A. Ojha and Y.S. Jain, Appl. Spectrosc. 24, 292 (1970).
3. The Out-of-Plane Vibrational Modes of Chlorobenzene in its Ground and First Singlet Excited States: Y.S. Jain and H.D. Bist, J. Mol. Spectrosc. 47, 126 (1973).
4. Thermodynamic Properties in the Gaseous State of Certain Monosubstituted Benzenes: V.N. Sarin, Y.S. Jain and H.D. Bist, Thermochim. Acta 6, 39 (1973).
5. The Ferroelectric Phase Transition in Ammonium Sulphate: Y.S. Jain, H.D. Bist and G.C. Upreti, Chem. Phys. Lett., 22, 572 (1973).
6. A Point Charge Model for the Ferroelectric Transition in Ammonium Sulphate: Y.S. Jain and H.D. Bist, Phys. Status Solidi 62b, 295 (1974).
7. Comment on the Paper on 'The Origin of Phase Transition in Ammonium Sulphate': Y.S. Jain and H.D. Bist, Solid State Communications xxx, 0000 (1974).
8. Optical Phonons in α -NiSO₄.6H₂O Single Crystal: Y.S. Jain, H.D. Bist and A.L. Verma, J. Raman Spectrosc., 2, 327 (1974).
9. On the Symmetry Behaviour of Metal-Aquo-Complex of $[M(OH_2)_6]^{2+}$ An Analysis for $[Ni(OH_2)_6]^{2+}$ in α -NiSO₄.6H₂O: Y.S. Jain and H.D. Bist. Appl. Spectrosc. 29, 0000 (1975). March - April Issue

Papers Published in Proceedings of Conferences

10. Optical Phonons in Molecular Crystals of Halogens; Y.S. Jain and H.D. Bist, Proc. Nucl. Phys. Solid State Phys. Symp., BARC 3, 485 (1970)
11. Optical Phonons and Conformations of Water Molecules in Hydrates of Barium Chlorides: Y.S. Jain, V.S. Tomar and H.D. Bist, Proc. Nucl. Phys. Solid State Phys. Symp., BARC 3, 381 (1972).
12. Optical Phonons and Ferroelectric Phase Transition in Ammonium Sulphate; Y.S. Jain, H.D. Bist and P. Venkateswarlu, Proc. Indo-Sov. Conf. on Solid State Materials (1972) Proceedings to be published.

13. Optical Phonons in Nickel Sulphate Hexahydrate Crystal: Y.S. Jain and H.D. Bist, Proc. Nucl. Phys. Solid State Phys. Symp. BARC, 15C, 483 (1973).
14. Laser Raman Scattering in α -Nickel Sulphate Hexahydrate Single Crystal: Y.S. Jain and H.D. Bist (Presented in the Symposium of Quantum Opto-Electronics (BARC), Bombay (1974).

CHAPTER I

INTRODUCTION

1.1 GENERAL

The physicochemical properties of a system of particles are governed by inter- and intra- particle interactions. These interactions can be of different nature and be understood by theoretical and experimental studies of the dynamics of the particles. Spectroscopic studies **involving** absorption or emission of electromagnetic radiations, scattering and diffraction of particles (photons, electrons, neutrons, etc.) are the most accurate tools to investigate the dynamics of a system of particles. Solids are the most complex systems having different kinds of interactions and large number of interacting particles, but are of great practical importance due to their wide application in scientific and industrial fields. Reasons of earlier slow progress towards the studies on solids had been the lack of required experimental tools and the knowledge of modern theories.

The recent developments in modern theories and availability of various machines on commercial basis have encouraged the studies of solids on a larger scale during the past few decades. The progress has been so fast that emphasis is now being given to more and more complex systems.

The present work is devoted to the study of optical phonons in $(\text{NH}_4)_2\text{SO}_4$, $(\text{NH}_4)_2\text{BeF}_4$ and $\alpha\text{-NiSO}_4 \cdot 6\text{H}_2\text{O}$ crystals with a view to investigate their lattice dynamics, ferroelectric phase transition (in ^{the}former two systems) and the effects of hydrogen-bond interaction. Infrared(IR) absorption and Raman scattering have been used as investigating tools. A brief discussion of various topics related to the present study has been made in this Chapter.

1.2 DYNAMICS OF A MOLECULE

The dynamics of N-atomic molecule can be described in terms of $3N$ degrees of freedom (3 translations + 3 rotations + $3N-6$ vibrations for a non-linear molecule or 3 translations + 2 rotations + $3N-5$ vibrations for a linear molecule)^{1,2}. When such a molecule occupies a position in a crystal, all its $3N$ degrees of freedom become oscillatory; the oscillations arising from translations and rotations of the molecule are known as translatory and libratory lattice vibrations, respectively. All these vibrations are governed by inter- and intra- molecular interactions, hence they are important to understand the related microscopic and macroscopic properties. As such the dynamics of a molecule or a solid appears to be quite complex but may be described in terms of simple modes of motion known as normal modes.

1.3 NORMAL MODE

A normal mode (or fundamental mode) has the following properties^{1,2},
 (i) each atom of the system oscillates about its equilibrium position with a simple harmonic motion having the same frequency and phase (ii) the relative velocity and the amplitude of individual atom depend on its mass

and the nature of motion; for internal modes of vibrations they are governed in such a way that no resultant translation or the rotation of the system as a whole takes place.

1.4 INFRARED ABSORPTION

The IR absorption is a phenomenon involving interaction between electromagnetic radiations and matter. To a first approximation, it occurs through changes in electric dipolemoment ($\vec{\mu}$) of the molecular unit arising due to its excitation to a higher energy level. It may also occur through changes in electric moments of higher order, magnetic moments, etc; however, the absorption through such interactions is generally found to be negligibly weak. Frequency of vibrations in molecules and solids match with the energy of IR photons, hence enough informations about the vibrations in these systems may be collected from IR absorption spectra.

Coblentz³ was among the first who made a systematic study of IR absorption in 1905. Its elementary theory dealing with vibration-rotation spectra was given by Bjerrum⁴ in 1914. Since then a number of theoretical and experimental studies have been made on the subject⁵.

1.5 RAMAN SCATTERING

Inelastic scattering of electromagnetic waves now known as Raman scattering was predicted theoretically by Smekal⁶ in 1923. Sir C.V. Raman⁷ observed it experimentally in 1928. The importance of the phenomenon lies in the fact that differences between the frequencies of scattered and incident radiations carry informations about the dynamics and structure of the scatterer.

The scattered radiations (excluding Rayleigh scattering) are found to have frequencies lower and higher than the frequency of incident light. The phenomenon in the former case is known as Stokes Raman scattering while in the latter case as anti-Stokes Raman scattering. Two types of these events are illustrated in Fig. 1.1. In Fig. 1.1a, the system of particles (say molecule) is unexcited initially. An incident photon at ν_e is absorbed and a Stokes photon at $\nu_S = \nu_e - \nu_v$ is emitted simultaneously. To conserve energy the molecule is excited to a higher level, (say vibrational) of energy $hc\nu_v$. If on the other hand, the molecule is initially in the excited state ($E = hc\nu_v$) as shown in Fig. 1.1b, an anti-Stokes photon at $\nu_{AS} = \nu_e + \nu_v$ may be emitted alongwith the de-excitation of the molecule from $v = 1$ to $v = 0$. Since anti-Stokes emission depends on the number of molecules being in the initial excited state, it is weaker than Stokes emission.

The modern theories of Raman effect explain the phenomenon in terms of creation and annihilation of photons⁸. For example in the first process (cf. Fig. 1.1a), a photon of frequency $\nu_S = \nu_e - \nu_v$ is created while one photon of frequency ν_e is annihilated resulting in the excitation of the molecule from $v = 0$ to $v = 1$. Similarly in the other process (cf. Fig. 1.1b) a photon of $\nu_{AS} = \nu_e + \nu_v$ is created alongwith the annihilation of a photon of frequency ν_e resulting in the deexcitation of the molecule from $v = 1$ to $v = 0$.

Raman scattering is usually weak in intensity, hence a high intensity source is needed for its observation. For this reason, a stimulated interest in its studies and applications arose only in the past decade after the invention of high power and highly monochromatic

continuous laser sources. As a result several new phenomena^{8,9} e.g. stimulated-, resonance-, **inverse**-, hyper-Raman effects, etc. have recently been observed.

Raman effect is the result of interaction between electromagnetic waves and induced dipole moment (\vec{p}) hence is fundamentally different from IR absorption. The two phenomena are complementary to each other in providing informations about the dynamics of a system. Whether a particular mode of vibration would appear in particular type of spectra is ascertained by the finite transition probability computed for it using appropriate transition moment.

1.6 TRANSITION PROBABILITY

The transition probability depends on the matrix element M_{fi} of the transition moment \tilde{M} associated with the transition between final and initial states respectively described by eigen-functions ψ_f and ψ_i .

we have

$$M_{fi} = \int \psi_f \tilde{M} \psi_i d\tau \quad \dots 1.6a$$

\tilde{M} can be either of the $\vec{\mu}$, \vec{p} , etc., depending on the nature of excitation.

1.7 IR BAND INTENSITY

The transition moment for IR absorption can be given by Eqn. 1.6a, if $\tilde{M} \equiv \vec{\mu}$. Thus

$$\mu_{fi} = \int \psi_f \vec{\mu} \psi_i d\tau \quad \dots 1.7a$$

The Einstein coefficient B_{fi} of the transition probability is related with

μ_{fi} through

$$B_{fi} = (8\pi^3/3ch^2) \cdot |\mu_{fi}|^2 \quad \dots 1.7b$$

and the intrinsic absorption corresponding to a transition between f and i states is given by

$$dI(\nu) = -hc\nu B_{fi} N_i \cdot I(\nu) \cdot dx \quad \dots 1.7c$$

where $\nu = \nu_{fi} = (E_f - E_i)/hc$, N_i is the number of absorbing centres per unit volume in the initial state, $I(\nu)$ is the intensity of light beam at frequency ν after traversing a distance dx in the absorbing medium and $dI(\nu)$ is the absorbed intensity at the same frequency. Population of excited centres, N_f , has been considered to be negligibly small. Eqn. 1.7c may also be expressed in terms of absorption coefficient k_ν at frequency ν as

$$dI(\nu) = -I(\nu) \cdot k_\nu \cdot dx \quad \dots 1.7d$$

where k_ν is given by

$$k_\nu = -\frac{1}{I(\nu)} \cdot \frac{dI(\nu)}{dx} = hc\nu B_{fi} N_i \quad \dots 1.7e$$

On integrating, the Eqn. 1.7d becomes

$$I(\nu) = I_o(\nu) \cdot \text{Exp}(-k_\nu x) \quad \dots 1.7f$$

where $I_o(\nu)$ is the total incident intensity at frequency ν . Eqn. 1.7f is known as Bouguer's or Lambert's law¹⁰ and may also be written as

$$k_\nu = \frac{1}{x} \log_e \frac{I_o(\nu)}{I(\nu)} = \frac{2.303}{x} \log_{10} \frac{I_o(\nu)}{I(\nu)} \quad \dots 1.7g$$

or in terms of absorbance A_ν , as

$$A_\nu = \log_{10} \frac{I_o(\nu)}{I(\nu)} = \frac{1}{2.303} \cdot k_\nu \cdot x = Kx \quad \dots \quad 1.7h$$

Here K is known as Bunsen Rascoe extinction coefficient¹⁰

Since every transition is having some finite width the integrated absorption over the full band is regarded to have more significance than the peak absorption. The former quantity in its absolute units may be defined as

$$k_{int} = \int_{band} k_\nu d\nu = \frac{2.303}{x} \int_{band} \log_{10} \frac{I_o(\nu)}{I(\nu)} d\nu = \frac{2.303}{x} A_{int} \quad \dots \quad 1.7i$$

where

$$A_{int} = \int_{band} A_\nu d\nu \quad \dots \quad 1.7j$$

Most of the commercial double beam IR instruments measure the quantity $I(\nu)$ (cf Eqn. 1.7f), while some have the provision to measure the quantity A_ν (cf Eqn. 1.7h). The computation of k_{int} from spectra obtained on either type of instruments becomes complicated because of the difficulties encountered in the measurements of $I_o(\nu)$ and /or x . However, A_{int} can be easily deduced from the spectra recorded on the latter type of instruments. A_{int} is of only relative importance, its approximate value can be found by multiplying peak absorptivity with full width at half the maximum intensity (FWHMI). We would use this method to estimate A_{int} in IR bands, although, there could be other methods; e.g. counting the squares on the graph paper or measuring the area of bands using a planimeter.

1.8 RAMAN BAND INTENSITY

The polarizability theory of Raman band intensity was developed by Placzek¹¹ in 1934 considering that Raman scattering arises from the ground state polarizability depending on molecular vibrations. The bond polarizability theory^{12,13} was discussed in later years. The recent developments on this subject have been reviewed by Tang and Albrecht¹⁴.

The transition probability for Raman scattering depends on the matrix element α_{fi} of electric polarizability tensor ($\tilde{\alpha}$). We have

$$\alpha_{fi} = \int \psi_f \tilde{\alpha} \psi_i d\tau \quad \dots \quad 1.8a$$

In single crystal studies the intensity of Raman band is usually treated in terms of scattering efficiency S defined as^{15,16}

$$S = \frac{N(\nu_s)}{N(\nu_e)} \quad \dots \quad 1.8b$$

where $N(\nu_s)$ is the number of scattered photons of frequency ν_s produced per unit time per unit cross sectional area of the crystal in the solid angle $d\Omega$ about the direction of observation and $N(\nu_e)$ is the number of incident photons of frequency ν_e per unit time per unit cross - sectional area. For right angle scattering and unpolarized light, Smith¹⁶ computed

$$S = \frac{3hLd\Omega(\nu_e - \nu)^4}{2\pi\sigma_c\nu} |\alpha_{fi}|^2 [1 - \text{Exp}(-hc\nu/kT)]^{-1} \quad \dots \quad 1.8c$$

where $\nu = \nu_{fi} = (E_f - E_i)/hc$ and L is the effective length of the crystal from which the scattered radiations are received at the slit of the spectrophotometer, σ is the density of scattering centres, k is the Boltzmann's constant and T is the absolute temperature.

The experimentally observed Raman band intensity, which is proportional to the related value of S , as such can be of only relative importance. Here also the integrated intensity of the band may be considered to be of more significance than the peak intensity. To a good approximation, the former may be computed by multiplying the latter with the FWHMI value of the same band.

To define the depolarization ratio (ρ), a scattering geometry is considered as shown in Fig. 1.2 where it has been assumed that the unpolarized incident light is propagating along c -axis while the scattered radiations are observed along a -axis of the crystal. Raman spectra in this set up can be recorded for scattered radiations polarized (i) in the plane and (ii) perpendicular to the plane of scattering, *ac*. If S_{\parallel} and S_{\perp} are the scattering efficiencies of a mode respectively in these two conditions then the depolarization ratio for this mode is given by

$$\rho = \frac{S_{\parallel}}{S_{\perp}} \quad \dots 1.8d$$

1.9 BAND SHAPES

Numerous formulae have been proposed to match the IR absorption and Raman band shapes¹⁷. The most commonly used functions for describing the band shapes are the following.

(i) for Gaussian shape

$$I(\nu) = I(\nu_0) \exp -(\nu - \nu_0)^2 / \underline{a} \quad \dots 1.9a$$

and (ii) for Lorentzian shape

$$I(\nu) = I(\nu_0) \frac{\underline{b}^2}{\underline{b}^2 + (\nu - \nu_0)^2} \quad \dots 1.9b$$

Here $I(\nu_0)$ is the maximum intensity at peak frequency (ν_0), and \underline{a} and \underline{b}

are adjustable parameters. In Eqn. 1.9b, \underline{b} is such that $2\underline{b}$ = FWHM of the band.

The observed band can in general be resolved into indefinite number of band components of either shape. However, it seems more reasonable to resolve an observed band into as many components as there are clear indications. The resolution is an arbitrary process to a certain extent and hence the resolved bands may have considerable uncertainties in peak position, FWHM and the intensity.

1.10 SELECTION RULES

An allowed transition between f and i states is defined by the non-zero value of M_{fi} (cf Eqn. 1.6a). However, in general it is difficult to find out the eigen-functions (ψ 's) of a system, and so the value of M_{fi} . Group theoretical methods are, therefore, used to predict the zero and non-zero values of M_{fi} . It can be noticed that the integrand of equation (1.6a) should be totally symmetric for non-zero values of M_{fi} and so for an allowed transition between f and i states.

a. Infrared Absorption

The IR absorption processes take place through $\vec{\mu} = e\vec{r}$. Since \vec{r} is a space vector, the product of the symmetry species of ψ_f and ψ_i should be the same as that of any component \vec{x} , \vec{y} or \vec{z} of this vector for an allowed transition.

b. Raman Scattering

This phenomenon takes place through the induced electric dipole-moment ($\vec{p} = \vec{\alpha}\vec{E}$; $\vec{\alpha}$ is the second rank tensor having bases of representation : xx, yy, zz, zx, xy and yz). Obviously, for an allowed Raman

transition the product of symmetry species of ψ_f and ψ_i must be similar to that of any basis of \tilde{Q} .

Conclusively, if the initial state is the ground state, the allowed vibration in infrared should belong to the species of x, y, or z and for Raman scattering to the species of xx, yy, zz, zx, xy or yz. The classification of normal modes into the species of symmetry point group, therefore, becomes essential.

1.11 CLASSIFICATION OF NORMAL MODES

The methods of classifying the normal modes of a free molecule with or without use of group theory have been discussed by several workers^{1,2,18-20}. For crystals the method known as the unit cell approach was suggested for the first time by Bhagavantam and Venkatarayudu²¹. Later, Halford²² gave a local symmetry approach which was discussed in detail by Hornig²³ and was proved to give the same results as obtained by the unit cell approach. Further, Winston and Halford²⁴ derived both methods by considering the motions of a crystal segment composed of an arbitrary number of unit cells and subjected to the Born - Von Karman²⁵ boundary conditions. The applications of these methods have been illustrated by several authors^{15,26-30}. Both approaches are briefly reviewed as follows.

a. Unit Cell Approach

In this approach the problem of classification of $3nN$ modes of the whole crystal (containing n unit cells of N atoms) is reduced to the problem of classifying $3N$ modes of the unit cell. Such a simplification is based on the assumption that atoms or molecules at equivalent lattice positions are in the same state of motion without any phase difference. Thus the

approach consists in finding the total character representation for the unit cell following the usual formula,

$$\chi(N) = N^R(\pm 1 + 2 \cos \phi_R) \quad \dots \quad 1.11a$$

Here N^R is the number of invariant atoms under a symmetry operation R which could be either a proper rotation (identity or n fold rotation) or improper rotation (inversion, reflection or reflection rotation) defined by angle ϕ_R ; $+1$ and -1 are accounted respectively for proper and improper rotations.

The reducible representation with bases as translational, librational or internal modes can also be obtained separately using the formulae:

(i) for translational lattice modes

$$\chi(t) = N^R(t) [\pm 1 + 2 \cos \phi_R] \quad \dots \quad 1.11b$$

(ii) for librational lattice modes

$$\chi(l) = N^R(l) [1 \pm 2 \cos \phi_R] \quad \dots \quad 1.11c$$

and (iii) for internal modes

$$\chi(i) = \chi(N) - [\chi(t) + \chi(l)] \quad \dots \quad 1.11d$$

where $N^R(t)$ is the total number of both atomic and polyatomic groups while $N^R(l)$ is the number of only polyatomic groups which remain invariant under symmetry operator R . The number of modes belonging to a particular species can be obtained by reducing the above representations using the formula²

$$n^s = \frac{1}{h} \sum_i c_i \chi_i \chi_i^s \quad \dots \quad 1.11e$$

where n^s is the number of irreducible representations (corresponding to the symmetry species s) present in a reducible representation. χ_i^s and χ_i are the characters of i^{th} class of operators describing irreducible representation (species s) and reducible representation, respectively, C_i is the order of i^{th} class and h is that of the group of symmetry operators. The sum goes over all classes in the point group.

b. Local or Site Symmetry Approach

Assuming the local potentials as mainly responsible for the dynamics of the mono- or polyatomic group in the crystal, Halford²² suggested to classify the normal modes into species of local symmetry point group. It can be done by correlating the symmetry species of the point group of 'free' molecular group to those of the local symmetry point group. This method neglects the interaction between different groups in the same unit cell. Hornig²³ considered such interactions and showed that by further correlating the species of the local and the crystal symmetry point groups, one obtains the same classification as obtained by the unit cell approach.

1.12 PHONONS

Phonons are the quantized vibrations or elastic waves in solids³¹. They are different from the vibrations of a molecule in liquid or vapour phase in the sense that for any excited mode of vibration, the disturbances confine only to the single molecule while they propagate in all directions in solids. Thus the free vibration of the molecule loses its identity to a large extent inside the solid where it is designated as a phonon. The phonon is characterized by discrete phase velocity v_q , frequency ν_q and wave vector \vec{q} .

When all the cell particles excute vibrations in the same phase and with the same amplitude, the phonons generated are called accustic phonons. There are only three such phonons defined for a crystal. The optical phonons, on the other hand, are characterized by the motions of particles in an unit cell without the shift of the centre of mass of the cell. There are $3N-3$ such branches in the unit cell having N particles.

The longitudinal and transverse branches of a phonon are, respectively, characterized by vibrations of particles along and perpendicular to the direction of propagation of a phonon mode. Since the electromagnetic radiations are transverse in nature, they can not interact with longitudinal phonons. Therefore, only transverse phonons can be studied in transmission spectroscopy. However, in Raman scattering and reflection spectroscopy one can study both types of phonons.

1.13 CONSERVATION LAWS FOR PHONONS

The correct momentum of a phonon (or photon) can be expressed in terms of wave vector \vec{q} (or \vec{k}) as $\hbar\vec{q}$ (or $\hbar\vec{k}$). The following conservation laws of energy and wave vector hold good.

$$\vec{k} + \underline{n}\vec{G} = \sum_i \pm \vec{q}_i \quad \dots \quad 1.13a$$

and

$$\hbar c\nu = \sum_i \pm \hbar c\nu_i \quad \dots \quad 1.13b$$

where \vec{k} and $\hbar c\nu$ are the wave vector and energy, respectively, of the incident photon, \vec{q}_i and $\hbar c\nu_i$ are the corresponding quantities for an i^{th} phonon, \vec{G} is the reciprocal lattice vector and \underline{n} is an integer. Positive and negative signs indicate the emission and absorption processes,

respectively. Since for IR photon $\vec{k} \approx 0$, we have

$$\vec{nG} = \sum_i \pm \vec{q}_i \quad \dots \quad 1.13c$$

For a single phonon process \underline{n} has to be zero. Obviously $\vec{k} = \vec{q}_1 \approx 0$ and such process would occur at the centre of Brillouin zone. On the other hand for multiphonon processes $\underline{n} = 0, \pm 1, \text{etc.}$ and the phonons involved may have finite wave vectors. Therefore, spectra due to multiphonon processes must be continuous; however some structure may be observed due to singularities in dispersion curves.

1.14 VIBRATIONAL SPECTRA

a. General

The vibrations in solids are governed by net effect of various type of interactions leading to the following force field potential¹⁵

$$V = \sum_i V_i + \sum_{i,j} \sum V_{ij} + V_e + V_{ei} \quad \dots \quad 1.14a$$

where $\sum_i V_i$ represents the sum of internal potential energies of individual molecules in the crystal and may lead to the static field splitting (site symmetry splitting), the second term contains all cross terms between the internal coordinates of different molecules and may lead to correlation field splitting, the third term (V_e) represents the net force field potential for external modes, while the last term represents the interaction between external and internal co-ordinates and leads to the coupling between the two.

It is apparent from Eqn. 1.14a that V is a complex function of normal modes Q_i . For the sake of simplicity, V can be expressed as a Taylor expansion¹,

$$\begin{aligned}
 V = V_0 + \sum_i \left(\frac{\partial V}{\partial Q_i} \right)_0 Q_i + \frac{1}{2!} \sum_{i,j} \left(\frac{\partial^2 V}{\partial Q_i \partial Q_j} \right)_0 Q_i Q_j \\
 + \frac{1}{3!} \sum_{i,j,k} \left(\frac{\partial^3 V}{\partial Q_i \partial Q_j \partial Q_k} \right)_0 Q_i Q_j Q_k + \dots \quad \dots \quad 1.14b
 \end{aligned}$$

Here V_0 is the equilibrium potential energy which may be taken as zero. The second term vanishes as there is no force acting when the system is in equilibrium.

b. First Order Spectra

First order spectra are those which may be explained in terms of simple harmonic approximation of vibrational modes. The expression (Eqn. 1.14b) may be reduced to one describing simple harmonic motion only when Q_i , Q_j , etc. have small amplitudes and the cross-interaction among Q 's is negligibly small. To a good approximation, such conditions may be achieved at low temperatures. Thus the simple harmonic approximation for the vibrations in solids is more valid at low temperatures. Otherwise, in general, the spectrum may also exhibit effects which arise due to other processes e.g. the second order effects, Fermi resonance, etc.

c. Second Order Spectra

The second order vibrational spectra arise mainly due to anharmonic part in the expression for potential energy V , i.e. the fourth term in Eqn. 1.14b. Such anharmonic parts result in the observation of multi-phonon processes, enhancement in bandwidths, etc. The second order effects some times lead to more intense bands for multi-phonon processes than those for single phonon processes especially where electrical anharmonicities are predominant.

d. Static and Correlation Field Splittings

The static force fields around atomic/molecular unit in a crystal define interactions when the neighbouring atoms/molecules are in stationary state. The interactions can shift a nondegenerate mode and/or split only the degenerate modes into components of lower symmetry. The correlation field interactions provide additional perturbations and arise due to relative motions of symmetrically situated similar atoms/molecules. These interactions are responsible for the correlation field splittings.

e. Fermi Resonance

Fermi resonance occurs when two energy levels of a molecule, having the same symmetry and approximately the same energy interact with each other; in other words when they are accidentally degenerate. The phenomenon results in the repulsion of two levels and large enhancement in the intensity of weaker transition.

The phenomenon was observed by Fermi³² for the first time in CO_2 and later by several workers in different molecules e.g. by Adel and Barker³³ in CH_3Cl , by Sarin³⁴ in $\text{C}_6\text{H}_5\text{CHO}$ and by us³⁵ in $\text{C}_6\text{H}_5\text{Cl}$. Analogous phenomenon may be exhibited by solids as observed in quartz³⁶.

Theoretically, if ψ_1^0 and ψ_2^0 represent the unperturbed wave functions of two states involved in Fermi resonance, the perturbed states would be defined by

$$\psi_1' = a_1 \psi_1^0 - a_2 \psi_2^0 \quad \dots \quad 1.14c$$

$$\psi_2' = a_2 \psi_1^0 + a_1 \psi_2^0 \quad \dots \quad 1.14d$$

where a_1 and a_2 are such that

$$a_1^2 + a_2^2 = 1 \quad \dots \quad 1.14e$$

and

$$a_1 = \left| \frac{\Delta + \delta}{2\Delta} \right|^{\frac{1}{2}}, \quad a_2 = \left| \frac{\Delta - \delta}{2\Delta} \right|^{\frac{1}{2}} \quad \dots \quad 1.14f$$

when $\delta = 0$, we obtain equal mixture of Ψ_1^0 and Ψ_2^0 and when δ is very large $\Psi_1' \rightarrow \Psi_1^0$ and $\Psi_2' \rightarrow \Psi_2^0$. Here δ is the separation between unperturbed energy levels while Δ is that observed between perturbed levels.

The ratio of intensities I_1' and I_2' of observed transitions may be computed in terms of intensities I_1 and I_2 of respective unperturbed transitions from the following equation³⁷

$$\frac{I_1'}{I_2'} = \frac{a_1^2 I_1 + a_2^2 I_2 \mp 2a_1 a_2 (I_1 I_2)^{\frac{1}{2}}}{a_2^2 I_1 + a_1^2 I_2 \pm 2a_1 a_2 (I_1 I_2)^{\frac{1}{2}}} \quad \dots \quad 1.14g$$

The choice of the combination of signs depends on whether the matrix element of perturbation potential $V_{12} > 0$ or < 0 . The intensity I_2 of unperturbed overtone (or combination) mode can reasonably be regarded as zero. We have, therefore

$$\frac{I_1'}{I_2'} = \frac{a_1^2}{a_2^2} = \frac{\Delta + \delta}{\Delta - \delta} \quad \dots \quad 1.14h$$

For known values of I_1' , I_2' and Δ , this equation can provide the value of δ .

f. Longitudinal and Transverse Splitting

The longitudinal and transverse phonon branches of a mode possess the same frequencies except in the case of polar mode where the former branch has higher frequency than the latter. According to Born and Huang³⁸ this happens due to the presence of long range electrostatic interaction. Thus large splittings are observed in ionic crystals.

The split frequencies are related to the static dielectric constant ϵ_0 and high frequency dielectric constant ϵ_∞ through the relation

$$\prod_i \frac{\nu_i^{(LO)}}{\nu_i^{(TO)}} = \left(\frac{\epsilon_0}{\epsilon_\infty} \right)^{\frac{1}{2}} \quad \dots \quad 1.14i$$

This relation is known as Lyddane-Sachs-Teller (LST) relation. Here the product over i includes every polar mode.

g. Forbidden Modes of a Free Molecular Unit in Solids

The forbidden modes of a free molecular unit may appear in ^{the} spectra of solids. It happens mainly because of the distortions in the symmetry of units. The intensity of such modes can, therefore, be used to estimate the distortions or vice versa. If the distortions are small, the transition moment M_{fi} (Eqn. 1.6a) would be almost zero for these modes, and the corresponding band would be weak; in case of large distortions, the bands are expected to be strong.

1.15 HYDROGEN BOND

A hydrogen bond (A-H...B) exists only when H atom in a molecule or crystal comes so close to an electronegative atom B that two atoms establish directed link among each other. This type of bond in general possesses both the ionic and covalent bond characteristics. Detailed discussion on this subject is available in the literature³⁹⁻⁴².

A hydrogen bond results in two main type of shifts^{43,44} viz (i) a downward shift of stretching frequencies and (ii) an upward shift of bending frequencies. Further, in general it is accompanied by broad bands especially in stretching region⁴³ because of anharmonicity in some

part of potential energy function which gives the strong combination bands in neighbourhood of true stretching bands.

The hydrogen stretching band may exhibit a doublet if the H- bond is very strong⁴⁵. The doublet arises due to double minimum potential along A-H...B hydrogen bridge. The form of potential well along A-H...B bond has been discussed by Lippincott and coworkers^{46,47} with ~~some~~ illustrations while Somorjai and Hornig⁴⁸ have discussed the energy levels, wave functions and selection rules for IR absorption and Raman scattering.

1.16 FERROELECTRICS

Ferroelectrics have widely been discussed⁴⁹⁻⁵⁹ in past few decades for their wide applications in electronic devices. Important aspects of ferroelectricity are briefly discussed as follows.

a. General

The ferroelectrics are a subgroup of pyroelectrics. The latter act as an electric dipole on heating or cooling. A ferroelectric crystal possesses spontaneous polarization along a definite direction, which can be reversed by applying the electric field; this process is known as switching.

The relation between the net polarization and externally applied electric field is given by a hysteresis loop. A ferroelectric crystal may have regions of homogenous polarization differing only in its direction; such regions are called ferroelectric domains. Ferroelectricity disappears usually above certain temperature known as transition temperature (T_c) and the crystal becomes paraelectric.

b. Curie Weiss Law

The dielectric constant ϵ of a ferroelectric crystal changes with

temperature above T_c obeying the Curie Weiss law expressed as⁵⁴

$$\epsilon = \epsilon' + \frac{C}{T - T_0} \quad \dots \quad 1.16a$$

Here ϵ' is the dielectric constant at very high temperature, C is Curie-Weiss constant and T_0 is the Curie Weiss temperature.

c. Classification of Ferroelectrics

A large number of ferroelectrics are known today. To facilitate the study, these are classified in four different ways depending on: (i) the nature of chemical bonds, (ii) number of directions allowed to the spontaneous polarization, (iii) symmetry of the non-polar phase of the crystal and (iv) the nature of phase change. These classifications have been discussed and illustrated with examples by Jona and Shirane⁵². However, the fourth way of classification is of more importance and almost all ferroelectrics can be put in only two classes.

Displacive Type: The crystals in which spontaneous polarization appears as a result of induced dipole moment arising due to relative displacement of oppositely charged ions (electric monopoles). These crystals possess the Curie Weiss constant of the order of 10^4 - 10^5 . Examples are BaTiO_3 , SrTiO_3 , KNbO_3 , etc.

Order-Disorder Type: The phase transition in these crystals involves order-disorder phenomenon which leads to Curie-Weiss constant of the order of 10^2 - 10^3 . The examples are NaNO_2 , KH_2PO_4 , etc.

Recently, the ferroelectrics have been grouped into two categories depending on whether the phase transition occurs through (i) polarization catastrophe³¹ or (ii) some other order parameter. The crystals belonging to the former class are known as proper ferroelectrics and those belonging to the latter class are known as improper ferroelectrics.

Improper ferroelectrics were predicted theoretically by Levanyuk and Sannikov⁶⁰. Cross et al⁶¹ studied $\text{Gd}_2(\text{MoO}_4)_3$ crystal as the first improper ferroelectric.

d. Theories of Proper Ferroelectrics

The occurrence of ferroelectricity can be theoretically understood either in terms of polarization catastrophe or a soft mode (a low frequency transverse optical phonon); the two terms are interrelated through LST relation. Devonshire⁵⁶ has discussed the thermodynamical theory of ferroelectrics, which may be briefly reviewed as follows.

The equilibrium structure of a crystal is defined by the minimum value of free energy, which depends on several parameters like internal stress (\vec{X}), spontaneous polarization (\vec{P}), etc. These parameters usually change with temperature (T). Therefore by changing temperature, the free energy of the crystal may change in such a way that the condition of minimum free energy value needs a change in the crystal structure at certain temperature (T_c) known as transition temperature. This results into a crystal transformation. The parameters which trigger this transition are known as order parameters. For example \vec{P} is the order parameter for the phase transition in proper ferroelectrics.

Expansion of Free Energy: Devonshire⁵⁶ considers the free energy of the crystal as $F(T, X, P)$ and for the sake of simplicity assumes that (i) all stresses are equal to zero; $X = 0$, (ii) polarization vector \vec{P} is directed along one of the crystallographic axes only and (iii) the non-polar phase is centrosymmetrical. One has after expansion of $F(T, P)$ ³¹

$$F(T, P) = \frac{1}{2}g_2P^2 + \frac{1}{4}g_4P^4 + \frac{1}{6}g_6P^6 \quad \dots \quad 1.16b$$

where coefficients g_n depend on T . To obtain the ferroelectric state, it is supposed that

$$g_2 = \gamma(T-T_0) \quad \dots \quad 1.16c$$

γ is a positive constant. T_0 could be equal^{to} or lower than T_c .

Second-Order Transition: If g_4 is positive, inclusion of g_6 term does not change the physics, we have for equilibrium

$$\left(\frac{\partial F}{\partial P}\right)_T = \gamma(T-T_0)P_s + g_4 P_s^3 = 0 \quad \dots \quad 1.16d$$

Therefore either

$$P_s = 0 \quad \dots \quad 1.16e$$

$$\text{or } P_s = \pm \left[(\gamma/g_4)(T_0-T) \right]^{\frac{1}{2}} \quad \dots \quad 1.16f$$

Thus for $T > T_c$, $P_s = 0$; and for $T < T_c$, P_s has values ranging from zero to some finite value. Obviously transition starts at $T_0 = T_c$.

In second-order transition specific heat vs temperature may show discontinuity at T_c , but latent heat is zero.

First Order Transition: If g_4 is negative, the term g_6 is retained and considered to be positive in order to restrain F from going to minus infinity. In equilibrium we have

$$\left(\frac{\partial F}{\partial P}\right)_T = \gamma(T-T_0)P_s - |g_4| P_s^3 + g_6 P_s^5 \quad \dots \quad 1.16g$$

Therefore either

$$P_s = 0$$

$$\text{or } P_s^2 = \left[|g_4| \pm \left(|g_4|^2 - 4\gamma(T-T_0)g_6 \right)^{\frac{1}{2}} \right] / 2g_6 \quad \dots \quad 1.16h$$

So free energy would be minimum for $P_s = 0$ and for a definite value of P_s . Obviously, the polarization would jump from zero to certain definite value on decreasing the temperature. It may be seen that T_0 would be less than T_c .

The first order phase transitions involve certain amount of latent heat and a change in dielectric constant in such a way that⁶²

$$\frac{\epsilon^+ - 1}{\epsilon^- - 1} = 4 \quad \dots \quad 1.16i$$

where ϵ^+ and ϵ^- are the dielectric constants just above and just below T_c . Further, the hysteresis curve just above T_c exhibits double loop⁵⁴.

e. Theory of Improper Ferroelectrics

Kobayashi et al⁶³ have discussed the elementary theory of improper ferroelectrics considering the form of free energy expansion as

$$F(T, \theta, P) = b_1(T - T_\theta)^2 \theta^2 + b_2 \theta P + b_3 P^2 \quad \dots \quad 1.16j$$

where θ is the order parameter whose definition may differ from crystal to crystal. b_1, b_2, b_3 etc. are the constants, T_θ is a constant temperature (a characteristic of the crystal). The behaviour of improper ferroelectrics is not very well understood. However, the recent work of Dvorak et al⁶⁴ and Takagi et al⁶⁵ have contributed significantly to an understanding of the improper ferroelectrics.

f. Effects of External Conditions and Isotopic Substitution on Phase Transition

The general features of the effects of external conditions such as electric field and pressure, etc. and of isotopic substitution have been discussed in most of the text books⁵¹⁻⁵⁴.

The d.c. biasing field promotes the upper transition and correspondingly T_c goes up, whereas the lower transition temperature, if it existed, goes down.

The external pressure affects the phase transition in different ways depending on the nature of the crystal and the order of phase transition⁵¹.

The isotopic substitution may or may not affect phase transition. For example⁵², (i) KH_2PO_4 has the transition at 123°K while KD_2PO_4 at 213°K . (ii) Both the $\text{NH}_4\text{Fe}(\text{SO}_4)_2 \cdot 12\text{H}_2\text{O}$ and $\text{ND}_4\text{Fe}(\text{SO}_4)_2 \cdot 12\text{D}_2\text{O}$ have the transition at 88°K . In fact, it depends on the extent of the role played by the isotopically substituted atom in triggering the phase transition.

g. Electro- and Elasto- Optic Effects

These effects have been discussed in detail by Kanzig⁵¹ and Fatuzzo and Merz⁵³. Electro-optic effect appears as the change in birefringence when a crystal is subjected to electric field, while the elasto-optic effects appear as the change in birefringence when the crystal is subjected to the stress. These effects are important in connection with the ferroelectric phase transitions which involve a change in the states of internal electric field and stress.

h. Symmetry Aspects of Ferroelectricity

A review on the symmetry aspects in the theory of ferroelectricity has been published by Shuvalov⁶⁶. These aspects are very important because the symmetry-changes on phase transitions and the crystallography of domain structure determine the properties of ferroelectrics. The knowledge of the

symmetry of the initial phase enables us to elucidate the behaviour of ferroelectrics and to predict many peculiarities involved.

i. Units

Debye: Debye is the unit of electric dipole moment. It is equal to the dipole moment of a dipole system of two oppositely charged particles of 10^{-10} e.s.u. separated by 1 \AA from each other. Thus $1 \text{ Debye} = 10^{-18}$ e.s.u. units of dipole moment (esu. cm) $= 1/3 \times 10^{-29}$ MKS units of dipole moment (Coulomb. metre)

Unit of Polarization: Polarization is the dipole moment per unit volume or is the charge per unit area of crystal surface perpendicular to the polarization \vec{P} . It is usually measured in micro Coulomb per cm^2 ($\mu\text{C}/\text{cm}^2$).

$$\begin{aligned} 1 \mu\text{C}/\text{cm}^2 &= 10^{-2} \text{ MKS (Coulomb/metre}^2) \\ &= 3 \cdot 10^3 \text{ e.s.u (esu charge/cm}^2) \\ &= 3 \cdot 10^{-3} \text{ Debye/\AA}^3 \end{aligned} \quad \dots \quad 1.16k$$

This leads to

$$\vec{P}(\text{in } \mu\text{C}/\text{cm}^2) = \frac{1000}{3v} \vec{p} \quad \dots \quad 1.16l$$

where v is the volume (in \AA^3) and \vec{p} is the dipole moment (in Debye) of the unit cell.

1.17 ATTENUATED TOTAL REFLECTION (ATR) SPECTROSCOPY

The well known phenomenon of total internal reflection defines⁶⁷ that the light travelling from a denser medium towards the rarer medium is totally reflected back (cf Fig. 1.3a) from the interface between the two

media if: (i) the angle of incidence θ_i satisfies the condition

$$\theta_i \geq \sin^{-1}(n_2/n_1) \quad \dots 1.17a$$

and (ii) the second medium is non-absorbing. Here n_1 and n_2 are refractive indices of denser and rarer media, respectively. However in case of absorbing rarer medium, the intensity of reflected light gets attenuated and the phenomenon is defined as attenuated total reflection (ATR)⁶⁷.

In as early as 1947, Goos and Hanchen⁶⁸ showed that there is a slight displacement of the totally reflected beam in the plane of reflection as shown in Fig. 1.3b; unlike the ordinary reflection, the reflected beam follows the path shown by continuous line instead of the broken line. They also showed that the beam penetrates to a depth d_p in the rarer medium and probably follows the curved path as shown in Fig. 1.3b.

Newton⁶⁹ had explained these observations in terms of attraction between light and matter which was assumed to be stronger for denser medium. It is now established that this explanation and picture given by Newton, although convenient, are incorrect. According to the present knowledge, a standing wave (cf Fig. 1.4a) normal to the reflecting surface is established in the denser medium while an evanescent, nonpropagating field in the rarer medium. The electric field amplitude of evanescent field decays exponentially with distance from the surface as shown in Fig. 1.4b.

In a case, when the rarer medium is absorbing, the energy from the incident beam is transferred to this medium through its interaction with evanescent field. Thus the intensity of the beam gets attenuated. The magnitude of attenuation depends on the depth of penetration d_p (cf : Fig. 1.4b) and the absorption coefficient of the medium. d_p is defined as

the distance required for the electric field amplitude to fall to e^{-1} of its value at surface and is given by⁶⁷

$$d_p = \frac{\lambda_{vac}}{2\pi n_1 [\sin^2 \theta_i - (n_2/n_1)^2]^{\frac{1}{2}}} \quad \dots \quad 1.17b$$

where λ_{vac} is the vacuum wavelength of incident radiation.

Now if we have an experimental set up to analyse spectroscopically the reflected beam, the spectra are seen to exhibit informations about absorption characteristics of the second medium. Several spectrophotometers and accessories useful to investigate such attenuated reflection have been designed and fabricated in other laboratories and are also available commercially^{70,71}.

In a Fahrenfort⁷² type accessory which we have in our laboratory, a hemicylindrical crystal of IR transparent material (like KRS-5, AgCl, Ge, etc.) is used as a medium of high refractive index. Fig. 1.5 depicts the cross sectional view of rays entering into and emerging out from such a crystal. The radius of curvature (r) of the cylinder is kept such that it satisfies the condition

$$d = \frac{r}{n_1 - 1} \quad \dots \quad 1.17c$$

where d represents the distance as shown in Fig. 1.5. The sample to be investigated is kept in optical contact with the plane back surface of the hemicylinder. The reflected radiations are arranged to focus on the slit of the spectrophotometer for spectroscopic analysis. Spectra thus obtained may be called as ATR spectra.

It has been established both experimentally and theoretically that ATR spectra should be more or less identical ~~with~~ the transmission spectra of absorbing medium if recorded at an angle θ_i greater than the critical angle (θ_c) by a few degrees. However, the spectra recorded at angles $\theta_i < \theta_c$, exhibit bands resembling the specular reflection spectra. There is a continuous transition from one type of spectrum to the other as θ_i crosses θ_c (cf Fig. 1.6)*. Thus it becomes clear that in order to get transmission like spectra of an absorbing medium, n_1 must be sufficiently larger than n_2 .

Attenuated total reflection spectroscopy has some decided advantages over normal transmission or reflection methods. The observed spectra do not involve matrix bands (e.g. mull bands in IR spectra). The problem like ion exchange, as it sometimes occurs in KBr disc technique used to record IR spectra, may be avoided. Samples, whether they are solids, liquids or pastes, can be studied in their natural forms. Crystal slabs of normal size can be used, while transmission spectroscopy requires slabs of a few micron thickness which are difficult to obtain by conventional methods. Good ATR spectra may be recorded by using samples as thin as about 10 microns. Although, there are some outstanding problems e.g. to have optical contact between sample crystal and ATR element, the ATR spectroscopy has been developing quite rapidly in past few years.

* In this figure $\theta_{c \text{ min}}$, $\theta_{c \text{ av}}$ and $\theta_{c \text{ max}}$, respectively, correspond to the minimum, average and maximum values of refractive index (n_2) over the absorption band.

REFERENCES

1. G. Herzberg, Infrared and Raman Spectra of Polyatomic Molecules, D. Van Nostrand, New York (1945).
2. E.B. Wilson Jr., J.C. Decius and P.C. Cross, Molecular Vibrations, McGraw Hill, New York (1955).
3. W.W. Coblentz, Investigations of Infrared Spectra, Carnegie Institute Publications, Washington, D.C. (1905).
4. N. Bjerrum, Verhandl. deut. Physik. Ges., 16, 737 (1914).
5. For Example Bibliography reported by (a) Herzberg (Ref.1), (b) K. Nakamoto, Infrared Spectra of Inorganic and Coordination Compounds, John Wiley, New York (1963) and (c) D. Bloor, Infrared Physics 10, 1 (1970).
6. A Smekal, Naturwissenschaften 11, 873 (1923).
7. C.V. Raman, Ind. J. Phys. 2, 387 (1928).
8. A. Yariv, Quantum Electronics, John Wiley, New York (1967).
9. For Example Bibliography reported (for 1968-69) in Laser Raman Spectroscopy, by M.C. Tobin, Wiley Inter Science, New York (1971).
10. H.H. Jaffe and M. Orchin, Theory and Applications of Ultraviolet spectroscopy, John Wiley, New York (1964).
11. G. Placzek, Handbuch Der Radiologie 2, 205 (1934).
12. L.A. Woodward in Raman Spectroscopy; Theory and Practice, Vol I, Ed. H.A. Szymanski, Plenum Press, New York (1967).
13. R.E. Hester in Raman Spectroscopy; Theory and Practice, Vol I, Ed. H.A. Szymanski, Plenum Press, New York (1967).
14. J. Tang and A.C. Albrecht in Raman Spectroscopy, Theory and Practice, Vol. II, Ed. by H.A. Szymanski, Plenum Press, New York (1970).
15. P.M.A. Sherwood, Vibrational Spectroscopy of Solids, Cambridge University Press, Cambridge (1972).
16. H. Smith, Phil. Trans. Roy. Soc. London A241, 105 (1948).
17. M.C. Tobin, Laser Raman Spectroscopy, Wiley Inter Science, New York (1971).

18. D.M. Dermison, Rev. Mod. Phys. 3, 280 (1931).
19. E.B. Wilson, Phys. Rev. 45, 706 (1934).
20. J.E. Rosenthal and G.M. Murphy, Rev. Mod. Phys. 8, 317 (1936).
21. S. Bhag^ovantam and T. Venkatarayudu, Proc. Ind. Acad. Sci. A9, 224 (1939).
22. R.S. Halford, J. Chem. Phys. 14, 8 (1946).
23. D.F. Hornig, J. Chem. Phys. 16, 1063 (1948).
24. H. Winston and R.S. Halford, J. Chem. Phys. 17, 607 (1949).
25. M. Born and Th. Van Karman, Z. Phys. 13, 297 (1912) cited in Handbuch der Phys. 7, 325 (1955).
26. S. Bhagvantam, Scattering of Light and The Raman Effect, Chemical Publication Co., New York (1942).
27. S.S. Mitra in Optical Properties of Solids Eds. S. Nudelman and S.S. Mitra, Plenum Press, New York (1969).
28. W.G. Fateley, N.T. McDevitt and F.F. Bentley, Appl. Spectrosc. 25, 155 (1971).
29. S.S. Mitra, Solid State Phys. 13, 1 (1962).
30. G. Turrell, Infrared and Raman Spectra of Crystals, Academic Press, London (1972).
31. C. Kittel, Introduction to Solid State Phys., John Wiley, New York (1971).
32. E. Fermi, Z. Physik 71, 250 (1931).
33. A. Adel and E.F. Barker, J. Chem. Phys. 2, 627 (1934).
34. V.N. Sarin, Ph.D. Thesis, Indian Institute of Technology Kampur, India (1970).
35. Y.S. Jain and H.D. Bist, J. Mol. Spectrosc. 47, 126 (1973).
36. J.F. Scott, Phys. Rev. Lett. 21, 907 (1968).
37. J.F. Bertran, L. Ballester, L. Dabrihalova, N. Sanchez and R. Arrieta, Spectrochim. Acta 24A, 1765 (1968).
38. M. Born and K. Huang, Dynamical Theory of Crystal Lattices, Oxford University Press, New York (1954).

39. L. Pauling, The Nature of Chemical Bond, Cornell University Press, London (1945).
40. W.C. Hamilton and J.A. Ibers, Hydrogen Bonding in Solids, Benjamin, New York (1968).
41. D. Hadzi, Editor, Hydrogen Bonding, Pergamon Press, New York (1957).
42. G. C. Pimental and A.L. McClellan, The Hydrogen Bond, Freeman, California (1960).
43. S. Bratoz, Adv. Quant. Chem. 3, 210 (1967).
44. J.C. Waddington, J. Chem. Soc., 4340 (1958).
45. S. Bratoz and D. Hadzi, J. Chem. Phys. 27, 991 (1957).
46. R. Schroeder and E.R. Lippincott, J. Phys. Chem. 61, 921 (1957).
47. E.R. Lippincott and R. Schroeder, J. Chem. Phys. 23, 1099 (1955).
48. R.L. Somorjai and D.F. Hornig, J. Chem. Phys. 36, 1980 (1962).
49. E.T. Jaynes, Ferroelectricity, Princeton University Press, Princeton (1953).
50. H.D. Megaw, Ferroelectricity in Crystals, Methuen, London (1957).
51. W. Kanzig, Ferroelectrics and Antiferroelectrics, Academic Press, New York (1957).
52. F. Jona and G. Shirane, Ferroelectric Crystals, Pergamon Press, Oxford (1962).
53. E. Fatuzzo and W.J. Merz, Ferroelectricity, North-Holland, Amsterdam (1967).
54. J.C. Burfoot, Ferroelectrics, D. Van Nostrand, London (1967).
55. W.J. Merz, Ferroelectricity: Progress in Dielectrics, Vol 4, Heywood, London (1962).
56. A.F. Devonshire, Adv. Phys. 3, 85 (1954).
57. P.W. Anderson, Moscow dielectric Conf. (1960).
58. W. Cochran, Adv. Phys. 2, 387 (1960).
59. V.L. Ginzburg, Sov. Phys. - Solid State 2, 1824 (1960).
60. A.P. Levanyuk and D.G. Samikov, Exp. i-Teor. Fiz. 55, 256 (1968).

61. L.E. Cross, A. Fouskova and S.E. Cummins Phys. Rev. Lett. 21, 812 (1968).
62. C. Kittel, Introduction to Solid State Physics 2nd edition, John Wiley, New York (1956).
63. J. Kobayashi, Y. Enomoto and Y. Sato, Phys. Status Solidi (b) 50, 335 (1972).
64. V. Dvorak and J. Petzelt, Phys. Lett A35, 209 (1971).
65. Y. Takagi, A. Sawada and Y. Ishibashi, J. Phys. Soc. Japan 34, 737 (1973).
66. L.A. Shuvalov, J. Phys. Soc. Japan Supl. 28, 38 (1970).
67. N.J. Harrick, Internal Reflection Spectroscopy, Inter Science, New York (1967).
68. F. Goos and H. Hanchen, Ann. Physik 1, 333 (1947).
69. I. Newton, Opticks, Dover Publications, New York (1952).
70. P.A. Wilks, Jr. and T. Hirschfeld in Applied Spectroscopy Review, Ed. E.G. Brame, Marcel Dekker, New York (1967).
71. W.W. Wendlandt and H.G. Hecht, Reflection Spectroscopy, Inter Science, New York (1966).
72. J. Fahrenfort, Spectrochim. Acta 17, 698 (1961), J. Fahrenfort and W.M. Visser, Spectrochim. Acta 18, 1103 (1962).

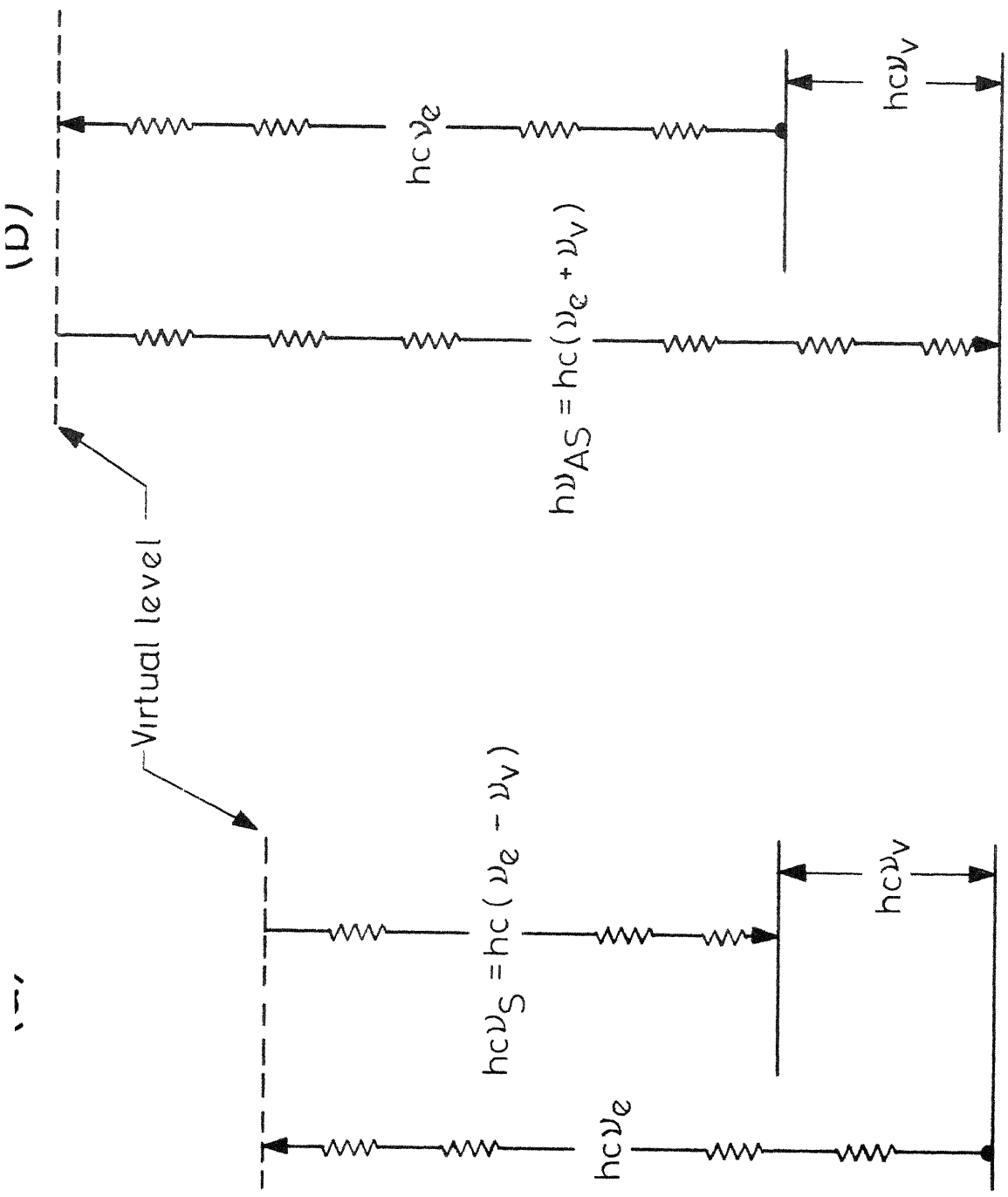


Fig.1.1 An illustration of (a) Stokes and (b) anti-Stokes Raman processes.

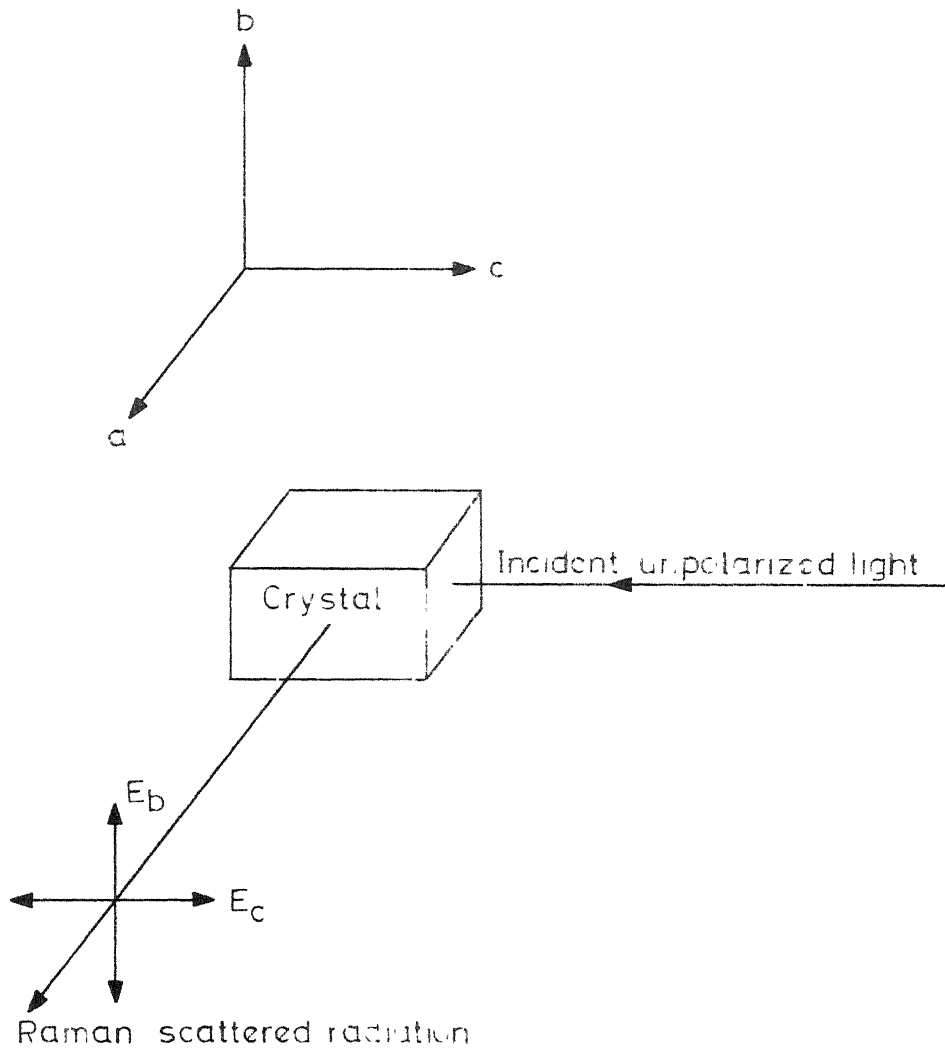
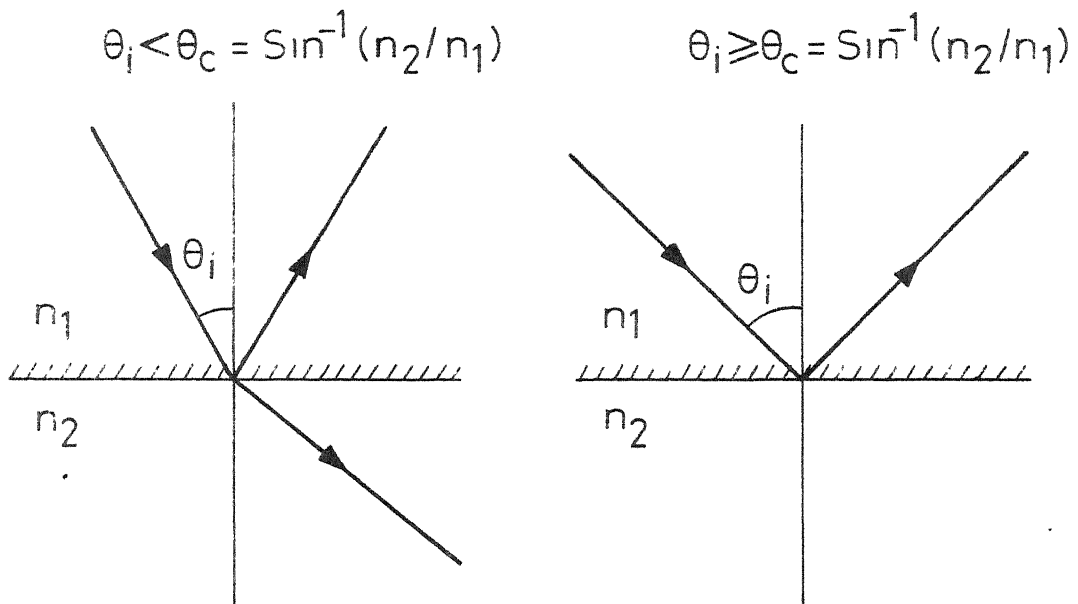


Fig.1.2 An illustration to define depolarization ratio $\rho = S_{||} / S_{\perp}$. For $S_{||}$ and S_{\perp} , intensity of scattered radiations polarized parallel to E_c and E_b respectively, are measured.

(a)



(b)

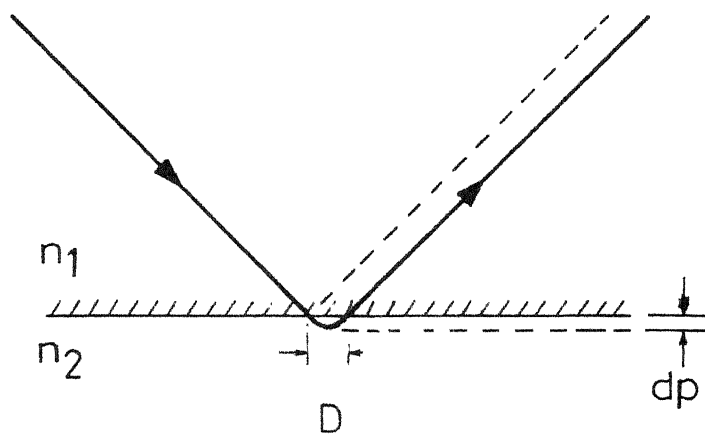
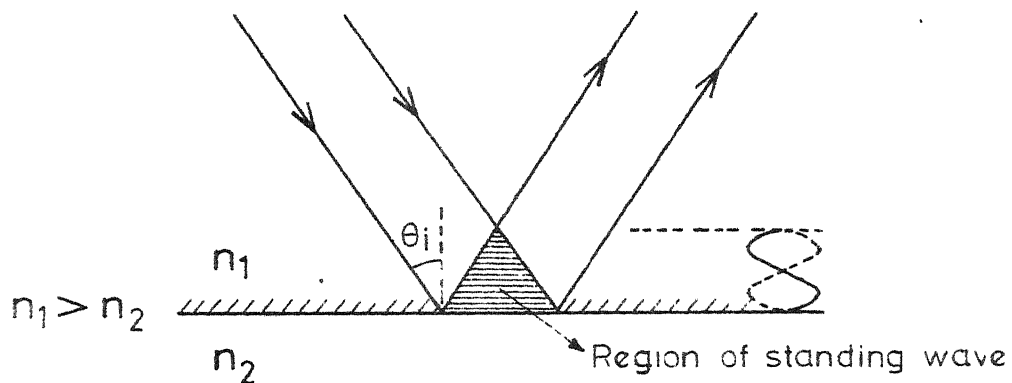


Fig.1.3 (a) An illustration showing total reflection phenomenon, (b) The totally reflected beam follows the path shown by solid line (—) instead of broken one (----).

(a)



(b)

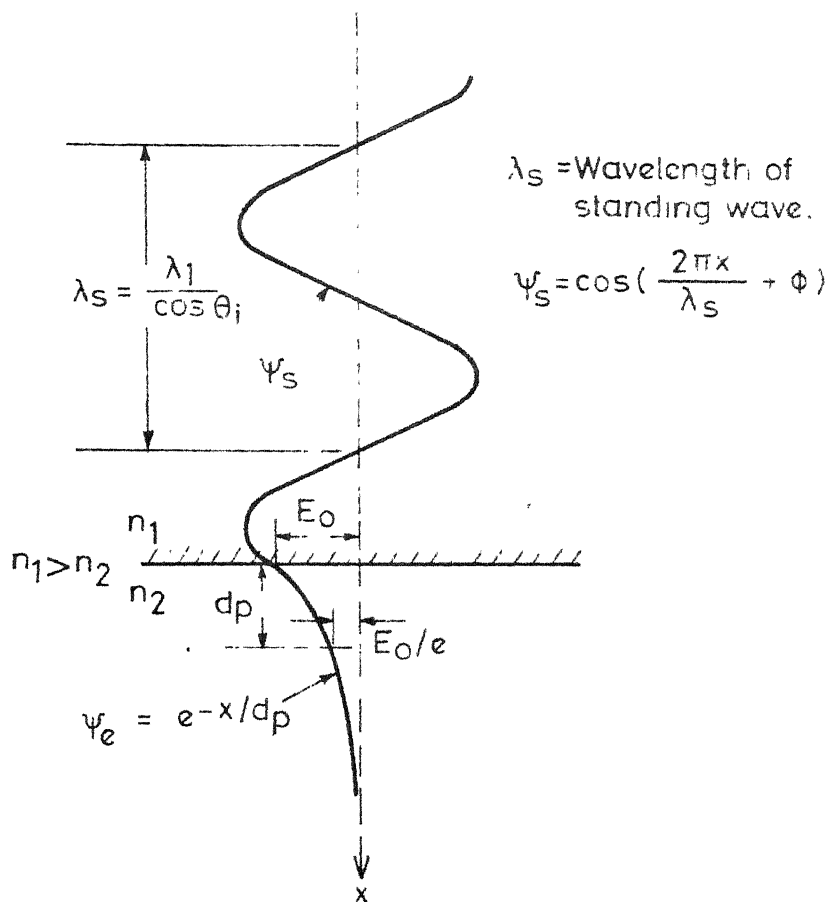


Fig.1.4 Total reflection phenomenon establishes (a) standing wave (ψ_s) in denser medium and (b) nonpropagating evanescent wave (ψ_e) in rarer medium.

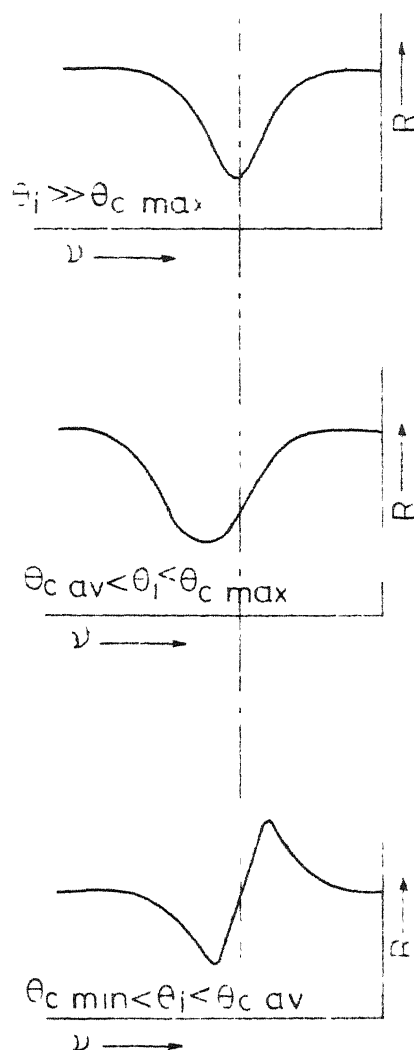
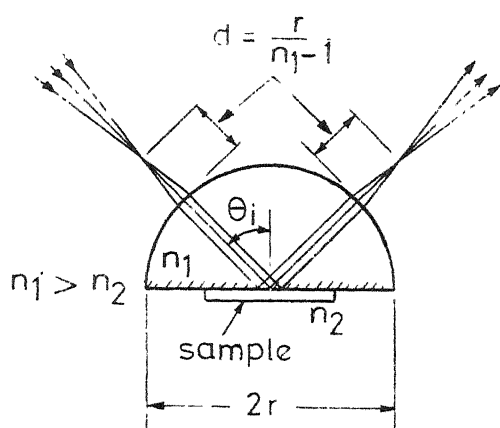


Fig.1.5 Rays of light going in and emerging out from a hemicylindrical ATR element

Fig.1.6 Transition from a normal absorption type spectrum to an anomalous absorption type with decreasing θ_i .

CHAPTER II

EXPERIMENTAL DETAILS

2.1 PURIFICATION OF SAMPLES

Compounds of analar grade or of high purity were obtained from British Drug House (BDH) Chemicals or Alfa Inorganics for present investigations. The compounds were further purified in this laboratory by slow evaporation of their aqueous solution in proper thermal conditions to ensure the high grade purity and correct chemical structure in case of hydrates. Transparent crystals of a few mm³ size were separated out from the material obtained after evaporation. These small crystals were further dissolved to grow large single crystals which were finally used for spectral investigations. Deionized distilled water was used to prepare solutions.

2.2 GROWTH OF LARGE SINGLE CRYSTALS

Large single crystals of each of the investigated systems were grown from aqueous solution of recrystallized compound. The simple seed suspension or rotating seed technique was employed. Both of these techniques have been discussed in detail by Holden and Singer¹ and Buckley². A rotatory crystallizer was fabricated for the latter method. The line diagram of the fabricated unit has been shown in Fig. 2.1. This contains

shynchronous motor (M) of 30 rpm. The motor is fixed rigidly on the upper platform of a metal framed box having three vertical sides of glass-sheet and one slidable perspex sheet. A stainless steel rod (R), which passes vertically through a central hole in the upper platform connects the motor M to a glass stirrer (S) through 90° gear system G. The stirrer (S) has a number of horizontally projected glass fins which are tilted in such a way that the solution is driven little upward when the stirrer is rotated. This tilt was found to give better results, probably because it keeps the solution homogeneous. The temperature inside the box is observed to vary at the maximum by $\pm 2^\circ$ in the air-conditioned laboratory.

2.3 CRYSTAL CUTTING AND POLISHING

Crystals for present investigations were prepared by adopting the following procedure. The crystallographic axes were first identified by the morphology of crystals and later were confirmed by X-ray diffraction (Laue pattern) method. Crystal pieces of orthorhombic shape (having sides parallel to the crystallographic axes) and appropriate size were cut from the grown crystals on a crystal cutting machine. These pieces were polished over a polishing kit; polishing powders of 302 $\frac{1}{2}$, 303 and 303 $\frac{1}{2}$ grades, obtained from British American optical company U.S.A. were used in succession with CCl₄ drops. For final finish, the crystals were polished with finest alumina powder and glycerine. Once again the Laue patterns were photographed to ensure the correctness of the determined crystallographic axes.

2.4 INFRARED INSTRUMENT AND ACCESSORIES

a. Instrument

Infrared spectra were recorded on the Perkin Elmer-521 double beam grating spectrophotometer³ which works on the principle of optical null method. The optical ray diagram is depicted in Fig. 2.2. Nernst glower is used as a source of infrared radiation and a high speed sensitive thermocouple fitted with blackened gold leaf and CsBr lens, as detector. The instrument employs two plane gratings G_1 and G_2 mounted on a common base facing back to back. G_1 has 100 lines/mm and is used in its first and second orders respectively in the regions from 630 to 2000 cm^{-1} and 2000 to 4000 cm^{-1} ; G_2 having 25 lines/mm is used only in first order in the region of 250 to 630 cm^{-1} . Automatic adjustment of interference filters have been provided to avoid radiations from unwanted orders. To scan high quality spectra the instrument has been provided with several adjustable parameters e.g. slit width, gain, scan speed, etc. The resolution of the instrument is 0.3 cm^{-1} at 1000 cm^{-1} with a reproduction of $\pm 0.5 \text{ cm}^{-1}$ with slit width 410 microns.

b. ATR Accessory

The line diagram of Fahrenfort⁴ type ATR accessory obtained from Perkin Elmer Corporation is shown in Fig. 2.3. The principal part of the accessory is the hemi-cylindrical crystal (CRY) of KRS-5 (Thallium bromide iodide) known as ATR element. The refractive index of KRS-5 is 2.37 at 1000 cm^{-1} which remains almost constant in the complete working range of PE-521 instrument. Crystals of Ge, Si and AgCl having appropriate size are also used instead that of KRS-5. Mirrors M_1 and M_2 are rigidly

fixed, while M_3 and M_4 move on carriages and ATR element rotates about its vertical axis. The geometry of the accessory is such that radiations after reflection from mirror M_4 always get focussed at the slit of the spectrophotometer. The accessory in its best conditions is reported to have about 35% transmittance; however, we observed only about 27%.

c. Low Temperature Cell

Spectra at low temperatures were recorded by mounting the pellet or the KBr/AgCl window on which polycrystalline film was deposited inside the cold finger block of the conventional Wagner-Hornig⁵ type cell (cf Fig. 2.4). The cell consists of a double walled reservoir (for coolant like liquid nitrogen) and an evacuable cell fitted with CsBr windows.

Copper-constantan thermocouple was attached to the centre of one side of the cold finger block. One end of the thermocouple was dipped in an ice-water mixture. Thermo e.m.f. was measured by a milli-voltmeter which was calibrated to read the temperature of the sample. The temperature was controlled by cooling the cold finger with liquid nitrogen and simultaneously heating the same electrically by controlled current in a nichrome coil wound around the kovar tube (cf Fig. 2.4). Both temperature stability and accuracy of its measurement could be maintained within $\pm 2^\circ\text{C}$.

2.5 SCAN OF IR SPECTRA

To get an adequate IR spectrum of an inorganic compound is difficult because of two main factors: (i) the highly absorbing nature and (ii) long range electrostatic interaction exhibited by such compounds. The former factor almost makes it impossible to record transmission spectra because of technical difficulties in getting the required thin sheet of the

single crystal, while the second one makes the spectra to depend on the shape, size and environment of the sample. Recently attention has, therefore, been paid towards the development of specular reflection and attenuated total reflection techniques^{4,6-8} and their application to the study of the IR spectra of single crystals. However, there are several limitations and difficulties in employing these techniques e.g. (i) the former technique needs sufficiently large size plane polished crystal and the recorded spectra exhibit very poor resolution and characteristic shift in band positions by several wave numbers and (ii) the latter technique requires optical contact between the sample crystal and ATR element, which is an outstanding problem to get more reliable spectra.

In this laboratory we have used ATR technique to record IR spectra of single crystals while mull, pellet and low scattering microcrystalline film techniques for powdered samples.

a. ATR Technique

The crystal to be investigated using ATR technique is cut to an appropriate size. The space provided for the sample with the accessory can accommodate a crystal of largest size: 19 mm in length, 8 mm in breadth and 2 mm in thickness⁹. However, adequate spectra are stated to have been obtained using only, effective sample area of 0.2 mm x 0.7 mm⁹. The largest faces of the sample crystal are rubbed with fine polishing powder with suitable liquid like CCl_4 in our cases to get uniform thickness. One of these faces is polished following the method discussed in section 2.3 to get high degree of planeness. The highly polished face is kept in contact with the plane face of ATR element and lightly pressed by tightening the screw over the pressure plate. The spectra are then recorded at desired angle

of incidence between the available range 25° to 65° .

b. Mull Technique

In this technique the solid sample is ground into a fine powder and then dispersed in a mulling agent to get a slurry or mull. The commonly employed mulling agent is the nujol (high boiling fraction from petroleum). Other mulling agents include hexachlorobutadiene, perfluoro-kerosene (fluorolube), etc. The absorption bands of nujol¹⁰ are found at 2915, 1462, 1376 and 719 cm^{-1} . In the present investigations we have also used nujol of extra pure quality as the mulling agent. In order to minimize its absorption nujol was also used in the reference cell. Plane polished CsBr windows were used in both sample and reference cells.

c. Pellet Technique

This method involves mixing a fine powder of the sample with a suitable matrix material (e.g. alkali halides) and pressing the mixture into a transparent disc.

We used dry KBr of analar grade to prepare pellets of our samples; fine powder of KBr was heated at about 100°C in a furnace for few hours before use. Pellets were prepared in a pellet making die which was connected to a vacuum pump to get more transparent pellets of uniform thickness.

In some cases mull and/or pellet techniques may provide inadequate spectra as a result of the effects arising due to several physical and chemical factors which have been discussed and reviewed by Duyckaerts¹¹. Attention was, therefore, paid to ensure the correctness and adequacy of the spectra recorded by using these techniques.

d. Low Scattering Microcrystalline Film Technique

Though the microcrystalline film technique is a simple one but is not very common in practice. In this technique the finely powdered sample is spread uniformly on a plane plate of alkali or silver halides. Few drops of suitable organic liquid of high vapour pressure like CCl_4 are used to wet the powder. The wet powder is subjected to the uniform pressure applied gently through a plane glass plate which is kept in slow sliding motion. The glass plate is eventually removed and the organic liquid is allowed to evaporate completely.

2.6 CALIBRATION IN IR REGION

The calibration of the spectrophotometer was checked by using rotational bands of atmospheric water vapour below 600 cm^{-1} and fine structure lines of CO_2 and HCl (vapour)¹². In rest regions lines of indene were recorded. The accuracy of reported frequencies varies between $\pm 2\text{ cm}^{-1}$ for sharp bands and $\pm 10\text{ cm}^{-1}$ for diffuse and broad bands.

2.7 RAMAN INSTRUMENTS AND ACCESSORIES

Raman spectra were recorded on spex model-1400 Raman spectrophotometer¹³. The optical ray diagram of this instrument is shown in Fig. 2.5. The grating double monochromator acts as dispersor. The square size gratings (102 mm x 102 mm) have 1200 lines per mm and are blazed at 5000 \AA . The gratings are driven by a sine-bar arrangement which yields a spectral output with wavelength as a linear function of drive screw rotation. The scanning speeds may be varied between 0.12 and $2300\text{ \AA}/\text{min}$. The bilateral, curved slits may be used upto a height of 50 mm; the resolution is 0.08 \AA at 6328 \AA . The wavelength counter mechanism is stated to be accurate to

1 Å and to be reproducible to 0.2 Å over a 6000 Å wavelength interval.

Argon ion laser model 52 (Coherent Radiation Laboratory) tuned at 4880 Å was used as a source of excitation. Interference filters were used to avoid plasma lines.

EMI-6256S photomultiplier and photon counting detection system were used to detect the scattered radiations.

2.8 SCAN OF RAMAN SPECTRA

Crystals used to record their Raman spectra were prepared by following the procedure discussed in section 2.3. The crystal to be investigated was mounted on a goniometer for better adjustment of its orientation. The correct knowledge of the orientation of the crystal is very important as it directly indicates which of the components of polarizability tensor changes during vibrations, producing a particular spectrum. The form of the scattering tensor can be predicted for a vibration of any given symmetry by standard group theoretical methods.

Loudon¹⁴ has listed the scattering tensors for all 32 point groups. For an uniaxial crystal Nedungadi¹⁵ has shown that 27 different types of Raman spectra may be obtained with transverse scattering of which only 12 are relatively important. However, the minimum number of geometries needed for the complete study of Raman tensor depends on the symmetry of the crystal or the number of independent components of Raman tensor.

A given component of the scattering tensor α_{xy} may be determined experimentally by arranging the geometry such that the incident light is

polarized in the x-direction and the scattered light in y-direction. For example the geometry in Fig. 2.6 allows the determination of phonons having xy polarizability characteristic.

Porto and coworkers¹⁶ have initiated very useful notation for defining the geometry used in recording a particular spectrum and in describing polarizability characteristic of the same. Four symbols, two inside parenthesis and two outside, describe the pertinent experimental parameters. For example in x(yz)y two outer symbols x and y denote the directions of propagation of incident and scattered light, respectively, while the inner symbols y and z indicate that incident light is polarized along y-direction and scattered one in z-direction. Further, these symbols in their combined form yz indicate that α_{yz} component of polarizability tensor changes to produce scattered radiations which are recorded. In such notations geometry is always assumed to be 90° scattering unless otherwise specified.

Fig. 2.7 depicts 12 different geometries used by us to record Raman spectra of a single crystal. The thick vertical arrow (in each of the six illustrations) represents exciting laser beam propagating parallel to the crystallographic axis marked near the arrow head. The horizontal thin line represents the scattered radiations coming out of the crystal parallel to the crystallographic axis marked near its arrow head. The lines with double arrow heads represent the state of polarization of the exciting and scattered light. These six illustrations as such define scattering geometries b(aa)c, a(cc)b, etc., involving only diagonal components of $\tilde{\alpha}$. The starred arrangements b(ab)c, a(ca)b, etc. involving off-diagonal components of $\tilde{\alpha}$ can be obtained by rotating the

analyzer by 90° from its respective positions in $b(aa)c$, $a(cc)b$, etc.

2.9 CALIBRATION OF RAMAN SPECTRA

The wavelength scale of Raman spectra of $(NH_4)_2SO_4$ was corrected for its constant error by measuring the Stokes and anti-Stokes bands in their lattice mode region. In cases of $(NH_4)_2BeF_4$ and $\alpha-NiSO_4 \cdot 6H_2O$ crystals, the calibration of Raman spectra was made using the sharp lines of neon discharge in 4880 \AA to 6000 \AA region.

2.10 DEUTERATION OF THE HYDRATED COMPOUNDS

The hydrated compound was first heated in a furnace at a temperature where it loses its whole content of water of hydration. The dehydrated compound thus obtained was taken out of the furnace and transferred soon into a dry flask. This flask was connected to a vacuum system at F_2 (cf Fig. 2.8) as soon as possible. Every precaution was taken to avoid the absorption of atmospheric water by the sample. D_2O was transferred into this flask from one connected at F_1 using vacuum distillation method. After the anhydrous compound got dissolved completely in D_2O , the latter was evaporated and transferred to another flask at F_3 again by using vacuum distillation method; the sample flask was kept at an appropriate temperature during this process to ensure the correct chemical structure.

REFERENCES

1. A. Holden and P. Singer, Crystal and Crystal Growing, University Press, Columbus (1960).
2. H.E. Buckley, Crystal Growth, John Wiley, New York (1951).
3. Instruction Manual for Model 521 Spectrophotometer, Perkin Elmer, Norwalk Connecticut (1965).
4. J. Fahrenfort, Spectrochim. Acta 17, 698 (1961); J. Fahrenfort and V.M. Visser, Spectrochim. Acta 18, 1103 (1962).
5. E.L. Wagner and D.F. Hornig, J. Chem. Phys. 18, 296 (1950).
6. W.W. Wendlandt and H.G. Hecht, Reflectance Spectroscopy, Inter-Science, New York (1966).
7. N.J. Harrick, Internal Reflection Spectroscopy, Inter-Science New York (1967).
8. P.A. Wilks and T. Hirschfeld, Applied Spectroscopy Reviews Ed. E.G. Brame, Marcel Dekker, New York (1967).
9. Instructions: Attenuated Total Reflectance Accessory, Perkin Elmer, Norwalk Connecticut (1963).
10. C.N.R. Rao, Chemical Applications of Infrared Spectroscopy, Academic Press, New York, p. 65 (1963).
11. G. Duyckaerts, Analyst 84, 201 (1959).
12. Tables of Wave Numbers for Calibration of Infrared Spectrophotometers, Butterworth (1961).
13. A. Anderson, The Raman Effect, Marcel Dekker, New York (1971).
14. R. Loudon, Adv. Phys. 13, 423 (1964).
15. T.M.K. Nedungadi, Proc. Indian Acad. Sci. A10, 197 (1939).
16. T.C. Damen, S.P.S. Porto and B. Tell, Phys. Rev. 142, 570 (1960) and Phys. Rev. 144, 771 (1966).

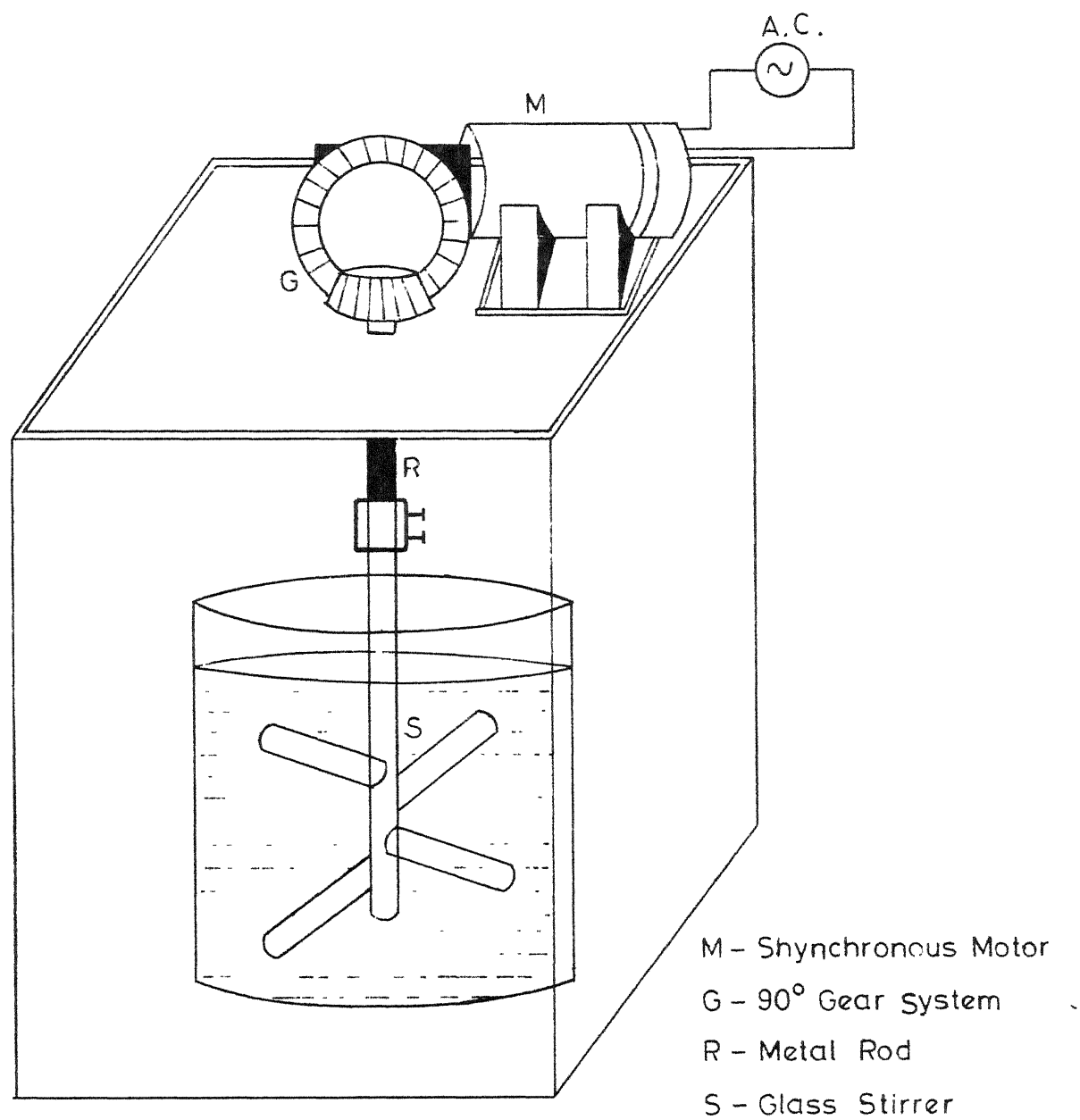


Fig.21 Line diagram of rotatory crystallizer.

PERKIN - ELMER - 521 INFRARED SPECTROPHOTOMETER.

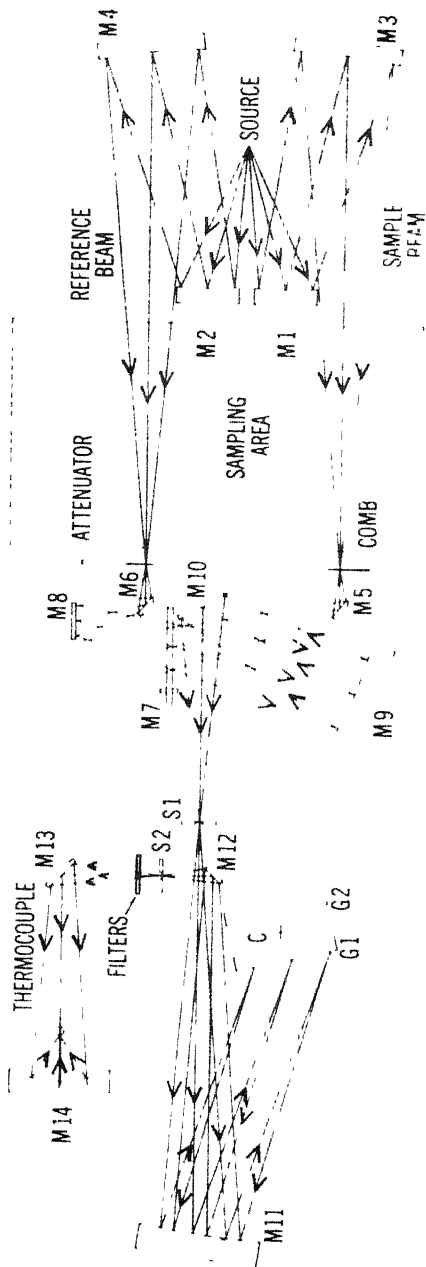
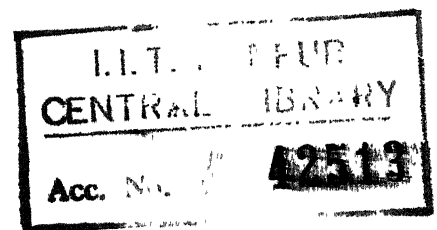
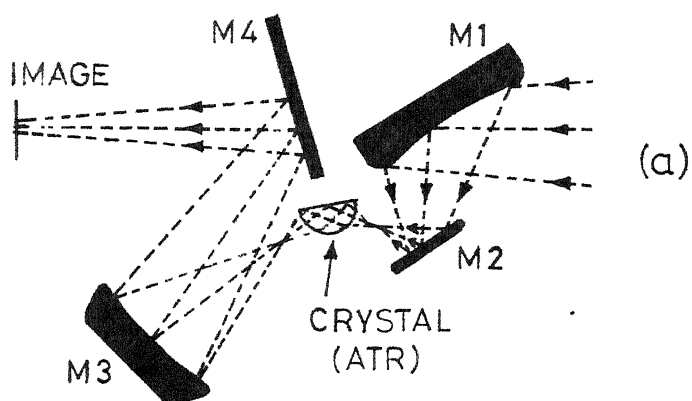


Fig. 2.2

Glower (Source); Mirrors ($M_1, M_2, M_3, M_4, M_5, M_6, M_7, M_8, M_9,$
 $M_{10}, M_{11}, M_{12}, M_{13}$ and M_{14}); Entrance slit (S_1); Exit slit (S_2),
 Grating (G_1 and G_2).





(a)

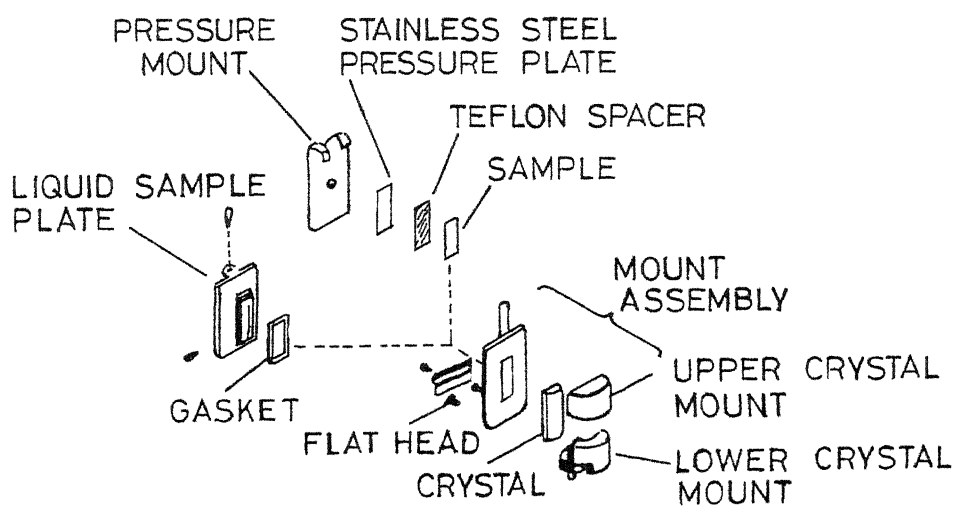


Fig.2.3 Fahrenfort type ATR accessory:
 (a) optical diagram and
 (b) sample unit.

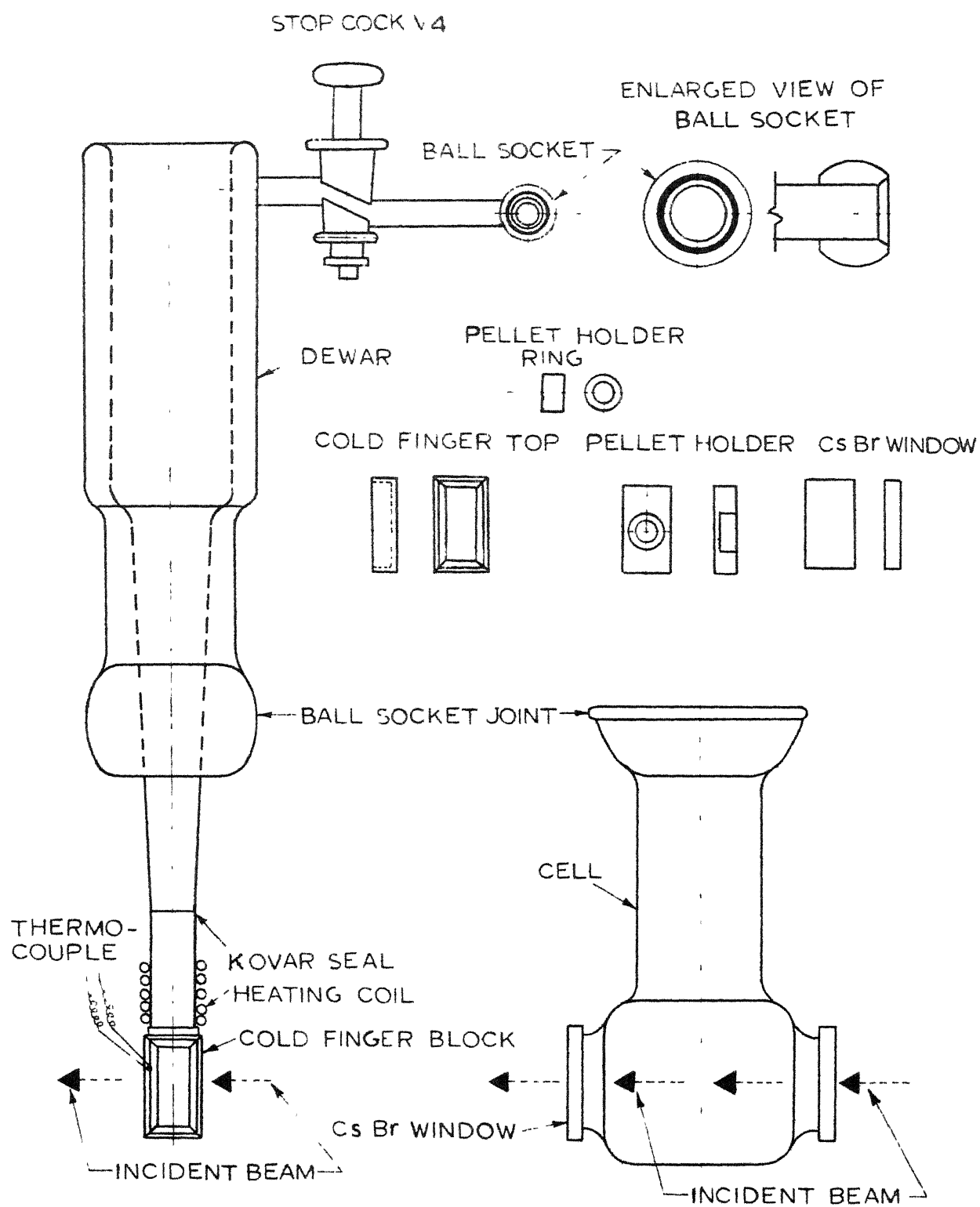


Fig.2.4 Low temperature cell

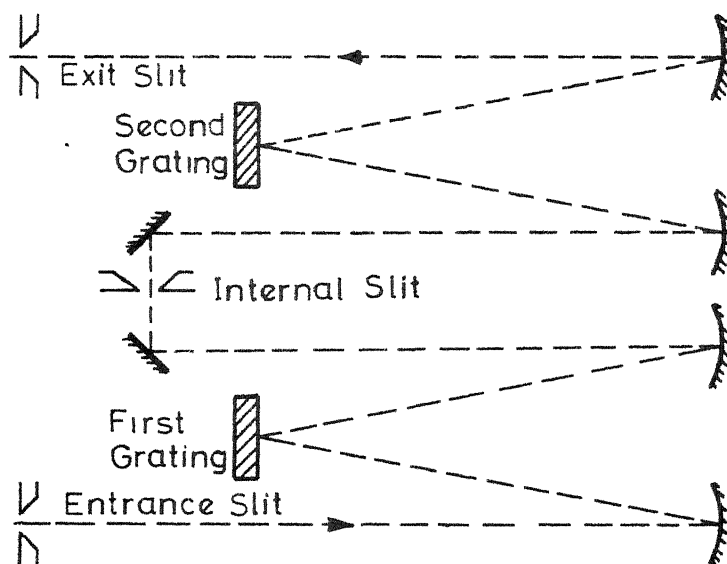


Fig. 2.5 Optical diagram of the spex model 1400 double monochromator .

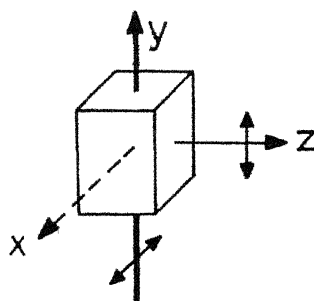
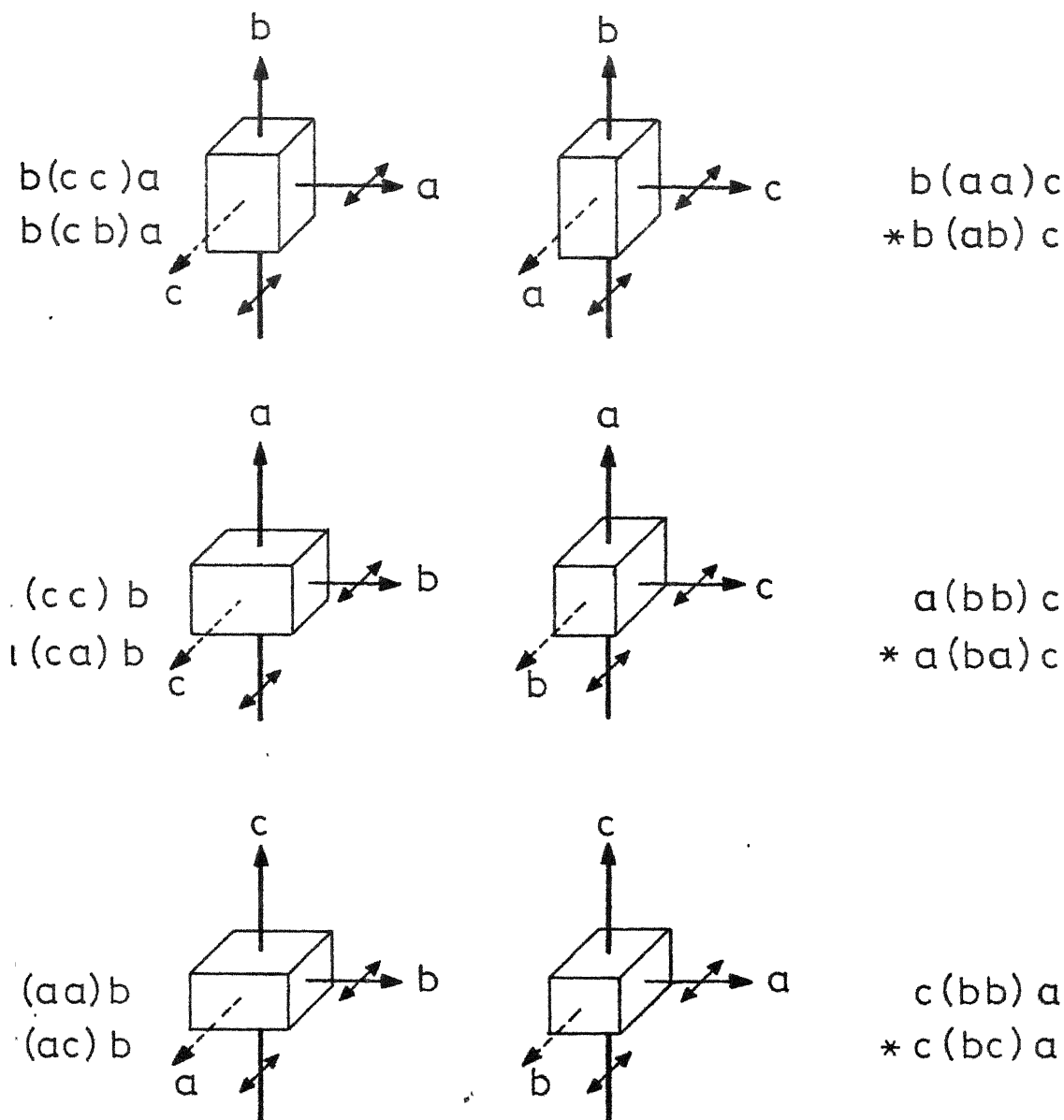


Fig.2.6 Excitation geometry, $y(xy)z$.



2.7 Twelve geometries to record Raman spectra of a crystal having orthonormal a -, b - and c -axes.

The $*$ geometry gives off-diagonal polarization and can be adjusted simply by rotating the analyzer by 90° .

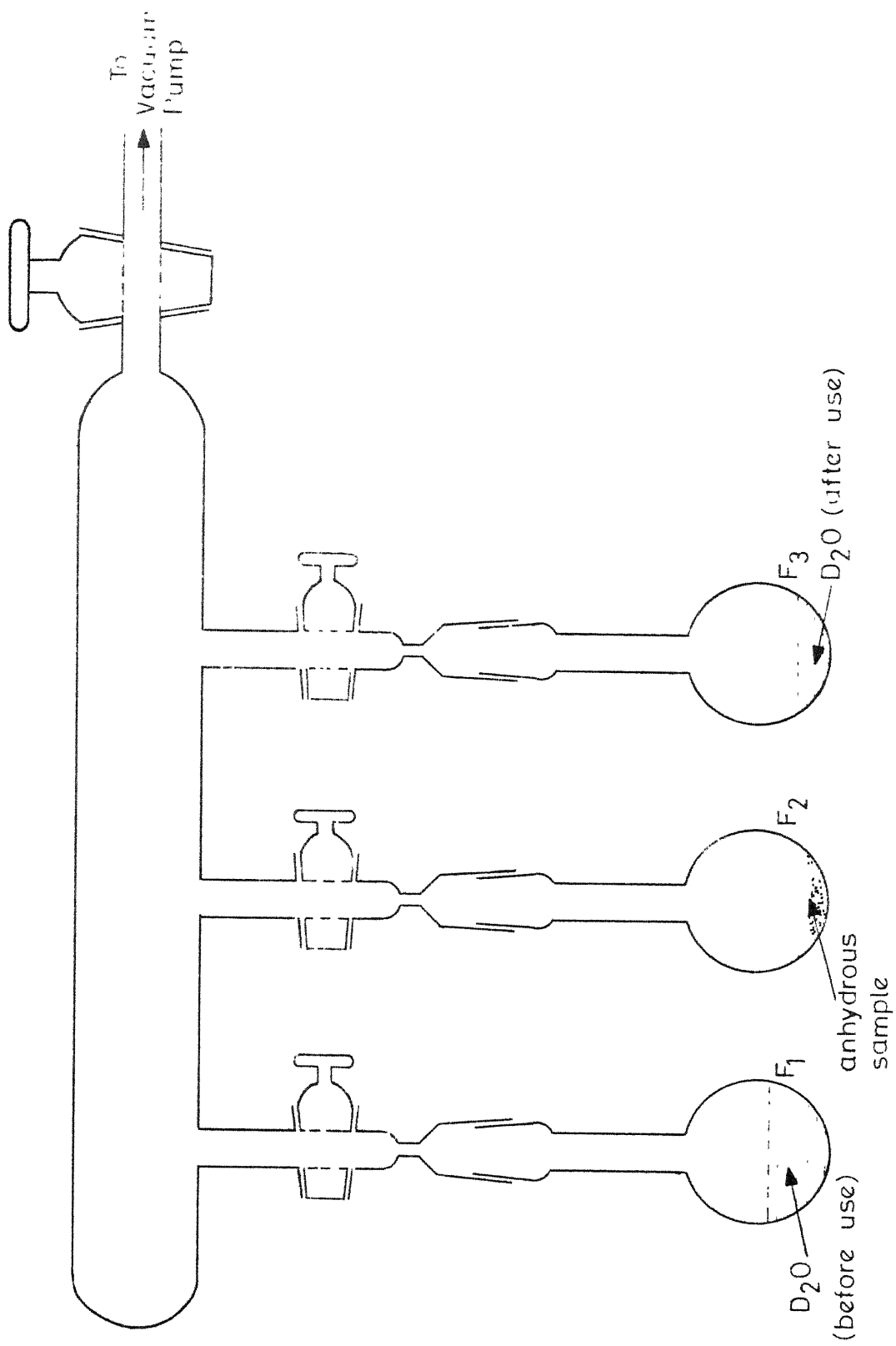


Fig. 2.8 Vacuum arrangement used to prepare deuterated analogue of hydrated samples.

CHAPTER III

OPTICAL PHONONS AND FERROELECTRIC PHASE
TRANSITION IN $(\text{NH}_4)_2\text{SO}_4$ CRYSTALABSTRACT

A brief review of up-to-date studies on $(\text{NH}_4)_2\text{SO}_4$ is presented in the introductory part of this Chapter. The dynamics of the crystal has been described in terms of 180 phonon modes under the unit cell approximation. The classification of these modes has been presented using both unit cell and site symmetry approaches.

Laser Raman spectra have been recorded in different geometries corresponding to six different components of polarizability tensor. The observed spectra have been comprehensively analysed*. It is inferred that the force fields describing the dynamics of crystallographically inequivalent $\text{NH}_4^+(\text{I})$ and $\text{NH}_4^+(\text{II})$ ions are not too different to produce distinguishable spectra. Strong Fermi interaction has been observed between ν_3 fundamental and $\nu_2 + \nu_4$ combination modes of NH_4^+ ion. The translational modes of NH_4^+ and SO_4^{2-} ions exhibit strong Raman bands between

*Presented in the Indo-Soviet Conference on Solid State Materials, Bangalore (1972). Proceedings to be published.

207-174 cm^{-1} and 73-38 cm^{-1} , respectively. Librational modes of NH_4^+ ions have been unambiguously assigned to weak Raman bands around 357 cm^{-1} . Indications are observed for the existence of proton tunneling in the double minimum potential along N-H...O hydrogen bridge.

IR (ATR) spectra of single crystal of $(\text{NH}_4)_2\text{SO}_4$ have been recorded for the first time. The important features of these spectra have been discussed.

The IR and Raman spectra of microcrystalline $(\text{NH}_4)_2\text{SO}_4$ in its both paraelectric and ferroelectric phases have been investigated in order to make comparative study of phonons in the two phases. The observed spectra are found to be consistent with the known crystal structure of $(\text{NH}_4)_2\text{SO}_4$ in respective phases.

The temperature dependence of integrated intensity of three thermo-sensitive IR bands has been investigated. It has been inferred that ferroelectric phase transition near 223°K in $(\text{NH}_4)_2\text{SO}_4$ is primarily due to sudden distortions of SO_4^{2-} ion which has almost tetrahedral symmetry in the paraelectric phase^{**}.

A point charge model[†] has been developed to compute the spontaneous polarization \vec{P} due to NH_4^+ and SO_4^{2-} ions in the crystal. The computed value of \vec{P} ($0.42 \mu\text{C}/\text{cm}^2$)

^{**} Published in Chem. Phys. Letters 22, 572 (1973).

[†] Published in Physica Status Solidi 62(b), 295 (1974).

agrees well with the experimentally known values from other studies. The nature of phase transition has been critically discussed.

In view of the present investigations and other experimental facts known about $(\text{NH}_4)_2\text{SO}_4$ crystal, a critical discussion has been made on the existing theories of transition in this crystal⁺.

3.1 INTRODUCTION

Ammonium sulphate, a naturally occurring material known as mascagnite, is colourless compound having molecular weight 132.14 and specific gravity 1.769¹ (at ~300°K). It is highly soluble in water and insoluble in alcohol, acetone and ammonia; it dissociates at 235°C¹.

Crenshaw and Ritter² inferred for the first time from the temperature dependence of specific heat that $(\text{NH}_4)_2\text{SO}_4$ undergoes a phase transition at 223°K. From the study of dielectric properties, Mitthias and Remeika³ later proved this transition to be ferroelectric in nature. The crystal has, therefore, been a subject of numerous studies in order to investigate its crystal structure⁴⁻¹¹ and several macroscopic properties^{2,3,12-43} and microscopic phenomena⁴⁴⁻⁹⁰. The investigated macroscopic properties include the study of thermodynamic^{2,12-18} dielectric^{3,18-37} and elastic³⁷⁻³⁹ properties, electrical conductivity⁴⁰, optical constants^{41,42} and birefringence^{35,43}. The studies of microscopic phenomena provide informations about NMR⁴⁴⁻⁴⁹, DMR⁵⁰⁻⁵⁵, DQR⁵⁶, NMR line

+ A part of this discussion has been accepted for publication in Solid State Communications.

width transition^{44,45} and its correlation with IR absorption^{57,58} proton⁴⁷ and deuteron⁵³⁻⁵⁵ relaxation times, electric field gradient tensor of NH_4^+ ions⁴⁹⁻⁵¹, defects in gamma irradiated crystals^{59,60}, domain structure^{33,61} thermoluminescence⁶², microwave absorption⁶³, IR absorption^{44,57,58,64-78}, Raman effect^{41,71,76,77,79-86} and neutron inelastic scattering⁸⁷⁻⁹⁰.

There are several phenomena yet to be carefully investigated to understand various characteristics of $(\text{NH}_4)_2\text{SC}_4$ and we undertook the study of phonon spectra and their temperature dependence for the following reasons.

(i) Studies of phonon spectra of $(\text{NH}_4)_2\text{SO}_4$ reported to-date either do not cover the complete range of phonon frequencies or their results are poor in quality. Further, these studies have not been comprehensively discussed which is of vital importance for the better understanding of phonons and their related phenomena.

(ii) The Raman spectra of a single crystal, in comparison to those of microcrystalline form, provide better understanding of the dynamical properties of a crystal. However, such studies are not available for $(\text{NH}_4)_2\text{SO}_4$ crystal.

(iii) Two different viewpoints have been proposed in relation to the microscopic phenomenon involved in the phase transition,— the one proposed by Schlemper and Hamilton¹¹ emphasizes the importance of hydrogen bonds in triggering the phase transition, while the other, proposed by O'Reilly and Tsang⁵⁵, relates the transition with order-disorder phenomenon involving permanent dipole moments associated with NH_4^+ ions. However, none of these viewpoints explains well the various properties of the crystal (as would be discussed later). Thus the microscopic mechanism involved in the phase transition is still not well understood. Attempts

have been made in this direction by Schutte and Heyns^{57,58} and Torrie et al⁷⁷ investigating the temperature dependence of phonon spectra of $(\text{NH}_4)_2\text{SO}_4$. The former authors showed that their results were consistent with crystallographic data reported by Schlemper and Hamilton¹¹ and thus supported their viewpoint, while Torrie et al⁷⁷ tried to establish the consistency between their results and the viewpoint proposed by O'Reilly and Tsang⁵⁵. One finds, therefore, two contradictory explanations of IR and Raman spectra recorded at different temperatures. In order to have most reliable explanation, it is worthwhile to carefully repeat such investigations.

(iv) The reported literature presents several controversies both in experimental observations and their interpretations. For example: (a) some investigations reveal that the dielectric constant in paraelectric phase does not depend on temperature¹², while on the contrary it exhibits weak temperature dependence in the range of T_c and $T_c + 50^\circ$ ²⁷ and obeys Curie Weiss law^{29,30}. (b) Miller et al⁴⁷ interpreted their NMR data showing that the phase transition is not accompanied by co-operative reorientation of NH_4^+ ions while O'Reilly and Tsang⁵⁵ made an otherwise interpretation of their DMR data. It can, however, be hoped that the present study of phonon spectra and their temperature dependence can dispel at least **some** of such controversies.

3.2 CRYSTAL STRUCTURE

The crystal structure of $(\text{NH}_4)_2\text{SO}_4$ is isomorphous to those of K_2SO_4 , Rb_2SO_4 , Cs_2SO_4 , etc.⁹¹ at room temperature. It has been investigated using diffraction of X-rays^{4-8,10}, electrons⁹ and neutrons^{10,11}.

Tetramolecular unit cell of the crystal at RT belongs to orthorhombic system having D_{2h}^{16} (Pnam) space group symmetry. The ferroelectric transition at 223°K leads to a change in its structure which has been examined using X-ray diffraction¹⁰ and neutron diffraction¹¹ methods. It has been found to belong to orthorhombic system having C_{2v}^G (Pna2₁) space group symmetry.

The unit cell dimensions as reported by Schlemper and Hamilton¹² are given in Table 3.1 which designate the crystal axes in the order of $b > a > c$. These notations would be used throughout this chapter.

The microscopic structure depicting the atomic arrangement in the unit cell projected in (001) plane is shown in Fig. 3.1 for both phases. The cell contains two distinct sets of four NH_4^+ ions. These sets are designated as NH_4^+ (I) and NH_4^+ (II) and are marked by I and II symbols, respectively, in the figure. For the convenience, different atoms (O, S, N and H) have been shown by circles in order of decreasing size (not to be related with their atomic sizes).

In paraelectric phase (cf Fig. 3.1A) NH_4^+ and SO_4^{2-} ions form a planar arrangement in (001) planes separated from each other by $c/2$ lattice distance. Atoms represented by blank and filled circles are considered to be located on (001) mirror planes at $c/4$ and $3c/4$ heights, respectively, from the base of the cell. The line-shaded circles denote pairs of O or H atoms which get interchanged with each other under mirror symmetry (σ_{ab}) operation. In ferroelectric phase this mirror symmetry vanishes with minor changes which are apparent in Fig. 3.1B.

3.3 PHONON BRANCHES IN THE CRYSTAL

The dynamics of $(\text{NH}_4)_2\text{SO}_4$ crystal containing 60 atoms per unit cell can be described in terms of 180 phonon branches (177 optical + 3 acoustical) under the unit cell approximation. These branches arise from different normal modes of constituting ions: $\text{NH}_4^+(\text{I})$, $\text{NH}_4^+(\text{II})$ and SO_4^{2-} .

Both the NH_4^+ and SO_4^{2-} ions are the five atomic AB_4 type perfect tetrahedra in their free state. AB_4 tetrahedron exhibits four frequencies for nine internal modes as defined by Herzberg⁹² by the notations: ν_1 (the totally symmetric stretching), ν_2 (the doubly degenerate symmetric bending), ν_3 (the triply degenerate anti-symmetric stretching) and ν_4 (the triply degenerate anti-symmetric bending). The former two modes belong to A_1 and E species, respectively while the latter two belong to F_2 species of T_d point group. These modes are shown diagrammatically in Fig. 3.2. The external degrees of freedom i.e. rotations (l) and translations (t) form the bases of F_1 and F_2 irreducible representations, respectively⁹². Since only A_1 , E and F_2 species are Raman active and F_2 species are infrared active, l are forbidden in both these spectra and the ν_1 and ν_2 are forbidden in IR spectra.

3.4 CLASSIFICATION OF PHONONS

a. Unit Cell Approach

The classification of 180 phonons using the unit cell approach has been worked out in Table 3.2 for the room temperature phase of the crystal. The number of atoms found invariant under different operations of D_{2h} point group are given by N^R (cf column 1 of the Table). The crystallographic data¹¹ reveal that 60 atoms remain invariant under E while

only 36 under mirror symmetry σ'_{ab} and none under other operations. Considering each of the polyatomic ions $\text{NH}_4^+(\text{I})$, $\text{NH}_4^+(\text{II})$ and SO_4^{2-} as single particle, the number of invariant particles are found to be 12 under each of the E and σ'_{ab} operations. Since there is no atomic ion, number of invariant particles $N^R(t)$ to account for the external translatory vibrations would be equal to $N^R(1)$ the number of invariant polyatomic units to account for the libratory external vibrations. Using these values of N^R , $N^R(t)$ and $N^R(1)$ thus found we computed the reducible representations $\chi(N) = N^R(\pm 1 + 2 \cos \phi_R)$, $\chi(t) = N^R(t) \cdot (\pm 1 + 2 \cos \phi_R)$ and $\chi(1) = N^R(1) \cdot (\pm 1 + 2 \cos \phi_R)$. All the 180 phonon modes form the bases of $\chi(N)$ while 36 translatory and 36 libratory external modes of $\chi(t)$ and $\chi(1)$, respectively. Reduction of these representations into irreducible representations of D_{2h} point group provides number of phonon modes belonging to different species. A similar classification for 180 modes has been presented in Table 3.3 for the ferroelectric phase of the crystal. We note that no atom remains invariant under any operation (except E) of C_{2v} symmetry of this phase.

b. Site Symmetry Approach

All the three $\text{NH}_4^+(\text{I})$, $\text{NH}_4^+(\text{II})$ and SO_4^{2-} tetrahedra in the crystal of $(\text{NH}_4)_2\text{SO}_4$ occupy $C_s(\sigma'_{ab})$ sites in its paraelectric phase while C_1 sites in the ferroelectric. The correlation schemes deduced for different species of T_d , $C_s(\sigma'_{ab})$ and D_{2h} point groups and T_d , C_1 and C_{2v} point groups are given in Tables 3.4 and 3.5, respectively, for the use in classifying 180 phonon modes in paraelectric and ferroelectric phases. The symmetry species and number of phonons arising from a definite mode of $\text{NH}_4^+(\text{I})$, $\text{NH}_4^+(\text{II})$ or SO_4^{2-} ion have been summarized in Table 3.6 and 3.7 for paraelectric and ferroelectric phases, respectively.

3.5 THE FORMS OF RAMAN TENSOR COMPONENTS

The Raman tensor components of the Raman active species A_g , B_{1g} , B_{2g} and B_{3g} of the symmetry group D_{2h} to which the crystal of $(NH_4)_2SO_4$ belongs at RT have the following form⁹³

$$\begin{aligned}
 A_g &= \begin{bmatrix} a & 0 & 0 \\ 0 & b & 0 \\ 0 & 0 & c \end{bmatrix} & B_{1g} &= \begin{bmatrix} 0 & 0 & 0 \\ 0 & 0 & d \\ 0 & d & 0 \end{bmatrix} \\
 B_{2g} &= \begin{bmatrix} 0 & 0 & e \\ 0 & 0 & 0 \\ e & 0 & 0 \end{bmatrix} & B_{3g} &= \begin{bmatrix} 0 & f & 0 \\ f & 0 & 0 \\ 0 & 0 & 0 \end{bmatrix}
 \end{aligned}$$

It shows that all the six components of the symmetric polarizability tensor are independent. Six different spectra having characteristics of these components would, therefore, be sufficient to describe the Raman active phonons in the crystal.

3.6 EXPERIMENTAL

a. Growth of Single Crystal

Single crystals of $(NH_4)_2SO_4$ of a few mm^3 size can be obtained by simple method of slow evaporation of its aqueous solution. However, methods of growing large single crystals of $(NH_4)_2SO_4$ are not simple and have been discussed by Mullin et al⁹⁴, Petrenko⁹⁵, and Godard and Drasko⁹⁶. The former method needs unwieldy amount of solution while the latter two need very precise control of the temperature. We, therefore, tried the rotating

seeds technique for which a rotatory crystallizer was fabricated in this laboratory (cf section 2.2). A good single crystal of about $1.5 \times 2 \times 4 \text{ cm}^3$ size could be obtained in about a month. The crystallizer was kept at ambient temperature varying at the maximum by $\pm 2^\circ\text{C}$. Better crystal was obtained when the crystal seed was rotated with 30 rpm rather than 15.

b. Determination of Crystallographic Axes

The crystallographic axes were first identified by using the knowledge of crystal morphology⁹⁷ and were later confirmed by X-ray diffraction (Laue pattern) method. The existence of perfect cleavage along (100) plane of the crystal helps considerably in fixing the axes.

c. Scan of Raman Spectra

Raman spectra were recorded in twelve different geometries (90° arrangements cf Fig. 2.7) using 4880 and 5145 Å ~~emission~~ lines from an argon ion laser as source of excitation and $(\text{NH}_4)_2\text{SO}_4$ single crystals grown from aqueous solution as well as purchased from Semi Elements Inc. Spex-1400 double monochromator was used to investigate the scattered radiations. Details of recording the spectra have been discussed in section 2.8.

Raman spectra were also recorded for the single crystal of $(\text{NH}_4)_2\text{SO}_4$ below its transition temperature by using the low temperature Raman cell and liquid nitrogen as coolant. However, the crystal shatters so vigorously that no polarization effect was observed. Therefore, spectra recorded for such shattered crystal both at 77°K and 300°K have been treated as of microcrystalline samples. The observed spectra show good similarity with those reported by Torrie et al⁷⁷ for microcrystalline samples supporting our consideration.

d. Scan of IR Spectra

ATR technique (cf section 2.5a) was used to record IR spectra of single crystal. A crystal piece of appropriate size was properly polished

and kept in contact with the ATR element of the accessory. The facing plane of the crystal was identified to be (100). Spectra were recorded at different angles of incidence.

IR spectra of microcrystalline sample were recorded by using mujol mull, KBr pellet and low scattering film techniques discussed in detail in section 2.5. The low scattering film was prepared on AgCl plate and was used to record spectra both at RT and LT. Spectra at different temperatures were recorded in selected regions in which extra-thermosensitive bands are observed. The temperature of the sample was controlled and monitored as described in section 2.4c.

All IR spectra were recorded on PE-521 spectrophotometer in 250-4000 cm^{-1} range.

3.7 RESULTS AND DISCUSSION

I. RAMAN PHONONS IN SINGLE CRYSTAL

a. Observed Spectra

Out of the twelve Raman spectra recorded for the single crystal of $(\text{NH}_4)_2\text{SO}_4$, the two having the same polarization characteristic but recorded for different geometries (e.g. b(ab)c and a(ba)c) were found to be identical, as expected. Thus only six different spectra were obtained whose representatives are shown in Figs. 3.3 and 3.4; the spectra in the former figure cover the region ($3400\text{-}400\text{ cm}^{-1}$) of the internal modes of NH_4^+ and SO_4^{2-} ions, while those in latter cover the region ($400\text{-}20\text{ cm}^{-1}$) of the external modes of the crystal. In these figures aa, bb, cc, etc. denote the polarization character of the spectra while A_g , B_{1g} , etc.

denote the corresponding symmetry species of D_{2h} point group. The number over each band are the frequencies of Raman shifts in the units of wave number (cm^{-1}).

In the N-H stretching region ($2600\text{--}3400\text{ cm}^{-1}$) of Fig. 3.3, the dotted curves are the manually resolved bands having Lorentzian shapes. The frequencies of band peaks of their resolved structure have been measured and marked. It may be noticed that the spectrum of ab polarization (giving B_{3g} species) is in lower expanded scale of frequency.

In Fig. 3.4 the spectra shown by dotted lines are on more expanded frequency scale (almost double of the regular spectra).

b. Frequency, Width and Intensity of Bands

Appendix 3.1 provides frequency (ν), the relative integrated intensity (I, in parenthesis) and the width (FWHMI, cm^{-1}) of various bands of observed spectra. The values are accurate within $\pm 2\text{ cm}^{-1}$ for well developed sharp bands. The frequencies of manually resolved or broad bands may have uncertainty as large as $\pm 10\text{ cm}^{-1}$. The I values were first determined by multiplying the corresponding FWHMI value and peak intensity of bands. These values as given in the appendix are relative with respect to an arbitrarily chosen value 10 for the intensity of the band due to $\nu_4^s(451\text{ cm}^{-1})$ and are computed separately for the spectrum of each polarization. The errors in I values lie within 5% for well developed strong bands but within 20% for those having weak and/or diffuse structure or obtained after resolution.

c. Assignments

Our assignments for observed Raman shifts both for single and multi-phonon processes are given in Table 3.8. The average frequencies (ν_{av}) of assigned modes are given in column 9 of this table. The ν_{av} values of single phonon processes have been used to compute frequencies of multiphonon processes which are given in column 10.

A critical examination of observed spectra reveals that force fields governing the dynamics of $\text{NH}_4^+(\text{I})$ and $\text{NH}_4^+(\text{II})$ are not too different from each other to produce distinguishable spectra, although they are crystallographically inequivalent. Therefore, modes of these ions have not been assigned separately. For the simplicity of discussion modes of NH_4^+ and SO_4^{2-} ions have been distinguished from each other by using superscripts n and s respectively.

Internal Modes of NH_4^+ and SO_4^{2-} Ions: These modes have been assigned on the basis of the knowledge of their frequencies in free state of NH_4^+ and SO_4^{2-} ions as quoted in Fig. 3.2.

The sharpest band is observed in each spectrum for $\nu_1^s(976 \text{ cm}^{-1})$ having FWHM of about 6 cm^{-1} . This mode appears as strongest band in aa, bb and cc polarized spectra but shows remarkably low intensity in other polarizations. This indicates that the associated mode is highly polarized and thus supports our assignment. All modes are group theoretically allowed in the spectrum of each polarization except the ν_1^n and ν_1^s which have only one A_g and one B_{3g} components allowed in Raman spectra. The weak bands at 976 cm^{-1} observed in spectra of B_{1g} and B_{2g} modes, therefore, arise due to spillover of strong A_g bands as a result of possible error in the scattering geometries.

The assignment of ν_1^n and ν_3^n modes is complicated by multiphonon processes originating from $2\nu_2^n$, $\nu_2^n + \nu_4^n$ and $2\nu_4^n$ modes expected to appear near 3340, 3110 and 2880 cm^{-1} respectively. The latter three modes can appear as strong bands by sharing intensity from fundamental modes through resonance phenomenon. Still the problem of seeking unique assignments of different modes falling in N-H stretching region (2700 - 3400 cm^{-1}) can be solved to a reasonable extent. Different bands of this region have been designated as u-, v-, ... y- and z- bands as given in Table 3.8 column 1.

Among all these bands x-bands are strongest in aa, bb and cc polarized spectra but weakest in ab and bc polarizations. This shows that x-bands correspond to remarkably low depolarization ratio and must arise due to ν_1^n mode. The weak band appearing at 3143 cm^{-1} in spectrum of B_{2g} modes has been associated with the spillover of strong A_g bands similar to those of ν_1^s mode (cf starred frequencies in Table 3.8).

The u- and z- bands are reasonably associated with $2\nu_2^n$ and $2\nu_4^n$ modes, respectively. It is interesting to note that the v- band is observed at 3292 cm^{-1} only in bb polarized spectrum. This band exhibits distinct sharpness (FWHMI = 60 cm^{-1}) among all bands of N-H stretching region; other bands have FWHMI values between 110-270 cm^{-1} (cf Appendix 3.1). As would be shown in a latter section this band appears at 3310 cm^{-1} and 3306 cm^{-1} , respectively in IR and Raman spectra of microcrystalline $(\text{NH}_4)_2\text{SO}_4$ (kept at LT), showing remarkable increase in its intensity and sharpness approximately by a factor of 2. Similar correlation was made earlier by Torrie et al⁷⁷ and this band was associated with a site splitted component of ν_3^n mode. On the other hand Schutte and Heyns⁵⁸

associated it with $2\nu_2^n$ and Stekhanov and Gabrichidze⁸⁴ with a component D.C.(I) of the doublet arising due to tunneling of proton along the N-H...O hydrogen bridge. In view of the specific properties of this band as mentioned above, the last assignment appears to be more unique.

Schmidt⁴⁰ measured the electrical conductivity of $(\text{NH}_4)_2\text{SO}_4$ along its b-axis and explained that the observed high conductivity can arise mainly due to proton tunneling. Since the bb polarization character of v-band, indicates its association with a linear vibration of proton along b-axis, the proton tunneling responsible for high conductivity along this axis may perhaps be correlated with the origin of v-band. Thus the observations reported by Schmidt⁴⁰ support the assignment for v-band proposed by Stekhanov and Gabrichidze⁸⁴.

Both the remaining w- and y-bands in spectra of A_g and B_{3g} modes can be associated with group theoretically allowed two components of ν_3^n mode. However, it is not consistent with the observation of x- and y-bands in spectra of B_{1g} and B_{2g} modes, since ν_3^n has only one allowed component under these species. In order to find the assignments for these bands we note that (i) the w- and y-bands in each spectrum have comparable intensity and FWHM values (cf Appendix 3.1) and (ii) the computed frequency of $\nu_2^n + \nu_4^n$ ($\sim 3098 \text{ cm}^{-1}$) falls almost at the centre of the two ($\sim 3108 \text{ cm}^{-1}$). It may, therefore, be asserted that w- and y-bands arise as a result of Fermi resonance between ν_3^n fundamental and F_2 component of $\nu_2^n + \nu_4^n$ ($F_1 + F_2$) combination mode. Thus both w- and y-bands have been associated with mixed modes* of ν_3^n and $\nu_2^n + \nu_4^n$. As already stated w- and y-bands have almost equal intensity within the errors of resolution therefore by putting $I_1 = I_2$ in Eqn. 1.14h,

* Designated as F.R.(I) and F.R.(II).

it can be shown that the unperturbed frequencies of both ν_3^n , $\nu_2^n + \nu_4^n$ fall at the centre of w- and y-bands i.e. 3108 cm^{-1} to a good approximation. It may be noted that Fermi resonance can not occur between $\nu_1^n (A_1)$ and $\nu_2^n + \nu_4^n (E_1 + E_2)$ modes, although the frequencies of two fall more close to each other.

The other internal modes ν_2^n , ν_4^n , ν_3^s , ν_4^s and ν_2^s could be unambiguously assigned to the bands having frequencies between 1654-1693, 1402-1475, 1062-1117, 612-628 and 446-451 cm^{-1} , respectively.

From these assignments of ν_i^s and ν_i^n ($i = 1, 2, 3$ and 4) modes we note that (i) the number of bands observed in different spectra are consistent with theoretical predictions except in the case of ν_4^n mode in aa polarized spectrum and ν_4^s mode in ab polarized spectrum where these modes separately show single band instead of expected two (ii) the ν_2^n and ν_2^s modes in general are weaker than ν_4^n and ν_4^s modes respectively in each spectrum of A_g modes but are stronger in spectra of B_{1g} , B_{2g} and B_{3g} modes; as an exception to it, only ν_2^n mode appears stronger than ν_4^n in bb polarized spectrum of A_g modes and (iii) the aa, bb and cc polarized spectra record modes of only A_g species but frequencies and intensities of bands associated with a single mode in these spectra are found to be different (cf column 1-6 of Appendix 3.1). Although, these observations seem to be interesting, the explanations require rigorous computations and are not attempted here.

Assignment of External Lattice Modes: In order to assign these modes we note that (i) the translatory (t^n) and libratory (l^n) modes of NH_4^+ ion can reasonably be expected to have higher frequencies than the respective ones (t^s and l^s) of SO_4^{2-} ion, since the mass and moment of inertia ratios

(for $\text{NH}_4^+ : \text{SO}_4^{2-}$) are 1:5.3 and 1:30, respectively, (ii) in both Raman and IR spectra, t^s and t^n modes are expected to exhibit strong bands, while the l^s and l^n , the weak (may be too weak to be observed), since the latter two are forbidden in these spectra for perfect NH_4^+ and SO_4^{2-} tetrahedra which are not very much distorted in $(\text{NH}_4)_2\text{SO}_4$.

Different bands observed below 400 cm^{-1} seem to arise due to external lattice modes. The bands may be readily arranged in five groups as indicated in Table 3.8 column 1. In view of the above mentioned points we assign t^n and t^s modes to strong Raman bands of group (II) and group (IV) respectively, while l^n modes to the weak bands of group (I). Remaining bands of groups (III) and (V) could be tentatively associated with (i) multiphonon processes involving t^s and l^s modes and/or (ii) single phonon processes involving l^s modes. Since the multiphonon modes involving t^s and l^s may be expected to be stronger than l^s modes which can easily be obscured by strong t^s modes or Rayleigh line, any unambiguous assignment of l^s modes could not be possible. However, it is interesting to note that weak shoulders of Rayleigh line appear at about 22 cm^{-1} in Raman spectra of $(\text{NH}_4)_2\text{SO}_4$ and its iso-structural other sulphates, $\text{Cs}_2\text{SO}_4^{98}$ and $\text{K}_2\text{SO}_4^{99}$ crystals. Since l^s modes in all these crystals may reasonably have almost equal frequency, hence may be assigned to the bands of group (V).

The subscripts a, b and c used with t^n , and t^s refer to phonons originating from translatory vibrations along crystallographic axes a-, b- and c-, respectively. Similarly these subscripts used with l^n and l^s modes represent librations about axes parallel to corresponding crystal axes. Since t_c^n and t_c^s modes are expected to appear only in bc and ac

polarized spectra, they can be separated from t_a and t_b components both of which are expected to appear in all other polarizations. Similarly l_c modes can be separated from l_a and l_b , since the former most are expected to appear in aa, bb, cc and ab polarizations while the latter two in only bc and ca polarizations.

Our assignments of t^n and l^n modes are corroborated by the following facts: (i) the NIS spectrum of $(NH_4)_2SO_4$ exhibits one strong band at 335 cm^{-1} and a broad band at about 200 cm^{-1} as reported by Rush and Taylor⁸⁷. Since protons have very high cross-section for neutron inelastic scattering, these bands evidently arise due to NH_4^+ ions, and (ii) the IR and Raman studies⁷⁷ of microcrystalline $(ND_4)_2SO_4$ reveal that bands around 355 cm^{-1} exhibit shift by a factor of $1/\sqrt{2}$ while those around 200 cm^{-1} only by $(18/22)^{\frac{1}{2}}$.

d. Comparison of Spectra of NH_4^+ and SO_4^{2-} Ions

Both NH_4^+ and SO_4^{2-} tetrahedra occupy the similar $C_s(\sigma'_{ab})$ site in RT phase of $(NH_4)_2SO_4$. The comparison of spectra of two ions may therefore be interesting. For this purpose we tabulate (cf Table 3.9) the ratios $\Delta\nu^n/\Delta\nu^s$ and $I^n/2I^s$ given by

$$\frac{\Delta\nu^n}{\Delta\nu^s} = \frac{\text{FWHMI of a mode of } NH_4^+ \text{ ion}}{\text{FWHMI of the same mode of } SO_4^{2-} \text{ ion}} \quad \dots 3.7a$$

and

$$\frac{I^n}{2I^s} = \frac{I \text{ value of a mode of } NH_4^+ \text{ ion}}{2(I \text{ value of the same mode of } SO_4^{2-} \text{ ion})} \quad \dots 3.7b$$

The factor of 2 in latter quantity has been introduced because there are

two NH_4^+ ions for each SO_4^{2-} ion in the crystal. Since the ν_3^n (F_2) exhibits considerable mixing with $\nu_2^n + \nu_4^n(F_1 + F_2)$ as a result of Fermi resonance, the I^n and $\Delta\nu^n$ used in computing above ratios are averaged for two Fermi components falling around, $\nu_{av} = 3183$ and 3041 cm^{-1} .

The $\Delta\nu^n/\Delta\nu^s$ and $I^n/2I^s$ thus computed and the observed spectra of well established internal modes reveal the following:

- (i) Each mode of NH_4^+ is broader than the similar one of SO_4^{2-} . For the probable reasons we note that there are two different NH_4^+ ions which may result in slightly different spectra and contribute to the width of NH_4^+ bands. Moreover, the force fields of NH_4^+ ions are perhaps more anharmonic than SO_4^{2-} ion due to H-bonding and possibly result in further broadening of NH_4^+ bands.
- (ii) The well separated ν_2^n and ν_4^n and the totally symmetric ν_1^n modes are in general weaker than the corresponding ones of SO_4^{2-} ion, although ν_2^n mode of bb polarization is an exception to it. One of the probable reasons for it could be the low scattering power of NH_4^+ ion in comparison to that of SO_4^{2-} ion, since the electron density in the former ion is lower than in the latter. However, the ν_3^n mode has more intense bands than ν_3^s except in the spectrum of aa polarization. This behaviour of ν_3^n may be attributed to the fact that many combination bands involving low lying lattice vibrations (e.g. t^n and l^n) arise in neighbourhood of true stretching modes as a result of anharmonicity in some part of the potential arising from strong H-bonding¹⁰⁰.
- (iii) The peak intensity of a band associated with NH_4^+ ion is smaller than the corresponding one of SO_4^{2-} ion (cf Fig. 3.3). This observation may also be attributed primarily to the more anharmonic force fields and low

scattering efficiency of NH_4^+ ion in comparison to those of SO_4^{2-} .

Now the critical look into the spectra of lattice modes (cf Fig. 3.4) and $\Delta\nu^n/\Delta\nu^s$ and $I^n/2I^s$ values (cf Table 3.9 columns 6 and 11) computed for translatory modes indicates that t^n bands exhibit higher FWHMI and lower integrated and peak intensities in comparison to t^s bands of the same spectra. This behaviour is identical to that shown by well established and well isolated ν_2 and ν_4 modes of NH_4^+ and SO_4^{2-} ions. This similarity may be considered as a support to our assignments of t^n and t^s modes and an indication for their low mixing with each other.

II IR(ATR) SPECTRA OF SINGLE CRYSTAL

Five typical ATR spectra of single crystal of $(\text{NH}_4)_2\text{SO}_4$ recorded for $\theta_i = 35^\circ, 37^\circ, 40^\circ, 45^\circ$ and 60° in $4000-2000\text{ cm}^{-1}$ range and four spectra recorded for $\theta_i = 40^\circ, 45^\circ, 60^\circ$ and 65° in $2000 - 250\text{ cm}^{-1}$ range are shown in Fig. 3.5a and 3.5b, respectively.

The bands arising due to N-H stretching modes falling between $3500 - 2700\text{ cm}^{-1}$ exhibit anomalous character for θ_i increasing upto about 40° ; a typical absorption type spectrum is observed for $\theta_i = 45^\circ$. The attenuation in reflected intensity almost vanishes in this region at $\theta_i = 60^\circ$. Almost the same behaviour is observed for bands appearing around 1400 cm^{-1} due to ν_4^n mode which shows some attenuation at $\theta_i = 60^\circ$.

The bands arising due to $\nu_3^s(1080\text{ cm}^{-1})$ and $\nu_4^s(612\text{ cm}^{-1})$ exhibit anomalous character for θ_i increasing upto 45° . Well shaped normal absorption type bands are observed due to these two modes for $\theta_i = 60^\circ$. No band appears due to ν_1 and ν_2 modes of NH_4^+ and SO_4^{2-} ions.

The critical angle for the system of KRS-5 and $(\text{NH}_4)_2\text{SO}_4$ crystals was estimated in non-absorbing regions of the latter crystal by studying the rate of decrease in reflected intensity with decreasing θ_i . It was seen that in $4000 - 1500 \text{ cm}^{-1}$ region, the reflected intensity rapidly decreases around $\theta_i = 41^\circ$, while in $1500 - 250 \text{ cm}^{-1}$ range around $\theta_i = 45^\circ$. Within the error limits of such estimations the θ_c may be stated to vary within $41 \pm 2^\circ$ in the former frequency range and within $45 \pm 2^\circ$ in the latter. Thus the refractive index of $(\text{NH}_4)_2\text{SO}_4$ in above mentioned frequency ranges is found to have values within $1.55 \pm .06$ and $1.67 \pm .06$, respectively. In the neighbourhood of absorption bands, the refractive index of the crystal has not been estimated since it varies rapidly with frequency and such estimations do not have much significance unless the frequency is specified.

The attenuation in reflected intensity shows a general decrease with increasing frequency from 250 to 4000 cm^{-1} . This phenomenon may be related to the effective depth of penetration of evanescent field in the sample which also decreases with increasing frequency (cf. Eqn. 1.17b).

The frequencies of bands read from two selected spectra ($\theta_i = 40^\circ$ and 45°) of $4000 - 2000 \text{ cm}^{-1}$ region and those ($\theta_i = 60^\circ$ and 65°) of $2000 - 250 \text{ cm}^{-1}$ region are tabulated in Table 3.10. These spectra were selected as they show better shapes of bands. Positions of anomalous dispersion type bands have been measured at points of maximum slope while those of normal absorption type at their peaks. Uncertainties estimated in these values are also given in the same table. We note that the frequencies of N-H stretching bands measured for anomalous type bands (i.e. corresponding to $\theta_i = 40^\circ$) differ considerably from those measured from

normal absorption type bands ($\theta_i = 45^\circ$). This is perhaps due to superposition of several bands in this region.

III RAMAN AND IR SPECTRA OF MICROCRYSTALLINE $(\text{NH}_4)_2\text{SO}_4$

Attempts were firstly made to investigate the Raman spectra of single crystal at LT (below T_c) in order to study phonons in the ferroelectric phase. However, it could not be possible because of the vigorous shattering of the crystal at T_c . The Raman and IR spectra of microcrystalline sample are therefore, investigated both at RT and LT.

a. Observed Raman Spectra

The spectra of microcrystalline sample recorded both at RT ($\sim 300^\circ\text{K}$) and LT ($\sim 77^\circ\text{K}$) are shown in Figs. 3.6A and 3.6C, respectively. The inset B of the latter figure shows some LT Raman bands recorded on expanded scale in order to depict their splitted structures which are not clear in the survey spectrum. The numbers marked over each band represent the frequencies (in cm^{-1}) of the corresponding Raman shapes.

b. Observed IR Spectra

It is shown in the Appendix 3.2 that $(\text{NH}_4)_2\text{SO}_4$ undergoes a strong ion exchange phenomenon with KBr. Therefore, the following discussion is based on the IR spectra recorded for microcrystalline low scattering film prepared on AgCl window. These spectra scanned at RT ($\sim 300^\circ\text{K}$) and LT ($\sim 120^\circ\text{K}$) are shown in Figs. 3.7(a) and (b) respectively. In these spectra the downward shift of the base line (on absorbance scale) with the decrease of frequency arises due to general scattering phenomenon. The spectral portion recorded under spectra(a) and (b) in $2600 - 3500 \text{ cm}^{-1}$ region represent the portions of respective spectra recorded after attenuating the reference beam.

The prominent bands of spectra (Figs. 3.7(a) and (b)) have been retraced in Fig. 3.8 after choosing appropriate base lines neglecting general scattering effects. The bands have been resolved into Lorentzian shaped components. The resolution has been made in such a way that the number of resolved components remain mostly equal to the number of bands looking apparent and the resolved band positions differ least from the apparent ones. The starred components in different bands are due to the asymmetry in bands on their low frequency sides. Such asymmetry may arise in spectra of low scattering films due to general scattering which is difficult to be accounted for completely by choosing the appropriate base line and reducing the bands on horizontal basis. The other reason of such asymmetry is the anharmonic effect which sometimes allows the combinations in the vicinity of fundamental bands.

c. Frequency, Width and Intensity of Raman and IR Bands

Appendix 3.3 provides frequency (ν), relative integrated intensity (I , in parenthesis) and width (FWHMI, cm^{-1}) of Raman bands in its first four columns and of IR bands in the last four columns. The Lorentzian resolution of complex Raman bands (e.g. N-H stretching band) although not shown in Fig. 3.6, was made to measure these data. The I values for Raman bands as given in the appendix are relative to an arbitrarily chosen value 10 for the integrated intensity of 618 cm^{-1} band in RT spectrum and 612 cm^{-1} band in LT spectrum. For IR bands they are relative to the integrated intensity (10) of full band at $\sim 610 \text{ cm}^{-1}$ in both RT and LT spectra. The error levels in ν and I values of both Raman and IR bands are identical to those mentioned for Raman bands in spectra of single crystal (cf section 3.7(I)b).

d. Assignments and Comparative Study of RT and LT Spectra

The assignments of different phonon modes in microcrystalline $(\text{NH}_4)_2\text{SO}_4$ as given in Table 3.11 are based on those discussed for single crystal (cf section 3.7(I)).

The band observed at 3292 cm^{-1} (FWHMI $\approx 60 \text{ cm}^{-1}$) in bb polarized Raman spectra of single crystal may be noticed only as very weak shoulder to N-H stretching band on its higher frequency side both in RT Raman and RT IR spectra (cf Figs. 3.6 and 3.8); after Lorentzian resolution corresponding bands are observed at $\approx 3290 \text{ cm}^{-1}$ in Raman and $\approx 3300 \text{ cm}^{-1}$ in IR spectra. At LT, the respective bands are seen, well separated from the broad complex band at 3306 and 3310 cm^{-1} having more sharp structure and increased intensity.

On lowering the temperature, the Raman and IR bands at $\approx 3200 \text{ cm}^{-1}$ do not show significant change in their frequencies; however the IR band ($\approx 3200 \text{ cm}^{-1}$) splits into 3215 and 3180 cm^{-1} components.

The ν_1^n mode showing Raman band at $\approx 3144 \text{ cm}^{-1}$ in RT spectrum (cf Fig. 3.6A) shifts to 3117 cm^{-1} and possesses imperceptible intensity in IR spectra (both at RT and LT); the downward shift is consistent¹⁰⁰ with increase in H-bond strength in LT phase as revealed from crystal data¹¹. The absence of this mode in IR is consistent with low distortions¹¹ in tetrahedral structure of NH_4^+ ions.

The γ -band assigned as a Fermi component (F.R.(II), cf Table 3.8) is observed at 3039 cm^{-1} in Raman and at 3030 cm^{-1} in IR spectra (RT). It exhibits three components having remarkably sharp structure both in LT Raman and LT IR spectra (cf Figs. 3.6B and 3.7b); the total intensity of three components is observed to be maximum both in Raman and IR spectra. On the

basis of maximum Raman intensity, this band may be assigned as ν_1^n mode in LT phase of $(\text{NH}_4)_2\text{SO}_4$; however its high intensity in IR and the triplet structure are inconsistent with this assignment. Here it may be noted that F.R.(II) component at RT exhibits almost equal mixing of ν_3^n fundamental and $\nu_2^n + \nu_4^n$ combination modes, since its intensity in most of the spectra is almost equal to that of F.R.(I) to a good approximation. However, F.R.(II) possesses more intensity than the F.R.(I) in LT spectra. It implies that F.R.(II) perhaps exhibits more contribution of ν_3^n fundamental at LT indicating that unperturbed frequency of ν_3^n mode falls more close to F.R.(II). Thus the unperturbed ν_3^n shifts towards lower frequencies on decreasing the temperature. Therefore it must have a value lower than 3108 cm^{-1} (the frequency of unperturbed ν_3^n at RT, cf Table 3.8 column 10). Thus unperturbed ν_3^n is found to be lower than ν_1^n both at RT and LT; of course the separation of about 20 cm^{-1} at RT is insignificant within the limits of experimental uncertainties. This observation is just reverse of that observed in general (i.e. anti-symmetric stretch ν_3 has higher frequency than symmetric stretch ν_1). Similar observations have also been reported in several cases¹⁰¹ e.g. for H_2O in ice at -78°C ($\nu_1 = 3400$ and $\nu_3 = 3220 \text{ cm}^{-1}$), NO_2 in NaNO_2 ($\nu_1 = 1328$ and $\nu_3 = 1261 \text{ cm}^{-1}$), etc. Plumb and Hornig¹⁰² also observed in NH_4F that ν_3^n (2810 cm^{-1}) falls lower than ν_1^n (2870 cm^{-1}). As explained by these authors such observation may be physically understood as follows in our case of $(\text{NH}_4)_2\text{SO}_4$.

Physically, the question is to understand how the energy required to distort the NH_4^+ ion symmetrically could be larger than that for anti-symmetric distortion. The possible answer is that during the ν_1^n mode all H atoms move away from N atoms while moving towards SO_4^{2-} ions. Since for

each SO_4^{2-} ion there are two NH_4^+ ions or eight protons, the ν_1^n mode would yield 2N^{3-} and $(\text{H}_8\text{SO}_4)^{6+}$ ions at the extreme. This is an energetically unfavourable configuration. On the other hand in ν_3^n mode one H atom moves away from N atom while three H atoms come nearer to it. At the extreme we may have neutral 2NH_3 and H_2SO_4 molecules in the lattice; this configuration is energetically more favourable. However, this implies that potential curve describing such motion of NH_4^+ ion or of protons possesses double minima. It is corroborated by the following study,— Schroeder and Lippincott¹⁰³ computed the nature of potential describing the linear motion of a proton along linear H-bonds (N-H...O) having $r_{\text{N-O}} = 3.05$ and 2.85 \AA . Under the assumption of stationary N and O atoms their results showed the existence of double minimum potential with barrier height of 40 and 20 kcal/mole respectively. These data give an approximate value of 25 kcal for the barrier height in the double minimum potential well of H-bond having $r_{\text{N-O}} = 2.90 \text{ \AA}$ which corresponds to a shortest H-bond in $(\text{NH}_4)_2\text{SO}_4$ ¹¹.

The unambiguously assigned ν_1^n mode shows a shift of 100 cm^{-1} towards higher frequency side of free ion frequency (3033 cm^{-1}) ⁹² opposite to the expected downward shift due to H-bonding. Such a phenomenon has also been observed in systems like NH_4Cl ^{104,105} and NH_4Br ¹⁰⁶ where ν_1^n shifts by 15 and 20 cm^{-1} in higher frequency side, respectively. The reason for such observations may be attributed to the modifications in the internal force fields of NH_4^+ ion arising due to several interactions which act in the crystalline state. However, on the other hand the unperturbed ν_3^n mode in $(\text{NH}_4)_2\text{SO}_4$ exhibits the expected downward shift by $\sim 25 \text{ cm}^{-1}$ from its free ion value (3134 cm^{-1}) ⁹² at RT and by some more magnitude at LT.

The lowest frequency band of H-H stretching region arising due to $2\nu_4^n$ mode splits into two components at LT. No significant change in total intensity of this mode is observed.

The ν_2^n mode at RT appears as a good intensity band (1671 cm^{-1}) in Raman spectrum. The corresponding band in IR spectrum is observed to be weak and diffuse indicating low distortions in NH_4^+ tetrahedra. In LT Raman spectrum it exhibits three frequencies while in LT infrared spectrum only two. The centre of ν_2^n bands shift towards higher frequency side on lowering the temperature. It is consistent with the increasing H-bond strength.

The ν_4^n ($\sim 1440\text{ cm}^{-1}$) mode shows two frequencies in both Raman and IR spectra of the sample at RT. At LT the Raman bands split into five components while IR bands into six without significant change in intensity. Similar behaviour is shown by ν_3^s ($\sim 1100\text{ cm}^{-1}$) mode.

The ν_1^s mode exhibits sharpest (FWHMI = 5 cm^{-1}) band in both Raman and IR spectra 976 and 972 cm^{-1} respectively. At RT this mode has very low IR intensity which increases by an approximate factor of about 10 at LT. The sharpness of this mode indicates that its force fields are harmonic to a good approximation; the fact that the mode is non-polar to a good extent might also be one of the reasons for its remarkably sharp character.

The ν_4^s mode appearing at 618 cm^{-1} in Raman spectrum (RT) splits into 2 components (628 and 612 cm^{-1}) at LT. It exhibits two components at 615 and 608 cm^{-1} and three components at 618 , 609 and 602 cm^{-1} in IR spectra recorded at RT and LT respectively.

The ν_2^s (450 cm^{-1}) shows two components in both Raman and IR spectra recorded at LT. It has imperceptible IR intensity and shows single band in Raman spectrum at RT.

The very weak band ($\sim 357\text{ cm}^{-1}$) arising due to l^n modes in Raman spectrum (RT) splits into three components ($387, 359$ and 339 cm^{-1}) at LT. In IR spectrum these modes show a sharp weak band (370 cm^{-1}) at LT.

A weak and diffuse band ($\sim 283\text{ cm}^{-1}$) is observed in Raman spectrum recorded at LT. It could have been obscured by strong wing of t^n bands in IR spectrum (LT). This band perhaps arises due to modes like N-H...O (hydrogen bond) stretching.

In frequency region below 250 cm^{-1} our Raman spectrum recorded at RT only shows three shoulders to exciting line at $213, 181$ and 106 cm^{-1} . However, the Raman spectrum (LT) shows four bands at $222, 209, 196$ and 170 cm^{-1} due to t^n modes and three bands at $78, 65$ and 36 cm^{-1} due to t^s modes; the rest 127 and 100 cm^{-1} bands seem to arise due to multiphonons involving t^s modes. A comparison of these frequencies of t^n and t^s with those observed for single crystal at RT, indicates that t^n modes exhibit slight increase in their frequencies on lowering the temperature while t^s modes do not show any significant change.

The crystal structural data¹¹ on $(\text{NH}_4)_2\text{SO}_4$ indicate that in ferroelectric phase (i) H-bonds are more strong, (ii) SO_4^{2-} ion has more distortions and (iii) NH_4^+ ions have low distortions in comparison to paraelectric phase. All spectroscopic observations summarized above are found to be consistent with these inferences. In addition, it may be stated that the C_{2v} symmetry of the LT phase allows more phonons in both IR and Raman spectra (cf Table 3.8). Under this point group the A_1, B_1 and B_2 species

are simultaneously IR and Raman active. Consequently, each of the phonons belonging to these species is expected to split into a LO and a TO component. Thus the already enriched RT Raman spectrum becomes more complex at LT.

IV FERROELECTRIC PHASE TRANSITION

a. Temperature Dependence of IR Bands

In order to understand the microscopic mechanism involved in the ferroelectric phase transition in $(\text{NH}_4)_2\text{SO}_4$, the temperature dependence of the integrated IR intensity of ν_1^s and ν_2^s modes of SO_4^{2-} ion and 3310 cm^{-1} band of NH_4^+ ions have been investigated. Since the last band (3310 cm^{-1}) appears as a part of the complex N-H stretching band, it was appropriately resolved and then studied.

Contours and intensity distributions in ν_1^s , ν_2^s and 3310 cm^{-1} bands are shown in Figs. 3.9(a), (c) and (e), respectively. The changes in the integrated intensity (I) with temperature (T) for these bands are depicted in Figs. 3.9(b), (d) and (f), respectively. The circles on these curves correspond to the temperatures at which different contours (shown vertically above) were recorded.

The ν_1^s mode which appears in IR as a very weak band for room temperature phase (e.g., the curve near 300°K in Fig. 3.9(a)) exhibits an abnormal enhancement in its intensity near $T_c = 223^\circ\text{K}$. Thereafter a very slow but gradual enhancement in intensity of this band continues right upto the lowest temperature studied. Likewise, the ν_2^s band which has almost imperceptible intensity above T_c , suddenly appears at T_c and simultaneously splits into two components (cf Fig. 3.9(c)). The discontinuity in T-I curves of SO_4^{2-} bands appears to last within 6° of our monitored temperature

which of course would represent the temperature gradient along the AgCl-plate within our experimental set up.

The above mentioned behaviour of ν_1^s and ν_2^s bands indicates that a sudden distortion takes place at T_c in the regular tetrahedral room temperature arrangement of SO_4^{2-} ion, since both these modes are IR forbidden for perfect tetrahedron.

The I vs. T curve for 3310 cm^{-1} band shows that structure and dynamics of NH_4^+ ions near T_c undergo changes which, however, are not as rapid as in case of SO_4^{2-} ion. All other studies^{44,45,55,77,90} related to NH_4^+ ions also indicate such changes.

These observations can reflect on the qualitative nature and microscopic mechanism of the ferroelectric transition in the crystal. For the completeness of the discussion it seems necessary to have the knowledge of quantitative changes in microscopic units of the crystal. A point charge model has, therefore, been used to compute the dipole moments associated with $\text{NH}_4^+(\text{I})$, $\text{NH}_4^+(\text{II})$ and SO_4^{2-} ions and their contributions to the net polarization.

b. The Point Charge Model

Both the NH_4^+ and SO_4^{2-} ions can be represented as AB_4^{n+} , where n is 1 for NH_4^+ and 2 for SO_4^{2-} ion. The point charge model defines AB_4^{n+} ion as having $\pm n/4$ electronic charge at crystallographic positions of each of the B atoms. This model describes the electronic charge distribution in AB_4^{n+} ion to a good approximation as discussed by Pauling¹⁰⁷ for a general case of molecular ion. This approximation should be valid for NH_4^+ and SO_4^{2-} ions in $(\text{NH}_4)_2\text{SO}_4$ crystal as they have only minor distortions. The net distortion

$\delta \vec{x}$ for any one of the twelve AB_4^{n+} ions in the unit cell can be expressed as a vector sum of the distortion components $\delta \vec{x}_i$ along the i -th crystallographic axis and we have

$$\delta \vec{x} = \sum_{i=1}^3 \delta \vec{x}_i = \sum_{i=1}^3 \sum_{r=1}^4 (\vec{B}_i^r - \vec{A}_i) \quad \dots 3.7c$$

where \vec{B}_i^r and \vec{A}_i are the components of position vectors respectively of r -th B atom and the A atom of the ion, along i -th crystallographic axis.

If $\delta \vec{x}$ is measured in angstroms, the corresponding \vec{p} (in Debye units) can be expressed by

$$\vec{p} = \sum_{i=1}^3 \vec{p}_i = \pm 1.2n \sum_{i=1}^3 \delta \vec{x}_i \quad \dots 3.7d$$

Considering the volume of the unit cell (496.2 \AA^3) at $\sim 180^\circ\text{K}$, the spontaneous polarization \vec{P} (in $\mu\text{C}/\text{cm}^2$) contributed by three different ions at this temperature would be given by

$$\vec{P} = 2.69 \sum_{i=1}^3 \sum_{\alpha=1}^3 p_i(\alpha) \quad \dots 3.7e$$

where the number 1, 2 and 3 (for α) refer to $NH_4^+(I)$, $NH_4^+(II)$ and SO_4^{2-} ions, respectively, and would retain this significance throughout this chapter.

The dipole moments $\vec{p}(\alpha)$ and their components $\vec{p}_a(\alpha)$, $\vec{p}_b(\alpha)$ and $\vec{p}_c(\alpha)$ along the crystallographic axes a , b and c , respectively, have been computed using Eqn. 3.7d and the crystal data¹¹ both for paraelectric ($\sim 298^\circ\text{K}$) and ferroelectric ($\sim 180^\circ\text{K}$) phases. These computed values for a single ion of each type are given respectively in columns 3, 4, 5 and 6 of Table 3.12.

It is observed that in the paraelectric phase all the three distinguishable ions possess the permanent dipole moments $\vec{p}(\alpha)$ having finite $\vec{p}_a(\alpha)$ and $\vec{p}_b(\alpha)$ and vanishing $\vec{p}_c(\alpha)$. Further, that the value of $\vec{p}(3)$ is about one fourth of each of the $\vec{p}(1)$ and $\vec{p}(2)$. The net dipole moment of the unit cell vanishes automatically due to inversion symmetry of this phase.

In ferroelectric phase all the components $\vec{p}_a(\alpha)$, $\vec{p}_b(\alpha)$ and $\vec{p}_c(\alpha)$ are finite. With respect to the corresponding values in paraelectric phase, $\vec{p}(3)$ shows an increase while $\vec{p}(1)$ and $\vec{p}(2)$ show a decrease and all the three have comparable magnitudes.

The magnitudes, directions and locations of $\vec{p}_a(\alpha)$, $\vec{p}_b(\alpha)$ and $\vec{p}_c(\alpha)$ for all the twelve ions in the unit cell of ferroelectric $(\text{NH}_4)_2\text{SO}_4$ have diagrammatically been shown in Fig. 3.10 for the better illustration of the situation. The starred locations refer to the set of ions which have one to one correlation with the data given in Table 3.12. The other locations and vectors can be obtained by symmetry operations of the C_{2v}^9 group.

The crystal symmetry of this phase C_{2v}^9 restricts the net polarization of the unit cell only along c-axis (the ferroelectric axis). Further, since $\vec{p}_c(1)$ opposes both $\vec{p}_c(2)$ and $\vec{p}_c(3)$. The Eqn. 3.7e simplifies to

$$\vec{P} = \vec{P}_c = 2.69 [\vec{p}_c(2) + \vec{p}_c(3) - \vec{p}_c(1)] \quad \dots 3.7f$$

Using this relation the net spontaneous polarization is found to be $0.42 \mu\text{C}/\text{cm}^2$ to which the contributions of different types of ions are given in column 7 of Table 3.12.

As the assumed point charge model represents only approximately the real charge distribution in AB_4^{n+} ion, the computed results may be supposed to have some error but certainly not of high order. This is evident from the fact that the computed value of polarization $0.42 \mu\text{C}/\text{cm}^2$ agrees well with experimentally reported values $0.45 \mu\text{C}/\text{cm}^2$ by Hoshino et al¹², $0.64 \mu\text{C}/\text{cm}^2$ by Ikeda and Fujibayashi³⁷ and $0.34 \mu\text{C}/\text{cm}^2$ obtained for 180°K from \vec{P} vs. T curve reported by Unruh³¹; the former two values are reported to be temperature independent. The NH_4^+ ions in paraelectric phase oscillate with large amplitudes which continue in the ferroelectric phase; $\text{NH}_4^+(\text{I})$ ion freezes at 160°K while $\text{NH}_4^+(\text{II})$ ion continues moderate oscillations upto $\sim 90^\circ\text{K}$ ⁵³. Consequently, the changes in the orientations of dipoles $\vec{p}(1)$ and $\vec{p}(2)$ and their effect on the orientation of $\vec{p}(3)$ are possible with the change in temperature. Such a change can lead to the temperature dependent polarization. Therefore, the spontaneous polarization data reported by Unruh^{and} coworkers^{31,32} seem to be more realistic.

It is noticed for the first time that the SO_4^{2-} ion which was not considered^{37,55} for contributing towards ferroelectricity, contributes a major part of about $0.23 \mu\text{C}/\text{cm}^2$ to the total polarization of about $0.42 \mu\text{C}/\text{cm}^2$.

It is also evident from Table 3.12 and Fig. 3.10 that orientations of dipoles in the ferroelectric phase do not define a state ordered better than that in the paraelectric phase. Rather the array of dipoles as it appears below T_c has the characteristic of a 'ferrielectric' structure with respect to the c-components of dipoles and of 'antiferroelectric' structure with respect to a- and b-components of dipoles. This provides an evidence for the inference made by Unruh and Rudiger³² that

As the assumed point charge model represents only approximately the real charge distribution in AB_4^{n+} ion, the computed results may be supposed to have some error but certainly not of high order. This is evident from the fact that the computed value of polarization $0.42 \mu\text{C}/\text{cm}^2$ agrees well with experimentally reported values $0.45 \mu\text{C}/\text{cm}^2$ by Hoshino et al.¹², $0.64 \mu\text{C}/\text{cm}^2$ by Ikeda and Fujibayashi³⁷ and $0.34 \mu\text{C}/\text{cm}^2$ obtained for 180°K from \vec{P} vs. T curve reported by Unruh³¹; the former two values are reported to be temperature independent. The NH_4^+ ions in paraelectric phase oscillate with large amplitudes which continue in the ferroelectric phase; $\text{NH}_4^+(\text{I})$ ion freezes at 160°K while $\text{NH}_4^+(\text{II})$ ion continues moderate oscillations upto $\sim 90^\circ\text{K}$ ⁵³. Consequently, the changes in the orientations of dipoles $\vec{p}(1)$ and $\vec{p}(2)$ and their effect on the orientation of $\vec{p}(3)$ are possible with the change in temperature. Such a change can lead to the temperature dependent polarization. Therefore, the spontaneous polarization data reported by Unruh^{and} coworkers^{31,32} seem to be more realistic.

It is noticed for the first time that the SO_4^{2-} ion which was not considered^{37,55} for contributing towards ferroelectricity, contributes a major part of about $0.23 \mu\text{C}/\text{cm}^2$ to the total polarization of about $0.42 \mu\text{C}/\text{cm}^2$.

It is also evident from Table 3.12 and Fig. 3.10 that orientations of dipoles in the ferroelectric phase do not define a state ordered better than that in the paraelectric phase. Rather the array of dipoles as it appears below T_c has the characteristic of a 'ferrielectric' structure with respect to the c-components of dipoles and of 'antiferroelectric' structure with respect to a- and b-components of dipoles. This provides an evidence for the inference made by Unruh and Rudiger³² that

the contributions to the macroscopic polarization due to NH_4^+ ions i.e. $\vec{P}_c(1)$ and $\vec{P}_c(2)$ must be antiparallel; $\vec{P}_c(1)$ and $\vec{P}_c(2)$ have been denoted respectively as \vec{P}_c^I and \vec{P}_c^{II} by these authors.

c. Microscopic Mechanism and Origin of Phase Transition

Order-Disorder Phenomenon: Our computations as discussed in above section contradict the order-disorder type of mechanism involved in the phase transition of $(\text{NH}_4)_2\text{SO}_4$ as proposed by O'Reilly and Tsang⁵⁵. These authors have shown¹⁰⁸ theoretically that the order-disorder phenomenon can be consistent with first order phase transition in $(\text{NH}_4)_2\text{SO}_4$, if the transition involves the cooperative reorientation of NH_4^+ ions at T_c . Similar phenomenon was proposed by Pauling¹⁰⁹ giving a qualitative explanation of the phenomenon at the time when much experimental data on the crystal were not available. This explanation was contradicted by Hamilton and Ibers¹¹⁰ on the basis of their neutron diffraction study of the crystal in both phases¹¹. Similarly, Miller et al⁴⁷ also showed by studying NMR spectrum of $(\text{NH}_4)_2\text{SO}_4$ that NH_4^+ ions do not undergo co-operative reorientation at T_c which is inconsistent with the phenomenon proposed by O'Reilly and Tsang^{55,108}. The phenomenon has also been critically discussed in later reports by O'Reilly and Tsang¹¹¹, Hamilton¹¹², and Ross and Hamilton¹¹³. However, no definite conclusion could be arrived at about this phenomenon.

Displacive Type Phenomenon: The crystal structural data¹¹ of $(\text{NH}_4)_2\text{SO}_4$ are not consistent with displacive type of phenomenon as exhibited by BaTiO_3 ^{114,115}. In order to visualize the clear picture of the situation, the positions (projected in bc-plane) of three different ions in the tetramolecular unit cell of para- and ferro-electric phases are shown in Fig. 3.11. Crystallographic data reported by Schlemper and Hamilton¹¹

have been used for these projections. We note that in ferroelectric phase SO_4^{2-} ion does not exhibit any shift while $\text{NH}_4^+(\text{I})$ and $\text{NH}_4^+(\text{II})$ ions exhibit shifts by + 0.005 c and -0.005 c respectively from their equilibrium positions in paraelectric phase. Considering monopoles of charge e^+ and $2e^-$ situated at positions (cf Fig. 3.11(b)) of NH_4^+ and SO_4^{2-} ions, respectively, the net polarization of the unit cell may be observed to vanish. This leaves no possibility of displacive type of mechanism to be responsible for the transition in $(\text{NH}_4)_2\text{SO}_4$.

Factual Phenomenon: The above discussion indicates that the usual displacive and order-disorder type of mechanisms are not responsible for the ferroelectric transition in $(\text{NH}_4)_2\text{SO}_4$. On the other hand, the changes in the distortions of $\text{NH}_4^+(\text{I})$, $\text{NH}_4^+(\text{II})$ and SO_4^{2-} ions occurring at T_c can explain the quantitative result of spontaneous polarization. The changes in the distortions of these ions can, therefore, be recognized as the main microscopic phenomenon responsible for the transition. Anistratov and Martynov³⁵ showed that the change in birefringence at T_c occurs mainly due to elasto-optical effect rather than electro-optical effect. All these inferences univocally indicate that $(\text{NH}_4)_2\text{SO}_4$ is not a proper ferroelectric and exhibits an ordinary molecular phase transition resulting ferroelectricity as a secondary effect. It has correctly been defined¹¹⁶ as an improper ferroelectric.

Order Parameter: From the above inferences it seems more probable that T_c is not affected by d.c. biasing field as observed by Hoshino et al¹² and corroborated by the observation that the hysteresis curve just above T_c exhibits a line shape³¹. Thus the observations of Kamiyoshi and Miyamoto²³ showing dependence of T_c on applied electric field do not appear to be correct. Conclusively, spontaneous strain rather than spontaneous

polarization acts as an order parameter to be used for describing the transition.

Origin of Phase Transition: The spontaneous strain, which acts as an order parameter, should arise due to covalency effects in directed bonds^{114,115}. $(\text{NH}_4)_2\text{SO}_4$ has three different types of directed bonds: N-H, N-H...O(H-bonds) and S-O, which could be equally responsible for the origin of driving interaction. However, the former two types of directed bonds appear to be of secondary importance because: (i) on deuteration, T_c is not affected¹² or is negligibly affected (by $0.6 \pm 0.1^\circ\text{K}$)³², (ii) the 3310 cm^{-1} band associated with NH_4^+ ion exhibits comparatively slow change in its intensity near T_c (cf Fig. 3.9(e) and (f)), while the crystal exhibits a sharp transition, (iii) the NMR line width is not affected by the transition⁴⁴ and (iv) the transition results in more distorted SO_4^{2-} ion and less distorted NH_4^+ ions in the ferroelectric phase in comparison to the respective ones in paraelectric phase: (Megaw¹¹⁴ has shown that the covalency effects in directed bonds tend to form angles leading to slightly distorted structure of lower symmetry in ferroelectric phase). This indicates that the main driving interaction has its origin in S-O bonds of SO_4^{2-} ion which triggers the transition by getting more distorted structure of lower symmetry; the NH_4^+ ions simply follow an appropriate change. This is probably the reason that studies related only with NH_4^+ ions indicate the phase transition as having characteristics of second order^{55,77,90}.

d. Theoretical Models Proposed (Earlier) for the Transition

Thermodynamical Theory: Ikeda et al¹¹⁶ considered a physically undefined order parameter (η) transforming like \vec{z} (the vector parallel to c-axis)

to develop the thermodynamic theory of the transition. The present study adds that η should be the localized strain or stress at the sites of SO_4^{2-} ion. This strain may polarize the SO_4^{2-} ion and can, therefore, exhibit interaction with \vec{P} .

Soft Mode Theory: The model developed by Sawada et al.¹¹⁷ attributes the origin of ferroelectric phase transition to a mixed mode of B_{1u} species of D_{2h} point group; the mode possesses large component of librational non-polar mode and a small component of translational polar mode, and becomes soft at $T = T_0$. This model is primarily based on the assumption that all the constituting ions $\text{NH}_4^+(\text{I})$, $\text{NH}_4^+(\text{II})$ and SO_4^{2-} exhibit perfect tetrahedral character in both phases and therefore internal modes of these ions do not involve in the transition.

However, we note the following: (i) The studies of NMR⁴⁴, DMR^{54,55} and IR absorption^{58,77} in $(\text{NH}_4)_2\text{SO}_4$ and its crystal structure¹¹ alongwith present investigations univocally reveal that NH_4^+ and SO_4^{2-} ions exhibit considerable distortions. (ii) The temperature dependence of the intensity of three thermosensitive IR bands of $(\text{NH}_4)_2\text{SO}_4$ discussed in section 3.7(IV)a reveals that the SO_4^{2-} ion suddenly gets distorted at T_c in a narrow range of temperature on cooling the crystal, while the NH_4^+ ions follow relatively a slow change. (iii) Calculations of $\vec{p}(1)$, $\vec{p}(2)$ and $\vec{p}(3)$ (cf Table 3.12) have indicated that distortions in NH_4^+ and SO_4^{2-} ions are sufficient to account for a spontaneous polarization of $0.42 \mu\text{C/cm}^2$; which agrees well with the experimentally measured results as already discussed. (iv) The translations and rotations form the bases of two different irreducible representations⁹² (i.e F_2 and F_4 , respectively) of T_d point group; obviously they can not mix unless NH_4^+ and SO_4^{2-} ions exhibit distortions. But a mixed

mode of translatory and rotatory vibrations of these ions forms the basis of this theoretical model. Thus the assumption of tetrahedral character of NH_4^+ and SO_4^{2-} ions seems to be unjustified and self contradictory. In conclusion this theory attributes the net spontaneous polarization \vec{P}_s of $(\text{NH}_4)_2\text{SO}_4$ to the relative shifts of $\text{NH}_4^+(\text{I})$, $\text{NH}_4^+(\text{II})$ and SO_4^{2-} ions along the c-axis from the equilibrium positions in paraelectric phase. Following this conclusion and using the known crystal structural data¹¹, Sawada et al¹¹⁷ computed a spontaneous polarization of $0.7 \mu\text{C}/\text{cm}^2$, while we find it to vanish under the same model involving displacive phenomenon (cf section 3.7(IV)d). Thus the soft mode theory as such proposed by Sawada et al¹¹⁷ appears to be inconsistent with both experimental and theoretical facts known to-date for $(\text{NH}_4)_2\text{SO}_4$.

In view of the experimental and theoretical knowledge including the inferences of the present study, we feel that an approach parallel to that developed by Sawada et al¹¹⁷ may lead to a consistent theory if the soft mode is considered to be a coupled mode of an appropriate symmetry having major component of asymmetric stretching (ν_3^s) and the asymmetric bending (ν_4^s) modes of SO_4^{2-} ion.

Recently, Aiju¹¹⁸ has discussed the new approach to develop a consistent theory for phase transition in $(\text{NH}_4)_2\text{SO}_4$ type crystals. Accordingly, there may exist a soft mode having wavelength equal to general rational number times the relevant lattice parameter i.e. $c = 5.993 \text{ \AA}$ in case of $(\text{NH}_4)_2\text{SO}_4$. However, on the basis of present investigations it seems difficult to examine the adequacy of this approach.

3.8 CONCLUSION

Raman spectra of single crystal of $(\text{NH}_4)_2\text{SO}_4$ have extensively been studied at RT. All modes except the 1^n and 1^s exhibit strong bands. The 1^n modes are assigned unambiguously to weak and diffuse bands around 355 cm^{-1} , while 1^s modes are tentatively assigned to weak shoulders to exciting line observed around 20 cm^{-1} . The t^n and t^s modes, which appear as strong bands around 200 cm^{-1} and below 80 cm^{-1} respectively, seem to have low mixing with each other. The force fields describing the dynamics of $\text{NH}_4^+(\text{I})$ and $\text{NH}_4^+(\text{II})$ ions are identical to a good approximation. The $\nu_2^n + \nu_4^n$ combination and ν_3^n fundamental exhibit strong Fermi interaction.

IR(ATR) spectra ($4000\text{--}250\text{ cm}^{-1}$) of the single crystal recorded at RT exhibit four strong bands due to ν_3^n , ν_4^n , ν_3^s and ν_4^s modes which are only IR active internal modes under T_d symmetry of NH_4^+ and SO_4^{2-} ions. A comparative study of RT and LT Raman and IR spectra of microcrystalline $(\text{NH}_4)_2\text{SO}_4$ has also been made.

The existence of proton tunneling along the strong H-bonds in $(\text{NH}_4)_2\text{SO}_4$ has been inferred; it is also supported by other studies. In general H-bonds become more strong in ferroelectric phase. SO_4^{2-} ion which has almost a tetrahedral structure in paraelectric phase gets distorted in a narrow range of temperature around T_c . The NH_4^+ ions also exhibit changes in their structure and dynamics but with slower rate. The overall observations reported in this chapter are consistent with the known crystallographic data of $(\text{NH}_4)_2\text{SO}_4$ in its both phases.

Within the limits of possible errors, the point charge model developed in the present investigations, explains the experimentally

known value of spontaneous polarization. It has been argued that the spontaneous polarization should possibly depend on the temperature. For the first time it has evidently been shown that SO_4^{2-} ion contributes about 50% of the total polarization at $\sim 180^\circ\text{K}$.

$(\text{NH}_4)_2\text{SO}_4$ seems to be an unique example where ferroelectricity is the secondary effect of an ordinary molecular phase transition. The order parameter coupled with spontaneous polarization seems to have several components including spontaneous strain in SO_4^{2-} ion as its major contributor. This strain appears to arise due to covalency effects in S-O bonds of SO_4^{2-} ion. Theoretical models developed by others to explain the origin and mechanism of phase transition in this crystal have been critically reviewed. Finally, it is hoped that the present study would be helpful in the development of an elegant theory of $(\text{NH}_4)_2\text{SO}_4$ type ferroelectrics and in the quantitative study of covalent bonds.

REFERENCES

1. R.C. Weast and S.M. Silby, Editors, Hand Book of Chemistry and Physics, The Chemical Rubber Comp. 47th edition, (1966-67).
2. J.L. Crenshaw and J. Ritter, Z. Physik Chem. B16, 143 (1932).
3. B.T. Matthias and J.P. Remeika, Phys. Rev. 103, 262 (1956).
4. A. Ogg and F.L. Hopwood, Phil. Mag. 32, 191, 518 (1916).
5. W. Taylor and T. Boyer, Proc. Manchester Lit. Phil. Soc. 72, 125 (1927-28).
6. A. Ogg, Phil. Mag. 5, 28, 354 (1928).
7. A. Ogg, Phil. Mag. 9, 665 (1930).
8. A.E.H. Tutton, Phil. Mag. 9, 58 (1930).
9. V.V. Udalova and Z.G. Pinskar, Sov. Phys. Crystallography 8, 433 (1964).
10. B. Singh, Doctoral Dissertation, The Pennsylvania University (1962).
11. E.O. Schlemper and W.C. Hamilton, J. Chem. Phys. 44, 4498 (1966).
12. S. Hoshino, K. Vedam, Y. Okaya and R. Pepinsky, Phys. Rev. 112, 405 (1958).
13. R. Ewald, Ann. Physik 44, 1223 (1914).
14. H.P. Klung and W.W. Johnson, J. Amer. Chem. Soc. 59, 2061 (1937).
15. I. Nitta and K. Suenaga, Bull. Chem. Soc. Japan 13, 36 (1938).
16. C.H. Shomate, J. Amer. Chem. Soc. 67, 1096 (1945).
17. R. Pepinsky and F. Jona, Phys. Rev. 105, 344 (1957).
18. F. Jona and G. Shirane, Ferroelectric Crystals, Pergamon Press, New York (1962).
19. A. Hettich, Z. Physik Chem. A168, 360 (1934).
20. R. Guillien, Compt. Rend. 208, 980 (1939).
21. S.T. Bayley, Trans. Faraday Soc. 47, 518 (1951).
22. M. Freymann, Compt. Rend. 233, 1449 (1951).
23. K. Kamiyoshi and T. Miyamoto, J. Chem. Phys. 22, 756 (1954).

24. L. Couture-Mathieu, S. Le Montagner, J. Le Bot and A. Le Traon, *Compt. Rend.* 242, 1804 (1956).
25. S. Le Montagner, Thesis, University of Paris (1957).
26. K. Kamiyoshi, *Rep. Res. Instt. Tohoku University*, A9, 94 (1957).
27. V.A. Koptsik, B.A. Strukov, A.A. Sklyankin and M.E. Levina, *Izv. Akad. Nauk SSSR Ser. Fiz.* 24, 1228 (1960).
28. V.A. Koptsik, B.A. Strukov and I.K. Nevodomsкая, *Izv. Akad. Nauk SSSR. Ser. Fiz.* 24, 1231 (1960).
29. E. Nakamura, T. Mitsui and J. Furuichi, *J. Phys. Soc. Japan* 18, 1477 (1963).
30. H.G. Unruh, *Phys. Lett.* 17, 8 (1965).
31. H.G. Unruh, *Solid State Commun.* 8, 1951 (1970).
32. H.G. Unruh and U. Rudiger, *J. de Physiq* 33, C2-77 (1972).
33. S. Toshev, *Proc. Int. Meet. Ferroelect.*, Prague 2, 31 (1966).
34. H. Ohshima and E. Nakamura, *J. Phys. Chem. Solids* 27, 481 (1966).
35. A.T. Anistratov and V.G. Martynov, *Sov. Phys. Crystallogra.* 15, 256 (1970-71).
36. M.E. Levina and G.I. Kolbeneva, *Vestn. Mosk. Univ. Khim.* 13, 211 (1972).
37. T. Ikeda and K. Fujibayashi, *J. Phys. Soc. Japan* 33, 1487 (1972).
38. S. Haussuhl, *Acta Cryst.* 18, 839 (1965).
39. Y. Luspín and G. Hauret, *C.R. Akad. Sci. Ser.* B274, 995 (1972).
40. V.H. Schmidt, *J. Chem. Phys.* 38, 2783 (1963).
41. J.C. Thrierr, *Compt Rend.* 253, 2917 (1961).
42. E.E.A. Chermack, *Diss. Abstr. Int.* B31, 2189 (1970).
43. B.A. Strukov, *Sov. Phys. Crystallogra.* 6, 511 (1961).
44. R. Blinc and I. Levstek, *J. Phys. Chem. Solids* 12, 295 (1960).
45. R.E. Richards and T. Schaefer, *Trans. Faraday Soc.* 57, 210 (1961).
46. I. Levstek, *Proc. Intern. Meet. Mol. Spectrosc. 4th Bologna (1959)*, 3, 1231 (1962).

47. S.R. Miller, R. Blinc, M. Brenman and J.S. Waugh, Phys. Rev. 126, 528 (1962).
48. R. Blinc, S.R. Miller, M. Brenman and J.S. Waugh, Proc. Collq. AMPERE 11, 199 (1962), Published in 1963.
49. R. Blinc, M. Mali, R. Osredkar, A. Prelesnik, J. Seliger and I. Zupancic, Chem. Phys. Lett. 14, 49 (1972).
50. T. Chiba, J. Chem. Phys. 36, 1122 (1962).
51. S.W. Rabindeau and P. Waldstein, J. Chem. Phys. 42, 3822 (1965).
52. D.W. Kydon, H.E. Petch and M. Pintar, Phys. Lett. 25, 360 (1967).
53. D.W. Kydon, M. Pintar and H.E. Petch, J. Chem. Phys. 47, 1185 (1967).
54. D.W. Kydon, H.E. Petch and M. Pintar, J. Chem. Phys. 51, 487 (1969).
55. D.E. O'Reilly and T. Tsang, J. Chem. Phys. 46, 1291 (1967).
56. R.R. Knispel, H.E. Petch and M. Pintar, J. Chem. Phys. 56, 676 (1972).
57. C.J.H. Schutte and A.M. Heyns, Chem. Phys. Lett. 1, 511 (1968).
58. C.J.H. Schutte and A.M. Heyns, J. Chem. Phys. 52, 864 (1970).
59. I. Barbur, Stud. Univ. Babes-Bolyai, Ser. Math. Phys. 13, 139 (1968).
60. A. Bodi, R. Baican and I. Barbur, Acta Phys. Pol. A39, 39 (1971).
61. B.A. Strukov and S. Toshev, Sov. Phys. Crystallogra. 9, 426 (1964).
62. C. Bettinali, G. Ferrarresso and J. W. Manconi, Atti. Acad. Naz. Lincei Rend., Cl. Sci. Fiz. Mat. Natur. 43, 536 (1967).
63. R. Guillien, Ann. Phys. 17, 334 (1942).
64. G. Hettner and F. Simon, Z. Physik Chem. B1, 293 (1928).
65. R. Pohlman, Z. Physik 79, 394 (1932).
66. J. Fock, Z. Physik 90, 38 (1934).
67. T.P. Myasnikova, Materialy 4-oi (Chetvertoi) Nauchn. Konf. Aspirantov Sb., 61 (1962).
68. T.P. Myasnikova and A.F. Yatsenko, Sov. Phys. Solid State 4, 475 (1962).
69. S.D. Ross, Spectrochim Acta 18, 1575 (1962).

70. V. Ananthanayanan, Ind. J. Pure Appl. Phys. 1, 58 (1963).
71. T.P. Mysnikova and I.M. Arefev, Opt. and Spectrosc. 16, 293 (1964).
72. J.E. Guerschais, A. Haumesser and R. Rohmer, Compt. Rend. 260, 5571 (1965).
73. L.L. Oden, Diss. Abstr. 26, 3654 (1966).
74. Z.A. Gabrichidze, I.P. Ereishvili and I.N. Dzhabaridze, Tr. Kutaio. Gos. Pedagog Instt., 32, 289 (1969).
75. M. Trefler and G.R. Wilkinson, Discuss. Faraday Soc. 48, 108 (1969).
76. M. Trefler, Can. J. Phys. 49, 1694 (1971).
77. B.H. Torrie, C.C. Lin, O.S. Binbrek and A. Anderson, J. Phys. Chem. Solids 33, 697 (1972).
78. P.K. Acharya and P.S. Narayanan, Ind. J. Pure Appl. Phys. 11, 514 (1973).
79. A. Da Silveira, Compt. Rend. 195, 521 (1932).
80. R. Ananthakrishnan, Proc. Ind. Acad. Sci. A5, 76 (1937).
81. H. Volkringer, M. Freymann and R. Freymann, Compt. Rend. 208, 1005 (1939).
82. R. Heerdt and J. Goubeau, Z. Anorg. Chem. 255, 309 (1948).
83. K. Schafer, Z. Electrochem. 52, 98 (1948).
84. A.I. Stekhanov and Z.A. Gabrichidze, Fiz. Tverd. Tela 5, 3105 (1963).
85. P.A. Bazherlin, T.P. Myasnikova and A.V. Rakov, Sov. Phys. Solid State 5, 1299 (1964).
86. F. Blomer and H. Moser, Z. Angew Phys. 27, 302 (1969).
87. J.J. Rush and T.I. Taylor, Inelastic Scattering of Neutrons in Solids and Liquids, Proc. Symp. 3rd Bombay, India, 2, 333 (1965).
88. P.S. Leung, T.I. Taylor and W.W. Havens, Jr., J. Chem. Phys. 48, 4912 (1968).
89. H.J. Kim, J. Korean Nucl. Soc. 4, 306 (1972).
90. U. Dahlborg, K.E. Larsson and E. Pirkmaser, Physica 49, 1 (1970).
91. W.G. Wyckoff, Crystal Structure, Inter Science, New York, Vol 3 (1965).

92. G. Herzberg, Infrared and Raman Spectra of Polyatomic Molecules, D. Van Nostrand, Princeton (1945).
93. R. Loudon, Adv. Phys. 13, 423 (1964).
94. J.W. Mullin, M. Chakraborty and K. Mehta, J. Appl. Chem. 20, 367 (1970).
95. D.S. Petrenko, Khim. Tekhnol. (Kharkov) 22, 55 (1971).
96. J. Godard and G. Drasko, Krist. Technol. 7, k11 (1972).
97. M.B. Porter and R.C. Spiller, The Barker Index of Crystals, Haffer and Sons, Cambridge, Vol. I (1951).
98. P. Venkateswarlu and H.P. Broida, Proc. Ind. Acad. Science 124A, 230 (1971).
99. P. Venkateswarlu, Private Communication.
100. S. Bratoz, Adv. Quant Chem. 3, 210 (1967).
101. K. Nakamoto, Infrared Spectra of Inorganic and Co-ordination Compounds, John Wiley, New York (1963).
102. R.C. Plumb and D.F. Hornig, J. Chem. Phys. 23, 947 (1955).
103. R. Schroeder and E.R. Lippincott, J. Phys. Chem. 61, 921 (1957).
104. E.L. Wagner and D.F. Hornig, J. Chem. Phys. 18, 305 (1950).
105. E.L. Wagner and D.F. Hornig, J. Chem. Phys. 18, 296 (1950).
106. J.R. During and D.J. Antion, Appl. Spectrosc. 24, 16 (1970).
107. L. Pauling, J. Chim. Phys. 45, 142 (1948).
108. D.E. O'Reilly and T. Tsang, J. Chem. Phys. 46, 1301 (1967).
109. L. Pauling, Phys. Rev. 36, 430 (1930).
110. W.C. Hamilton and J.A. Ibers, Hydrogen Bonding in Solids, Benjamin, New York (1968).
111. D.E. O'Reilly and T. Tsang, J. Chem. Phys. 50, 2274 (1969).
112. W.C. Hamilton, J. Chem. Phys. 50, 2275 (1969).
113. F.K. Ross and W.C. Hamilton, Proc. Amer. Crystallogra. Assoc. Meet. Columbia, S.C. Feb. (1971).

114. H.D. Megaw, *Ferroelectricity in Crystals*, Mathuen, London (1957).
115. W. Kanzig, *Ferroelectrics and Anti-Ferroelectrics*, Academic Press, New York (1957).
116. T. Ikeda, K. Fujibayashi, T. Nagai and J. Kobayashi, *Phys. Stat. Solidi* 16a, 279 (1973).
117. A. Sawada, Y. Takagi and Y. Ishibashi, *J. Phys. Soc. Japan* 34, 748 (1973).
118. K. Aizu, *J. Phys. Soc. Japan* 34, 1567 (1973).

TABLE 3.1
 Crystal structural data^x of $(\text{NH}_4)_2\text{SO}_4$

	RT	LT
Crystal system probable	Orthorhombic	Orthorhombic
space group formula	$D_{2h}^{16}(\text{Pnam})$	$C_{2v}^9(\text{Pna}2_1)$
units/unit cell		
a	7.782 Å	7.837±0.007 Å
b	10.636 Å	10.61 ±0.01 Å
c	5.993 Å	5.967±0.006 Å
Volume	496.0 Å ³	496.2 Å ³

^xTaken from ref. 11.

[illegible]

^x For different notations used in this Table see sections 1.10 and 1.11.

^ySuperscripts n and s represent modes of NH₄⁺ and SO₄²⁻ ions, respectively.

Classification of phonons in ferroelectric phase of $(\text{NH}_4)_2\text{SO}_4$ (an unit cell approach)^x

C_{2v}^9	E	C_2 c	σ' ac	σ'' bc	Reduced representations			Bases of representations ^y
					A ₁	A ₂	B ₁ B ₂	
A ₁	1	1	1	1				
A ₂	1	1	-1	-1				
B ₁	1	-1	1	-1				
B ₂	1	-1	-1	1				
ϕ_R	0	π	0	0				
$\beta = \pm 1 + 2\cos\phi_R$	3	-1	1	1	1		1	Space vector \vec{r}
$\beta' = \beta \cdot 2\cos\phi_R$	6	2	2	2	3	1	1	Polarizability tensor α
$\beta'' = 1 + 2\cos\phi_R$	3	-1	-1	-1		1	1	Angular moment \vec{L}
N^R	60	0	0.	0				
$N^R(t) = N^R(1)$	12	0	0	0				
$\chi(N) = N^R \cdot \beta$	180	0	0	0	45	45	45	Total phonon modes
$\chi(t) = N^R(t) \cdot \beta$	36	0	0	0	9	9	9	Translations $t^n + t^s$
$\chi(1) = N^R(1) \cdot \beta''$	36	0	0	0	9	9	9	Librations $l^n + l^s$
$\chi(i)$	108	0	0	0	27	27	27	Internal modes $\nu_i^n + \nu_i^s$

^xFor different notations used in this Table see sections 1.10 and 1.11.^ySuperscripts n and s represent modes of NH_4^+ and SC_4^{2-} ions, respectively.

TABLE 3.4

Correlation between symmetry species of T_d , C_s and D_{2h} point groups

Symmetry species ^x		
T_d	$C_s(\sigma_{ab})$	D_{2h}
A_1	A	$A_g + B_{3g} + B_{1u} + B_{2u}$
E	A + B	$(A_g + B_{3g} + B_{1u} + B_{2u}) + (A_u + B_{3u} + B_{1g} + B_{2g})$
F_1	A + 2B	$(A_g + B_{3g} + B_{1u} + B_{2u}) + 2(A_u + B_{3u} + B_{1g} + B_{2g})$
F_2	2A + B	$2(A_g + B_{3g} + B_{1u} + B_{2u}) + (A_u + B_{3u} + B_{1g} + B_{2g})$

^xSymmetry species A_1 , E and F_2 of T_d , A and B of C_s and A_g , B_{1g} , B_{2g} and B_{3g} of D_{2h} are Raman active while F_2 of T_d , A and B of C_s and B_{1u} , B_{2u} and B_{3u} of D_{2h} are IR active.

TABLE 3.5

Correlation between symmetry species
of T_d , C_1 and C_{2v} point groups

Symmetry species ^x		
T_d	C_1	C_{2v}
A_1	A_2	$A_1 + A_2 + B_1 + B_2$
E	2A	$2(A_1 + A_2 + B_1 + B_2)$
F_1	3A	$3(A_1 + A_2 + B_1 + B_2)$
F_2	3A	$3(A_1 + A_2 + B_1 + B_2)$

^xSymmetry species A_1 , E and F_2 of T_d , A of C_1 and A_1 , A_2 , B_1 and B_2 of C_{2v} are Raman active while F_2 of T_d , A of C_1 and A_1 , B_1 and B_2 of C_{2v} are IR active.

TABLE 3.6

Classification of phonons in paraelectric phase
of $(\text{NH}_4)_2\text{SO}_4$ crystal (The site symmetry approach)

Modes of AB_4 type T_d ion	Species under D_{2h}								N^x
	A_g	B_{1g}	B_{2g}	B_{3g}	A_u	B_{1u}	B_{2u}	B_{3u}	
$\nu_1(\text{A}_1)$	1	-	-	1	-	1	1	-	4
$\nu_2(\text{E})$	1	1	1	1	1	1	1	1	8
$\nu_3(\text{F}_2)$	2	1	1	2	1	2	2	1	12
$\nu_4(\text{F}_2)$	2	1	1	2	1	2	2	1	12
Rotations (F_1)	1	2	2	1	2	1	1	2	12
Translations (F_2)	2	1	1	2	1	2	2	1	12
Total ^y	9	6	6	9	6	9	9	6	60
Grand total ^z	27	18	18	27	18	27	27	18	180

^x N represents total number of phonon modes originating from particular mode of an AB_4 type tetrahedral ion in tetramolecular unit cell.

^yTotal accounting for the phonons originating from any one of the $\text{NH}_4^+(\text{I})$, $\text{NH}_4^+(\text{II})$ and SO_4^{2-} ions.

^zTotal, accounting for the phonons originating from all the three types of ions.

TABLE 3.7

Classification of phonons in ferroelectric phase of $(\text{NH}_4)_2\text{SO}_4$ crystal (A site symmetry approach)

Modes of AB_4 type T_d ion	Species under C_{2v}				N^x
	A_1	A_2	B_1	B_2	
$\nu_1(\text{A}_1)$	1	1	1	1	4
$\nu_2(\text{E})$	2	2	2	2	8
$\nu_3(\text{F}_2)$	3	3	3	3	12
$\nu_4(\text{F}_2)$	3	3	3	3	12
Rotations (F_1)	3	3	3	3	12
Translations (F_2)	3	3	3	3	12
Total ^y	15	15	15	15	60
Grand total ^z	45	45	45	45	180

^x N represents total number of phonon modes originating from particular mode of an AB_4 type tetrahedral ion in tetramolecular unit cell.

^yTotal accounting for the phonons originating from **any one** of the $\text{NH}_4(\text{I})$, $\text{NH}_4(\text{II})$ and SO_4 ions.

^zTotal accounting for the phonons originating from all the three types of ions.

TABLE 3.8

Frequencies (in cm^{-1}) of phonons observed in Raman spectra of single crystal of $(\text{NH}_4)_2\text{SC}_4$

Specifi- cations ^a	A _g			B _{3g}	B _{1g}	B _{2g}	Assignment ^b	ν_{av}^c	HFMP ^d
	aa	bb	cc	ab	bc	ca			
1	2	3	4	5	6	7	8	9	10
u-band						3322	$2\nu_2^n$	3322	3338
v-band		3292					D.C.(I)	3292	
w-bands	3185	3190	3180	3190	3194	3186	F.R.(I)	3187	<u>3108</u>
x-bands	3140	3122	3122	3113	3143*		ν_1^n	3124	
y-bands	3005	3040	3005	3016	3045	3060	F.R.(II)	3029	<u>3098</u>
z-bands	2865	2850	2865	2820	2850	2845	$2\nu_4^n$	2849	2858
			2525				?	2525	
			2025	2010	2080		$\nu_1^s + \nu_3^s$	2038	2063
			1795				$\nu_4^n + 1^n$	1795	1786
				1715			$\nu_3^s + \nu_4^s / \nu_2^n$	1715	1705
	1654	1662	1660	1674	1693	1668	ν_2^n	1669	
-	1410	1470	1439	1475			ν_4^n	1429	
		1417	1402	1423	1417	1412			
			1231			1204	$2\nu_4^s$	1218	1236
					1130		$\nu_3^s + t^s$	1130	1132
	1105	1105	1102	1117			ν_3^s	1087	
	1062	1068	1062	1073	1080	1095			
	976	976	976	976	976*	976*	ν_1^s	976	
			910				$2\nu_2^s$	910	900
		735	735		735	706	21^n	728	710
	628	625	625			628*	ν_4^s	618	
-		612	612	616	612	612			

contd.

Table 3.8 contd.

1	2	3	4	5	6	7	8	9	10
		530	530		530	530	$t^n + l^n$	530	546
	451	451	446	449	451	451	ν_2^s	450	
group I	370	357	357	347			l_c^n	357	
					370	340	l_a^n and l_b^n		
	-	207	-	197			t_b^n or t_a^n	202	
group II					192	200	t_c^n	196	
	178	178	174	-			t_a^n or t_b^n	177	
		163?	149				$2t_b^s$	156	146
group III				149	152	152	$t_b^s + t_c^s$	151	143
	105						$t_a^s + t_b^s$	105	115
	73	73	73	-			t_b^s or t_a^s	73	
group IV					66	73	t_c^s	70	
	38	38	-	58			t_a^s or t_b^s	45	
group V	22	15	22			22	$l^s?$	20	

^aUsed to facilitate the discussion.

^bD.C.(I): a doublet component arising due to double minimum potential along N-H...O hydrogen bond; F.R.(I) and (II): two components arising from Fermi resonance between ν_3^n fundamental and $\nu_2^n + \nu_4^n$ combination modes, superscripts n and s refer to the modes of NH_4^+ and SO_4^{2-} ions, respectively, l and t represent the librational and translational modes, respectively, subscripts a, b and c distinguish the librations about or the translations along the axes parallel to the crystallographic ones, the bands corresponding to starred (*) frequencies arise due to spillover of strong bands in other polarizations.

^c ν_{av} represents the average of all frequencies of a mode.

^dHFMP = harmonic frequency of multiphonon process computed from average values of involved single phonon processes, underlined value 3108 cm^{-1} is the estimated unperturbed ν_3^n , while 3098 cm^{-1} is the HFMP ($\nu_2^n + \nu_4^n$).

TABLE 3.9

Relative FWHMI $(\Delta\nu^n/\Delta\nu^s)^a$ and intensity $(I^n/2I^s)^a$ obtained for Raman spectra of single crystal of $(\text{NH}_4)_2\text{SO}_4$, at room temperature ($\sim 300^\circ\text{K}$)

Polarization	$\Delta\nu^n/\Delta\nu^s$					$I^n/2I^s$				
	ν_1	ν_2	ν_3	ν_4	t_o	ν_1	ν_2	ν_3	ν_4	t_o
aa	26.0	3.3	3.7	3.5	3.6	0.50	0.75	0.65	0.50	0.15
bb	23.0	3.3	4.6	3.5	2.0	0.37	1.25	1.03	0.31	0.72
cc	27.0	7.5	7.6	7.0	2.0	0.56	0.25	1.50	0.32	0.83
ab	10.0	6.0	3.2	5.6	3.0	0.33	0.35	1.87	0.83	0.06
bc	10.0	4.0	5.0	6.7	2.0	0.50	0.25	1.83	0.50	0.33
ca	?	9.0	5.3	8.9	2.8	?	0.20	1.95	0.33	0.25

^aFor significance see Eqns. 3.7a and 3.7b and the related text.

TABLE 3.10

IR active phonon frequencies (in cm^{-1}) observed in IR(ATR) spectra^a of single crystal of $(\text{NH}_4)_2\text{SO}_4$ recorded at angle of incidence θ_i

$\theta_i = 40^\circ$	$\theta_i = 45^\circ$	Assignments	$\theta_i = 60^\circ$	$\theta_i = 65^\circ$	Assignments
3260 ± 10	3190 ± 5	$\nu_3^n/\nu_2^n + \nu_4^n$	1405 ± 2	1405 ± 2	ν_4^n
2990 ± 10	3020 ± 20	$\nu_3^n/\nu_2^n + \nu_4^n$	1070 ± 10	1070 ± 5	ν_3^s
	2860 ± 20	$2\nu_4^n$	610 ± 2	612 ± 2	ν_4^s

^aRecorded on ATR accessory fitted with KRS-5 by keeping (100) plane of the sample crystal in contact.

TABLE 3.11

Frequencies of phonons (in cm^{-1}) observed in Raman and IR spectra of microcrystalline $(\text{NH}_4)_2\text{SO}_4$ recorded both at RT and LT.

Raman		Assignments ^x	IR	
300°K	77°K		300°K	120°K
1	2	3	4	5
3290	3306	D.C.(I)	3300	3310
3205	3191	F.R.(I)	3200	3235 3160
3144	3117	ν_1^n	-	-
3039	3047 3025 3004	F.R.(II)	3030	3080 3040 3010
2881	2922 2845	$2\nu_4^n$	2840	2930 2855
		$2\nu_3^s$		2110
	2048	$\nu_2^n + 1^n$		2060
	1820	$\nu_4^n + 1^n$	1790	1830 1782
1671	1714 1683 1673	ν_2^n	1700	1710 1682
1460	1490 1469 1446	ν_4^n	1460	1485 1465 1445 1435 1425
1414	1423 1414		1410	1405
	1162			1150
	1147			1140
1100	1127 1081	ν_3^s	1120 1065	1120 1090
1060			1018?	1060
	1047			1038

contd.

Table 3.11 contd.

1	2	3	4	5
976	976	ν_1^s	972	972
618	628 612	ν_4^s	615 608	618 609 602
450	462 450	ν_2^s		456 445
357	387 359 339	1^n	$(335)^y$	370
	283	?	?	?
213 181	222 209 196 170	t^n	(230)	
153 106	127 100	MPP(t^s)	(140) (120) (95)	
	78 65 36	t^s	(65)	

^xD.C.(I): a doublet component arising due to double minimum potential along N-H...O hydrogen bond, F.R.(I) and (II) two components arising from Fermi resonance between ν_3^n fundamental and $\nu_2^n + \nu_4^n$ combination modes, superscripts n and s refer to the modes of NH_4 and SO_4 , respectively, MPP(t^s): multiphonon processes involving translations of SO_4 , t^s .

^yFrequencies in parentheses have been read from the spectrum (RT) reported by Nyquist and Kagel, *Infrared spectra of Inorganic Compounds*, Academic Press, New York (1971).

TABLE 3.12

Computed values of dipole moments $\vec{p}(\alpha)$, their components^x $\vec{p}_a(\alpha)$, $\vec{p}_b(\alpha)$ and $\vec{p}_c(\alpha)$ in Debye units and the spontaneous polarization $\vec{P}_c(\alpha)$ in $\mu\text{C}/\text{cm}^2$ associated with a single ion of each type^y in $(\text{NH}_4)_2\text{SO}_4$.

Phase	Ions (α)	$p(\alpha)$	$\vec{p}_a(\alpha)$	$\vec{p}_b(\alpha)$	$\vec{p}_c(\alpha)$	Contributed polarization $\vec{P}_c(\alpha)$
Paraelectric (298°K)	1	0.246	0.037	0.243	0	
	2	0.302	-0.232	-0.191	0	
	3	0.071	-0.058	-0.041	0	
Ferroelectric (180°K)	1	0.163	-0.143	0.061	-0.050	-0.13
	2	0.154	0.043	-0.084	0.122	0.32
	3	0.161	-0.113	-0.076	0.086	0.23

The net polarization $P = P_c = 0.42 \mu \text{C}/\text{cm}^2$

^xThe components \vec{p}_a , \vec{p}_b and \vec{p}_c are taken along crystallographic axes a, b and c respectively.

^yThe three distinguishable ions $\text{NH}_4^+(\text{I})$, $\text{NH}_4^+(\text{II})$ and SO_4^{2-} in the unit cell are denoted under α by numbers 1, 2 and 3 respectively.

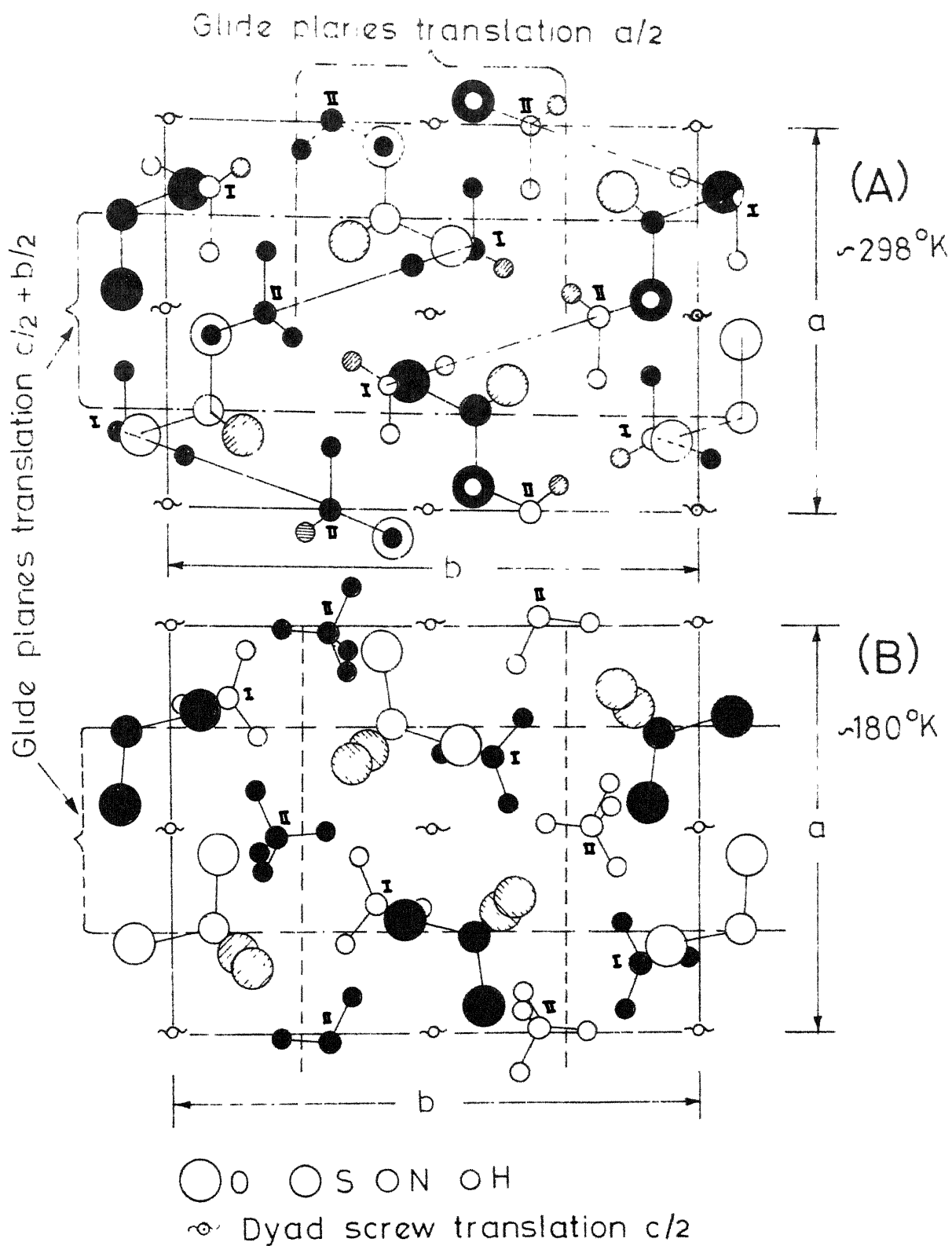
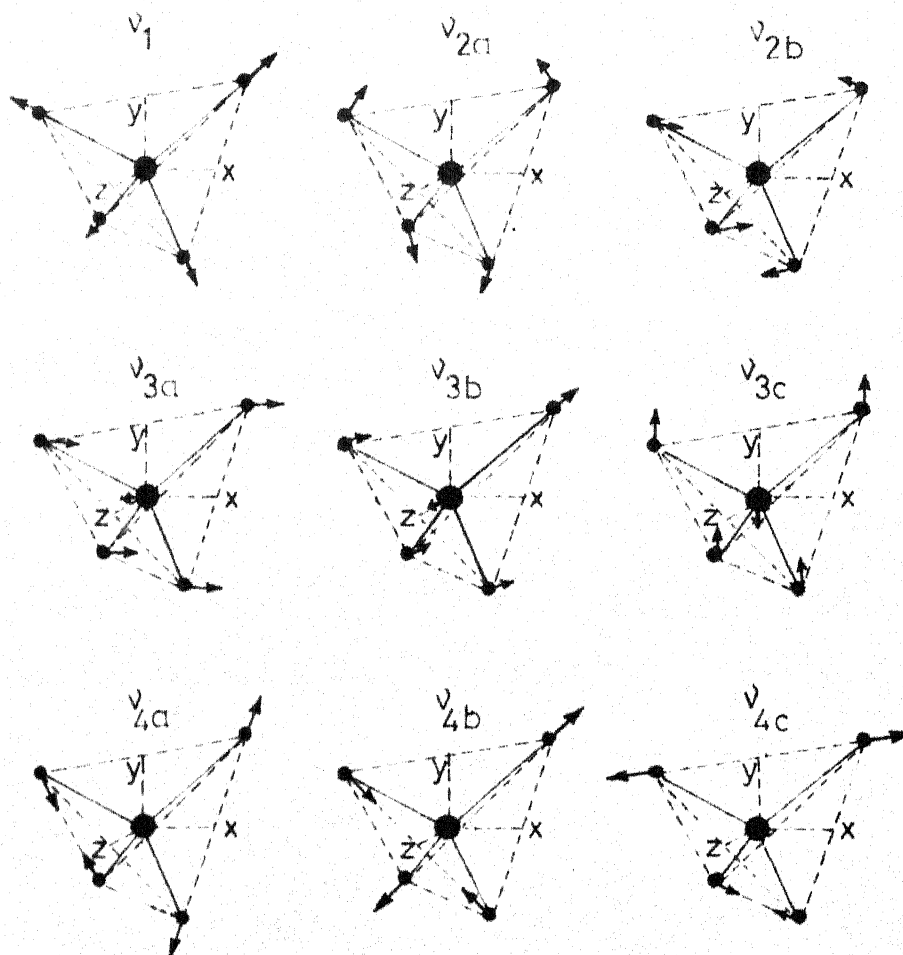


Fig. 3.1 Crystal structure of $(\text{NH}_4)_2\text{SO}_4$ projected in (001) plane (A) above T_c (B) below T_c



Frequencies of free ions from ref. 92

MODE	ν_1	ν_2	ν_3	ν_4
NH_4^+	3033	1685	3134	1397
SO_4^{2-}	981	454	1104	613

Fig. 32 Internal modes of AB_4 type tetrahedral molecule.

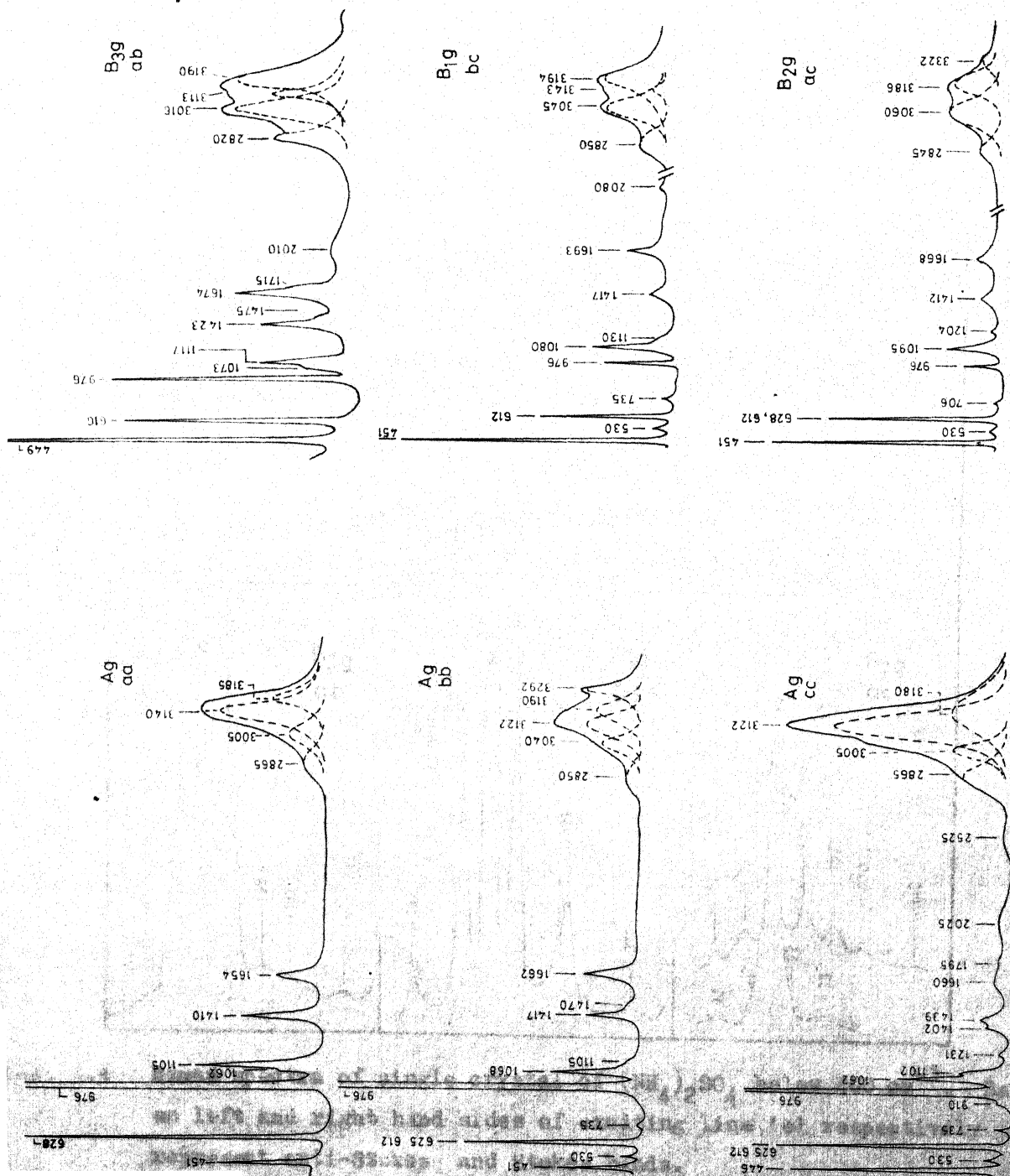


Fig. 3.3 Raman spectra of single crystal of $(\text{NH}_4)_2\text{SO}_4$ in $3400\text{--}400\text{ cm}^{-1}$ region. Two frequencies marked over some bands in $612\text{--}628\text{ cm}^{-1}$ range correspond to their two components shown in spectra on more expanded abscissa.

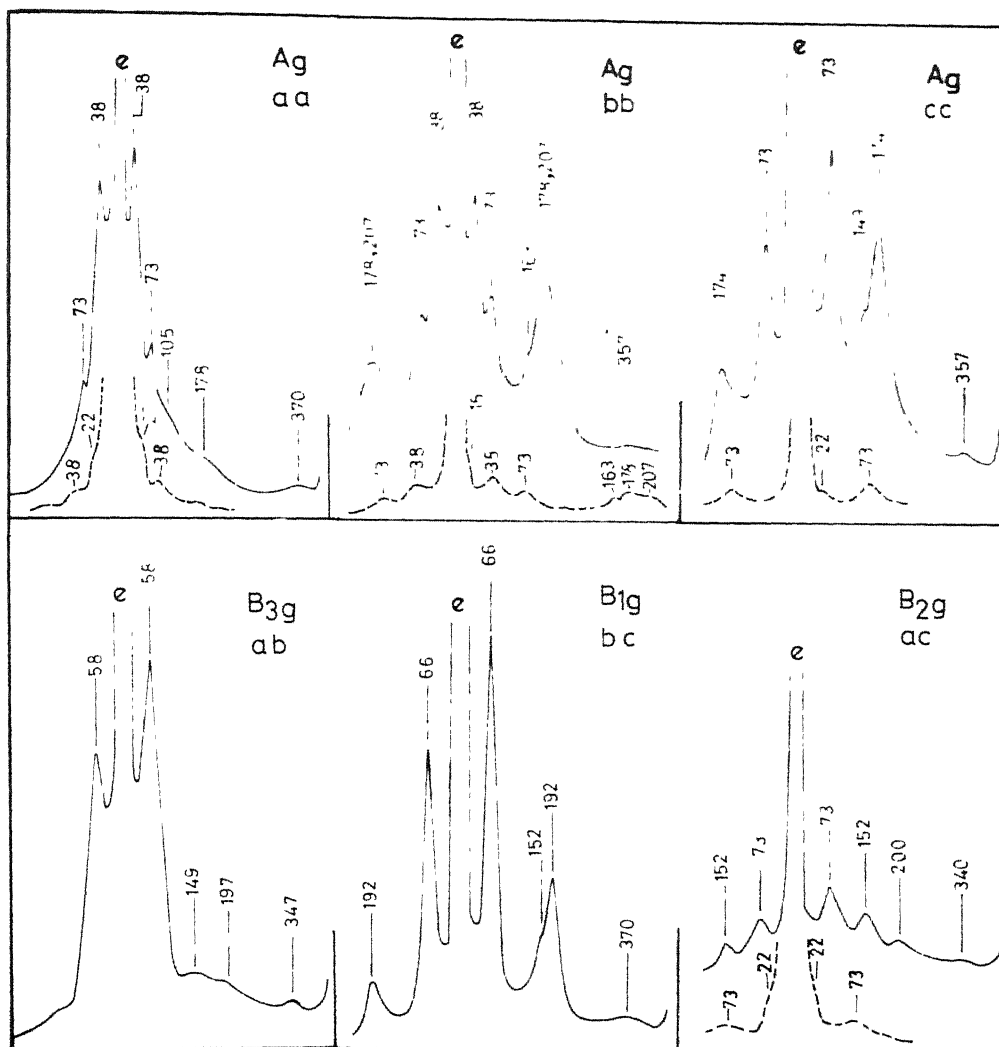


Fig. 3.4 Raman spectra of single crystal of $(\text{NH}_4)_2\text{SO}_4$ below 400 cm^{-1} . Bands on left and right hand sides of exciting line 'e' respectively represent anti-Stokes and Stokes bands.

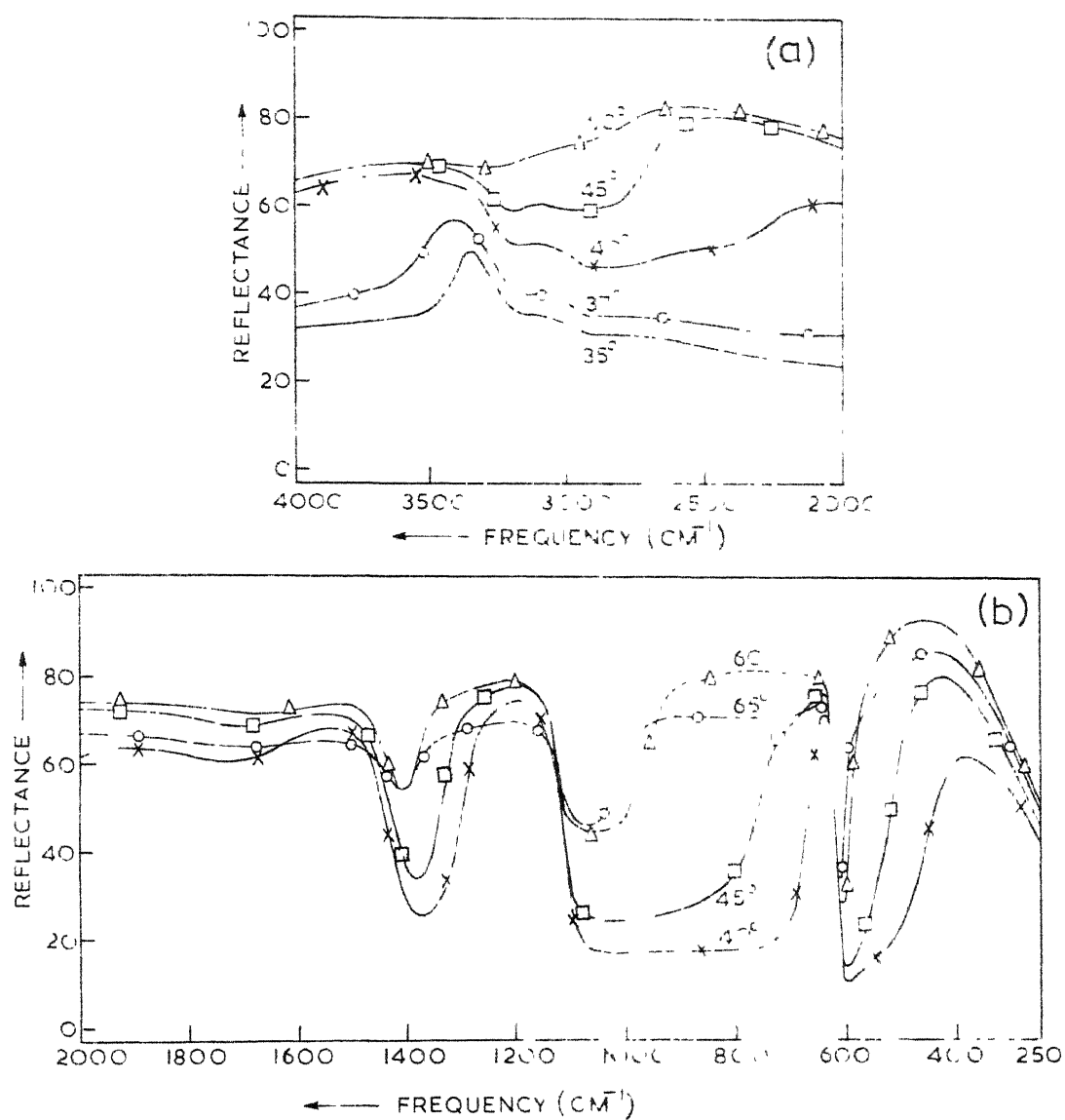


Fig. 3.5 IR (ATR) spectra of single crystal of $(\text{NH}_4)_2\text{SO}_4$ in (a) 4000-2000 cm^{-1} (b) 2000-250 cm^{-1} range recorded by keeping its (100) plane in contact with KRS-5 crystal.

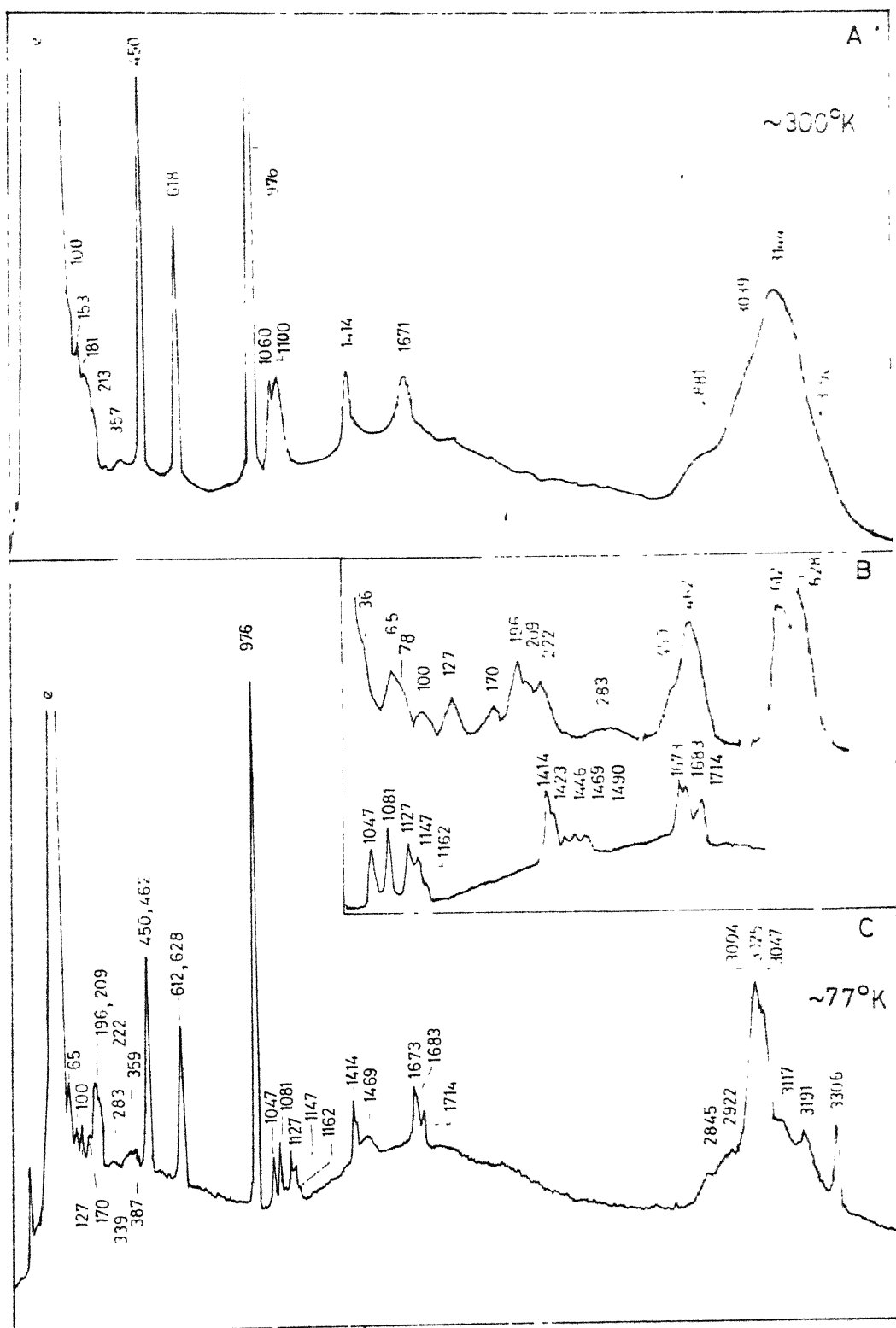


Fig. 3.6 Raman spectra of microcrystalline $(\text{NH}_4)_2\text{SO}_4$.

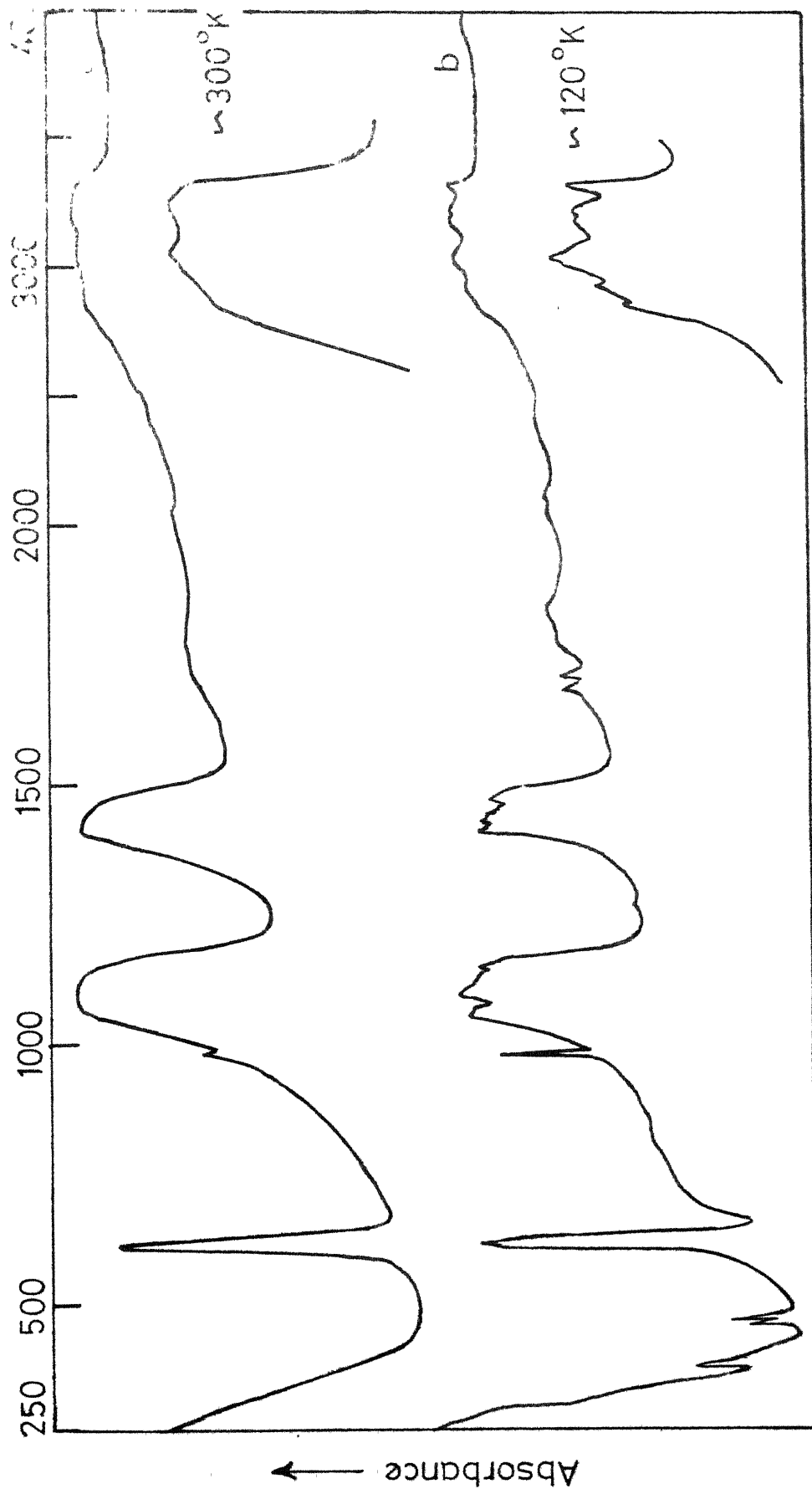


Fig. 3.7 IR spectra of low scattering microcrystalline film of $(\text{NH}_4)_2\text{SO}_4$ prepared on AgCl plate.

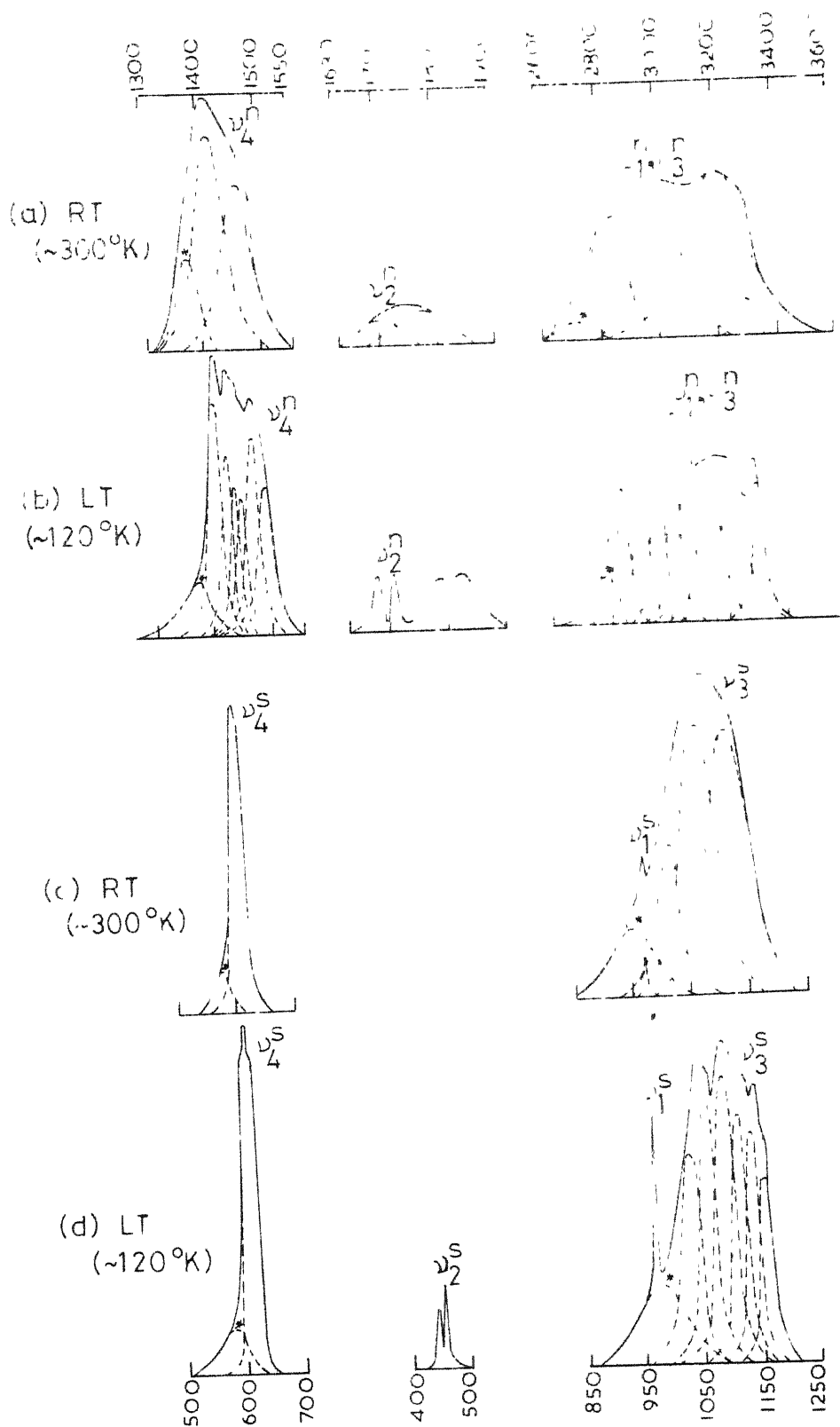


Fig.3.8 Replotted IR spectra of microcrystalline $(\text{NH}_4)_2\text{SO}_4 \cdot \text{NH}_4^+$ bands are shown in parts (a) & (b), SO_4^{2-} bands in (c) & (d). Upper frequency (cm^{-1}) scale is for (a) & (b) while the lower for (c) & (d), see also the text.

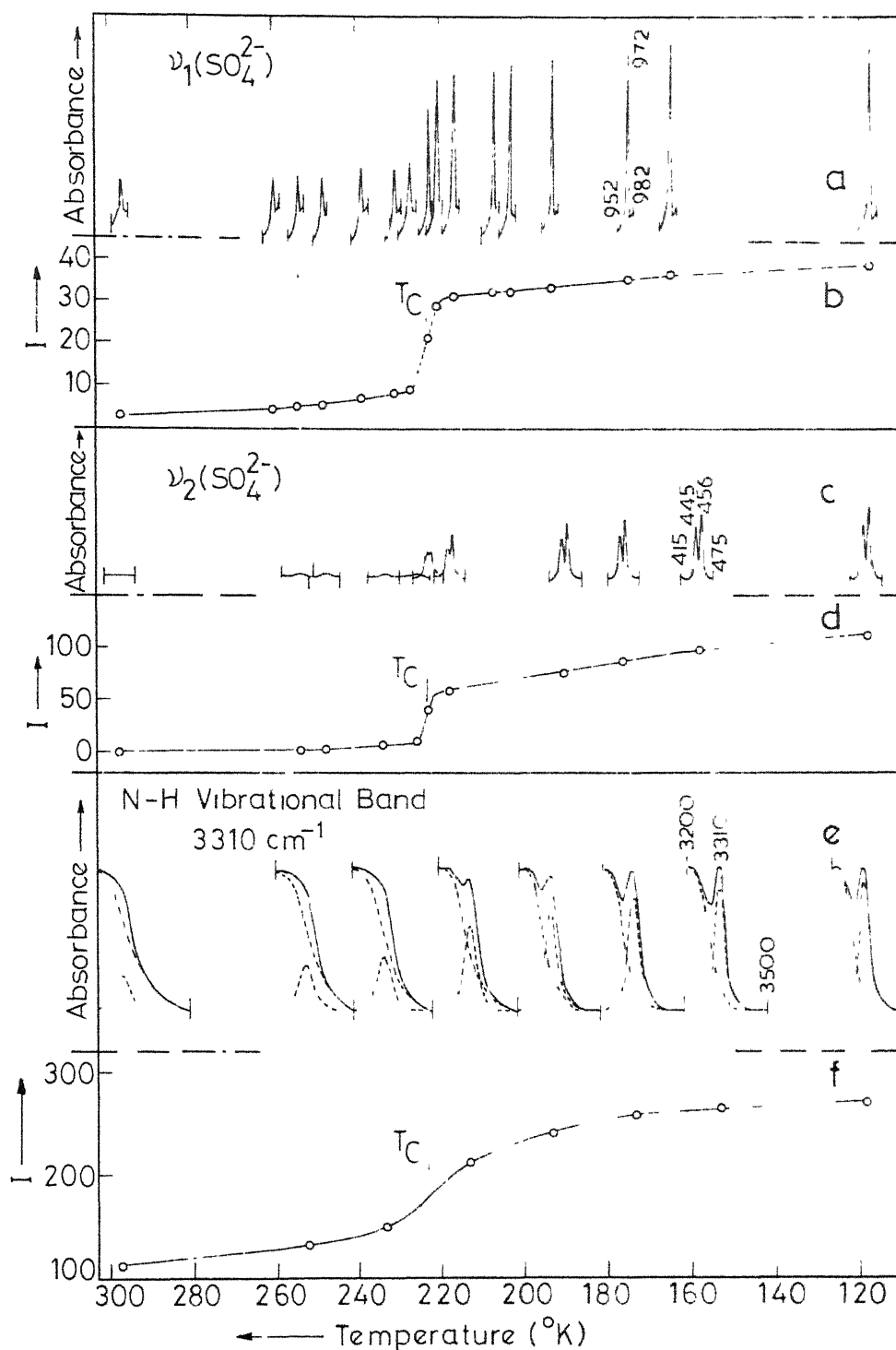
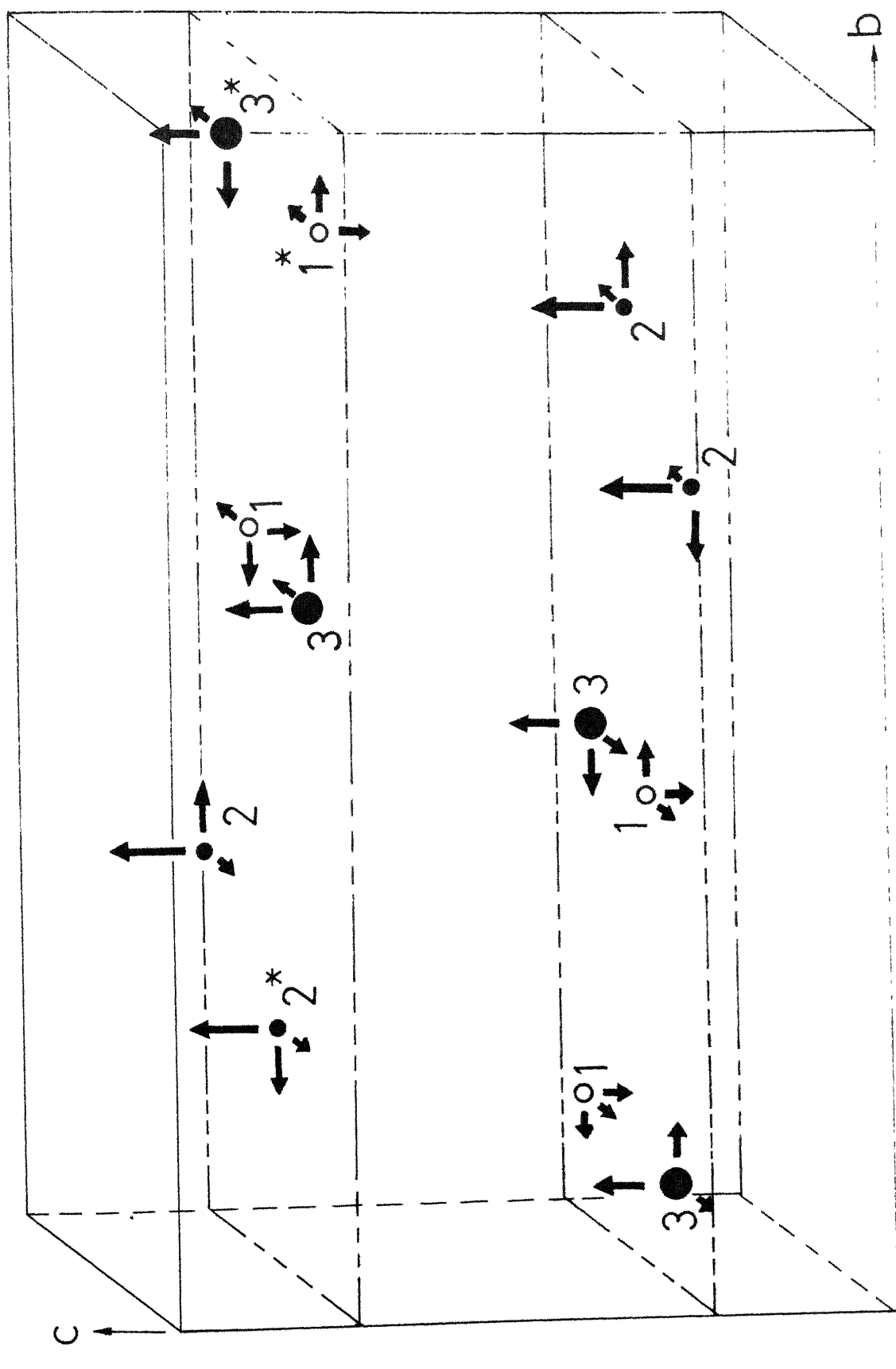


Fig. 3.9 Temperature (T) dependence of IR bands and their integrated intensities (I, in arbitrary units) in $(\text{NH}_4)_2\text{SO}_4$. Curves (b), (d) and (f) represent the variation of I in contours shown in (a), (c) & (e) respectively, with T.



a Fig. 3.10 Relative magnitudes and directions of components of dipoles $\vec{p}(\alpha)$
in the unit cell of $(\text{NH}_4)_2\text{SO}_4$ at 180°K (see also the text).

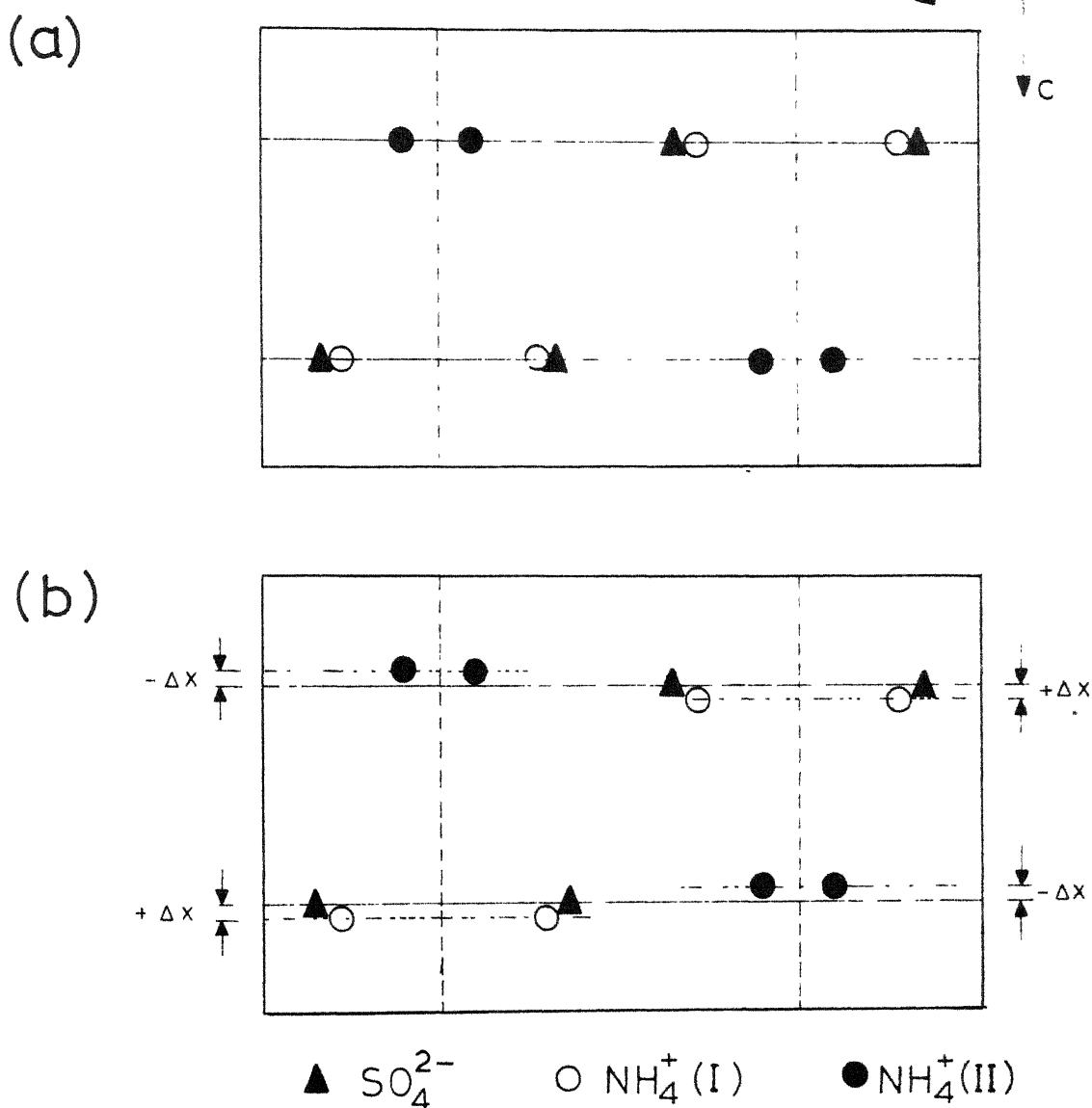


Fig. 3.11 Positions of different ions in the unit cell of $(\text{NH}_4)_2\text{SO}_4$ projected in its bc -plane. (a) Paraelectric phase and (b) ferroelectric phase, $\Delta x = 0.005c$.

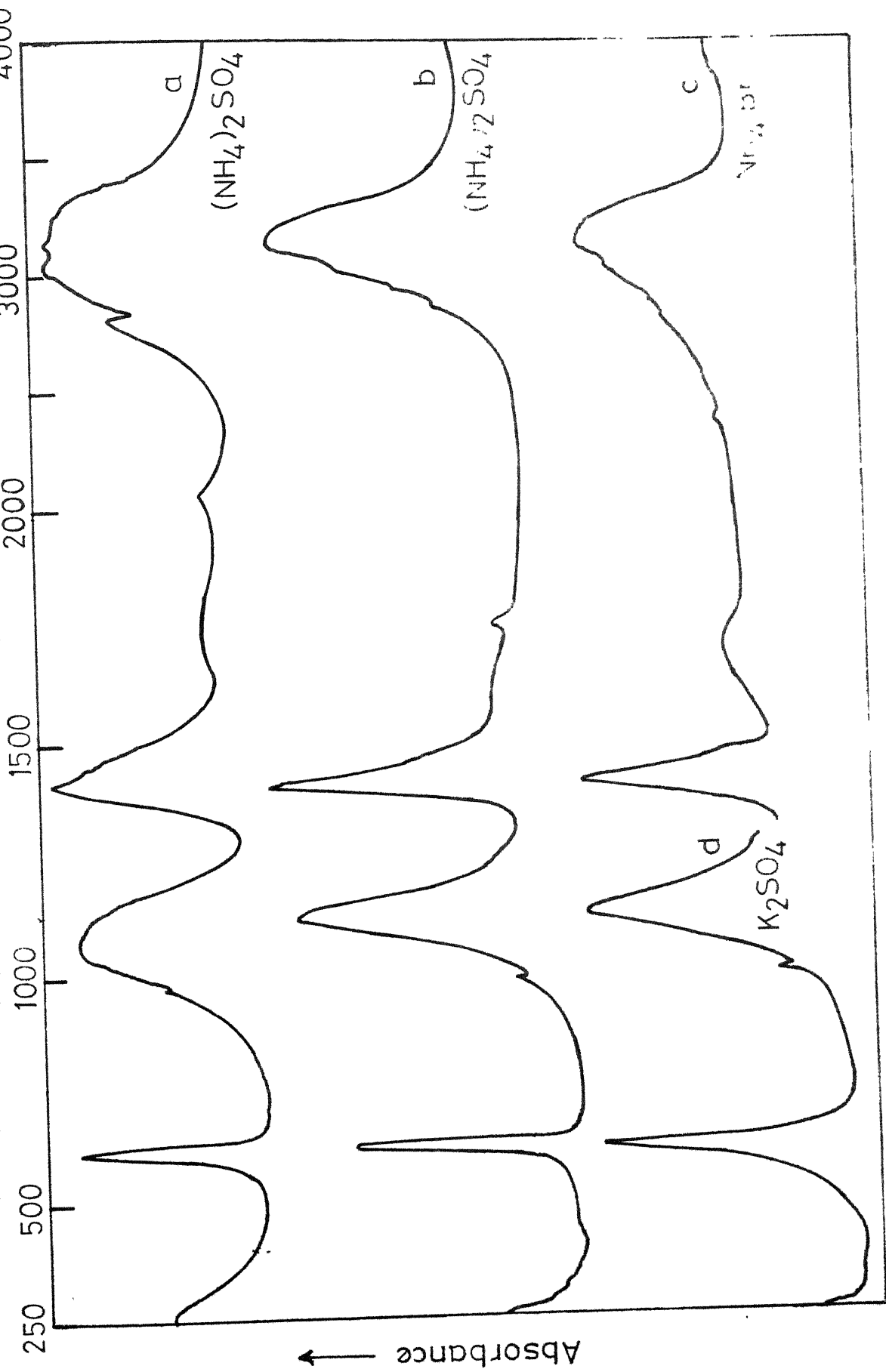


Fig. 3 12 IR spectra of indicated microcrystalline samples (a) in nujol mull

(b) (c) & (d) in KBr pellet .

APPENDIX 3.1

Frequency (ν , in cm^{-1}), relative integrated intensity (I, in parenthesis) and FWHMI of Raman bands in spectra of single crystal of ammonium sulphate

aa		bb		cc		ab		bc		ca	
ν	(I) FWHMI	ν	(I) FWHMI	ν	(I) FWHMI	ν	(I) FWHMI	ν	(I) FWHMI	ν	(I) FWHMI
1	2	3	4	5	6	7	8	9	10	11	12
		3292	(30) 60							3322	sh
3185	(35) 110	3190	(46) 120	3180	(50) 270	3190	(25) 180	3194	(35) 160	3186	(30) 150
3140	(80) 130	3122	(70) 140	3122	(90) 160	3113	(2) 60	3143	(2) 80		
3005	(30) 150	3040	(36) 110	3005	(22) 110	3016	(20) 140	3045	(30) 140	3016	(32) 170
2865	(20) 180	2850	(25) 180	2865	(25) 170	2820	(6) 110	2850	(15) 150	2845	(10) 140
				2525	df						
				2025	df	2010	(2) 250	2080	(1) 60		
				1795	df	1715	sh				
1654	(13) 50	1662	(25) 50	1660	(5) 120	1674	(7) 60	1693	(5) 40	1688	(4) 90
		1470	sh	1439	(5) 70	1475	sh				
1410	(18) 35	1417	(15) 30	1402	(2) 50	1423	(5) 45	1417	(5) 80	1412	(4) 80
				1231	(1) 35						
1105	(25) 35	1105	sh	1102	(4) 25	1117	(6) 50	1130	sh	1204	(?) ?

contd.

Appendix 3.1 contd.

1	2	3	4	5	6	7	8	9	10	11	12
1062	sh	1068	(20) 25	1062	(8) 25	1073	sh	1080	(9) 30	1095	(8) 30
976	(80) 5	976	(95) 6	976	(80) 6	976	(3) 6	976	(2) 8	976	(2) 10
				910	sh						
		735	(?) ?	735	(?) ?			735	(?) ?	706	(?) ?
628	(18) 10	625	(8) 10	625	(2) 10					628	(2) 7
		612	(16) 7	612	(9) 7	615	(3) 8	615	(5) 12	615	(6) 9
		530	(?) ?	530	(?) ?			530	(?) ?	530	(?) ?
451	(10) 15	451	(10) 15	446	(10) 16	449	(10) 10	451	(10) 10	451	(10) 10
370	df	357	df	357	df	347	df	370	df	340	df
		207	(80) 50			197	(1) 75	192	(12) 40	200	(4) 110
178	(7) 80	178	(150) 55	174	(20) 50						
105	sh	163?	sh	149	sh	149	(1) 75	152	sh	152	(5) 35
73	(8) 25	73	(60) 25	73	(12) 25			66	(18) 20	73	(8) 40
38	(15) 20	38	(100) 25			58	(8) 25				
22	sh	15	sh	22	sh					22	sh

Obtained after Lorentzian resolution although not shown in full range of observed spectra depicted in Figs. 3.3, 3.4, sh = shoulder, df = diffuse.

APPENDIX 3.2

ION EXCHANGE BETWEEN $(\text{NH}_4)_2\text{SO}_4$ AND KBr

Fig. 3.12(a) shows the IR spectrum of finely powdered $(\text{NH}_4)_2\text{SO}_4$ in Nujol mull; the spectrum of Nujol has been compensated. Fig. 3.12(b) depicts the spectrum of the sample in KBr pellet. A comparison of these two spectra clearly indicates that they are not identical to each other in position, width and intensity of different bands. The major difference is observed in latter two quantities. For example the band width of N-H stretching mode (around 3200 cm^{-1}) is about 700 cm^{-1} in the former spectrum while it is about 350 cm^{-1} in the latter. Such remarkable difference is also observed for other bands. The difference in the intensity of bands is quite visible from these spectra.

The spectra of NH_4Br and K_2SO_4 in KBr pellet are, respectively represented by curve(c) (in $4000 - 1300\text{ cm}^{-1}$ region) and curve(d) (in $1300 - 250\text{ cm}^{-1}$ region) in Fig. 3.12. The former curve depicts the bands of NH_4^+ ions while the latter depicts those of SO_4^{2-} ion. A comparison of spectra (c) + (d) with those represented by the curves (a) and (b) establishes the identity of (c) + (d) with (b). This proves that the spectrum (b) of Fig. 3.12 recorded in KBr pellet is the sum of the spectra of K_2SO_4 and NH_4Br rather than that of $(\text{NH}_4)_2\text{SO}_4$. Thus the ion exchange occurs between $(\text{NH}_4)_2\text{SO}_4$ and KBr.

APPENDIX 3.3

Frequency (ν , in cm^{-1}), relative integrated intensity (I, in parenthesis) and width (FWHMI, in cm^{-1}) of Raman and IR bands of microcrystalline ammonium sulphate at RT and LT.

Raman(RT=300°K)		Raman(LT=77°K)		IR(RT=300°K)		IR(LT=120°K)	
ν	(I) FWHMI	ν	(I) FWHMI	ν	(I) FWHMI	ν	(I) FWHMI
1	2	3	4	5	6	7	8
3290	(5) 60	3306	(4) 20	3300	(2.7) 70	3310	(5.0) 45
3205	(50) 180	3191	(35) 70	3200	(38) 240	3235	(7.0) 90
3144	(80) 140	3117	(30) 75			3160	(8.0) 35
		3047	(35) 30			3080	(5.6) 60
3039	(40) 140	3025	(40) 30	3030	(30) 200	3040	(6.0) 50
		3004	(35) 30			3010	(5.3) 55
		2922	(25) 80			2930	(5.6) 60
2881	(45) 160	2845	(15) 70	2840	(14) 140	2855	(4.7) 70
						2110	(0.3) 20
		2048	df			2060	(0.3) 20
		1820	df			1830	(2.3) 80

contd.

Appendix 3.3 contd.

1	2	3	4	5	6	7	8
				1790	(1.2) 90	1782	(2.0) 60
		1714	(1.0) 20	1700	(0.8) 70	1710	(0.5) 15
		1683	(1.0) 10			1682	(0.6) 20
1671	(10) 50	1673	(1.0) 10				
		1490	(0.5) 15			1485	(2.8) 30
1460	sh	1469	(0.5) 15	1460	(.9) 60	1465	(3.5) 25
		1446	(0.5) 15			1445	(1.8) 20
						1435	(1.5) 16
		1423	(1.0) 15			1425	(2.1) 16
1414	(.6) 35	1414	(1.0) 10	1410	(13) 55	1405	(4.2) 25
				1370	(.3) 40	1365	(1.8) 60
		1162	(0.3) 10			1150	(2.4) 20
		1147	(2.0) 20			1140	(4.4) 25
1100	(.8) 30	1127	(2.0) 15	1120	(21) 70	1120	(4.9) 25
1060	(.5) 25	1081	(2.0) 10	1065	(18) 60	1090	(8.8) 35
		1047	(2.0) 15	1018	(.6) 40	1038	(2.4) 38
976	?	976	?	972	(0.02) 5	972	(0.2) 5

contd.

Appendix 3.3 contd.

1	2	3	4	5	6	7	8
618	(10) 25	628	(5) 10	615 608	(10) 30	618 609 602	(10) 25
		612	(10) 20				
		462	(10) 10			456	(0.3) 6
450	(12) 15	450	(10) 20			445	(0.3) 12
357		387 359 339	(1.5) 80			370	(0.3) 20
		283	df				
213	sh	222	(4) 22				
		209	(2) 18				
181	sh	196	(3) 22				
153	sh	170	(1.5) 20				
		127	(2.5) 18				
100	sh	100	(2.0) 22				
		78	(2.0) 15				
		65	(2.0) 12				
		38	sh				

*For relativeness of these values see the text.

CHAPTER IV

OPTICAL PHONONS AND FERROELECTRIC
PHASE TRANSITION IN $(\text{NH}_4)_2\text{BeF}_4$ ABSTRACT

Laser excited Raman spectra of single crystal of $(\text{NH}_4)_2\text{BeF}_4$ have been investigated. These spectra have been analysed in terms of 180 phonon modes originating from different degrees of freedom of constituting ions, under the unit cell approximation. The force fields describing the dynamics of crystallographically different $\text{NH}_4^+(\text{I})$ and $\text{NH}_4^+(\text{II})$ ions in the crystal are observed to be identical to a good approximation. The ν_3 fundamental and $\nu_2 + \nu_4$ combination modes of NH_4^+ ions exhibit considerable mixing with each other as a result of resonance interaction between the two.

The IR spectra of microcrystalline $(\text{NH}_4)_2\text{BeF}_4$ in its both paraelectric and ferroelectric phases are examined. The observed spectra of NH_4^+ ions in this crystal closely resemble with those due to these ions in isostructural $(\text{NH}_4)_2\text{SO}_4$. Indications are observed

for the existence of proton tunneling along the strong N-H...F bonds in the crystal below T_c .

The BeF_4^{2-} ion, which has almost a tetrahedral structure in paraelectric phase, acquires considerable distortions in ferroelectric phase. The temperature dependence of the integrated intensity of ν_1 mode of BeF_4^{2-} ion indicates that the transition is close to being of a second order. The nature of phase transition has been critically discussed in view of all the known facts about the crystal. It is concluded that the contributions of BeF_4^{2-} ion to the spontaneous polarization of the crystal can not be neglected and the mechanism of the phase transition is not as simple as order-disorder type involving reorientation of only NH_4^+ ions.

4.1 INTRODUCTION

Ammonium tetrafluoroberyllate, $(\text{NH}_4)_2\text{BeF}_4$, is a colourless compound having molecular weight 121.09 and specific gravity 1.683. It is isostructural¹ with $(\text{NH}_4)_2\text{SO}_4$ (discussed in the preceeding chapter). $(\text{NH}_4)_2\text{BeF}_4$ and $(\text{NH}_4)_2\text{SO}_4$ exhibit various similar and dissimilar properties, e.g. (i) Both are highly soluble in water and insoluble in alcohols. (ii) $(\text{NH}_4)_2\text{BeF}_4$ also becomes ferroelectric² below 176°K showing spontaneous polarization along b-axis³ which makes 90° angle from the similar axis (i.e. c-axis) in $(\text{NH}_4)_2\text{SO}_4$. (iii) The Curie constants⁴ for both crystals are found to be of the order of 10°K. (iv) Although, the transition in both

crystals is of first order, the hysteresis curve just above T_c is observed to show a double loop in case of $(\text{NH}_4)_2\text{BeF}_4$ while a line shape in case of $(\text{NH}_4)_2\text{SO}_4$. From these considerations, studies of $(\text{NH}_4)_2\text{BeF}_4$ are as important as those of $(\text{NH}_4)_2\text{SO}_4$. However, the former crystal has been subjected to very limited investigations on: its crystal structure^{3,6-12}, its dielectric^{2,4,5,13-15}, thermodynamic¹⁴⁻¹⁷ and birefringence¹⁸⁻²⁰ properties, its ferroelectric domains²¹⁻²³ and its NMR spectra providing informations about the dynamics of proton²⁴⁻³¹, deuteron³²⁻³⁴ (in deuterated analogue) and fluorine(19)³⁵. The IR absorption spectra in $250\text{--}4000\text{ cm}^{-1}$ have so far been studied for microcrystalline samples of $(\text{NH}_4)_2\text{BeF}_4$ by Tedenac and Cot⁹ and Blinc and Levstek²⁴ without attempting their analysis. No report is available on Raman and neutron inelastic scattering spectra of this crystal. Thus extensive investigations are needed for better understanding of the dynamics and properties $(\text{NH}_4)_2\text{BeF}_4$.

Here we report the detailed study of Raman spectra of single crystal and IR spectra of microcrystalline sample of $(\text{NH}_4)_2\text{BeF}_4$. The temperature dependence of ~~some~~ thermo-sensitive IR bands has also been attempted.

4.2 CRYSTAL STRUCTURE

The crystal structure of $(\text{NH}_4)_2\text{BeF}_4$ has been investigated using X-ray^{3,6-10}, electron¹¹ and neutron¹² diffraction methods. Okaya et al³ reported that the crystal of $(\text{NH}_4)_2\text{BeF}_4$ exhibits super structure. However, all later reports⁹⁻¹² contradict the existence of super structure and support the results of earlier studies⁶⁻⁸. Accordingly, it is believed that the tetramolecular unit cell at RT belongs to the orthorhombic system

having D_{2h}^{16} (Pnam) space group symmetry isomorphous to that of $(NH_4)_2SO_4$. The crystallographic axes⁹ are found to be $a = 7.641 \pm .003$, $b = 10.437 \pm .003$ and $c = 5.922 \pm .003$ Å. Some confusion arises in the literature of K_2SO_4 type crystals owing to variations in axial notations. For orthorhombic crystals the axial notations should follow the convention* $c < a < b$ which we have used in the present study. From the isostructural behaviour of $(NH_4)_2BeF_4$ and $(NH_4)_2SO_4$ we know that (i) both NH_4^+ and BeF_4^{2-} ions occupy $C_s(\sigma_{ab})$ sites in paraelectric phase while C_1 sites in ferroelectric phase and (ii) the unit cell contains two crystallographically inequivalent NH_4^+ ions designated as $NH_4^+(I)$ and $NH_4^+(II)$. This is corroborated by the magnetic resonance studies, e.g.³⁰.

4.3 PHONON BRANCHES IN THE CRYSTAL

The dynamics of $(NH_4)_2BeF_4$ crystal can be understood in terms of 180 phonon branches (177 optical + 3 acoustical) arising from different normal modes of $NH_4^+(I)$, $NH_4^+(II)$ and BeF_4^{2-} tetrahedra. The IR and Raman activity and the description of the normal modes of such tetrahedral units have already been discussed (cf section 3.3).

4.4 CLASSIFICATION OF PHONONS

It is evident that $(NH_4)_2BeF_4$ crystal can be obtained on replacing SO_4^{2-} ion in $(NH_4)_2SO_4$ by BeF_4^{2-} . Thus the classification of 180 phonon modes in $(NH_4)_2BeF_4$ can be found in Tables 3.2 and 3.6 for its paraelectric phase and in Tables 3.3 and 3.7 for ferroelectric phase. However, it must be noted (while consulting these tables) that every mode of SO_4^{2-} ion is to be considered that of BeF_4^{2-} .

*J.D.H. Dornay and W. Nowacki, Crystal Data, Geological Society of America, Memoir 60, New York (1954).

4.5 FORMS OF RAMAN TENSOR COMPONENTS

The forms of Raman tensor components discussed in section 3.5 are useful for the study of Raman spectra of $(\text{NH}_4)_2\text{BeF}_4$ crystal, since this crystal is isostructural with $(\text{NH}_4)_2\text{SO}_4$. Therefore, here also the six different spectra recorded in appropriate geometries may be sufficient to study the Raman active phonon modes.

4.6 EXPERIMENTAL

a. Purification of Sample

$(\text{NH}_4)_2\text{BeF}_4$ was obtained from Alfa Inorganics Inc. Massachusetts. It was purified by its crystallization several times from the aqueous solution prepared in distilled deionized water by slow evaporation at RT ($\sim 300^\circ\text{K}$).

b. Growth of Single Crystal

Single crystals of $(\text{NH}_4)_2\text{BeF}_4$ were obtained by seed suspension technique using the solution of the purified sample, which was allowed to evaporate slowly at RT. A good single crystal of about $2 \times 20 \times 12 \text{ mm}^3$ size was obtained in about a month.

c. Determination of Crystallographic Axes

The crystallographic axes were first identified by using the knowledge of crystal morphology³⁶. The existence of perfect cleavage along (100) planes helps considerably in this identification. The axes thus determined were confirmed by X-ray diffraction method (Laue pattern).

d. Scan of Raman Spectra

Twelve spectra were recorded in different geometries (cf Fig.2.7) using 4880 Å emission line from an argon ion laser as a source of excitation. Spex-1400 double monochromator was used to analyse the scattered radiations. Detailed discussions are given in section 2.7 and 2.8.

e. Scan of IR Spectra of Microcrystalline Sample

The IR spectra of microcrystalline $(\text{NH}_4)_2\text{BeF}_4$ were recorded in the manner as discussed in detail for $(\text{NH}_4)_2\text{SO}_4$ (cf section 3.7d).

4.7 RESULTS AND DISCUSSION

I. RAMAN PHONONS IN SINGLE CRYSTAL

a. Observed Spectra

As expected theoretically for a crystal of D_{2h} symmetry, six different spectra were observed corresponding to six independent components of polarizability tensor. Representatives of these spectra are shown in Figs. 4.1 to 4.4. In these figures aa, bb, cc, etc. represent the polarization characters of the spectra, while A_g , B_{1g} , etc. represent the corresponding symmetry species of D_{2h} point group.

Fig. 4.1 depicts spectra in N-H stretching region (i.e 2700 - 3500 cm^{-1}). The dotted curves represent the resolved band structure, having Lorentzian shapes. Spectra of A_g modes characterizing aa, bb and cc polarizations are shown in Fig. 4.2, while those of B_{3g} , B_{1g} and B_{2g} modes (characterizing ab, bc and ca polarizations respectively) in Fig. 4.3. In order to visualize the details of lattice mode region,

spectra recorded in appropriate conditions are shown in Fig. 4.4.

b. Frequency, Width and Intensity of Bands

Appendix 4.1 provides the frequency (ν), relative integrated intensity (I, in parenthesis) and width (FWHM, $\Delta\nu$) of various bands in observed spectra. The ν values are accurate to within $\pm 2 \text{ cm}^{-1}$ for sharp bands and $\pm 10 \text{ cm}^{-1}$ for broad bands. The I values were first determined by multiplying the corresponding $\Delta\nu$ and peak height of bands. These values as given in the appendix are relative to an arbitrarily chosen intensity 10 of a band appearing within $3230 \pm 22 \text{ cm}^{-1}$ and the other appearing within $1688 \pm 11 \text{ cm}^{-1}$ for bands of $3500 - 2700 \text{ cm}^{-1}$ and $1800 - 30 \text{ cm}^{-1}$ regions respectively. The errors in I values lie within 5% for well developed strong bands and 20% for weak, broad and manually resolved bands.

c. Assignments

The assignments for observed Raman shifts are given in Table 4.1. The average frequencies (ν_{av}) of assigned modes are given in column 9 of this table. The ν_{av} values of single phonon processes have been used to compute the harmonic frequencies of multiphonon processes (HFMP) which are given in column 10.

As found in $(\text{NH}_4)_2\text{SO}_4$, a critical examination of observed Raman spectra of $(\text{NH}_4)_2\text{BeF}_4$ reveals that $\text{NH}_4^+(\text{I})$ and $\text{NH}_4^+(\text{II})$ exhibit almost identical force fields. The spectra may therefore be analysed as arising due to one type of NH_4^+ ion to a good approximation. The modes of NH_4^+ and BeF_4^{2-} have been distinguished by using superscripts n and b, respectively. Though a detailed discussion of IR spectra of microcrystalline $(\text{NH}_4)_2\text{BeF}_4$ would be made in section 4.7(II) but the observed spectra (cf Fig. 4.5)

and band positions (cf Table 4.2) may be referred in the following discussion.

Internal Modes of NH_4^+ Ion: In $3500 - 2700 \text{ cm}^{-1}$ region, the ν_1^n and ν_3^n fundamentals are expected alongwith $2\nu_2^n$, $\nu_2^n + \nu_4^n$ and $2\nu_4^n$ modes. It is observed that four bands centred around their average frequencies ν_{av} at 3228 , 3125 , 3040 and 2858 cm^{-1} appear in this region. This becomes more clear when band envelopes observed in spectra (cf Fig 4.1) of different polarizations are resolved into Lorentzian components. For convenience of the discussion bands observed in this region have been designated as w-, x-, y- and z- bands (cf column 1, Table 4.1).

The x- bands appear as the strongest bands in aa, bb and cc polarized spectra. These bands have been associated with ν_1^n mode as it is expected to be stronger than all other modes falling in the N-H stretching region of these spectra. This assignment is also corroborated by the fact that any strong band does not appear near 3125 cm^{-1} in IR spectra where this mode is forbidden for tetrahedral NH_4^+ ion. The classification of phonons arising due to this mode also allows its one component in ab polarized spectrum where it may be assigned to weak x- band at 3122 cm^{-1} . The spectra of bc and ca polarizations also indicate the appearance of weak bands near 3133 and 3160 cm^{-1} , respectively. One of the origins for these bands could be the spillover of strong ν_1^n band from other polarizations. The z- bands ($\nu_{av} = 2858 \text{ cm}^{-1}$) may be associated with $2\nu_4^n(A_1 + E + E_1 + E_2)$ having computed harmonic frequency, 2864 cm^{-1} .

The remaining w- and y- bands are respectively observed to have $\nu_{av} = 3228$ and 3040 cm^{-1} . According to the theoretical analysis (cf Table 3.7), both these bands in spectra of A_g and B_{3g} modes can be

associated with components of ν_3^n mode of appropriate symmetry. However, ν_3^n mode has only one component of each of the E_{1g} and B_{2g} species, therefore one of the w- and y- bands must have some other origin. Here we note that the computed harmonic frequency of $\nu_2^n + \nu_4^n$ ($\sim 3112 \text{ cm}^{-1}$) falls reasonably close to the centre ($\sim 3134 \text{ cm}^{-1}$) of w- and y- bands. This indicates that F_2 component of $\nu_2^n + \nu_4^n(F_1 + F_2)$ combination possibly undergoes Fermi interaction with $\nu_3^n(F_2)$ fundamental. Thus w- and y- bands have been associated with mixed modes (designated as F.R.(I) and F.R.(II)) of ν_3^n and $\nu_2^n + \nu_4^n$. Since the w- band has more intensity on the average in comparison to y- band, ν_3^n fundamental may be regarded as having more contribution to F.R.(I) assigned to the former band. The unperturbed ν_3^n is also considered to be more close to the w- band i.e. higher than the centre ($\sim 3134 \text{ cm}^{-1}$) of w- and y- bands. Thus ν_3^n has higher frequency than ν_1^n in the RT phase of $(\text{NH}_4)_2\text{BeF}_4$. This is an usual observation but is different from that ($\nu_3^n < \nu_1^n$) observed in the isostructural $(\text{NH}_4)_2\text{SO}_4$. Unlike $(\text{NH}_4)_2\text{SO}_4$ a sharp intense band like the v- band (3292 cm^{-1}) is also not observed in any spectrum of $(\text{NH}_4)_2\text{BeF}_4$. This perhaps indicates that the observation of v- band was correctly correlated with the observation of $\nu_3^n < \nu_1^n$ in $(\text{NH}_4)_2\text{SO}_4$ crystal.

The ν_2^n mode has been assigned to bands centred around 1688 cm^{-1} . In spectra of aa, bb, cc and bc polarizations, this mode exhibits a single band. However, in ab polarized spectrum two distinct bands are observed at 1679 and 1720 cm^{-1} and in ca polarized spectrum, the strong band of 1678 cm^{-1} has weak shoulder at 1708 cm^{-1} . Under the assumption of identical force fields for $\text{NH}_4^+(\text{I})$ and $\text{NH}_4^+(\text{II})$ (as it seems to be consistent with observed spectra in other regions) both these bands of ab and ca

polarizations can not be attributed to ν_2^n mode, since this mode is expected to show only one component in each Raman spectrum. However, all frequencies 1679, 1720, 1678 and 1708 cm^{-1} are quite reasonable for ν_2^n mode in view of its 1685 cm^{-1} frequency for isolated NH_4^+ ion³⁷. Moreover, the other possible mode $\nu_4^n + l^n$, which could be assigned to 1720(ab) and 1708(ac) cm^{-1} bands, is observed at 1795 cm^{-1} in IR spectrum (cf Fig. 4.5b). This indicates that the assignment of $\nu_4^n + l^n$ mode for 1720(ab) and 1708(ac) cm^{-1} is not more appropriate. Thus it seems more reasonable to state that these bands also arise due to ν_2^n mode and the assumption of identical force fields for $\text{NH}_4^+(\text{I})$ and $\text{NH}_4^+(\text{II})$ does not hold here as an exception.

The ν_4^n mode has been assigned to the bands falling in 1413 - 1459 cm^{-1} range. The number of bands for ν_4^n in each spectrum are found to be consistent with allowed number of components in each polarization under the assumption of identical force fields for $\text{NH}_4^+(\text{I})$ and $\text{NH}_4^+(\text{II})$ ions.

Internal Modes of BeF_4^{2-} Ion: Quist et al³⁸ investigated Raman spectra of $(\text{NH}_4)_2\text{BeF}_4$ in dilute aqueous solution and Li_2BeF_4 and Na_2BeF_4 in melts. From the first spectrum the frequencies of ν_1^b , ν_3^b and ν_4^b modes are reported to be 548, 795 and 380 cm^{-1} , respectively; the ν_2^b mode, which is not observed in this spectrum has a frequency around 255 cm^{-1} as observed in other spectra. The following assignments of these modes of BeF_4^{2-} in $(\text{NH}_4)_2\text{BeF}_4$ are found to be consistent with these frequencies.

In our spectra of $(\text{NH}_4)_2\text{BeF}_4$ single crystal, the sharpest (FWHMI = 11 cm^{-1}) band appears at 558 cm^{-1} exhibiting maximum intensity in aa, bb and cc polarizations. The intensity becomes very low in spectra of ab and bc polarizations. Such a behaviour of 558 cm^{-1} band reveals

that it arises due to ν_1^b mode and indicates that BeF_4^{2-} exhibits tetrahedral symmetry to a good approximation in paraelectric phase of $(\text{NH}_4)_2\text{BeF}_4$. This inference is confirmed by its remarkably low intensity in IR spectrum (cf Fig. 4.5b, the band at 553 cm^{-1}). The ν_1^b mode is group theoretically allowed only in spectra of A_g and B_{3g} modes. Therefore, it may be argued that very weak band at 558 cm^{-1} in spectrum of B_{1g} modes arises due to the spillover of strong A_g bands.

Theoretically, the ν_3^b mode must show two bands in each spectrum of A_g and B_{3g} modes while one in each of the B_{1g} and B_{2g} . However, the observed spectra of A_g and B_{1g} modes show only one band having $\nu_{av} = 791\text{ cm}^{-1}$; no band is observed due to two B_{3g} and one B_{2g} components in respective spectra. This observation may be attributed to either the overlap of $2A_g$ components or the low scattering efficiency of ~~the~~ absent components. The strong IR band observed at 790 cm^{-1} confirms this assignment.

The ν_4^b mode has been attributed to bands having $\nu_{av} = 388\text{ cm}^{-1}$. Only cc polarized spectrum of A_g modes shows two allowed components separately at 402 and 381 cm^{-1} . In other spectra of A_g and B_{3g} modes two allowed components of this mode appear as a single band. The reason for it could be either the low scattering efficiency of one component or the overlap of both components of similar species. In bc and ac polarized spectra, this mode has a single band (as expected) at 385 and 379 cm^{-1} , respectively. This mode is also allowed in IR spectrum. Thus a good intensity band observed at 375 cm^{-1} (cf Fig. 4.5b) confirms this assignment.

One band in each of the six Raman spectra is observed due to ν_2^b around 273 cm^{-1} as expected group theoretically. This mode is not allowed

in IR spectra under perfect T_d symmetry of BeF_4^{2-} . It may, therefore, assume only very weak absorption which may be obscured by strong IR band arising due to translations of NH_4^+ ion expected to fall below 250 cm^{-1} .

Additional Bands: In addition to the above discussed bands, weak and sharp ($\text{FWHMI} \sim 8\text{ cm}^{-1}$) bands are observed at 981 cm^{-1} in spectra of A_g and B_{3g} modes. Very weak bands also appear around 463 cm^{-1} in bb, ab, bc and ca polarized spectra and around 627 cm^{-1} in aa, bb, cc, ab and bc polarized spectra. The IR spectra (cf Fig. 4.5) also show additional weak bands at 1100 and 620 cm^{-1} . In view of the intensity and positions, these bands in both Raman and IR spectra seem to arise due to internal modes of SO_4^{2-} ion which is probably contained as an impurity in the commercially purchased sample from Alfa Inorganics. This impurity remained in the crystal of $(\text{NH}_4)_2\text{BeF}_4$ even after the repeated crystallization. The reason for it probably lies in the fact that $(\text{NH}_4)_2\text{SO}_4$ and $(\text{NH}_4)_2\text{BeF}_4$ are isostructural having almost equal lattice parameters. $(\text{NH}_4)_2\text{BeF}_4$ was therefore purchased from K and K Laboratories, New York. This sample was also found to show SO_4^{2-} impurity. Gravimetric analysis of $(\text{NH}_4)_2\text{BeF}_4$ sample (used in the present investigations) to find SO_4^{2-} ion concentration following the usual method of BaCl_2 treatment could not be possible because BaBeF_4 also gets precipitated. The extent of impurity of SO_4^{2-} ion was therefore estimated in the following manner.

According to the informations furnished by Alfa Inorganics, the purity of their supplied $(\text{NH}_4)_2\text{BeF}_4$ lies between 97-99%. Considering the total impurity due to SO_4^{2-} ion only as $(\text{NH}_4)_2\text{SO}_4$, it can be shown that SO_4^{2-} contents in our sample lie between 2.18 - 0.73%. For the following discussion we consider it to be the maximum i.e. 2.18%.

In the presence of this impurity it is very much desirable to discuss its effects on observed spectra. Noting that BeF_4^{2-} and SO_4^{2-} have molecular weight around 85 and 96 amu, respectively, it can be asserted that 2 out of 100 BeF_4^{2-} ions are replaced by SO_4^{2-} ions in our crystal. In other words every 12 unit cell contains one SO_4^{2-} ion on the average. This implies that one SO_4^{2-} ion from the other is separated by **3-4** lattice parameters, if uniform distribution is assumed. Additionally we note that both BeF_4^{2-} and SO_4^{2-} ions are tetrahedral units of the same ionic character and both $(\text{NH}_4)_2\text{BeF}_4$ and $(\text{NH}_4)_2\text{SO}_4$ are isostructural having almost equal lattice parameters. Therefore it would be reasonable to state that this impurity would not affect the spectra of internal modes of NH_4^+ and BeF_4^{2-} ions. This is also evident from the simple structure of bands arising due to such modes.

Librational Modes of NH_4^+ and BeF_4^{2-} Ions: These modes are expected to be weak in both Raman and IR spectra, since for perfect T_d symmetry they are forbidden. In isostructural $(\text{NH}_4)_2\text{SO}_4$, l^n modes have been observed in $370 - 340 \text{ cm}^{-1}$ range (cf Table 3.8). In the IR spectrum (cf Fig. 4.5b) of $(\text{NH}_4)_2\text{BeF}_4$, the combination $\nu_4^n + l^n$ appears at 1795 cm^{-1} from which the frequency of l^n mode is deduced to be 370 cm^{-1} under the harmonic approximation. No clear band is observed around 370 cm^{-1} in our Raman spectra of $(\text{NH}_4)_2\text{BeF}_4$ perhaps because weak l^n modes may be obscured by strong bands appearing due to ν_4^b (388 cm^{-1}) and ν_2^b (273 cm^{-1}) on both high and low frequency sides. A critical examination of these spectra indicates three weak shoulders at $315(\text{cc})$, $328(\text{ab})$ and $315(\text{ca}) \text{ cm}^{-1}$ which are close to 370 cm^{-1} within the error limits of these frequencies and may therefore be attributed to l^n modes.

Translations of NH_4^+ Ions: In isostructural $(\text{NH}_4)_2\text{SO}_4$, t^n modes are observed as strong Raman bands in $170\text{--}210\text{ cm}^{-1}$. In view of this knowledge, t^n modes in $(\text{NH}_4)_2\text{BeF}_4$ have been assigned to strong bands having frequencies lower than those observed due to ν_2^b ($\sim 273\text{ cm}^{-1}$). Such strong bands are observed in $145\text{--}197\text{ cm}^{-1}$ range.

Translations of BeF_4^{2-} Ion: The translatory lattice vibrations t^b in $(\text{NH}_4)_2\text{BeF}_4$ crystal may be expected to have frequencies close to those of t^s (translations of SO_4^{2-} ion) in isostructural $(\text{NH}_4)_2\text{SO}_4$. The t^s modes appear as strong and distinct bands in $38\text{--}76\text{ cm}^{-1}$ range in Raman spectra of latter crystal (cf Table 3.8). Thus t^b modes in $(\text{NH}_4)_2\text{BeF}_4$ are assigned to the strong bands appearing in $30\text{--}60\text{ cm}^{-1}$ range. However, these bands exhibit weak shoulders on their low and high frequency sides. These shoulders perhaps arise due to SO_4^{2-} impurity in our crystal.

II IR SPECTRA OF MICROCRYSTALLINE $(\text{NH}_4)_2\text{BeF}_4$

a. Observed Spectra

Fig. 4.5(a) depicts the IR absorption spectrum in $4000\text{--}250\text{ cm}^{-1}$ range recorded in mull of $(\text{NH}_4)_2\text{BeF}_4$; spectra (b) and (c) were recorded for low scattering microcrystalline film of the sample at RT ($\sim 300^\circ\text{K}$) and LT ($\sim 120^\circ\text{K}$), respectively. The base line in latter two spectra shifts downward with decreasing frequency on absorbance scale. This arises because of general scattering of the film. Choosing an appropriate base line, both these spectra were retraced on horizontal base and observed bands were appropriately resolved into Lorentzian components in a manner shown in Fig. 3.8 for similar spectra of $(\text{NH}_4)_2\text{SO}_4$.

b. Frequency, Width and Intensity of Bands

Frequency(ν), width (FWHMI, $\Delta\nu$) and relative integrated intensity(I) of bands observed in IR spectra of microcrystalline $(\text{NH}_4)_2\text{BeF}_4$ are given in Appendix 4.2. The ν values are accurated within $\pm 2 \text{ cm}^{-1}$ for sharp bands and within $\pm 10 \text{ cm}^{-1}$ for broad bands. The I values as given in the appendix are relative to the arbitrarily chosen intensity(10) of bands at 790 cm^{-1} in RT spectrum and at 800 cm^{-1} in LT spectrum. These values may have uncertainties of about 5% for isolated band and about 20% for manually resolved bands.

c. Assignments

In N-H stretching region of IR spectrum(RT), three bands are observed at 3240 , 3040 and 2860 cm^{-1} . First two bands have been assigned to Fermi components, F.R.(I) and F.R.(II), arising due to resonance interaction between ν_3^n fundamental and $\nu_2^n + \nu_4^n$ combination modes. The 3240 cm^{-1} band is slightly more intense than 3040 cm^{-1} band which is consistent with our inference "that ν_3^n fundamental perhaps contributes more to F.R.(I) falling around 3240 cm^{-1} " drawn from the analysis of Raman spectra.

In IR spectrum recorded at LT, 3240 cm^{-1} band splits into two components at 3260 and 3180 cm^{-1} while 3040 cm^{-1} band into three components at 3100 , 3035 and 2980 cm^{-1} . The sum of the integrated ^{intensity} of latter three components is observed to be more than that of the former two. This perhaps indicates that in LT phase ν_3^n fundamental contributes more to F.R.(II) and its unperturbed frequency lies below the centre ($\sim 3140 \text{ cm}^{-1}$) of F.R.(I) and F.R.(II). Thus the ν_3^n is found to shift towards lower frequency side on cooling the crystal, indicating that H-bonds in ferroelectric phase become more strong and unperturbed ν_3^n has frequency lower

than ν_1^n in LT phase. It is perhaps corroborated by the observation of 3315 cm^{-1} band which seems to be analogous to 3310 cm^{-1} band observed in IR spectrum (LT) of $(\text{NH}_4)_2\text{SO}_4$ indicating that the former band is also a component D.C.(I) of doublet arising due to proton tunneling along strong N-H...F bonds. The $2\nu_4^n$ mode falling at 2860 cm^{-1} in RT spectrum splits into two components at 2920 and 2850 cm^{-1} in LT spectrum. The ν_2^n mode, which gives rise to weak and diffuse band around 1675 cm^{-1} at RT, shows a weak but well shaped band at the same frequency. The ν_4^n mode at RT shows a strong band which seems to have three components around 1465 , 1415 and 1372 cm^{-1} . Six components are observed due to this mode in LT spectrum. The ν_3^b mode also shows a broad and strong band at 790 cm^{-1} in RT spectrum. The asymmetric structure of the corresponding band observed in LT spectrum indicates that this mode splits into three components (845 , 800 and 750 cm^{-1}) in ferroelectric phase. The strong IR band at 370 cm^{-1} both in RT and LT spectra arises due to ν_4^b mode while the weak and sharp band at 553 cm^{-1} due to ν_1^b mode. Few remaining weak bands are associated with multiphonon processes; the assignments of $\nu_2^n + 1^n$ and $\nu_4^n + 1^n$ modes (cf Table 4.2) reveal that 1^n modes have frequencies lying in $360\text{--}380\text{ cm}^{-1}$ region.

Finally by comparing the Raman and IR spectra of NH_4^+ modes in $(\text{NH}_4)_2\text{BeF}_4$ with respective ones in isostructural $(\text{NH}_4)_2\text{SO}_4$ crystal, we observe that these spectra are identical to a good approximation. Few dissimilarities are: (i) that the unperturbed ν_3^n at RT in the former crystal has higher frequency than that in the latter, (ii) that ν_3^n mode in $(\text{NH}_4)_2\text{BeF}_4$ is observed to have higher frequency than ν_1^n , while an opposite situation seems to exist in $(\text{NH}_4)_2\text{SO}_4$, (iii) that the force fields describing ν_2^n mode of $\text{NH}_4^+(\text{I})$ and $\text{NH}_4^+(\text{II})$ in $(\text{NH}_4)_2\text{BeF}_4$ are slightly different but are almost identical in $(\text{NH}_4)_2\text{SO}_4$ and (iv) that in ferroelectric phase

ν_2^n mode shows single weak band in IR spectrum of $(\text{NH}_4)_2\text{BeF}_4$ but two weak bands in that of $(\text{NH}_4)_2\text{SO}_4$. From these observations it may be inferred that on an average the H-bonds in $(\text{NH}_4)_2\text{BeF}_4$ are slightly weaker than those in $(\text{NH}_4)_2\text{SO}_4$ and the distortions in both types of NH_4^+ ions in former crystal are slightly different from those in the latter crystal, although the difference does not appear to be very significant.

III SPECTRA OF SO_4^{2-} ION IN $(\text{NH}_4)_2\text{BeF}_4$

As pointed out earlier, SO_4^{2-} ion is contained by our investigated sample of $(\text{NH}_4)_2\text{BeF}_4$ as an impurity; on an average, the lattice positions of this ion are separated from each other by 3-4 lattice parameters. Therefore, it may be argued that the correlation field interaction between these SO_4^{2-} ions would be negligibly weak and the static field potentials would mainly affect the dynamics of the ion. The study of the modes of this ion may thus be used to sense the static crystalline fields at its sites in $(\text{NH}_4)_2\text{BeF}_4$.

The observed Raman spectra of single crystal (cf Fig. 4.2 and 4.3) exhibit sharp band of good intensity in each spectrum of A_g modes at 981 cm^{-1} ; at the same frequency a band of miserable intensity is seen in the spectrum of B_{3g} modes while no band in spectra of B_{1g} and B_{2g} modes. These bands arise due to ν_1^s mode.

Very weak bands also appear due to $\nu_4^s(627\text{ cm}^{-1})$ in all spectra except the one of ca polarization. Equally weak bands also appear due to $\nu_2^s(463\text{ cm}^{-1})$ mode in bb, ab, bc and ca polarizations. It is interesting to note that ν_2^s bands in ab, bc and ca polarized spectra are more intense than ν_4^s in respective spectra. Such an intensity behaviour of ν_2^s and ν_4^s modes is identical to that observed for these modes in Raman

spectra of $(\text{NH}_4)_2\text{SO}_4$ single crystal in which SO_4^{2-} ion has $C_s(\sigma_{ab})$ site. All these observations reveal that SO_4^{2-} ion also occupies $C_s(\sigma_{ab})$ site in $(\text{NH}_4)_2\text{BeF}_4$ and goes substitutionally at the position of BeF_4^{2-} ion.

The ν_3^s mode, which is not observed in Raman spectra probably because of low scattering efficiency, shows a band of good intensity at 1105 cm^{-1} in room temperature IR spectrum (cf Fig. 4.5b). A band of similar intensity appears at 620 cm^{-1} due to ν_4^s mode. On going to LT, the former band splits into three components of slightly different intensity at 1122, 1109 and 1092 cm^{-1} and the latter does not show such structure. Thus the distortions acquired by SO_4^{2-} ion in ferroelectric phase lead to site symmetry splittings in ν_3^s which are separated by $10 - 20\text{ cm}^{-1}$. The same order of separation in site symmetry splitted components of the similar ν_3^b mode may be expected. Thus the observed total width ($\sim 165\text{ cm}^{-1}$) of ν_3^b mode observed in IR spectra may be attributed to the correlation field interactions. Such a strong correlation field interaction seems to arise due to the strong polar character of ν_3^b . This inference may be corroborated by the fact that non-polar ν_1^b mode has a width of about 10 cm^{-1} . The positive shift of ν_4^s mode by 7 cm^{-1} in going from RT to LT may be attributed to the difference in the crystalline fields in two phases.

It may also be interesting to note that ν_1^s and ν_3^s (S-O stretching) modes of SO_4^{2-} ion in $(\text{NH}_4)_2\text{BeF}_4$ have frequencies equal to the free ion values within experimental errors, while the angular deformation ν_2^s and ν_4^s modes are observed to be higher by about 10 cm^{-1} . In view of the ion concentration ratio ($\text{BeF}_4^{2-}:\text{SO}_4^{2-}::98:2$) in our $(\text{NH}_4)_2\text{BeF}_4$ crystal, the average Raman intensity ratio ($I(\nu_1^b):I(\nu_1^s)::100:10$) is consistent with more ionic character^{39,40} of Be-F bonds in BeF_4^{2-} than S-O bonds in SO_4^{2-} .

IV FERROELECTRIC PHASE TRANSITION

a. Temperature Dependence of IR Bands

The IR intensity of ν_1^b mode changes remarkably with temperature. Band contours observed due to this mode (having peak at 553 cm^{-1}) scanned over 575 to 525 cm^{-1} range, are shown in Fig. 4.6a; the changes in the integrated intensity (I) with temperature (T) are depicted in Fig. 4.6b. Closed circles on I vs. T curve correspond to the temperature at which different contours, shown vertically above were recorded.

The ν_1^b mode appears as very weak band near RT (cf contour recorded at 273°K in Fig. 4.6a). This mode exhibits a slow increase in its intensity on cooling the sample except in the temperature range $200 - 160^\circ\text{K}$ in which the rate of increase of I becomes noticeably faster. This behaviour of ν_1^b mode indicates that BeF_4^{2-} ion, which has almost a tetrahedral structure at RT, gets slowly distorted on cooling; distortions occur with faster rate within $\pm 20^\circ$ around T_c . From other studies^{26,30,33} related only to NH_4^+ ions, we learn that the structure and the dynamics of NH_4^+ ions also undergo equally slow (if not slower) change around T_c . Evidently, the major structural changes in $(\text{NH}_4)_2\text{BeF}_4$ take place in a wide range of temperature. Although, the minor discontinuity must occur to account for the change in spontaneous polarization by about $0.04\text{ }\mu\text{C/cm}^2$ suddenly occurring at T_c ; it is possible that these changes are not reflected in I vs T curve for ν_1^b mode examined by us. Thus our observations are consistent with the fact that the transition closely resembles with second order changes.

b. Microscopic Mechanism and Origin of Phase Transition

Since the detailed informations are not available about the structure of $(\text{NH}_4)_2\text{BeF}_4$, it is difficult to explore more adequately the

microscopic mechanism and the origin of phase transition. However, from all known facts about this crystal, some conclusions may be arrived at.

The hysteresis curves just above T_c exhibit double loop. It reveals that (i) the transition is basically of the first order, (ii) the driving interactions are of electrostatic type and (iii) the spontaneous polarization acts as the major component of the order parameter which may be used to describe the phase transition. This makes it clear that origin of ferroelectric phase transition in $(\text{NH}_4)_2\text{BeF}_4$ is fundamentally different from that involved in the isostructural $(\text{NH}_4)_2\text{SO}_4$.

According to O'Reilly et al³³ two types of NH_4^+ ions have dipole moments of about 0.0 and 0.09D within the comparable limits of errors; in paraelectric phase these dipoles acquire disordered state and an ordered state in ferroelectric phase. This model, based on the order-disorder phenomenon, neglects the role of BeF_4^{2-} ion in occurrence of transition in this crystal. O'Reilly et al³³ presume that the transition is accompanied by the co-operative reorientation of NH_4^+ ions in order to keep consistency between order-disorder phenomenon and the first order nature of the transition. Contrary to this presumption Miller et al²⁶ have concluded that the dynamics of NH_4^+ ions in $(\text{NH}_4)_2\text{BeF}_4$ can be described in terms of the motion of independent ions. Moreover, our present investigations reveal that BeF_4^{2-} ion has considerably large distortions at T_c which get enhanced on further lowering the temperature. Therefore, contributions of BeF_4^{2-} ion to the spontaneous polarization at any temperature can not be neglected. Obviously the mechanism of transition in this crystal can not be as simple as attributed by O'Reilly et al³³.

Here we note that Be-F bonds in the crystal possess ionic character as high as 72%^{39,40} which therefore dominates over the covalent character.* Thus the dynamics of BeF_4^{2-} ion is governed by the electrostatic interactions to the larger extent. This leads us to propose the following model for the phase transition occurring in $(\text{NH}_4)_2\text{BeF}_4$ crystal. Accordingly, the relative displacements of Be^{2+} and F^- ions under electrostatic forces result in the existing phase transition. Thus the phase transition involves displacive type of mechanism. Under this model, the double loop exhibited by the hysteresis curve just above T_c and the sudden appearance of spontaneous polarization at T_c may consistently be rationalized. This model may also explain the following properties which need coherent explanations.

The Curie-Weiss constant for this crystal is observed to be around $15^\circ\text{K}^{4,14}$, while for the well known displacive type of ferroelectrics (e.g. BaTiO_3) this constant assumes a value of the order of 10^5°K^{41} . According to Devonshire⁴², the Curie-Weiss constant under the model based on the lattice dynamics of ferroelectric crystal, is given by

$$C = \frac{aN_e^2}{6bk} \quad \dots \quad 4.7a$$

where N is the number of oscillating ions per unit volume, e is the ionic charge, k is the Boltzmann's constant, a and b are the constants, such that the potential energy (V) of oscillating particle is given by

$$V = ax^2 + bx^4 \quad \dots \quad 4.7b$$

This indicates that C can have smaller values if the anharmonic constant b is larger. Thus the low value of C for $(\text{NH}_4)_2\text{BeF}_4$ may be rationalized if the

oscillations involving displacements of F^- ions (considered as the origin of

*It implies that, in BeF_4^{2-} ion, Be and F atoms can be regarded as separate particles of electrostatic charge $2e^+$ and e^- respectively, to a good

transition under the proposed model) are highly anharmonic. Such an anharmonic character may be exhibited by modes involving displacements of F^- ions because of interactions like H-bonding (N-H...F).

The transition temperature for $(ND_4)_2BeF_4$ is reported¹⁵ to be higher by 3° than that for $(NH_4)_2BeF_4$. This indicates that NH_4^+ ions also play some role in triggering the transition. It can be understood in view of the fact that the modes of BeF_4^{2-} are not completely isolated from those of NH_4^+ ions, e.g. the ν_2^b mode falling around 273 cm^{-1} may get mixed to some extent with t^n ($\sim 200\text{ cm}^{-1}$) modes. For this possibility we note that (i) under ν_2^b mode only F atoms get displaced from their mean positions in directions perpendicular to Be-F bonds and (ii) the NH_4^+ and F^- ions have almost equal weights. Thus the desired mixing of displacements of F^- and NH_4^+ ions may be observed under the dominating ionic interactions. It is also noted that in crystals like KH_2PO_4 , where the dynamics of protons play the major role in triggering the existing ferroelectric phase transition in such crystals, T_c shows considerably large shift on deuteration. For example T_c in KH_2PO_4 ($123^\circ K$) and KD_2PO_4 ($213^\circ K$) are in 1.0:1.732 ratio¹¹, while the ratio of the square roots* of proton and deuteron masses ($m_H^{1/2}:m_D^{1/2}$) is 1.0:1.414 which is of the equal order of magnitude to a good approximation. On the other hand, T_c for $(NH_4)_2BeF_4$ ($176^\circ K$) and $(ND_4)_2BeF_4$ ($179^\circ K$) are in 1.0:1.017 ratio which is more close to that (1.0:1.098) of square roots of NH_4^+ and ND_4^+ ion masses in comparison to $m_H^{1/2}:m_D^{1/2} = 1.0:1.414$. This supports our model indicating that the soft mode, which may describe the phase transition in $(NH_4)_2BeF_4$, has some contribution from translatory modes of NH_4^+ ion but is not consistent with the

*In vibrational motion the square root of the mass of a particle has more significance than other roots.

order-disorder type of mechanism involving orientations of NH_4^+ ions, i.e. the ~~the~~ displacements of protons around the fixed N atom.

The transition does not affect the line width and the second moment of PMR spectrum²⁴ of $(\text{NH}_4)_2\text{BeF}_4$. It indicates that the average environment of protons above and below T_c is not different. This fact may imply that the dynamics of protons does not play the major role in triggering the transition. Thus the NH_4^+ sites do not seem to be the centres of the major driving interactions for the transition. On the other hand such interactions might be centred at BeF_4^{2-} site as indicated by the following observation.

In Fig. 4.6c, we have shown the IR band contours ($1140-1040\text{ cm}^{-1}$) recorded at different temperatures around T_c . As already discussed, these bands arise due to ν_3 mode of SO_4^{2-} ion occupying BeF_4^{2-} site in the investigated $(\text{NH}_4)_2\text{BeF}_4$. Upto a temperature around 253°K , the contour shows no structure but two components are clearly seen near T_c ; initially below T_c , the higher frequency component shows relatively more increase in I than that of lower frequency component. However, on further lowering the temperature, the former component splits into two and the latter exhibits relatively more increase in I. These observations reveal that crystalline fields at the site of BeF_4^{2-} ion starts changing well above T_c and the site symmetry of this ion is effectively lower in ferroelectric phase in comparison to that in paraelectric phase. Thus the transition in $(\text{NH}_4)_2\text{BeF}_4$ seems to be initiated by the interactions centred at BeF_4^{2-} site; the NH_4^+ ions follow an appropriate change. The fact that the changes in birefringence in $(\text{NH}_4)_2\text{BeF}_4$ at T_c can be accounted for as electro-optic effect²⁰, also supports our model.

4.8 CONCLUSION

The Raman spectra of single crystal and IR spectra ($4000 - 250 \text{ cm}^{-1}$) of microcrystalline sample (RT) of $(\text{NH}_4)_2\text{BeF}_4$ are found to be consistent with the fact that this crystal has the same structure as that of $(\text{NH}_4)_2\text{SO}_4$. The IR spectrum recorded at LT can also be consistently analysed in view of the C_{2v}^9 space group symmetry of $(\text{NH}_4)_2\text{BeF}_4$ in ferroelectric phase. An extensive analysis of observed spectra indicates that the force fields describing the dynamics of crystallographically inequivalent $\text{NH}_4^+(\text{I})$ and $\text{NH}_4^+(\text{II})$ ions are identical to a good approximation. Frequencies of all modes except the librations of BeF_4^{2-} ion have been determined. Only the IR active ν_3 and ν_4 modes of both NH_4^+ and BeF_4^{2-} ions exhibit strong bands in IR spectra; ν_1 and ν_2 modes show very weak IR bands at both 300 and 120°K indicating that both ions have minor distortions in their T_d structure. But the distortions seem to be sufficient to account for the spontaneous polarization in the crystal.

The contribution of BeF_4^{2-} ion to the spontaneous polarization is not negligible. The driving interactions of the transition are mainly of electrostatic type and seem to be centred at the sites of BeF_4^{2-} ion which triggers the transition and NH_4^+ ions follow an appropriate change. The order parameter needed to develop the phenomenological theory of the transition may have several components but the spontaneous polarization acts as its major component. It has been shown that the mechanism of transition is not as simple as order-disorder involving NH_4^+ dipoles. It seems rather of displacive type involving displacements of F^- and NH_4^+ ions.

The soft mode which may describe the phase transition appears to be a mixed mode having major contribution from the modes involving displacements of F^- ions; mixing of modes involving displacements of NH_4^+ also needs consideration. The fundamental difference between the mechanism of transitions in this crystal and the isostructural $(NH_4)_2SO_4$ lies in the fact that Be-F bonds have ionic character to a large extent, while the S-O bonds are covalent to a high degree.

REFERENCES

1. R.W.G. Wyckoff, Crystal Structure, Vol. 3, Inter-Science, New York (1965).
2. R. Pepinsky and F. Jona, Phys. Rev. 105, 344 (1957).
3. Y. Okaya, K. Vedam and R. Pepinsky, Acta Cryst. 11, 307 (1958).
4. H. Oshima and E. Nakamura, J. Phys. Chem. Solids 27, 481 (1966).
5. B.A. Strukov, N.D. Gavrilova and V.A. Koptsik, Sov. Phys. Crystallogra. 6, 625 (1961).
6. R. Hultgren, Z. Krist. A88, 233 (1934).
7. P.L. Mukherjee, Current Sci. 3, 66 (1934).
8. P.L. Mukherjee, Ind. J. Phys. 18, 148 (1944).
9. J.C. Tedenac and L. Cot, C.R. Acad. Sci. Paris Ser. C 268, 1687 (1969).
10. C. Avinens, L. Cot and M. Maurin, Ann. Chim. 5, 423 (1970).
11. V.V. Udalova, Sov. Phys. Crystallogra. 6, 504 (1961).
12. Yu. Z. Nozik and L.F. Tokar, Latv. PSR Zinat. Akad. Vestis Fiz. Techn. Ser. (SSSR) 4, 75 (1969).
13. B.A. Strukov, T.L. Skomorokhova, V.A. Koptsik, A.A. Boiko and A.N. A.N. Izrailenko, Kristallogra. 18, 143 (1973).
14. V.A. Koptsik, B.A. Strukov, A.A. Sklyankin and M.E. Levina, Bull. Acad. Sci. USSR Phys. Ser. 24, 1230 (1960).
15. S. Hoshino, K. Vedam, Y. Okaya and R. Pepinsky, Phys. Rev. 112, 405 (1958).
16. B.A. Strukov and V.A. Koptsik, Sov. Phys. Crystallogra. 7, 182 (1962).
17. K.N. Semenenko and A.P. Savchenkova, Zh. Neorg. Khim. 18, 2285 (1973).
18. V.A. Koptsik, B.A. Strukov and I.K. Nevedomskaya, Bull. Acad. Sci. USSR Phys. Ser. 24, 1233 (1960).
19. B.A. Strukov, Sov. Phys. Crystallogra. 6, 511 (1961).
20. A.T. Anistratov, Rev. Phys. Appl. (France) 7, 77 (1972).
21. I. Zheludev, Proc. Ind. Acad. Sci. A57, 361 (1963).
22. S.D. Toshev, Sov. Phys. Crystallogra. 8, 87 (1963).

23. S.D. Toshev, Intern. Meet. Ferroelect. Prague 2, 31 (1966).
24. R. Blinc and I. Levstek, J. Phys. Chem. Solids 12, 295 (1960).
25. G. Burns, Phys. Rev. 123, 64 (1961).
26. S.R. Miller, R. Blinc, M. Brenman and J.S. Waugh, Phys. Rev. 126, 528 (1962).
27. A.G. Akhmedov, R.A. Dantov and G.T. Petrov, Sov. Phys. Solid State 8, 685 (1966).
28. J.C. Cotz, R. Schaeffer and A. Clouse, Inorg. Chem. 6, 620 (1967).
29. I.P. Aleksandrova, L.I. Zherebtsova and T.I. Leiborich, Sov. Phys. Crystallogra. 14, 218 (1969).
30. D.W. Kydon, H.E. Petch and M. Pintar, J. Chem. Phys. 51, 487 (1969).
31. I.P. Aleksandrova, K.S. Aleksandrov and L.I. Zherebtsova, Bull. Acad. Sci. Phys. Ser. 33, 228 (1969).
32. D.W. Kydon, H.E. Petch and M. Pintar, Phys. Lett. 25A, 360 (1967).
33. D.E. O'Reilly, E.M. Peterson and T. Tsang, Phys. Rev. 160, 333 (1967).
34. I.P. Aleksandrova and U.N. Shcherbakov, Sov. Phys. Crystallogra. 14, 608 (1970).
35. G.M. Mikhailov, L.G. Lundin and S.P. Gabuda, Sov. Phys. (JETP) 14, 977 (1962).
36. M.B. Porter and R.C. Spiller, The Barker Index of Crystals, Vol I (part 2), Haffer and Sons Cambridge (1951).
37. G. Herzberg, Molecular Spectra and Molecular Structure, Vol. II, D. Van Nostrand, New York (1945).
38. A.S. Quist, J.B. Bates and G.E. Boyd, J. Phys. Chem. 76, 78 (1972).
39. L.A. Woodward, Trans. Faraday Soc. 54, 1271 (1958).
40. I.P. Aleksandrova and M.L. Afanas'ev, J. Struct. Chem. 9, 807 (1968).
41. F. Jona and G. Shirane, Ferroelectric Crystals, Pergamon Press, Oxford (1962).
42. A.F. Devonshire, Adv. Phys. 3, 85 (1951).

TABLE 4.1

Raman phonon frequencies (in cm^{-1}) observed in
 spectra of the single crystal of $(\text{NH}_4)_2\text{BeF}_4$
 (MPP(t^b) denotes multiphonon processes involving t^b .)

	A_g			B_{3g}	B_{1g}	B_{2g}	Assign- ments	ν_{av}	HFMP
	aa	bb	cc	ab	bc	ca			
1	2	3	4	5	6	7	8	9	10
w-bands	3220	3235	3244	3209	3208	3252	F.R.(I)	3228	3112
x-bands	3130	3121	3127	3122	3133*	3160*	ν_1^n	3125	
y-bands	3037	3024	3030	3039	3051	3060	F.R.(II)	3040	3112
z-bands	2867	2852	2876	2854	2873	2826	$2\nu_4^n$	2858	2864
	1669	1685	1667	1720 1679	1699	1708 1678	ν_2^n	1688	
	1442 1422	1440 1413	1437 1419	1459 1417	1432	1429	ν_4^n	1432	
	982	981	981	981			ν_1^s	981	
	795	786	790		793		ν_3^b	791	
	633	623	627	627	625		ν_4^s	627	
	558	558	558	558	558	558	ν_1^b	558	
		462		466	464	460	ν_2^s	463	
	403 -	- 376	402 381	- 388	385	379	ν_4^b	388	
			315	328		315	1^n	319	
	276	275	265	272	274	274	ν_2^b	273	
			197 150		183 150		t^n	180 150	
	145 106	154 96 92 84	106	101		129 96 88	MPP(t^b)		
					90				
	58 45	47 43 32	53	54 44	41? 37	?	t^b		

For different notations, see foot notes to Table 3.8

TABLE 4.2

Phonon frequencies (in cm^{-1}) observed in
IR spectra of microcrystalline $(\text{NH}_4)_2\text{BeF}_4$

Freq- uency (RT)	Assignment	Freq- uency (LT)	Freq- uency (RT)	Assignment ^x	Freq- uency (LT)
?	D.C.(I)	3315			
			1105	ν_3^s	1122 1109 1092
3240	F.R.(I)	3260 3180			
			930	$\nu_1^b + \nu_4^b$	950 920
3040	F.R.(II)	3100 3035 2980			
			790	ν_3^b	845 800 750
2860	$2\nu_4^n$	2920 2850			
			655	$\nu_2^b + \nu_4^b$	670
2040	$\nu_2^n + 1^n$	2065	620	ν_4^s	627
			553	ν_1^b	553
1795	$\nu_4^n + 1^n$	1845 1805 1780			
			472	$\nu_4^b + 1^b ?$	474 430
1675	ν_2^n	1675			
			370	ν_4^b	370
1465		1484 1456 1436			
1415	ν_4^n	1420 1397 1370			
1372					

^x Superscripts n, b and s refer to the modes of NH_4^+ , BeF_4^{2-} and SO_4^{2-} ions, respectively. See the text for other notations.

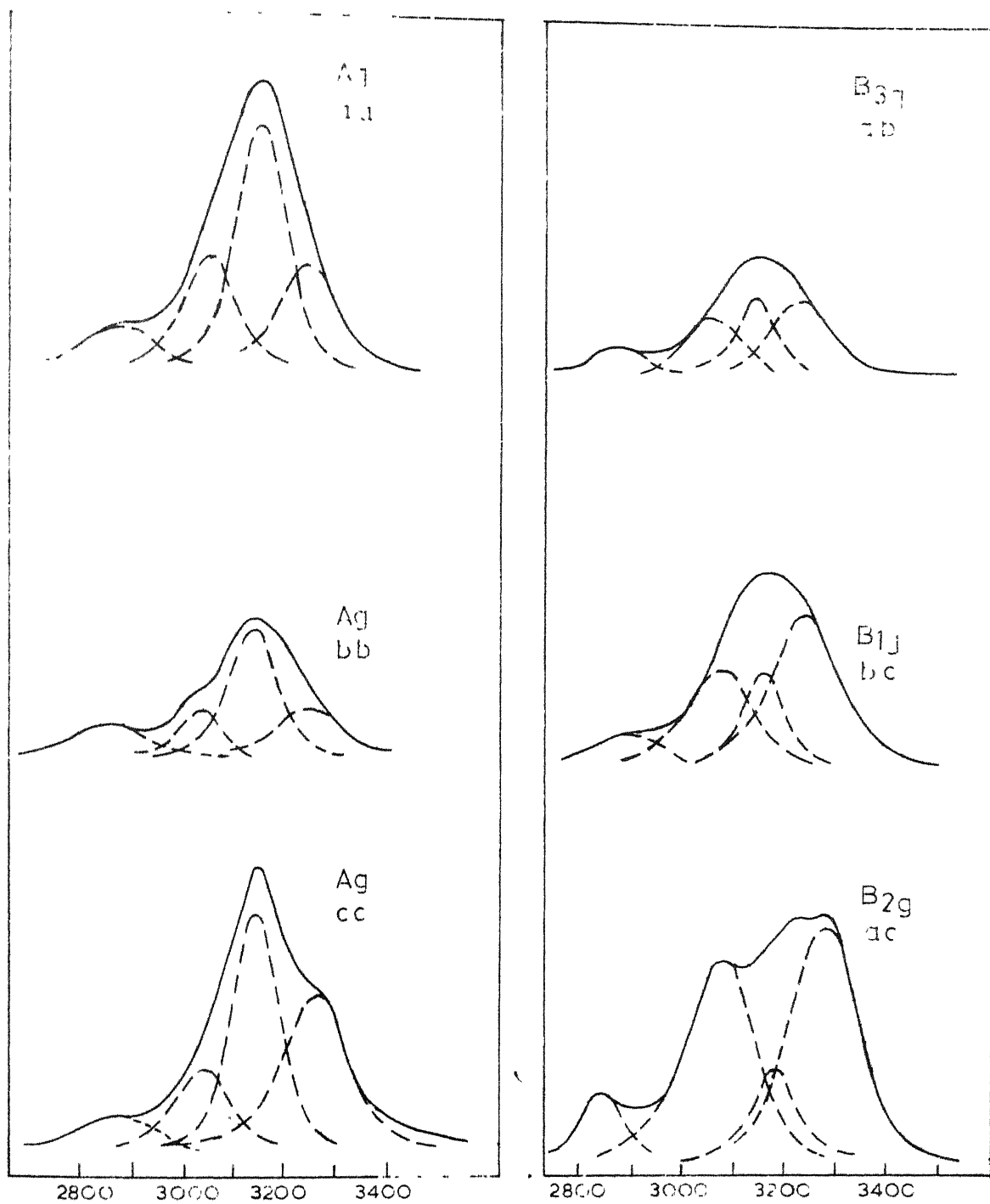


Fig.4.1 Raman spectra of $(\text{NH}_4)_2\text{BeF}_4$ single crystal in N-H stretching region.

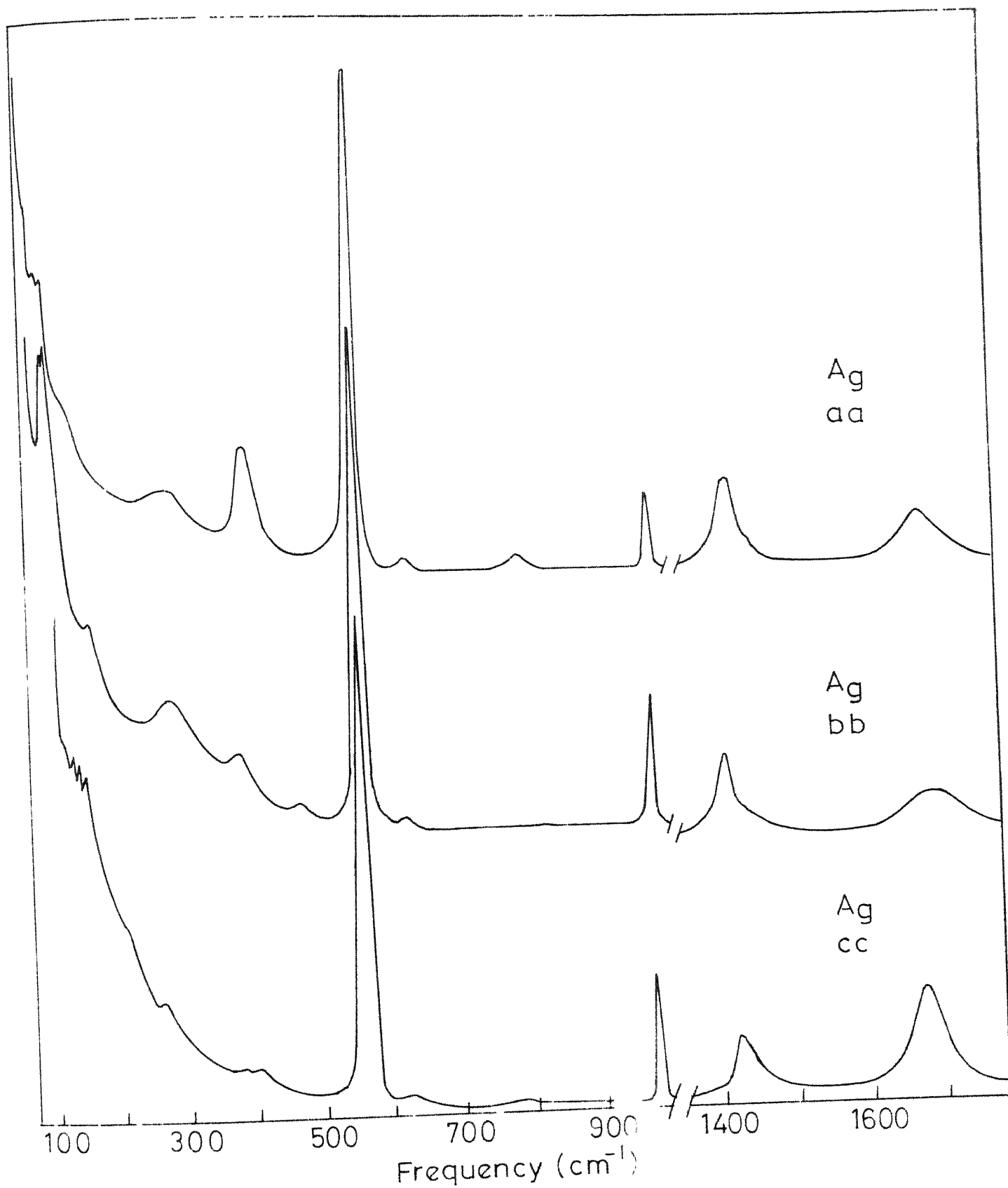


Fig.4.2 aa bb & cc polarized Raman spectra of $(\text{NH}_4)_2\text{BeF}_4$ single crystal below 1800 cm^{-1} .

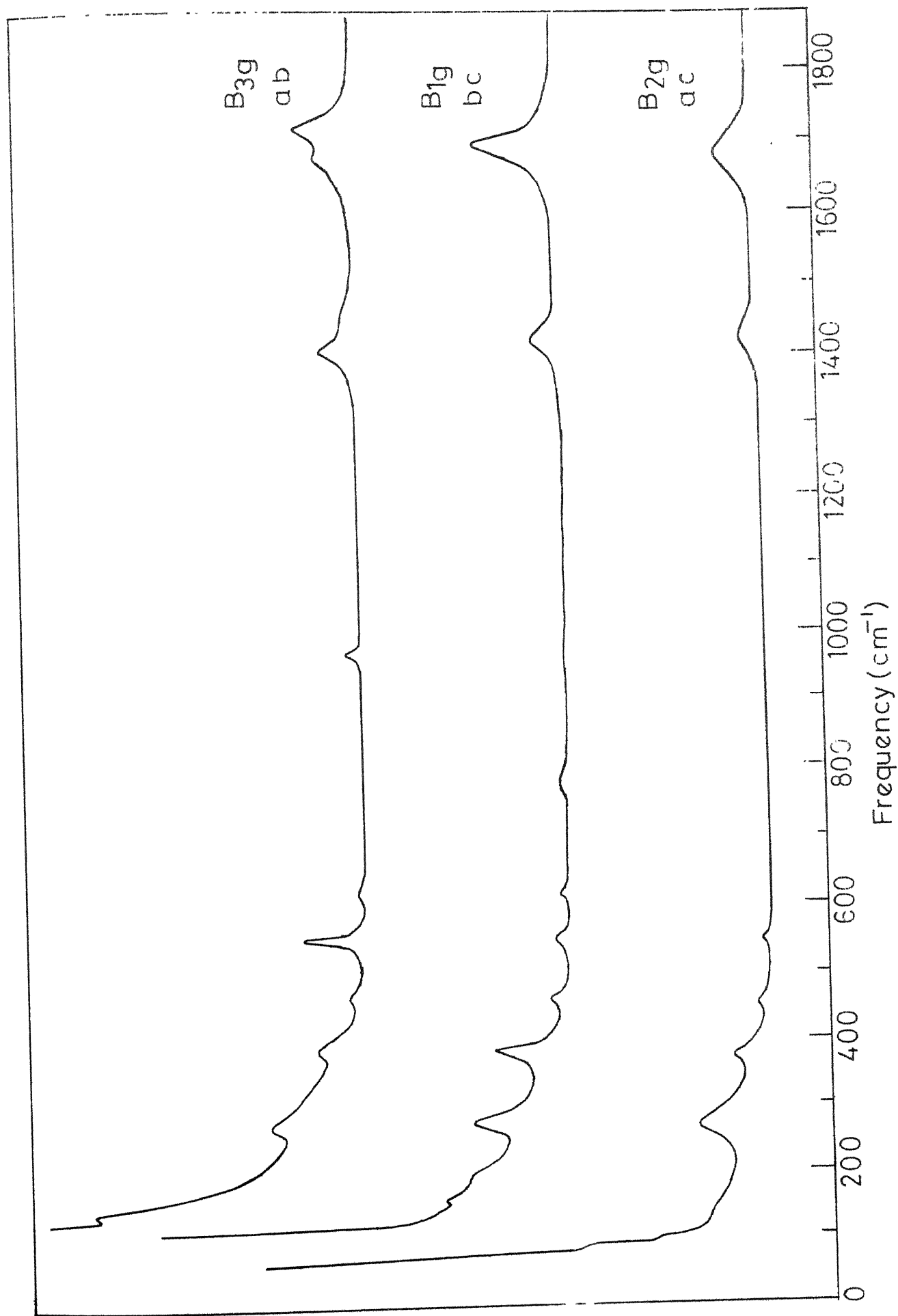
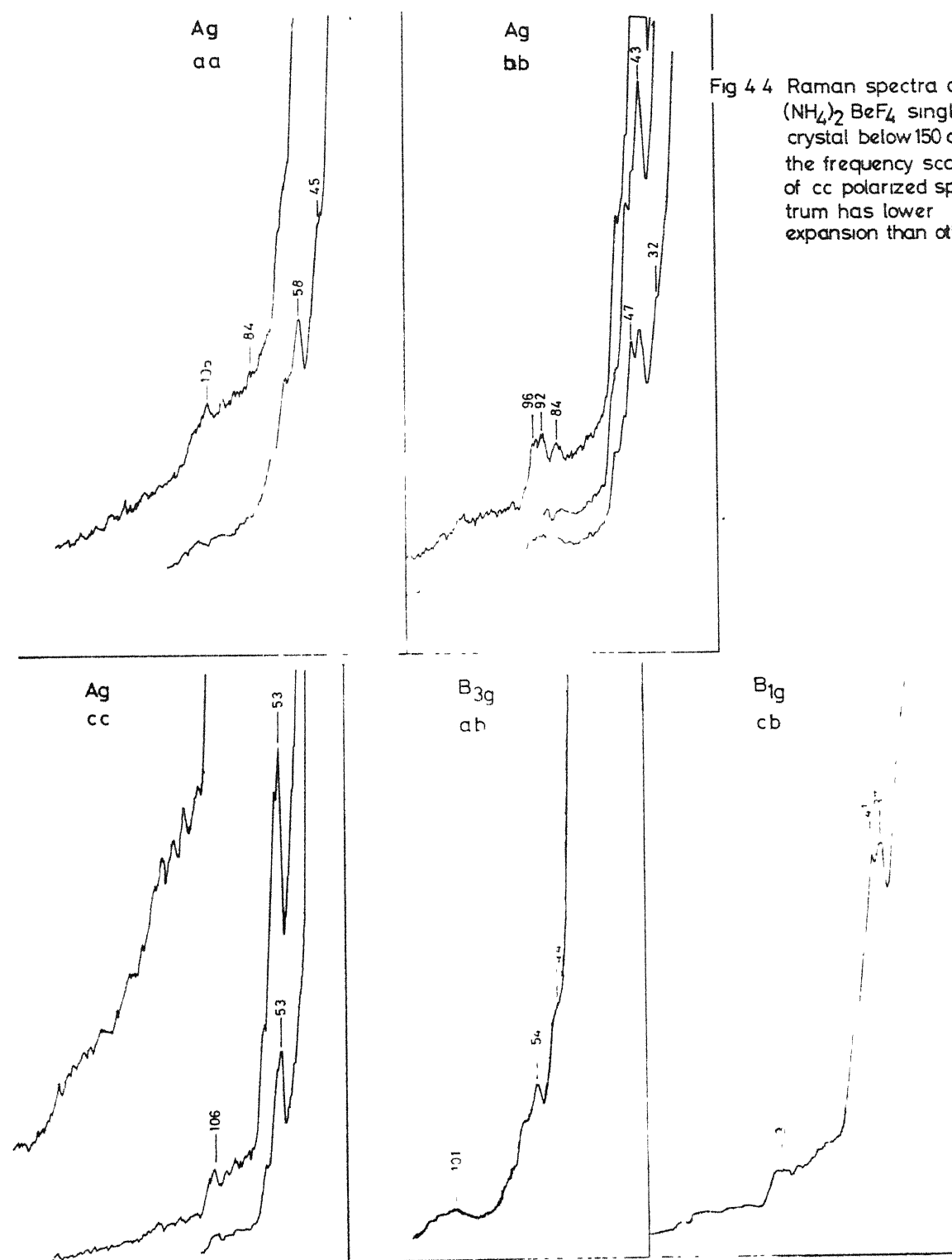


Fig.4.3 ab bc & ca polarized Raman spectra of $(\text{NH}_4)_2\text{BeF}_4$ single crystal below 1800 cm^{-1}



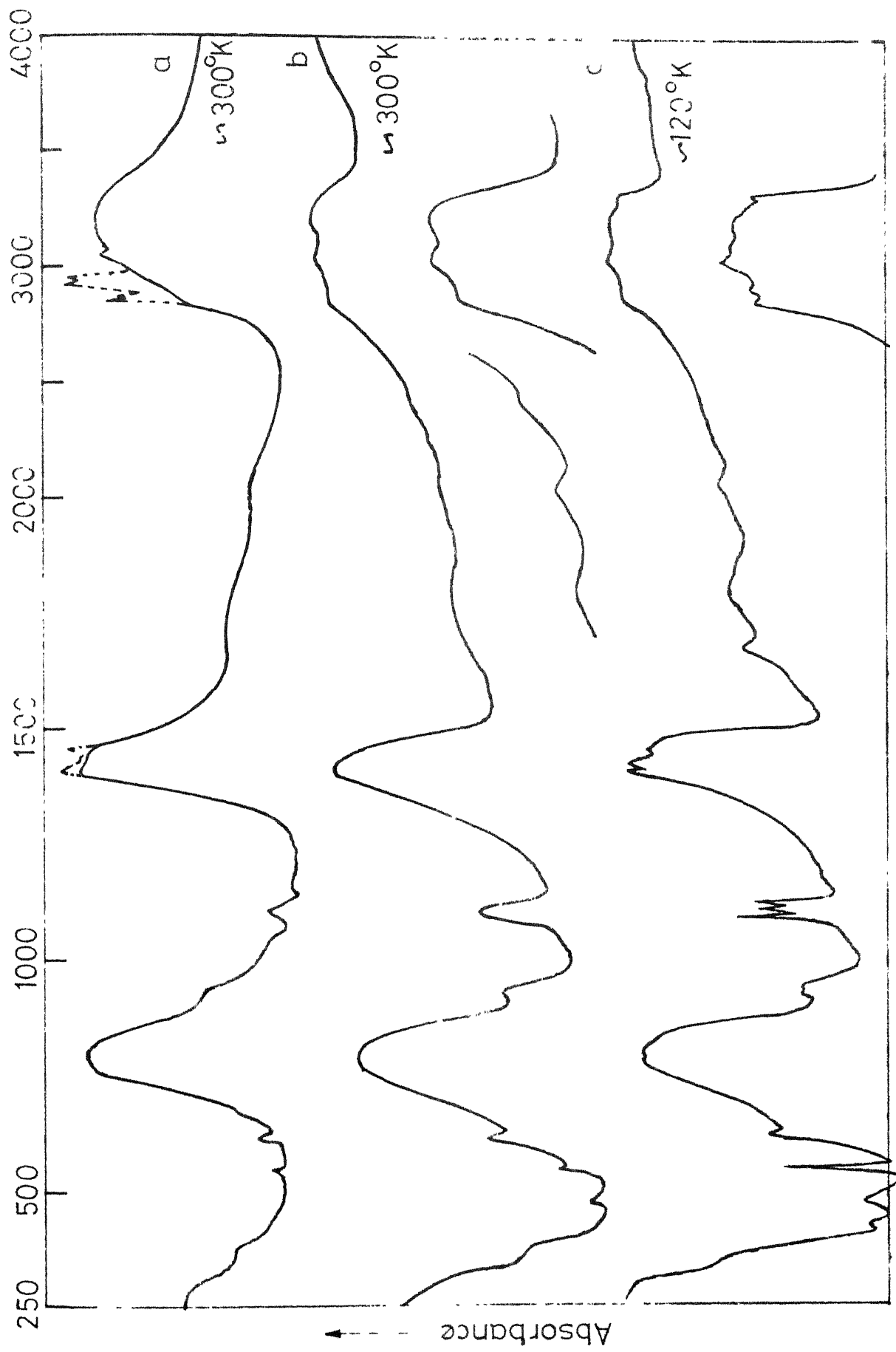


Fig. 4.5 IR spectra of microcrystalline $(\text{NH}_4)_2\text{BeF}_4$ (a) nujol mull; (b) & (c) film scattering film prepared on AgCl plate.

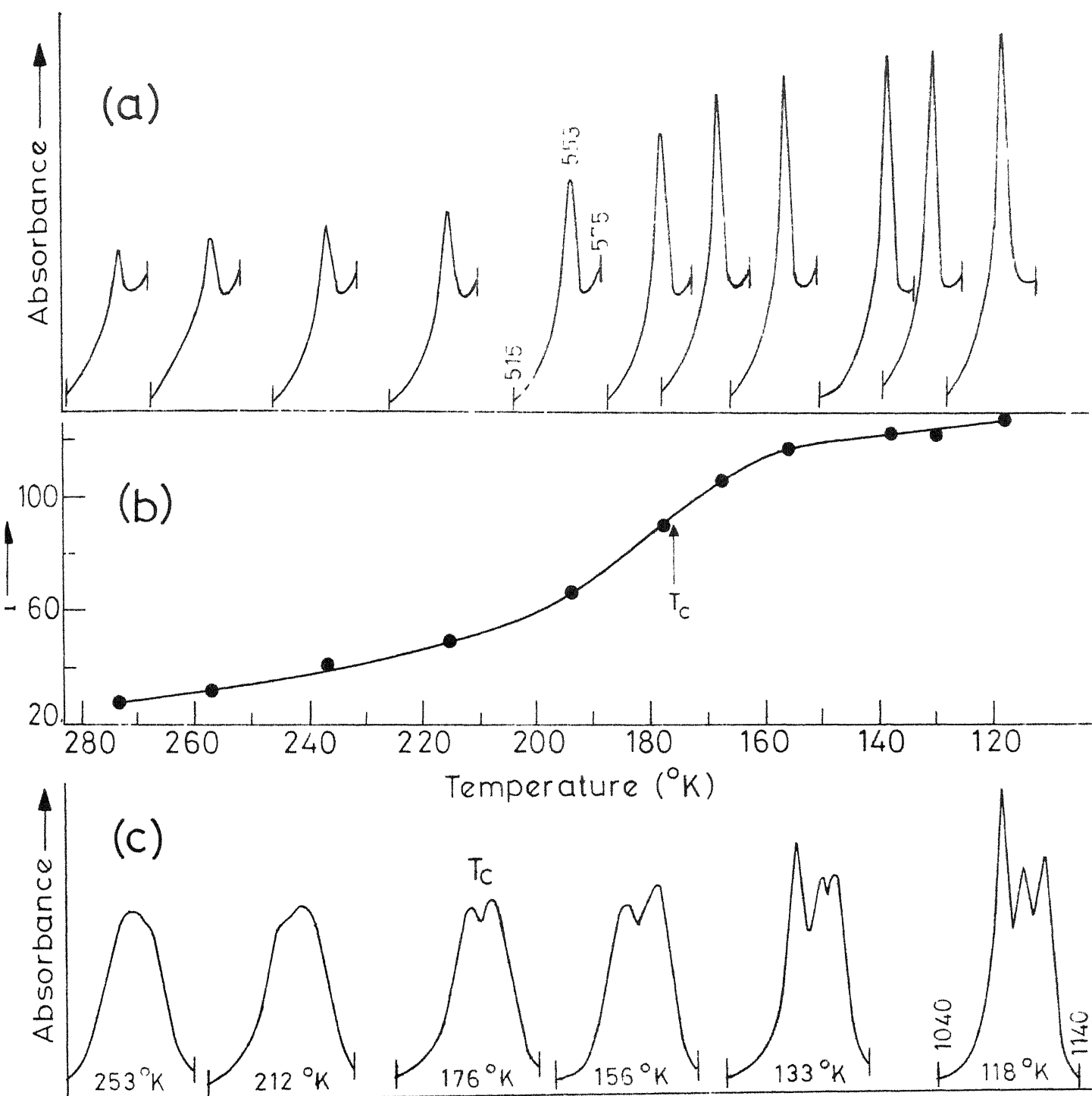


Fig. 4.6 Temperature dependence of IR (a) band contours and (b) integrated intensity (I , in arbitrary units) of $\nu_1(\text{BeF}_4^{2-})$ in $(\text{NH}_4)_2 \text{BeF}_4$, and (c) band contours of ν_3 mode of SO_4^{2-} in $(\text{NH}_4)_2 \text{BeF}_4$

APPENDIX 4.1

Frequency (ν , in cm^{-1}), relative integrated intensity (I, in parenthesis) and FWHMI of Raman bands^x in spectra of single crystal of $(\text{NH}_4)_2\text{BeF}_4$

aa		bb		cc		ab		be		ca	
ν	(I) FWHMI	ν	(I) FWHMI	ν	(I) FWHMI	ν	(I) FWHMI	ν	(I) FWHMI	ν	(I) FWHMI
1	2	3	4	5	6	7	8	9	10	11	12
3220	(10) 140	3235	(10) 145	3244	(10) 155	3209	(10) 150	3208	(10) 155	3252	(10) 155
3130	(21) 120	3121	(21) 110	3127	(12) 115	3122	(7) 110	3133	(4) 96	3160	(2) 96
3037	(9) 120	3024	(5) 90	3030	(4) 125	3039	(7) 145	3051	(6) 145	3060	(9) 170
2867	(4) 160	2852	(5) 140	2876	(2) 175	2854	(3) 140	2873	(2) 155	2826	(1) 90
						1720	(9) 42			1708	sh
1669	(10) 70	1685	(10) 91	1667	(10) 53	1679	(10) 61	1699	(10) 42	1678	(10) 61
1442	sh	1440	sh	1437	sh	1459	sh				
1422	(7.3) 30	1413	(6.8) 27	1419	(4.1) 30	1417	(6.4) 35	1432	(3.1) 38	1429	(3.6) 38
982	(1.5) 8	981	(2.0) 8	981	(2.0) 8	981	(0.5) 8				
795	(1.0) 25	786	?	790	?			793	(0.8) 25		
633	(0.5) 15	623	(0.6) 15	627	(0.3) 15	627	(0.3) 15	625	(0.2) 15		
558	(15) 11	558	(18) 11	558	(11) 11	558	(3.0) 11	558	(0.4) 11	558	(0.3) 11
		462	(1.9) 30			466	(1.1) 25	464	(0.9) 20	460	

contd.

Appendix 4.1 contd.

1	2	3	4	5	6	7	8	9	10	11	12
403 (8.2) 25				402 (1.0) 30							
		376 (6.2) 40		381 (1.0) 30		388 (5.0) 40		385 (6.2) 30		379 (4.2) 30	
				315 sh		328 sh				315 sh	
276 (6.4) 75	275 (7.8) 50			265 (1.6) 30		272 (4.6) 35		274 (4.5) 30		274 (10) 40	
				197 sh				183 (1.0) 25			
145 sh	154 sh			150 sh		154 sh		150 sh			
106				106		101				129 (1.3) 30	
		96 (6.0) 8								96 sh	
		92 (6.0) 8						90 (2.0) 10			
		84 (6.0) 8								88 sh	
58 (18) 10	47			53 (16) 15		54 (15)					
45 sh	43 (30) 16					44 sh					
	32 sh							37 (10) 20			

^xObtained after Lorentzian resolution (although not shown in Figs. 4.2 - 4.4) of observed spectra; for relativeness of I values see the text. sh = shoulder.

APPENDIX 4.2

Frequency (ν), relative integrated intensity (I, in parenthesis) and FWHMI of bands observed in IR spectra of microcrystalline $(\text{NH}_4)_2\text{BeF}_4$. (For relativeness of I values see the text, df = diffuse and bd = broad).

RT(300°K)			LT(120°K)		
ν	I	FWHMI	ν	I	FWHMI
			3315	4.9	60
3240	6.1	200	3260	4.1	70
			3180	11.1	110
			3100	6.8	75
3040	5.8	180	3035	6.2	65
			2980	4.4	65
2860	4.6	175	2920	8.2	90
			2850	8.2	90
2040	df	bd	2065	df	bd
			1845		
1795	df	bd	1805	df	bd
			1780		
1675	df	bd	1675	0.7	40
			1484	4.4	30
1465	2.3	55	1456	3.4	25
			1436	3.2	22
1415	2.9	55	1420	4.5	25
			1397	4.6	28
1372	2.2	55	1370	2.7	25
			1122	0.5	9
1105	0.7	42	1109	0.4	8
			1092	0.9	12
			950	1.1	35
930	0.7	55	920	1.1	40
			845	9.8	58
790	10.0	165	800	10.0	55
			750	11.8	65
655	1.4	80	670	7.1	75
620	0.1	20	627	0.6	20
553	0.03	12	553	0.9	10
			474	0.14	15
472	0.04	20	430	0.1	15
370	0.7	45	370	3.3	45

CHAPTER V

OPTICAL PHONONS IN α -NiSO₄·6H₂O CRYSTALABSTRACT

This Chapter reviews some earlier but important investigations dealing with the dynamics of H₂O molecule in crystal hydrates and summarizes the up-to-date studies of α -NiSO₄·6H₂O (henceforth abbreviated as NSH) in the introduction. The investigations reported here deal with the lattice dynamics of NSH.

The dynamics of this crystal has been discussed in terms of 288 phonon modes under the unit cell approximation. These branches have been described in terms of internal and librational modes of H₂O molecules, internal modes of SO₄²⁻ ion, quasi-internal modes of (NiO₆^w)²⁺ complex ion (O^w represents H₂O as a single particle) and libratory and translatory external lattice modes of the crystal.

On the basis of consistent site symmetry correlations, it has been shown that (NiO₆^w)²⁺ part of

the $[\text{Ni}(\text{OH}_2)_6]^{2+}$ complex behaves as a quasi-molecule having C_h symmetry; the intermolecular interactions involving H atoms in this complex are too weak to affect its dynamics hence these atoms may be neglected*.

A symmetry classification of 288 phonon modes has been presented using both unit cell and site symmetry approaches.

Laser Raman spectra** of single crystal have been recorded at RT and attributed to phonons originating from the Raman active modes of isolated $\text{H}_2\text{O}(C_{2v})$, $\text{SO}_4^{2-}(T_d)$ and $(\text{NiO}_6^w)^{2+}(O_h)$ units. A discussion has been made on LO-TO splittings of polar phonons of E species of D_4 point group (the symmetry of NSH).

IR(ATR) spectra of single crystal of NSH have also been recorded in $250\text{--}4000\text{ cm}^{-1}$ range. Important features of these spectra are discussed.

IR spectra of microcrystalline NSH and its deuterated analogue have been measured at RT in $250\text{--}4000\text{ cm}^{-1}$ range; LT spectra of microcrystalline NSH are also discussed[†]. Librational modes of H_2O molecules which appear as weak and diffuse bands in Raman spectra

*Accepted for publication in Appl. Spectroscopy.

**Presented in the Symposium on Quantum-Opto-Electronics (BARC), Bombay (1974) and accepted in J. Raman Spectroscopy.

[†]Published in Proc. Nucl. Phys. Solid State Phys. (BARC) Chandigarh, 15c, 483 (1972).

exhibit 9 strong bands both at RT and LT. These modes exhibit remarkable enhancement in their sharpness and peak intensity. A simple model has been used to compute the force constants involved in libratory vibrations of H_2O molecules.

5.1 INTRODUCTION

The studies of optical phonons in hydrates of different metal compounds have received due attention in recent years. Such studies provide informations about interactions like metal-oxygen co-ordination and H-bonding which determine many bio-physical and bio-chemical processes as well as the properties of investigated system. These studies can also answer the central question whether the hydrate-complex consisting of water molecules surrounding a central metal ion can be regarded as a quasi-molecule for its dynamical behaviour in its crystal lattice. Additional interest in these studies arose since it was shown by Heber¹ that the electronic excitation energy of rare earth and transition metal ions in hydrated crystals is transferred to the lattice via the vibrational excitation of the shell of water molecules. The relaxation times of the excited electronic states are thus determined in part by the density of the vibrational states of this surrounding shell.

One more reason of interest in IR and Raman studies of hydrates of different metal compounds has been the aim to find some empirical relations between observed frequencies, widths and intensities of different modes of H_2O and appropriate parameters like length of O-H or O-H...X bonds, angle between two O-H bonds, etc. Attempts in this direction

have been made by several workers. For example: (i) Glemser and Hartert^{2a} demonstrated that O-H stretching frequency decreases monotonically with decreasing (OH....O) distance in hydrates, (ii) Lucchesi and Glasson^{2b} have observed an inverse relation between the stretching and bending frequencies of hydrated water, (iii) Hartert^{2c} reported a correlation between the symmetry of the water environment and width of bending mode, (iv) Saumagne and Josien^{2d}, Saumagne^{2e}, Glew^{2f} and Bellamy et al^{2g} have related symmetric O-H stretching with asymmetric O-H stretching mode for wide class of hydrates, (v) Gamo^{2h} has concluded that a linear relation exists between frequency of librational band appearing around 700 cm^{-1} and cation-water distance showing that such modes are considerably influenced by this distance. Van der Elsken and Robinson²ⁱ and Schiffer^{2j} have also commented over this inference.

However, all the proposed correlations do not hold good in general. Reasons probably lie in the facts that: (i) all the vibrations of a molecular unit are more or less affected by different parameters; the effect of a single parameter is difficult to isolate and (ii) the correlations are based on data and assignments which themselves are sometimes incorrect and ambiguous. Obviously, it is understood that better correlations are only possible when unambiguously analysed data of better quality are available. An extensive programme has, therefore, been initiated in this laboratory to make detailed and careful investigations of IR and Raman spectra of hydrates of transition and alkaline earth metal compounds. NSH is one of the systems undertaken in this programme.

The blue coloured NSH^{3,4} has molecular weight 262.68, specific gravity 2.07; it is highly soluble in water, alcohols and ammonium

hydroxide. NSH, in one or more forms is widely used as catalyst⁴, optical filters^{5,6} in determination of the emissive power of a laser⁷, etc.

For NSH extensive investigations have earlier been carried out on optical absorption⁸⁻¹⁵, optical activity¹⁶⁻²⁸, magneto-optical activity^{18,19,29-34}, circular dichroism^{20,24,27,35-38}, thermodynamics^{39,40}, magneto-thermodynamics⁴⁰⁻⁴⁴, magnetic susceptibility^{15,45-55}, kinetics of dehydration⁵⁶⁻⁶¹, crystal structure⁶²⁻⁶⁶ and crystal dislocations^{67,68}. Few reports are available on the study of birefringence⁶⁹, NMR⁷⁰, fluorescence⁷¹ and neutron inelastic scattering⁷² phenomena in this crystal. The IR absorption⁷³⁻⁸¹ and Raman scattering⁸¹⁻⁸³ have also been investigated by several workers. However, results of IR and Raman studies either do not cover the full range of phonon frequencies or are not of good quality. Moreover, the results have not been comprehensively analysed. **Some** of several possible reasons for it might have been the following:

(i) NSH is optically active, when laser sources were not available, it was necessary to illuminate a large volume of the crystal to obtain sufficient intensity to record its Raman spectra. Large crystal dimensions allow appreciable angles of optical rotation resulting ⁱⁿ considerable depolarization errors in spectra.

(ii) The point group symmetry D_4 of the crystal has E representation. Modes belonging to E are simultaneously Raman and IR active. When such a mode is observed in Raman effect, the long range electric field associated with the vibration splits the phonon into a transverse and a longitudinal component of different frequencies. This complicates the already enriched Raman spectrum.

(iii) In most IR and Raman studies NSH has been chosen as one member of a group of similar hydrates and, therefore, it has not been subjected to intensive investigations.

To clarify several ambiguities and discrepancies in results and up-to-date assignments, we present the results of our IR and Raman investigations on a single crystal of NSH. We would also discuss the important features of ATR spectra recorded for the first time. IR spectra of microcrystalline NSH and its deuterated analogue have also been studied particularly to make unambiguous assignments of librational modes of H_2O molecules.

5.2 CRYSTAL STRUCTURE

The positions of Ni, S and O atoms in the crystal lattice of NSH have been determined by several workers using X-ray diffraction methods⁶²⁻⁶⁵. The locations of H atoms have also been investigated by employing two dimensional neutron diffraction method⁶⁶. The crystal belongs to $D_4^4(4_12_12)$ or $D_4^8(4_32_12)$ space group symmetry of tetragonal (422) system.

Four formula unit cell of the crystal appears as shown in Fig. 5.1 which depicts the locations of different atoms projected in (001) plane. Circles of different radii in decreasing order of magnitude (i.e. in order of the atomic radii⁸⁴; 1.15, 1.04 and 0.74 Å of Ni, S and O, respectively), represent these atoms in the figure. The structure appears to be stacking of equal number of $[\text{Ni}(\text{CH}_2)_6]^{2+}$ octahedra and SO_4^{2-} tetrahedra. The numbers 0, 1/4, 1/2 and 3/4 in this figure denote the heights of the central atoms of these polyhedra in units of c. The crystal exhibits perfect cleavage along (001) plane.

The crystal data reported for the deuterated analogue of NSH and relevant to the present discussion are given in Table 5.1. From this table, it may be learnt that the crystal contains three crystallographically inequivalent water molecules which may be designated as $H_2O(I)$, $H_2O(II)$ and $H_2O(III)$. Columns 3-5 of the table read the bond lengths or the distances between two bonded particles. All the molecules have bond angles (cf column 6) greater than that in vapour phase (104.52°)⁸⁵ and closer to that in ice ($\sim 109.5^\circ$)⁸⁵. The Ni...O distances lie in 2.02-2.04 Å⁸⁶; values from Ref. (66) are given in column 7, Table 5.1.

5.3 PHONON BRANCHES IN THE CRYSTAL

The dynamics of NSH crystal can be described in terms of 288 phonon branches including 3 acoustical ones under the unit cell approximation. These phonons must originate from the normal modes of molecular units in the unit cell. According to the crystal structure the lattice contains two molecular units: $[Ni(CH_2)_6]^{2+}$ and SO_4^{2-} .

A critical look into our observed spectra and earlier IR and Raman studies^{81,87,88} on similar compounds provides definite evidences showing that the $[Ni(CH_2)_6]^{2+}$ complex behaves dynamically like a molecular unit. However, the correct symmetry behaviour of the complex, which is of vital importance for the unique explanation of spectroscopic observations and the chemical and physical properties of crystals containing such complexes, is not well understood. The detailed discussion presented in Appendix 5.1 concludes that $(NiO_6^w)^{2+}$ part of the complex behaves as a molecular unit of O_h point group symmetry; O^w represents the water molecule as a single particle. It also reveals that for librational

and internal modes, each H_2O molecule of the complex behaves as separate entity. The 288 phonons in NSH crystal can, therefore, be understood as originating from librational and internal modes of $\text{H}_2\text{O(I)}$, $\text{H}_2\text{O(II)}$, $\text{H}_2\text{O(III)}$, SO_4^{2-} and $(\text{NiC}_6\text{H}_6)^{2+}$ and translations of the last two units; translations of H_2O molecules are accounted for by modes of $(\text{NiC}_6\text{H}_6)^{2+}$. For convenience of discussion modes of H_2O molecules, SO_4^{2-} ion and $(\text{NiC}_6\text{H}_6)^{2+}$ complex would be distinguished by using superscripts w, s and c, respectively. The descriptions of the normal modes of these units may be discussed in brief as follows.

a. Normal Modes of H_2O

The H_2O molecule in its free state belongs to C_{2v} point group and has nine normal modes of motion⁸⁹ (3 translations + 3 rotations + 3 internal vibrations). When the molecule occupies a position in crystal lattice, its three translations result in three translatory vibrations. Like wise, the three rotations about the principal (a-, b- and c-) axes of moments of inertia (cf Fig. 5.2a) give rise to three librations: Wagging (W^w), twisting (T^w) and rocking (R^w), respectively. Three internal modes of H_2O are shown in Fig. 5.2b. These vibrations have been denoted by ν_1^w , ν_2^w and ν_3^w having significance similar to ν_1 , ν_2 and ν_3 notations used respectively by Herzberg⁸⁹. For perfect C_{2v} symmetry of the molecule, all internal and librational modes are active in Raman spectra; all modes except T^w are also active in IR spectra⁸⁹.

There are eight of each of the $\text{H}_2\text{O(I)}$, $\text{H}_2\text{O(II)}$ and $\text{H}_2\text{O(III)}$ molecules in the unit cell of NSH. Every mode of each of these would therefore contribute 8 phonon branches. The total contribution becomes $8 \times 3 = 24$ from internal and $8 \times 3 = 24$ from librational modes of one type

of H_2O and $(24 + 24) \times 3 = 144$ from all the three types.

b. Normal Modes of $(\text{NiC}_6^{\text{W}})^{2+}$ Complex

As concluded in Appendix 5.1, the complex behaves as XY_6 type molecule having O_h symmetry. Thus the complex would have 21 degrees of freedom (3 translational + 3 rotational + 15 internal). The 15 internal degrees of freedom are accounted for by six vibrations⁸⁹: $\nu_1^{\text{c}}(\text{A}_{1\text{g}})$, $\nu_2^{\text{c}}(\text{E}_\text{g})$, $\nu_3^{\text{c}}(\text{F}_{1\text{u}})$, $\nu_4^{\text{c}}(\text{F}_{1\text{u}})$, $\nu_5^{\text{c}}(\text{F}_{2\text{g}})$ and $\nu_6^{\text{c}}(\text{F}_{2\text{u}})$. The descriptions of these modes have been depicted in Fig. 5.3. Modes ν_1^{c} , ν_2^{c} and ν_5^{c} are Raman active while ν_3^{c} and ν_4^{c} are IR active for O_h symmetry. The ν_6^{c} and l^{c} modes of the complex are forbidden in both IR and Raman spectra under this symmetry⁸⁹. Since there are four units of $(\text{NiC}_6^{\text{W}})^{2+}$ complex in the unit cell, the net phonon branches originating from its different normal modes may be counted to be 84 (60 internal + 12 librational + 12 translational).

c. Normal Modes of SO_4^{2-} Ion

The form of the normal modes of SO_4^{2-} ion and their degeneracies along with their Raman and IR activity have been discussed in section 3.5. This unit adds 60 phonon branches to 144 contributed by H_2O molecules and 84 by $(\text{NiC}_6^{\text{W}})^{2+}$ complex. This sums up the total of 288 phonon branches sufficient for the description of the dynamics of the crystal.

5.4 CLASSIFICATION OF PHONONS

a. Unit Cell Approach

The classification of 288 phonon branches using the unit cell approach has been worked out in Table 5.2. The crystallographic data reveal that (i) no atom remains invariant under C_{21} , C_{41} and C_2 symmetry

operations of D_4^4 space group, (ii) only Ni and S atoms remain invariant under C_2' and (iii) as there are two C_2' axes forming one class of operations of D_4^4 and eight atoms of Ni and S in an unit cell, four of these would not change their positions under one C_2' . This leads to 96 and 4 invariant atoms (N^R) under E and C_2' operations, respectively. This invariance results in a reducible representation $\chi(N)$ whose bases are the total 288 phonons. Similarly, we find that 32 and 4 particles $N^R(t)$ retain their positions under E and C_2' operations, respectively, when H_2O , Ni and SO_4^{2-} are considered to be separate single particles. But out of the 28 polyatomic units ($24H_2O$ and $4SO_4^{2-}$) in the unit cell, only 2 SO_4^{2-} units ($N^R(1)$) are found to be rigid under C_2' . Using these invariant characters of the unit cell, we computed $\chi(t)$, $\chi(1)$ and $\chi(i)$ reducible representations whose bases are 96 translational, 84 librational and 108 internal modes, respectively (cf corresponding rows in Table 5.2). The reduction of these representations results the number of phonons belonging to different symmetry species (cf columns 8-12 of Table 5.2).

However, the translations of six H_2O molecules appear to mix considerably with those of Ni^{2+} ion. These modes can, therefore, be described in terms of translations, librations and internal vibrations of $(NiO_6^W)^{2+}$ complex. Obviously, 96 translatory modes of H_2O , Ni and SO_4^{2-} forming the bases of $\chi(t)$ need further classification in terms of pure translatory lattice modes of the crystal and the internal and librational modes of $(NiO_6^W)^{2+}$. For this purpose we need to consider the unit cell as a system of four $(NiO_6^W)^{2+}$ (as the polyatomic units) and four SO_4^{2-} (as single particle). The invariance character of such a unit cell is given by N' (for total 96 modes), $N'(t)$ (for 24 pure translatory lattice modes

and $N'(1)$ (for 12 librational modes) of the complex. Corresponding reducible representations may be given by $\chi(t) = \chi(N')$, $\chi'(t)$ and $\chi'(1)$ respectively (cf Table 5.2). The representation $\chi'(i)$ for quasi-internal modes of $(\text{NiO}_6^{\text{w}})^{2+}$ may be obtained from

$$\chi'(i) = \chi(t) - (\chi'(1) + \chi'(t)) \quad \dots 5.4a$$

The reduction of $\chi'(t)$, $\chi'(1)$ and $\chi'(i)$ gives the desired classification of 96 translations (cf last three lines of Table 5.2).

b. Site Symmetry Approach

The correlations between different species of C_{2v} for H_2O , T_d for SO_4^{2-} and O_h for $(\text{NiO}_6^{\text{w}})^{2+}$ with those of D_4 point group of the crystal are given in Table 5.3. Using these correlations, symmetry species and number of phonon branches arising from a definite mode of free state H_2O , SO_4^{2-} or $(\text{NiO}_6^{\text{w}})^{2+}$ are given in Table 5.4. This table has been divided into four sections. Section (i) presents the classification of 144 modes (72 internal + 72 librational of H_2O molecules, while sections (ii) and (iii) present the classification of 36 internal modes of SO_4^{2-} and 60 internal modes of $(\text{NiO}_6^{\text{w}})^{2+}$ respectively. The classification of 12 librations of SO_4^{2-} and 12 librations of $(\text{NiO}_6^{\text{w}})^{2+}$ and 24 translatory lattice modes (21 optical + 3 acoustical) is separately given in the last section (iv). The number given in first seven rows of section (i) are for the one type of H_2O molecule. The three different types of H_2O molecules have been accounted for in the total given in the eighth row.

5.5 FORM OF THE RAMAN TENSOR COMPONENTS

The point group symmetry D_4 of the crystal of NSH has five irreducible representations: A_1 , A_2 , B_1 , B_2 and E^{89} . Phonons of all

species except those of A_2 are Raman active and have the following forms of Raman Tensor⁹⁰

$$A_1 = \begin{pmatrix} a & 0 & 0 \\ 0 & a & 0 \\ 0 & 0 & b \end{pmatrix} \quad B_1 = \begin{pmatrix} c & 0 & 0 \\ 0 & -c & 0 \\ 0 & 0 & 0 \end{pmatrix} \quad E_2 = \begin{pmatrix} 0 & d & 0 \\ d & 0 & 0 \\ 0 & 0 & 0 \end{pmatrix}$$

$$E(\vec{a}) = \begin{pmatrix} 0 & 0 & 0 \\ 0 & 0 & e \\ 0 & e & 0 \end{pmatrix} \quad \text{and} \quad E(-\vec{b}) = \begin{pmatrix} 0 & 0 & e \\ 0 & 0 & 0 \\ e & 0 & 0 \end{pmatrix}$$

Rotating the crystal by 45° around c axis, so that the new frame of axes become $\vec{a}' = (\vec{a} + \vec{b})/\sqrt{2}$ and $\vec{b}' = (\vec{a} - \vec{b})/\sqrt{2}$, A_1 tensor remains unchanged. The other tensors, however, have the following forms

$$B_1 = \begin{pmatrix} 0 & c & 0 \\ c & 0 & 0 \\ 0 & 0 & 0 \end{pmatrix} \quad B_2 = \begin{pmatrix} -d & 0 & 0 \\ 0 & d & 0 \\ 0 & 0 & 0 \end{pmatrix}$$

$$E(\vec{a}') = \begin{pmatrix} 0 & 0 & e \\ 0 & 0 & e \\ e & e & 0 \end{pmatrix} \quad \text{and} \quad E(-\vec{b}') = \begin{pmatrix} 0 & 0 & -e \\ 0 & 0 & e \\ -e & e & 0 \end{pmatrix}$$

The phonons belonging to E representation are also infrared active hence each one of them is expected to split into a LO and a TO component. The polarization associated with these phonons is given in parenthesis.

The crystal symmetry thus leads to five independent components of polarizability tensor. Raman spectra of different polarizations can be

recorded using appropriate geometrical arrangements in view of the above forms of Raman tensors. Fig. 5.4 depicts such geometries, equivalents of which can also be used. Crystallographic axes are denoted by a , b and c in this figure. The set of axes denoted by a' and b' represent axes making 45° angle with a and b axes in ab plane. The wave vectors of incident and scattered light and the phonons taking part in scattering processes are denoted by \vec{k}_i , \vec{k}_s , and \vec{q} , respectively. It can be easily understood that spectra recorded in $b(aa)c$ or its equivalent would provide informations about phonons of mixed species, $A_1 + B_1$. In order to isolated phonons of B_1 species geometry $b'(a'b')c$ shown in Fig. 5.4 (v) or its equivalent can be used. Similarly, we note that ac polarized spectra arise due to phonons exhibiting change in dipole moment along b -axis. Such spectra recorded in $c(ac)b$ geometry would scan both TO and LO components of phonons of E species. In order to isolate TO components, geometry $c(ac)a$ shown in Fig. 5.4 (vi) or its equivalent may be used.

5.6 EXPERIMENTAL

a. Growth of Single Crystals

$\text{NiSO}_4 \cdot x\text{H}_2\text{O}$ of Analar quality was obtained from BDH (British Drug House) chemicals. It was subjected to the crystallization process involving slow evaporation of its aqueous solution in order to obtain NSH at 32°C ⁹¹.

Large single crystals of NSH were obtained by recrystallization of the crystallized sample using seed suspension technique as discussed by Holden and Singer⁹¹. Blue colour crystals thus grown appear to have well developed octahedral shape

The deuteration of the sample was done following the procedure discussed in section 2.10. For this purpose, anhydrous sample was obtained by heating the finely powdered NSH in a furnace at $\sim 300^\circ\text{C}$ for about 8 hours. A solution of this sample was prepared in D_2O as discussed in section 2.10. Finally, deuterated NSH was obtained by evaporating D_2O (under vacuum) from the solution which was kept at a temperature above 32°C to ensure correct chemical structure.

b. Determination of Crystallographic Axes

The property of perfect cleavage along (001) plane of the crystal was used to fix c-axis. The a- and b- axes of the crystal were fixed using the knowledge of crystal morphology⁹² and were confirmed by X-ray diffraction (Laue-pattern) method. Crystals of appropriate size were cut and polished by following the procedure described in section 2.3.

c. Scan of Raman Spectra

The crystal of NSH shows maximum transmission¹⁷ and minimum optical rotatory power²⁰ near 4900 \AA . The c-axis behaves as an optical axis. The rotatory power decreases from $0^\circ/\text{mm}$ at 4900 \AA to $-1.85^\circ/\text{mm}$ at 6000 \AA through $0.2^\circ/\text{mm}$ at 4880 \AA ²⁰. The 4880 \AA emission line of Ar^+ ion laser is found to be most suitable to excite Raman effect in this crystal.

A clear and transparent crystal of about $6 \times 5 \times 3 \text{ mm}^3$ size having plane polished faces was used in different orientations so as to get scattering geometries defined by first four parts of Fig. 5.4 and their equivalents. Although, spectra recorded in last two geometries (cf Fig. 5.4 (v), (vi)) could be, respectively, useful to isolate phonons of A_1 and B_1 species and the LO and TO components of E modes, however we are unable to

produce them here. To minimise the effect of rotatory power of crystal on the observed spectra, light from laser was allowed to enter the crystal within 1 mm of the crystal face closest to the spectrophotometer and only first 2 mm of the thread like passage of light was focused on the slit. Since the crystal of NSH exhibits some absorption at 4880 \AA , the laser beam with its maximum power was found to make holes in it. In order to avoid this phenomenon, the power of the laser was reduced appropriately. Other instrumental details are discussed in sections 2.7 and 2.8.

d. Scan of IR Spectra

The ATR technique was used to record IR spectra of single crystal of appropriate size ($15 \times 6 \times 2 \text{ mm}^3$) with incident unpolarized light falling at various angles (i.e. 35° , 37.5° , 40° , 45° and 50°) on its well polished (001) plane following the procedure discussed in section 2.5a.

IR spectra of micro-crystalline sample were recorded using KBr pellet which was used in situ to record spectrum at LT. To ensure the adequacy of the spectrum, nujol mull technique was also employed at RT. Spectrum of deuterated microcrystalline NSH was also recorded at RT.

All these spectra were recorded on PE-521 spectrophotometer in $250\text{--}4000 \text{ cm}^{-1}$ range.

5.7 RESULTS AND DISCUSSION

I. RAMAN PHONONS IN SINGLE CRYSTAL

a. Observed Spectra

Raman spectra of single crystal of NSH having aa and bb polarization and ac and bc polarization characteristics were found to be identical.

Thus only four out of twelve spectra were found to be distinct. Representatives of these four spectra are shown in Figs. 5.5 and 5.6; the former figure depicts only O-H stretching region, while the latter figure covers the complete region at lower frequencies. In these figures aa, bb, cc, etc. denote the polarization character of respective spectra, while A_1 , B_1 , etc. denote the corresponding symmetry species of D_4 point group. The dotted curves are the manually resolved bands having Lorentzian shapes.

b. Frequency, Width and Intensity of Bands

Appendix 5.2 provides frequency (ν), width (FWHMI, cm^{-1}) and relative integrated intensity (I, in parenthesis) of various bands observed in different spectra. The ν values are accurate within $\pm 2 \text{ cm}^{-1}$ for well developed sharp bands. The frequencies of the manually resolved bands showing sharp structure and of those showing broad or diffuse structure may have uncertainty as large as ± 5 and $\pm 10 \text{ cm}^{-1}$, respectively. The I values have been determined by the same method as discussed in section 3.7a. These values for bands of O-H stretching region are unrelated with those of lower frequency region. In the former case they are relative with respect to an arbitrarily chosen value, 10, for the intensity of lowest frequency band in each spectrum (cf frequencies marked with an asterisk in the Appendix). Similarly for bands below 2900 cm^{-1} , these I values are relative with respect to a value 10, chosen for the band falling between $1083\text{--}1095 \text{ cm}^{-1}$ in each spectrum (cf bands marked with ** in the Appendix). The accuracy in I values lies within 20% and 5%, respectively, for bands of O-H stretching and lower frequency (i.e. below 2900 cm^{-1}) regions.

c. Assignments

The assignments of observed Raman bands, as given in Table 5.5, are discussed in detail in the following subsections:

Internal Modes of H₂O Molecules: The bands appearing in 2900-3500 cm⁻¹ region of spectra of NSH should reasonably be due to ν_1^w and ν_3^w fundamental and 2 ν_2^w overtone modes of H₂O(I), H₂O(II) and H₂O(III) molecules (cf Table 5.1). The structural data⁶⁶ for these molecules, as given in Table 5.1, reveal that H₂O(I) exhibits considerable asymmetry while H₂O(II) and H₂O(III) are symmetric to a good approximation. The increasing H-O' and O-O' distances on going from H₂O(I) to H₂O(III) (cf columns 4 and 5 of Table 5.1 where O and O' represent oxygen atoms of H₂O and SO₄²⁻, respectively) indicate that on an average H₂O(I) exhibits strongest H-bonds while H₂O(III), the weakest among the three. The stretching modes of H₂O(I), H₂O(II) and H₂O(III) should therefore fall in an ascending order of frequency.

For the symmetric type of H₂O molecules ν_1^w and ν_3^w modes are related with each other to a reasonable accuracy through the empirical relation^{2f}.

$$(3657 - \nu_1^w) = 0.8333(3756 - \nu_3^w) \quad \dots \quad 5.7a$$

Assuming that 3428(A₁), 3455(A₁ + B₁, B₂) and 3460(E) cm⁻¹ bands arise due to ν_3^w (III) mode of H₂O(III), the corresponding frequencies for ν_1^w (III) were computed to be 3384(A₁), 3406 (A₁ + B₁, B₂) and 3410(E) cm⁻¹, respectively, using the Eqn. 5.7a. These frequencies lie reasonably close to 3375 (A₁, A₁ + B₁), 3360(B₂) and 3404(E) cm⁻¹ of observed bands which have, therefore, been associated with ν_1^w (III) mode. Similarly, attributing

3290(A_1), 3285($A_1 + B_1$), 3282(B_2) and 3310(E) cm^{-1} bands of observed spectra to $\nu_3^w(\text{II})$ mode of $\text{H}_2\text{O}(\text{II})$, we computed the respective frequencies 3269(A_1), 3265($A_1 + B_1$), 3262(B_2) and 3285(E) cm^{-1} for $\nu_1^w(\text{II})$ mode. These values are about 20 cm^{-1} lower than those of $\nu_3^w(\text{II})$. We observe the bands at 3190(A_1), 3198($A_1 + B_1$), 3230(B_2) and 3223(E) cm^{-1} which are lower than these computed values by 79, 67, 32 and 62 cm^{-1} , respectively; thus it is not reasonable to assign these bands as $\nu_1^w(\text{II})$.

Here it is observed that the average frequency of ν_2^w mode lies around 1630 cm^{-1} (cf Tables 5.6 and 5.7). Therefore, $2\nu_2^w$ mode of A_1 symmetry of C_{2v} point group may share intensity (through Fermi resonance interaction) from ν_1^w mode of the same symmetry, if the latter falls near the computed harmonic frequency ($\sim 3260 \text{ cm}^{-1}$) of the former. It is observed that the average frequency of $\nu_1^w(\text{III})$ lies at 3379 cm^{-1} hence $2\nu_2^w(\text{III})$ must be weak. But the ν_{av} ($\sim 3271 \text{ cm}^{-1}$) of $\nu_1^w(\text{II})$, computed by using ν_{av} ($\sim 3292 \text{ cm}^{-1}$) of $\nu_3^w(\text{II})$ in Eqn. 5.7a, is close to 3260 cm^{-1} . Consequently, $\nu_1^w(\text{II})$ and $2\nu_2^w(\text{II})$ undergo Fermi resonance and these modes get mixed with each other. One of the two mixed levels of these modes may finally fall on lower frequency side alongwith the other on higher frequency side of 3260 cm^{-1} . The lower frequency component, which may perhaps have larger contribution of $2\nu_2^w(\text{II})$, has been assigned to 3230(ab) and 3223(ac) cm^{-1} bands, while the higher frequency component which may perhaps have larger contribution of $\nu_1^w(\text{II})$ seems to superimpose the $\nu_3^w(\text{II})$ bands. The $2\nu_2^w(\text{II})$ bands ($\nu_{av} = 3227 \text{ cm}^{-1}$), which are not clearly observed in cc and bb(or aa) polarized spectra, might have been obscured by strong bands at 3190 and 3198 cm^{-1} , respectively. Finally, we associate the remaining unassigned bands of 3190(A_1), 3198($A_1 + B_1$), 3144(B_2) and

3134(E) cm^{-1} with $\nu_1^{\text{W}}(\text{I})$ mode. Here we note that the former two frequencies are higher by about 60 cm^{-1} from the latter two. This may be due to the fact that $2\nu_2^{\text{W}}(\text{II})$ also contributes to the intensity in the former two bands on their higher frequency side. The assignment of $\nu_3^{\text{W}}(\text{I})$ would be discussed later while analysing IR spectra of micro-crystalline NSH.

Nakamoto et al⁹³ correlated O-H stretching band positions with O-H...C' bond lengths. Using these correlations and our assignments of stretching modes, we estimated O-H...O' bond lengths for $\text{H}_2\text{O}(\text{I})$, $\text{H}_2\text{O}(\text{II})$ and $\text{H}_2\text{O}(\text{III})$ molecules. The values obtained are 2.74 \AA , 2.78 \AA and 2.85 \AA , respectively. Within the uncertainties of such estimations, these values are found to be in good agreement with the corresponding ones, known from crystallographic data (cf column 5 Table 5.1) and thus support our assignments.

The ν_2^{W} mode could not be observed in Raman spectra of single crystal. This mode appears as weak broad band at 1625 cm^{-1} in IR(ATR) spectra of single crystal and at 1635 cm^{-1} in the spectrum of micro-crystalline NSH.

Internal Modes of SO_4^{2-} Ion: The ν_1^{S} and ν_3^{S} modes of this ion fall in isolated frequency regions of the vibrational fundamentals in NSH crystal. These modes could, therefore, be unambiguously assigned as shown in Table 5.5. The former mode appears as the sharpest band ($\text{FWHMI} \approx 5-7 \text{ cm}^{-1}$) in each of the four spectra. The number of bands appearing due to ν_1^{S} in each spectrum are consistent with theoretical predictions (cf Table 5.4).

The ν_3^s mode shows one band at 1083 and 1095 cm^{-1} , respectively, in cc and ab polarized spectra as expected theoretically (cf Table 5.4). However, two bands are observed both in bb(or aa) and ac(or bc) polarized spectra while three allowed components of $A_1 + 2B_1$ and $3E$ species are respectively expected on the basis of theoretical analysis. Moreover, in bb polarized spectrum, 1123 cm^{-1} band has negligibly weak intensity and perhaps arises due to the spillover of strong 1130(ac) cm^{-1} band. Thus the ν_3^s mode exhibits a strong band of frequency lying in 1083 - 1095 cm^{-1} range of all the four recorded spectra. A strong band at 1130 cm^{-1} is also observed only in ac polarized spectrum. This specific appearance in ac polarization leads us to assign TO and LO components of $3E$ phonon modes of ν_3^s to 1089 and 1130 cm^{-1} bands, respectively. These bands have a separation of 41 cm^{-1} . The well established LO and TO components of similar type of ν_3 ($\sim 980 \text{ cm}^{-1}$) mode of ClO_3^- ion in NaClO_3 crystal⁹⁴ have separation of the same order. Perhaps it may be considered as a support to the above assignments.

The ν_2^s and ν_4^s modes fall around 450 and 610 cm^{-1} , respectively where librational modes of H_2O molecules may also appear. However, the appearances of one or two strong bands in 645 - 603 cm^{-1} and two in 475 - 426 cm^{-1} regions of observed spectra indicates that water librations are weak and diffuse and all these strong bands arise due to SO_4^{2-} modes. The weak and diffuse bands due to H_2O librations in 865 - 752 cm^{-1} range of bb and ac polarized spectra (cf Fig. 5.6) corroborates this inference. This has also been shown by Jager and Schaack⁸¹ by investigating Raman and IR spectra of NSH and deuterated NSH.

Following these arguments we note that as far as the number of bands observed for triply degenerate ν_3^s and ν_4^s modes are concerned, the two exhibit identical behaviour. Therefore, the three strong bands $603(A_1)$, $618(A_1 + B_1)$ and $619(E_2)$ cm^{-1} have been associated with non-polar components of ν_4^s mode and the two bands $616(E)$ and $645(E)$ cm^{-1} respectively to TO and LO components of $3E$ polar phonons.

It is interesting to note that (i) all the allowed components of doubly degenerate ν_2^s mode appear as separate bands unlike triply degenerate ν_3^s and ν_4^s modes which show only single band in all spectra except that of E phonons and (ii) the ν_2^s and ν_1^s modes do not show any observable difference in the frequencies of LO - TO splittings of their components of E species. The latter observation leads us to conclude that SO_4^{2-} ion is not much distorted from its tetrahedral structure for which ν_1^s and ν_2^s modes are IR forbidden and thus do not have strong polar character.

Librational Modes of H_2O Molecules: As already mentioned, these modes are not observed as well developed bands in Raman spectra, hence their detailed discussion would be presented in section 5.7(III) dealing with IR spectra of microcrystalline NSH.

Quasi-Internal Modes of $(\text{NiO}_6^w)^{2+}$ Complex: By studying Raman and IR spectra of NSH and deuterated NSH, Jager and Schaack⁸¹ have shown that bands observed in $400 - 200 \text{ cm}^{-1}$ region arise due to quasi-internal modes of $(\text{NiO}_6^w)^{2+}$ complex; however, some of their assignments seem to be incorrect. The crystallographic data⁶⁶ reveal that $(\text{NiO}_6^w)^{2+}$ complex does not exhibit much distortion in its octahedral symmetry. Consequently,

only $\nu_1^c(A_g)$, $\nu_2^c(E_g)$ and $\nu_5^c(F_{2g})$ modes are expected to be strong in Raman spectra, while $\nu_3^c(F_{1u})$ and $\nu_4^c(F_{1u})$ in the IR spectra.

Our assignment of the totally symmetric ν_1^c mode to the bands observed around 380 cm^{-1} is based on the following facts: (i) the bands observed around 380 cm^{-1} correspond to the least depolarization ratio among all those of $400 - 200\text{ cm}^{-1}$ region and (ii) the low temperature IR spectrum of microcrystalline NSH exhibits a weak and sharp band (FWHMI $\approx 20\text{ cm}^{-1}$) at 375 cm^{-1} (cf Appendix 5.3); similar behaviour is shown by well identified totally symmetric ν_1^s mode which is also IR forbidden, like ν_1^c .

All remaining bands of $400 - 200\text{ cm}^{-1}$ region are found to be centred around 298, 273, 251 and 215 cm^{-1} . The bands near 298 cm^{-1} appear only in cc polarized spectrum with **good** intensity and in ab polarized spectrum with very low intensity. The bands near 273 cm^{-1} are observed in all the four spectra, though as weak bands in ab polarization. On the other hand bands centred near 251 do not have their representatives in cc polarized spectrum. Here, we note that bands centred near 273 and 251 cm^{-1} differ in frequencies under different polarization as much as by 10 cm^{-1} , while those centred at 215 cm^{-1} have fixed frequency within the experimental errors. Moreover, 251 cm^{-1} bands are separated from **bands** around 215 cm^{-1} by 36 cm^{-1} while from 273 cm^{-1} bands by about 22 cm^{-1} . A **critical** examination of these observations reveals that bands near 215 cm^{-1} should be due to a different mode while those near 251 and 273 cm^{-1} could be due to the one and the same mode. Following the general observation that stretching modes fall at higher frequencies than bending modes, the $\sim\nu_2^c(\text{Ni}---\text{O}^w\text{ stretching})$ mode has been assigned to bands centred at 273

and 251 cm^{-1} , while the ν_5^c (angular deformation) mode to 215 cm^{-1} bands. The number of bands observed in each spectrum is equal to those expected theoretically for doubly degenerate ν_2^c mode, while only single band appears for ν_5^c triply degenerate mode. This behaviour is identical to that observed for doubly degenerate ν_2^s and triply degenerate ν_3^s and ν_4^s modes of SO_4^{2-} ion.

As reported by Jager and Schaaack⁸¹, the bands $297(\text{A}_1)$ and $298(\text{B}_1)$ cm^{-1} could have also been attributed to ν_2^c mode. But the symmetry classification (cf Table 5.4) reveals that ν_2^c mode has only one allowed component in these spectra. These frequencies are also not too high to attribute them to $\nu_3^c(\text{Ni}---\text{O}^w \text{ stretching})$ mode which is only IR active for perfect O_h symmetry. But the high intensity of $297(\text{A}_1)\text{ cm}^{-1}$ band is not compatible with very low distortions⁶⁶ in octahedral structure of the complex. Moreover, the IR spectra do not exhibit any strong band due to ν_3^c mode near this frequency. Therefore, the $297(\text{A}_1)$ and $298(\text{B}_2)\text{ cm}^{-1}$ bands appear to arise due to a multi-phonon process involving low-lying quasi-internal modes of the complex. A most unique assignment for this band has been found to be $2\nu_6^c(\text{A}_g + \text{E}_g + \text{F}_{1g} + \text{F}_{2g})$,— the first overtone of $\nu_6^c(\text{F}_{2u})$ mode. The high intensity of $297(\text{A}_1)\text{ cm}^{-1}$ band may be understood in terms of resonance interaction of E_g component of $2\nu_6^c$ with $\nu_2^c(\text{E}_g)$ falling nearby. This assignment of $2\nu_6^c$ mode reveals that ν_6^c mode must have frequency of about 149 cm^{-1} which is quite reasonable for this mode.

It is important to note that none of the IR forbidden ν_1^c , ν_2^c and ν_5^c modes exhibit observable LO - TO splittings in their components of E species analogous to ν_1^s and ν_2^s modes which are also forbidden in IR.

This indicates that $(\text{NiO}_6^{\text{w}})^{2+}$ complex is not significantly distorted (as is also known from crystal data⁶⁶) from its octahedral structure and thus ν_1^{c} , ν_2^{c} and ν_5^{c} do not acquire significant polar character.

The above discussion on Raman spectra of NSH crystal does not provide any information about IR active ν_3^{c} and ν_4^{c} modes of the complex. Therefore, to complete the understanding of the dynamics of the complex we may look into the assignments for IR bands reported by Jager and Schaack⁸¹. These authors observed five bands in IR spectrum of A_2 species at 345(vw), 326(vw), 251(s), 227(w) and 217(w) cm^{-1} ; the abbreviations vw, s and w respectively refer to bands of very weak, strong and weak intensity. IR bands of almost similar frequencies and intensities are also observed in the spectrum of powdered NSH reported by Nyquist and Kagel⁹⁵. Jager and Schaack⁸¹ associated all the three bands (251, 227 and 217 cm^{-1}) with A_2 branches of ν_4^{c} mode. However, it looks more reasonable to associate the strongest band at 251 cm^{-1} to ν_3^{c} mode while those at 227 and 217 cm^{-1} to ν_4^{c} since (i) the asymmetric $\text{Ni}-\text{O}^{\text{w}}$ stretching mode ν_3^{c} is expected to have more intense bands of higher frequency than those of ν_4^{c} and (ii) the ν_4^{c} mode has only two components of A_2 species (cf Table 5.4). The very weak IR bands at 345(A_2) and 326(A_2) cm^{-1} could be assigned as $\nu_6^{\text{c}} + \nu_5^{\text{c}}$ ($A_{1u} + E_u + F_{1u} + F_{2u}$) mode and not as ν_3^{c} since their intensity does not seem to be compatible with the latter mode.

External Lattice Modes: All the strong bands observed below 200 cm^{-1} have been associated with allowed optical translatory external modes ($2A_1 + 4B_1 + 2B_2 + 5E(\text{LO}) + 5E(\text{TO})$). Few bands exceeding in number over these allowed modes are observed in different spectra as weak bands and sometimes as shoulders to the exciting line or strong Raman bands.

Frequencies of such bands are marked with double asterisk(**) in Table 5.5. These bands may be attributed to: (i) the spillover of strong bands from other polarizations, (ii) multiphonon processes and/or (iii) external rotations of SO_4^{2-} and $(\text{NiO}_6^{\text{W}})^{2+}$ which can only correspond to weak bands, since they are forbidden in both IR and Raman spectra for their perfectly symmetric states. Although, it is difficult to find unambiguous assignments for these weak bands, the spillover of strong bands seems to be the main reason for their appearance.

In the spectrum of ac(or bc) polarization 10 strong bands appear below 200 cm^{-1} . These bands arise from 5E(LO) and 5E(TO) components of allowed external translatory modes. Frequencies of these bands can be arranged into five pairs as shown in column 4, section (v) of Table 5.5. The lower frequency band of each pair has been attributed to a TO component while the higher one to a LO component of a polar translatory phonon mode of E species. From these assignments it is noted that TO component has higher intensity than the LO component analogous to such components of ν_4^{S} but opposite to those of ν_3^{S} modes of SO_4^{2-} .

Although, the spectrum recorded in a(ca)c is needed to establish the assignments of LO and TO components of phonons belonging to E species, the observation of 10 strong bands below 175 cm^{-1} in the spectrum of ac polarization (cf the bottom curve in Fig. 5.6) for 5E phonons (translatory external modes) evidently support our assignments.

II IR(ATR) SPECTRA OF SINGLE CRYSTAL OF NSH

Five typical IR(ATR) spectra of single crystal of NSH recorded at $\theta_i = 35^\circ, 37.5^\circ, 40^\circ, 45^\circ$ and 50° are shown in Fig. 5.7. From these

spectra we observe the following: (i) The bands arising due to O-H stretching modes falling in $2700 - 3600 \text{ cm}^{-1}$ region exhibit anomalous character for θ_i increasing upto about 40° . For $\theta_i = 45^\circ$, a normal typical absorption type spectrum is observed,— the intensity of which diminishes considerably at $\theta_i = 50^\circ$. Similar behaviour is shown by the ν_2^w band ($\sim 1625 \text{ cm}^{-1}$). (ii) For $\theta_i = 40^\circ$, a normal absorption type sharp band is observed at 1100 cm^{-1} due to ν_3^s mode. The higher frequency wing of this peak, however, exhibits anomalous absorption band type shape at the same angle. A broad and strong band is also observed at about 1060 cm^{-1} due to this mode. The frequencies of 1100 and 1060 cm^{-1} bands shift to 1105 and 1070 cm^{-1} respectively in the spectrum for $\theta_i = 50^\circ$, at which both bands have normal absorption band type shapes and (iii) the superposition of large number of bands appearing in $250 - 900 \text{ cm}^{-1}$ region makes it difficult to identify whether the bands have the normal absorption type shapes as they appear to have at every measured angle, θ_i . The spectra in this region do not change much in band shapes on increasing θ_i but small increase in band frequencies and decrease in attenuated intensity are observed.

In absorbing regions, where the refractive index changes considerably with change in frequency, the estimate of critical angle for the system of NSH and KRS-5 may not have much significance. However, in non-absorbing regions between $1100 - 4000 \text{ cm}^{-1}$ its value was estimated to be $41 \pm 1^\circ$ by studying the rate of decrease in reflected intensity with decrease in θ_i ; at $\theta_i = \theta_c$ the reflected intensity decreases with maximum rate. From this value of θ_c the refractive index of NSH crystal with respect to that of vacuum may be estimated to be $1.56 \pm .03$ using

refractive index of KRS-5 i.e. 2.37 which remains almost constant in above mentioned frequency range.

It is also observed that the attenuation in reflected intensity shows a general decrease with increasing frequency from 250 to 4000 cm^{-1} . This phenomenon may be related with the effective depth of penetration of evanescent field which also decreases with increasing frequency.

The frequencies of bands read from three selected spectra corresponding to $\theta_i = 37.5, 45$ and 50° are given in Table 5.6. The positions of anomalous dispersion like bands have been measured at the points of maximum slope, while for normal absorption like bands at the peak points. These measured frequencies are accurate upto $\pm 2\text{ cm}^{-1}$ for well shaped bands but upto $\pm 10\text{ cm}^{-1}$ for broad or anomalous dispersion type bands. The difference observed between positions of a band in different spectra is not significantly large within the limits of experimental errors.

III IR SPECTRA OF MICROCRYSTALLINE NSH

a. Observed Spectra

The IR spectra of microcrystalline NSH are shown in Figs. 5.8 and 5.9. Spectra (a) and (b) of the former figure represent those recorded in KBr pellet and Nujol mull, respectively. A good similarity between these two spectra establishes that KBr and NSH do not undergo ion exchange phenomenon and thus an otherwise observation reported by Janik et al⁷⁴ is not true. This is also corroborated by the good similarity between spectrum (a) of Fig. 5.8 and ATR spectrum of single crystal (cf Fig. 5.7, $\theta_i = 50^\circ$) in $1700 - 250\text{ cm}^{-1}$ region in which the latter spectrum shows intense bands of transmission like character. Fig. 5.8(c) depicts

the spectrum of the deuterated analogue of NSH. The extent of deuteration was estimated to be more than 90% from the integrated intensity of O-D and O-H stretching bands.

Figs. 5.9a and 5.9b depict spectra of KBr pellet recorded at RT ($\sim 300^\circ\text{K}$) and LT ($\sim 120^\circ\text{K}$). These spectra have been retraced in Figs. 5.9c and 5.9d respectively after correcting the former two for general scattering of KBr pellet. The latter two spectra have been resolved into optimum number of Lorentzian shaped bands.

b. Frequency Width and Intensity

Appendix 5.3 provides frequencies (ν), FWHMI(cm^{-1}) and integrated intensity (I) of each resolved band of spectra c and d shown in Fig. 5.9. The ν values are accurate upto $\pm 2 \text{ cm}^{-1}$ for sharp bands but may have errors upto $\pm 10 \text{ cm}^{-1}$ for broad bands. The I values have been determined by multiplying peak absorbance with FWHMI measured in wave numbers. These values as given in the appendix are relative to an arbitrarily chosen value 10 for 1102 cm^{-1} band in RT spectrum and for 1095 cm^{-1} band in LT spectrum. The uncertainties in these values lie within 5 % for well developed bands and within 20% for broad and weak or manually resolved bands.

c. Assignments

The frequencies ν measured from Figs. 5.9c and 5.9d have also been tabulated in Table 5.7 alongwith their assignments. Band positions observed in the spectrum of deuterated analogue (cf Fig. 5.8c) are also given in column 4 of this table. The $\nu_{\text{H}}/\nu_{\text{D}}$ values (computed from the observed frequencies ν_{H} and ν_{D} of a similar mode in RT spectra of NSH and deuterated NSH respectively) are given in the last column to facilitate the discussion.

Internal Modes of H_2O : The O-H stretching region of RT and LT spectra exhibit three and five prominent bands, respectively. The latter spectrum also shows two weak residual bands which may reasonably arise due to anharmonic force fields, general scattering effect of KBr pellet (possibly persisting even after the correction of base line), etc. We note that the highest frequency RT band of 3460 cm^{-1} splits into a strong component of 3480 cm^{-1} and a little weaker component of 3410 cm^{-1} at LT. Similarly, the next higher frequency RT band of 3290 cm^{-1} splits into a strong component of 3310 cm^{-1} and a little weaker component of 3240 cm^{-1} . In view of assignments discussed for Raman spectra of single crystal 3480 and 3410 cm^{-1} bands have been attributed to $\nu_3^{\text{w}}(\text{III})$ and $\nu_1^{\text{w}}(\text{III})$ respectively. Relative intensity of $\nu_3^{\text{w}}(\text{III})$ with respect to that of $\nu_1^{\text{w}}(\text{III})$ clearly supports these assignments since the former is expected to be stronger than the latter in IR. The 3310 cm^{-1} strong band has been associated simultaneously with $\nu_3^{\text{w}}(\text{II})$ and $\nu_1^{\text{w}}(\text{II})$. The $2\nu_2^{\text{w}}(\text{II})$ mode has been assigned to 3240 cm^{-1} band whose high intensity may be understood in terms of strong resonance interaction with $\nu_1^{\text{w}}(\text{II})$.

The lowest frequency IR band in O-H stretching region has frequency of 3045 cm^{-1} . But the lowest frequency Raman band has an average value of 3139 cm^{-1} and has been associated with $\nu_1^{\text{w}}(\text{I})$ (cf Table 5.5). Since these frequencies of IR and Raman spectra differ by significant value of about 100 cm^{-1} they must have the different origins. Thus $\nu_3^{\text{w}}(\text{I})$ can be assigned to 3045 cm^{-1} IR band on the basis that it should be stronger than $\nu_1^{\text{w}}(\text{I})$ which perhaps has very weak band at 3139 cm^{-1} in IR; for its low intensity, the latter band might have been obscured by lower frequency wing of strong IR band due to $2\nu_2^{\text{w}}(\text{II})$ modes. Similarly, the $\nu_3^{\text{w}}(\text{I})$

appearing around 3045 cm^{-1} perhaps has very low intensity in Raman spectra. The asymmetry of $\text{H}_2\text{O(I)}$ may be one of the reasons for such a behaviour of $\nu_1^{\text{W}}(\text{I})$ and $\nu_3^{\text{W}}(\text{I})$ modes.

The ν_2^{W} mode, which is not observed in any Raman spectra of single crystal, appears as weak and broad band at 1635 and 1642 cm^{-1} , respectively, in RT and LT spectra (IR). It does not exhibit observable change in its intensity and width on lowering the temperature. Since the band does not exhibit any structure even at LT, the separate assignment of this mode of $\text{H}_2\text{O(I)}$, $\text{H}_2\text{O(II)}$ and $\text{H}_2\text{O(III)}$ could not be possible.

Internal Modes of SO_4^{2-} Ion: Two internal modes of SO_4^{2-} ion ν_1^{S} and ν_3^{S} fall in the isolated frequency region $900 - 1300\text{ cm}^{-1}$ of vibrational spectra of NSH. ν_1^{S} appears as a band of negligible intensity at 983 cm^{-1} in RT and at 985 cm^{-1} in LT spectra. Such a low intensity of this mode indicates that SO_4^{2-} ion has almost a tetrahedral structure in NSH crystal. The similar inference was also made on the basis of Raman spectra. On lowering the temperature the intensity of this mode, increases, although not very significantly. One of the reasons for it could be the increase of distortion in T_d structure of SO_4^{2-} on lowering the temperature.

The broad IR band of 1100 cm^{-1} could be appropriately resolved into three components of 1148 , 1102 and 1065 cm^{-1} at RT. In LT spectrum, these components have frequencies 1148 , 1095 and 1065 cm^{-1} . The 1065 cm^{-1} components may more reasonably be associated with $\nu_2^{\text{S}} + \nu_4^{\text{S}}(F_1 + F_2)$ having computed harmonic frequency about 1060 cm^{-1} . Its intensity can be understood in terms of resonance interaction of its F_2 component with $\nu_3^{\text{S}}(F_2)$ fundamental mode. The remaining two higher frequency components seem to arise due to ν_3^{S} mode.

The ν_2^s ($\sim 450 \text{ cm}^{-1}$) mode which is forbidden in IR for tetrahedral symmetry of SO_4^{2-} can only be expected to have very low intensity in IR spectrum and may be obscured by strong bands due to librations of H_2O molecules.

However, the ν_4^s mode which appears usually as a strong band near 613 cm^{-1} is also superimposed by bands of H_2O librations. The comparative study of spectra of NSH and its deuterated analogue reveals that all bands in $400 - 900 \text{ cm}^{-1}$ region (except the one at 610 cm^{-1}) exhibit frequency shifts by a factor of about $1/\sqrt{2}$; the 610 cm^{-1} band is observed to be at about 620 cm^{-1} in the spectrum of deuterated analogue. Similarly, the comparison of RT and LT spectra indicate that, except the 610 cm^{-1} band, all bands shift to higher frequencies by $10 - 20 \text{ cm}^{-1}$ with enhanced peak intensity and sharpness in LT spectrum. Both these observations reveal that ν_4^s mode should be assigned to 610 cm^{-1} band only.

The increasing frequency of ν_4^s on deuteration indicates strong H-bond interaction between O atoms of SO_4^{2-} ion and H atoms of H_2O molecules in the crystal. This fact is also evident from the increase in FWHM of ν_3^s mode by an approximate factor of 1.2 on deuteration of NSH. Other reason for ν_4^s shift could ^{be} the overlap of librations of H_2O and D_2O in different ways in respective spectra.

Librational Modes of H_2O Molecules: It is clear from the discussion of above subsection that all the nine bands, except 610 cm^{-1} in $400 - 900 \text{ cm}^{-1}$ region, arise due to librational modes of H_2O molecules. The possibility of any band being due to a transition between low lying translational and higher frequency librational modes is rejected since none of the

observed frequencies in this region corresponds to such a difference. As apparent from the observed spectra all the nine bands of $400 - 900 \text{ cm}^{-1}$ range can be arranged into three groups as indicated in column 1, Table 5.7.

The NSH crystal contains three crystallographically inequivalent water molecules (cf Table 5.1). The librational modes rocking (R^W), wagging (W^W) and twisting (T^W) of each of these water molecules may produce 9 bands in all as observed. Although, the intermolecular interaction between eight H_2O molecules of the same type in the unit cell of NSH may split each of these modes (cf section 1, Table 5.4), an interpretation of the absorption bands on the basis of correlation splitting is rejected in view of the simplicity of spectra and the relative isolation and lack of mutual perturbation of water molecules as shown in Appendix 5.1.

The T^W mode is forbidden for perfect C_{2v} symmetry of H_2O molecule. Therefore, it can appear as weak IR band owing to some asymmetry in the structure of H_2O molecules occupying C_1 sites in NSH crystal. Thus T^W modes of three different types of H_2O molecules have been assigned to the first three weaker bands at 735 , 575 and 410 cm^{-1} in RT spectrum. It is interesting to note that these bands are the lowest frequency bands of groups (a), (b) and (c) respectively. We also observe that the central frequency band shows maximum peak intensity in its own group. The integrated intensity of this band is also found to be maximum in groups (a) and (c). However, in group (b) the maximum integrated intensity is attained by its highest frequency (660 cm^{-1}) band. Such a differential behaviour may perhaps be attributed to the mixing of librational modes of H_2O with $\nu_4^s(610 \text{ cm}^{-1})$ mode of SO_4^{2-} ion which falls in the centre of the group. This mixing may also be responsible for comparatively more sharp structure of bands of group (b).

Miyazawa⁹⁶ showed that the wagging mode must be about 2.7 times more stronger than the rocking mode of H_2O . Although, the validity of this criterion has not been established in general, it has been found to hold good in some cases where unambiguous assignments of W^W and R^W modes are known⁹⁷. In view of this criterion, we assign the W^W modes to the central frequency band of each group; the remaining R^W modes could be assigned to the highest frequency bands.

It can be argued that the librational modes of H_2O exhibiting stronger H-bonds must have higher frequencies than the one exhibiting weaker H-bonds. Thus the librational modes of $H_2O(I)$ denoted by $R^W(I)$, $W^W(I)$ and $T^W(I)$ have been assigned to three bands of group (a), while those of $H_2O(II)$ and $H_2O(III)$ to the bands of groups (b) and (c), respectively.

From these assignments we computed the ratio $[I(W^W): I(R^W)]$ of integrated intensity of W^W and R^W modes of each type of H_2O molecules. This ratio for $H_2O(I)$ and $H_2O(III)$ is found to be about 1.8 and 1.5 respectively. To a good approximations these values are consistent with intensity criterion of Miyazawa⁹⁶. However, for $H_2O(II)$ the ratio is observed to be about 0.9 but this inconsistency seems to arise due to the mixing of librational modes of this water molecule with $\nu_4^s(610\text{ cm}^{-1})$ mode through H-bonding as we have already pointed out.

IV FORCE FIELD CONSTANTS FOR LIBRATIONS OF H_2O MOLECULE

Considering the H_2O as a rigid molecule, Blue⁹⁸ developed the following equations for the frequencies (measured in wave numbers) of its rotatory modes.

$$\text{Wagging: } \nu_W = (1/2\pi c) \cdot \left[\frac{k_H r_H^2 \sin^2 \phi + \frac{1}{2} k_O r_O^2}{I_a} \right]^{1/2} \quad \dots 5.7b$$

$$\text{Twisting: } \nu_T = (1/2\pi c) \cdot \left[\frac{k_H r_H^2 \cos^2 \phi}{I_b} \right]^{1/2} \quad \dots 5.7c$$

$$\text{Rocking: } \nu_R = (1/2\pi c) \cdot \left[\frac{k'_H r_H^2 + \frac{1}{2} k'_O r_O^2}{I_c} \right]^{1/2} \quad \dots 5.7d$$

The significance of r_H , r_O and ϕ may be understood from the geometry of H_2O molecule shown in Fig. 5.10. I_a , I_b and I_c are the principal moments of inertia about a-, b- and c- axes as shown in the same figure. k_H and k_O are the force constants respectively involved when H and O atoms get displaced from their mean positions in directions perpendicular to the plane of the molecule. k'_H and k'_O are the similar force constants which come into play for the displacements in the plane of H_2O molecule in appropriate directions for the Rocking mode. Using the geometry of free H_2O and moment of inertia values from Ref.(85), Eqns. 5.7(b-d) can be reduced to:

$$k_H + 0.0078k_O = 0.1340 \times 10^{-5} \cdot \nu_W^2 \quad \dots 5.7e$$

$$k_H = 0.1190 \times 10^{-5} \cdot \nu_T^2 \quad \dots 5.7f$$

$$k'_H + 0.0025k'_O = 0.1237 \times 10^{-5} \cdot \nu_R^2 \quad \dots 5.7g$$

Here k_H , k'_H , etc. are measured in mdyne/Å.

In computing above mentioned force constants, Van der Elsken and Robinson²ⁱ assumed that (1) the librational modes do not mix with intramolecular vibrations which is implied from the rigidity of the

molecule, (2) the centre of mass in the water molecule is the same in the crystal as it is in the gaseous phase, i.e. that the moments of inertia of the free molecule can be used. For the third assumption two alternatives were employed; (3a) that during the libration the centre of mass of the molecule remains fixed in the unit cell and does not oscillate and (3b) that the force constants opposing hydrogen and oxygen displacements are the same regardless of the axis about which the molecule librates.

Under the assumptions (1), (2) and (3a) the displacement of the oxygen atom is proportional to that of the hydrogens; thus their force constants are not independent and are related through $k_C = 16k_H$ and $k'_O = 16k'_H$. The force constants k_H and k'_H thus computed are reported²¹ to be around 0.2 and 0.1 mdyne/Å respectively. Consequently, k_C and k'_C must have values around 3.2 and 1.6 mdyne/Å in the same order.

Under the assumptions (1), (2) and (3b), we have $k_H = k'_H$ and $k_C = k'_O$ (as also used by Blue⁹⁸) which were computed to have values of the order of 0.1 and 50 mdyne/Å respectively.

However, we note that: (i) in librational modes of H_2O the displacements of O atoms usually occur in directions normal to metal-oxygen bond to a good approximation, (ii) the frequencies of corresponding translatory vibrations (i.e. excluding those against metal atom) of H_2O in large number of hydrates have values lying in 100 - 300 cm^{-1} range and (iii) the frequency (ν_t) of such translatory modes may be given by the following relation under the approximation of simple harmonic motion.

$$\nu_t = (1/2\pi c) \cdot \left[\frac{k_C + 2k_H}{m_w} \right]^{1/2} \quad \dots 5.7h$$

where m_w represents the mass of H_2O molecule. Similar relation may be written for translations involving k'_O and k'_H .

The limiting frequencies 100 and 300 cm^{-1} of these modes when used in above equation (assuming $k_H = 0$ for an instant) reveal that k_C must lie in $0.11 - 0.96\text{ mdyne/\AA}$. As some force field is definitely provided by the displacement of H atoms, the factual values of k_C and k'_C may not be expected to exceed 0.96 mdyne/\AA . Thus the force constants k_C or k'_C computed by Van der Elsken and Robinson²¹ under first and second sets of assumptions seem to be large by factors of 10 and 100, respectively which are quite significant to observe.

More accurate values of k_O and k'_O may be computed using the frequency of appropriate translatory modes of H_2C in Eqn. 5.7h; since in most of the cases, it would be difficult to isolate translatory modes involving k_O and k'_O , an average frequency may be used. k_C and k'_C may also be assumed to be equal to a reasonable accuracy.

In NSH crystal H_2C molecules occupy positions at the corners of an approximate octahedra. This makes it reasonable to assume $k_O = k'_O$. The average frequency of translatory vibrations (excluding those against Ni atom may be considered to be 200 cm^{-1} both for RT and LT. It gives $k_C = k'_C = 0.42\text{ mdyne/\AA}$ neglecting the contribution to the force field potentials due to displacements of H atoms. This value is used in Eqns. 5.7e and 5.7g to compute k'_H and k_H which are tabulated in columns 3 and 4 of Table 5.8 respectively. The values of k_H as given in column 5 of the same table can also be computed independently using frequency of T^W mode and Eqn. 5.7f. The average value of k_H deduced from those given in columns 4 and 5 are given in column 6. The k_H values given in column 8 of this table are the deviations of k_H values given in columns 4 or 5 from the mean k_H values. Since k_H values deduced from two independent Eqns. 5.7e

and 5.7i are expected to be equal, the deviations Δk_H may be regarded as error limits in mean k_H values. Similar errors are obviously expected in k'_H . The source of these errors perhaps lies in the assumptions of H_2O as a rigid molecule and its structure identical to that in vapour phase.

Finally it is observed from Eqns. 5.7e and 5.7g that unless k_O and k'_O are of the order of $10 \text{ mdyne}/\text{\AA}$ (which does not seem reasonable as it is greater than the force constant of any single covalent bond), k_H and k'_H are not significantly affected. For example the $0.42 \text{ mdyne}/\text{\AA}$ value of k_O and k'_O taken by us affects the k_H and k'_H by 0.003 and $0.001 \text{ mdyne}/\text{\AA}$ respectively. These values are insignificant in comparison to the errors involved owing to the simplicity of the model. Thus, the terms containing k_O and k'_O can be dropped from Eqns. 5.7e and 5.7g respectively, to compute k_H and k'_H . Thus we have

$$k_H = 0.1340 \times 10^{-5} \cdot \nu_W^2 \quad \dots 5.7i$$

$$k'_H = 0.1237 \times 10^{-5} \cdot \nu_R^2 \quad \dots 5.7j$$

revealing that librations are mainly described by k_H and k'_H . From these relations we have

$$\frac{\nu_R}{\nu_W} = 1.041 \cdot (k'_H/k_H)^{1/2} \quad \dots 5.7k$$

This indicates that for $k'_H = k_H$, the rocking mode would be higher from the wagging by about 4%. However, the condition of $k'_H = k_H$ may perhaps be considered to hold good when (-H...X bond is almost linear. Similarly k'_H may be considered to exceed k_H for in plane bent H-bonded H_2O , while k_H may exceed k'_H for bifurcated (out-of-plane bent) H-bonded H_2O . Obviously

ν_R would be greater than ν_W for in plane bent H-bonded H_2O while reverse would happen for bifurcated H-bonded H_2O .

We also have from Eqns. 5.7f and 5.7i that

$$\frac{\nu_W}{\nu_T} = 0.942 \quad \dots 5.71$$

It reveals that wagging mode must have lower frequency than the twisting. Our assignments made on the basis of intensity criterion provide ν_W/ν_T values lying in 1.05 - 1.12 range and thus are incompatible with Eqn. 5.71. Since it would be unreasonable to attribute a stronger IR band to the twisting mode (IR forbidden for perfect C_{2v} symmetry) and a weaker one to the wagging mode of H_2O , this incompatibility seems to be the result of the simplicity of our model.

Finally using $\nu_t (\sim 200 \text{ cm}^{-1})$ and $k_H (0.20 \text{ and } 0.92 \text{ mdyne/\AA}, - \text{ the minimum and maximum values respectively, of Table 5.8})$ in Eqn. 5.7h, the k_0 values are computed to be 0.02 and -1.42 mdyne/ \AA respectively; it may be noted that earlier we computed $k_0 = 0.42 \text{ mdyne/\AA}$ considering $k_H = 0$. The negative value of k_0 thus obtained indicates that the relation (Eqn. 5.7h) can not be rigorously applied to determine the frequency of translatory modes of H_2O in the crystal lattice. It can be rationalized since the translatory modes of different units in the crystal exhibit mixing with each other. Normal co-ordinate analysis accounting for several inter-particle (molecule and/or atom) interactions, are therefore needed to have more accurate values of force constants like k_0 . Thus $k_0 = 0.42 \text{ mdyne/\AA}$ computed on the basis of assumptions as specified before may be treated correct only in its order of magnitude.

5.8 CONCLUSION

Frequencies of different phonon modes in NSH crystal have been determined on the basis of an extensive analysis of Raman and ATR spectra of single crystal at about 300°K and IR spectra of microcrystalline sample at about 300°K and 120°K. The bending mode ν_2^w , appearing around 1630 cm^{-1} in IR spectra, is not observed in Raman spectra, although it is allowed. The librational modes of H_2O molecules show weak and diffuse bands in Raman spectra but bands of good intensity in IR spectra. Among the other modes only those, which are allowed in respective spectra under O_h symmetry of $(\text{NiO}_6^w)^{2+}$, T_d symmetry of SO_4^{2-} , exhibit strong Raman and IR spectra. The librational modes of $(\text{NiO}_6^w)^{2+}$ and SO_4^{2-} ions could not be identified.

It is interesting to note that the doubly degenerate angular deformation mode ν_2^s has different components having maximum separation of about 50 cm^{-1} while the triply degenerate modes ν_3^s and ν_4^s which involve changes in both bond lengths and bond angles have only one component each having frequency within 1089 ± 6 and $611 \pm 8\text{ cm}^{-1}$, respectively (excluding the frequencies of LO components). On the other hand the triply degenerate angular deformation mode ν_5^c exhibits a single band at 215 cm^{-1} while the doubly degenerate stretching mode ν_2^c has its different components lying between $248 - 278\text{ cm}^{-1}$. These observations may indicate that the force field for SO_4^{2-} ion is more distorted from the tetrahedral symmetry in respect of bond angle (O-S-O) while that for $[\text{Ni}(\text{OH}_2)_6]^{2+}$ is more distorted from the O_h symmetry in respect of the bond length (Ni---O). Within the limits of standard deviations, the crystallographic data reveal that (i) all S-O bonds have equal lengths while different O-S-O bond angles

vary between 106° to 111° and (ii) the Ni---O bonds have lengths lying between 2.01 to 2.11 Å while different O---Ni---O bond angles vary between 88° to 93° ⁶⁶. These results thus corroborate our inferences of present investigations.

A simple model has been used to compute the force field constants describing 1^W modes in the crystal. It has been shown that O_h point group describes more consistently the symmetry behaviour of $[\text{Ni}(\text{OH}_2)_6]^{2+}$ complex in NSH crystal. It concludes that (i) the intermolecular interactions involving H atoms in complex are weak and may be neglected, (ii) the complex behaves as a molecular unit for its modes which may be described in terms of translatory degrees of freedom of $6\text{H}_2\text{O}$ molecules and one Ni atom and (iii) each of the six H_2O molecules behaves as separate entity for its librational and internal modes of H_2O . Finally it is argued that the above conclusions could be valid in general for the metal-aquo-complex of $[\text{Ni}(\text{OH}_2)_6]^{2+}$ type.

REFERENCES

1. J. Hober, *Phys. Kondens. Materie* 6, 381 (1967).
2. (a) O. Glemser and E. Hartert, *Naturwiss* 42, 534 (1955), (b) P.J. Lucchesi and W.A. Glasson, *J. Am. Chem. Soc.* 78, 1347 (1956), (c) E. Hartert, *Naturwiss* 43, 275 (1956), (d) P. Saumagne and M.L. Josier, *Bull. Soc. Chim. France* 813 (1958), (e) P. Saumagne, *J. Chem. Phys.* 53, 3768 (1970), (f) D.N. Glew in *Hydrogen Bonded Solvent Systems*, Eds. A.K. Covington and P. Jones, Taylor and Francis, p. 133 (1968), (g) L.J. Bellamy, M.J. Blandama, M.C.R. Symons and D. Waddington, *Trans. Faraday Soc.* 67, 3435 (1971), (h) I. Gamo, *Bull. Chem. Soc. Japan* 34, 760 (1961), (i) J. Van der Elsen and D.W. Robinson, *Spectrochim Acta* 17, 1249 (1961), (j) J. Schiffer, Thesis, Princeton Univ., Princeton (1964).
3. R.C. Weast and S.M. Selby (Eds.), *Hand Book of Chemistry and Physics*, Chemical Rubber Company, 47th ed. (1966-67).
4. J.W. Mellor, *A. Comprehensive Treatise on Inorganic Chemistry* 15, 459 (1961).
5. S.F. Pellicori, *Appl. Opt.* 3, 361 (1964).
6. C.L. Braga and M.D. Lumb, *J. Sci. Instrum.* 43, 341 (1966).
7. D.F. Scott, *J. Sci. Instrum.* 43, 940 (1966).
8. R. Trehin, *Ann. Phys.* 20, 372 (1945).
9. C.K. Jorgensen, *Acta Chem. Scand.* 9, 1362 (1955).
10. H. Hartmann and H. Miller, *Disc. Faraday Soc.* 26, 49 (1958).
11. A.D. Liehr and C.J. Ballhausen, *Ann. Phys.* 6, 134 (1959).
12. J. Arris and J.A. Duffy, *J. Chem. Soc.* 5850 (1964).
13. J. Reedijk, P.W.N.M. Van Leeuwen and W.L. Groeneveld, *Rev Trav. Chim.* 87, 130 (1968).
14. M.H.L. Pryce, G. Agnetta, T. Garofamo, M.B. Plama-Vittorelli and M.U. Palma, *Phil. Mag.* 10, 477 (1964).
15. R. Chatterjee, *Can. J. Phys.* 45, 2121 (1967).
16. L. Rosenfeld, *Z. Physik* 52, 161 (1928).
17. N. Underwood, F.G. Slack and E.B. Nelson, *Phys. Rev.* 54, 355 (1938).
18. F.G. Slack and P. Rudnick, *Phil Mag.* 28, 24 (1939).

19. L.R. Ingersoll, P. Rudnick and F.G. Slack, Phys. Rev. 55, 672A (1939).
20. L.R. Ingersoll, Phys. Rev. 57, 1145 (1940).
21. P. Rudnick, F.G. Slack and J.J.O'Connor, Phys. Rev. 58, 1003 (1940).
22. W.C. Knopf, Jr. and W.C. Gilmore, Jr., J. Opt. Soc. Amer. 32, 619 (1942).
23. P. Rudnick and L.R. Ingersoll, J. Opt. Soc. Amer., 32, 622 (1942).
24. J.P. Mathieu and G. Vuldy, Compt. Rend. 222, 223 (1946).
25. M.J. Stephen, Proc. Cambridge Phil. Soc. 54, 81 (1958).
26. W. Moffit and A. Moscovitz, J. Chem. Phys. 30, 648 (1959).
27. R.D. Gillard in Physical Methods in Advanced Inorganic Chemistry, Eds. H.A.O. Hill and P. Day, Interscience, New York, p. 189 (1968).
28. R. Strickland and F.S. Richardson, J. Chem. Phys. 57, 589 (1972).
29. L. Longchampon, Compt. Rend. 173, 89 (1921).
30. R.W. Roberts, J.H. Smith and S.S. Richardson, Phil. Mag. 44, 912 (1922).
31. W. Koenig, Ann. Physik 17, 736 (1933).
32. F.G. Slack, R.T. Lagenman and N. Underwood, Phys. Rev. 54, 358 (1938).
33. J. Bequerel, J. Van der Handel and H.A. Kramers, Physica 17, 717 (1951).
34. M. Levy and J. Van der Handel, Physica 17, 737 (1951).
35. P.L. Meredith and R.A. Palmer, Chem. Comm., 1337 (1969).
36. F. Castano, Spectrochim. Acta 25A, 401 (1969)
37. R. Ginter, M.J. Harding and S.F. Mason, J. Chem. Soc. A, 667 (1970).
38. M.J. Harding J. Chem. Soc. 68, 234 (1972).
39. J.W. Stout, R.C. Archibald, G.E. Brodale and W.F. Giaque, J. Chem. Phys. 44, 405 (1966).
40. J.W. Stout and W.B. Hadley, J. Chem. Phys. 40, 55 (1964).
41. R.A. Fisher, F.W. Hormung, G.E. Brodale and W.F. Giaque, J. Chem. Phys. 46, 4945 (1967)., 48, 3728 (1968)

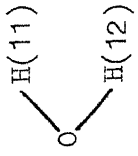
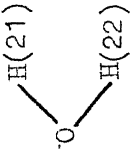
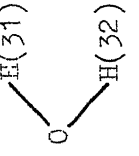
42. R.A. Fisher and E.W. Hornung, J. Chem. Phys. 48, 4284 (1968).
43. R.A. Fisher, G.E. Brodale, E.W. Hornung and W.F. Giaque, J. Chem. Phys. 49, 4046 (1968).
44. R.A. Fisher, E.W. Hornung, G.E. Brodale and W.F. Giaque, J. Chem. Phys. 51, 1959 (1969).
45. L.C. Jackson, Phil. Trans. Roy. Soc. A224, 1 (1924).
46. R. Schlapp and W.G. Penney, Phys. Rev. 42, 666 (1932).
47. K.S. Krishnan, N.C. Chakravorty and S. Banerjee, Phil. Trans. Roy. Soc. A232, 99 (1933).
48. R.B. Janes, Phys. Rev. 48, 78 (1935).
49. K.S. Krishnan and A. Bose, Nature 141, 329 (1938).
50. K.S. Krishnan, A. Mookerji and A. Bose, Phil. Trans. Roy. Soc. A238, 125 (1939).
51. J.W. Stout and M. Griffie, J. Chem. Phys. 18, 1449 (1950).
52. B.C. Guha, Proc. Roy. Soc. A206, 353 (1951).
53. A. Bose and D. Schoenberg, Trans. Bose, Res. Instt. (Calcutta) 20, 1 (1955).
54. T. Watanabe, J. Phys. Soc. Japan 17, 1856 (1962).
55. A. Bose and R. Chatterjee, Proc. Phys. Soc. 82, 23 (1963).
56. O.I. Luk'yanova, P.A. Rebinder and G.M. Belousova, Doklady Akad. Nauk SSSR 130, 816 (1960).
57. P. Lumme and J. Petonen, Suomen Kemistilehti 37B, 162 (1964).
58. B. Loranta, Z. Anal. Chem. 219, 256 (1966).
59. J.M. Thomas and G.D. Ranshaw, J. Chem. Soc. A, 2749 (1969).
60. J.M. Thomas and G.D. Ranshaw, J. Chem. Soc. A, 2753 (1969).
61. J.M. Thomas and G.D. Ranshaw, J. Chem. Soc. A, 2756 (1969).
62. C.A. Beevers and H. Lipson, Z. Krist. 83, 123 (1932).
63. R.B. Corey and R.W.G. Wyckoff, Z. Krist. 84, 477 (1933).
64. C. Frondel and C. Palache, Amer. Mineralogist 34, 188 (1949).

65. H. Fuess, U. Koenig, G. Will and E. Woelfel, Diskussionstag Neutronphys. Forschungsreaktoren Vortragskuzfassungen 3rd, 144 (1967).
66. B.H. O'Connor and D.H. Dale, Acta Cryst. 21, 705 (1966).
67. J.M. Thomas, Chem. Brit. 6, 60 (1970).
68. L.G. Berg and U.P. Kovyrizina, Zh. Neorg. Khim. 9, 29 (1964).
69. N. Kruzman, Compt. Rend. 256, 3446 (1963).
70. A. Bose, H. Chatterjee and A.S. Chakraborty, Paramagnetic Resonance, Proc. International Conf. (Jerusalem) 1, 155 (1962); Pub.(1963).
71. L.A. Rossiello, Ric. Sci. Rend. Sez. A6, 437 (1964).
72. A. Bajorek, J.A. Janik, J.M. Janik, I. Natkaniec, K. Parlinski, J.N. Pokotilovskij, M. Sudnik-Hryniewicz, V.E. Komarov, R.P. Ozerov and S.P. Solerev, Proc. IAEA Symp. Neut. Inelastic Scatt. Vienna Vol. II, 143 (1968).
73. C. Schaefer and M. Schubert, Am. Physik. 50, 283 (1916).
74. J.M. Janik, G. Pytasz and T. Stanek, Acta Phys. Polon. 35, 997 (1969).
75. A.I. Stekhanov, Z.A. Gabrichidze, A.A. Klochikhim and E.A. Popova, Fiz. Probl. Spektroskopii Akad. Nauk SSSR, Materialy 13-go (Trinadt-satogo) Soveshch, Laningrad 2, 25 (1960); Pub. (1963).
76. M. Mamiya, Bunseki Kagaku 9, 609 (1960).
77. S.N. Andreev and T.G. Balicheva, Dokl. Akad Nauk SSSR 148, 86 (1963).
78. T.G. Balicheva and S.N. Andreev, J. Strukt. Khim. 5, 29 (1964).
79. S.N. Andreev and T.G. Balicheva, Vodoradnaya Svyaz Akad. SSSR Inst. Khim. Fiz. - Sb. - Statti, 144 (1964).
80. L. Ben-Dor and R. Magralith, Inorg. Chim. Acta 1, 49 (1967).
81. J. Jager and G. Schaack, Z. Naturforsch. 28a, 738 (1973).
82. A.I. Stekhanov and Z.A. Gabrichidze, Optika i Spektroskopiya 11, 359 (1961).
83. D. Krishnamurthi, Proc. Ind. Acad. Sci. 48A, 355 (1958).
84. C.N.R. Rao, M.V. George, J. Mahanty and P.T. Narasimhan, A Handbook of Chemistry and Physics, East-West Press, New Delhi, p.209 (1967).
85. D. Eisenberg and W. Kauzman, The Structure of Water, Clarendon Press, Oxford (1969).

86. R.W.G. Wyckoff, Crystal Structure, Vol.3, 2nd ed., Wiley, New York (1965).
87. I. Nakagawa and T. Shimanouchi, Spectrochim. Acta 20, 429 (1964).
88. P. Diem, K.H. Hellwege, J. Jager, G. Schaack and F.J. Schedewie, Phys. Kondens Materie. 7, 76 (1968).
89. G. Herzberg, Molecular Spectra and Molecular Structure, Vol.II, D. Van Nostrand, New York (1945).
90. R. Loudon, Adv. Phys. 13, 423 (1964).
91. A. Holden and P. Singer, Crystal and Crystal Growing, University Press, Columbus (1960).
92. M.B. Porter and R.C. Spiller, The Barker Index of Crystal Vol.I, Haffer and Sons, Cambridge (1951).
93. K. Nakamoto, M. Margoshes and R.E. Rundle, J. Amer. Chem. Soc. 77, 6480 (1955).
94. C.M. Hartwig, D.L. Rousseau and S.P.S. Porto, Phys. Rev. 188, 1328 (1969).
95. R.A. Nyquist and R.C. Kagel, Infrared Spectra of Inorganic Compounds, Academic Press, New York (1971).
96. T. Miyazawa, Bull. Chem. Soc. Japan 34, 202 (1961).
97. K. Ichida, Y. Kuroda, D. Nakamura and M. Kubo, Spectrochim. Acta 28A, 2433 (1972).
98. R.W. Blue, J. Chem. Phys. 22, 280 (1954).

TABLE 5.1

Crystal structural data^x of α -nickel sulphate hexahydrate

	r_{O-H}	$r_{H-O'}$	$r_{O-O'}$	2ϕ	r_{Ni-O}	Other details of unit cell
$H_2O(I)$		0.93 Å	1.77 Å	2.69 Å	112° 58'	Symmetry D_{4h}^4 or D_{4h}^8 $a = b = 6.790 \pm .003$ Å $c = 18.305 \pm .004$ Å $N = 4$
		1.00 Å	1.83 Å	2.81 Å	2.02 Å	
$H_2O(II)$		0.97 Å	1.86 Å	2.77 Å	107° 32'	
		0.97 Å	1.79 Å	2.74 Å		
$H_2O(III)$		0.96 Å	1.94 Å	2.84 Å	109° 41'	
		0.96 Å	1.80 Å	2.75 Å	2.10 Å	

^x Reported for deuterated analogue α -NiSO₄·6D₂O by O' Conner Ref. 66; r represents the distance between two atoms as indicated; unprimed and primed O represent oxygen atoms of H₂O and SO₄²⁻, respectively. 2ϕ represents the bond angle between two O-H bonds of H₂O molecule, a , b and c represent crystallographic axes and N , the number of formula units per unit cell.

TABLE 5.2

Classification of phonons in α -NiSO₄·6H₂O crystal (an unit cell approach)^x

	D_4^4	E	$C_{2,1}$	$2C_{4,1}$	$2C_2$	$2C_2'$	Reduced representations					Bases of representations ^y		
							A_1	A_2	A_2	B_1	B_2	E		
	1	2	3	4	5	6	7	8	9	10	11	12	13	
A_1		1	1	1	1	1	1							
A_2		1	1	1	-1	-1	-1							
B_1		1	1	-1	1	1	-1							
B_2		1	1	-1	-1	-1	1							
E		2	-2	0	0	0	0							
ϕ_R		0	π	$\pi/2$	π	π								
$\beta = 1 + 2\cos\phi_R$		3	-1	1	-1	-1	-1	1				1	Space vector \vec{r}	
$\beta' = \beta \cdot 2\cos\phi_R$		6	2	0	2	2	2	2	1	1		1	Polarizability tensor $\vec{\alpha}$	
$\beta'' = 1 + 2\cos\phi_R$		3	-1	1	-1	-1	-1	1				1	Angular moment \vec{L}	
N^R		96	0	0	0	0	4							
$N^R(t) = N^R$		32	0	0	0	0	4							
$N^R(1)$		28	0	0	0	0	2							
$\chi(N) = N^R \cdot \beta$		288	0	0	0	0	-4	35	37	37	35	72	Total phonon modes	
$\chi(t) = \chi(N^R) \cdot \beta$		96	0	0	0	0	-4	11	13	13	11	24	Translations $t^n + t^s + t^w$	
$\chi(1) = N^R(1) \cdot \beta$		84	0	0	0	0	-2	10	11	11	10	21	Librations $l^s + l^w$	
$\chi(i)$		108	0	0	0	0	2	14	13	13	14	27	Internal modes $\nu_i^s + \nu_i^w$	

contd.

Table 5.2 contd.

	1	2	3	4	5	6	7	8	9	10	11	12	13
$N'(t)$			8	0	0	0	4						
$N'(l)$			4	0	0	0	2						
$\chi'(t)=N'(t) \cdot \beta$			24	0	0	0	-4	2	4	4	2	6	External translations
$\chi'(l)=N'(l) \cdot \beta''$			12	0	0	0	-2	1	2	2	1	3	Librations l^c
$\chi'(i)$			60	0	0	0	2	8	7	7	8	15	Quasi-internal modes ν_i^c

x_N^R , $N^R(t)$ and $N^R(l)$ respectively, represent the number of atoms, atomic + molecular units and only molecular units in the tetramolecular unit cell of the crystal remaining invariant under different symmetry operations; N' , $N'(t)$ and $N'(l)$, respectively, represent the similar number when H_2O and SO_4^{2-} are considered as atomic units and $[Ni(OH_2)_6]^{2+}$ complex as a molecular unit. For other notations see sections 1.10 and 1.11.

γ Superscripts n, s, w and c refer to the modes of Ni, H_2O , SO_4^{2-} and $[Ni(OH_2)_6]^{2+}$, respectively.

TABLE 5.3

Correlation between different species of C_{2v} , T_d , O_h and D_4 point groups

	Symmetry species			N_s^y	N_m^z
	Free State ^x	Site ^x	Crystal ^x D_4		
$H_2O(C_{2v})$: Site C_1	A_1, A_2, B_1, B_2	A	$A_1+A_2+B_1+B_2+2E$	3	8
$SO_4^{2-}(T_d)$: Site C_2	A_1	A	A_1+B_2+E	1	4
	E	$2A$	$2A_1+2B_2+2E$		
	F_1, F_2	$A+2B$	$A_1+2A_2+2B_1+B_2+3E$		
$[NiO_6]^{2+}(O_h)$: Site C_2	A_{1g}	A	A_1+B_2+E	1	4
	E_g	$A+B$	$A_1+A_2+B_1+B_2+2E$		
	F_{1g}, F_{1u}	$A+2B$	$A_1+2A_2+2B_1+B_2+3E$		
	F_{2g}, F_{2u}	$2A+B$	$2A_1+A_2+B_1+2B_2+3E$		

^xAll the four species of C_{2v} ; A_1 , E and F_2 of T_d ; A_{1g} , E_g and F_{2g} of O_h and A_1 , B_1 , B_2 and E of D_4 point groups are Raman active, while A_1 , B_1 and B_2 of C_{2v} ; F_2 of T_d ; F_{1u} of O_h and A_2 and E of D_4 are IR active. Under site symmetry C_1 or C_2 all species are both Raman and IR active.

^y N_s = number of inequivalent sites for respective molecular unit in the unit cell.

^z N_m = number of molecular units at one type of site.

TABLE 5.4

Classification of phonons in α -NiSO₄·6H₂O crystal (the site symmetry approach)

Phonon ^x		Species under D ₄					N ^y
		A ₁	A ₂	B ₁	B ₂	E	
1		2	3	4	5	6	7
(i) H ₂ O(C _{2v})							
	ν ₁ ^w (A ₁)	1	1	1	1	2	8
	ν ₂ ^w (A ₁)	1	1	1	1	2	8
	ν ₃ ^w (B ₂)	1	1	1	1	2	8
Rocking:	ν ₄ ^w (B ₂)	1	1	1	1	2	8
Twisting:	ν ₅ ^w (A ₂)	1	1	1	1	2	8
Wagging:	ν ₆ ^w (B ₁)	1	1	1	1	2	8
		6	6	6	6	12	48
	Total ^z	18	18	18	18	36	144
(ii) SO ₄ ²⁻ (T _d)							
	ν ₁ ^s (A ₁)	1	-	-	1	1	4
	ν ₂ ^s (E)	2	-	-	2	2	8
	ν ₃ ^s (F ₂)	1	2	2	1	3	12
	ν ₄ ^s (F ₂)	1	2	2	1	3	12
	Total	5	4	4	5	9	36
(iii) [NiO ₆ ^w] ²⁺ (O _h)							
	ν ₁ ^c (A _{1g})	1	-	-	1	1	4
	ν ₂ ^c (E _g)	1	1	1	1	2	8
	ν ₃ ^c (F _{1u})	1	2	2	1	3	12
	ν ₄ ^c (F _{1u})	1	2	2	1	3	12
	ν ₅ ^c (F _{2g})	2	1	1	2	3	12
	ν ₆ ^c (F _{2u})	2	1	1	2	3	12
	Total	8	7	7	8	15	60

Contd.

Table 5.4 contd.

1	2	3	4	5	6	7
(iv) External modes						
Rotations of $\text{SO}_4^{2-}(\text{F}_1)$	1	2	2	1	3	12
Rotations of $[\text{NiO}_6^{\text{w}}]^{2+}(\text{F}_{2g})$	1	2	2	1	3	12
Optical translations t_o	2	3	4	2	5	21
Acoustical translations t_a	-	1	-	-	1	3
Total	4	8	8	8	12	48
Grand Total	35	37	37	35	72	288

^xSuperscripts w, s and c refer to the modes of H_2O , SO_4^{2-} and $[\text{NiO}_6^{\text{w}}]^{2+}$, respectively.

^yTotal phonon modes originating from particular mode of an unit.

^zTotal accounting for the phonon modes originating from all the three crystallographically inequivalent H_2O molecules.

TABLE 5.5

Frequencies^x (in cm^{-1}) and assignments of Raman phonons in $\alpha\text{-NiSO}_4 \cdot 6\text{H}_2\text{O}$ single crystal

A_1 a(cc)b	A_1+B_1 a(bb)c	B_2 b(ab)c	E c(ac)b	Assignments ^y	ν_{av}^z
1	2	3	4	5	6

(i) Internal Modes of H_2O Molecules

3428	3455	3455	3460	$\nu_3^w(\text{III})$	3450
3375	3375	3360	3404	$\nu_1^w(\text{III})$	3379
3290	3285	3282	3310	$\nu_3^w(\text{II}), \nu_1^w(\text{II})$	3292
		3230	3223	$2\nu_2^w(\text{II})$	3227
3190	3198	3144	3134	$\nu_1^w(\text{I})$	3139
-	-	-	-	ν_2^w	1630

(ii) Internal Modes of SO_4^{2-} Ion

1083	1123* 1087	1095	1130(LO) 1089(TO)	ν_3^s	1130 1089
983	985	985	987	ν_1^s	985
603	618	619	645(LO) 616(TO)	ν_4^s	645 614
461	472 445*	475 446	475 446	ν_2^s	471 446
426	428	428*	426*		427

(iii) Librational Modes of H_2O Molecules

-	865	-	860	$R^w(\text{I})$	863
-	752	806	796	$W^w(\text{I})$	786
-	-	-	-	$T^w(\text{I})$	-

contd.

Table 5.5 contd.

1	2	3	4	5	6
obscured by ν_4^S mode ?				$R^W(II), W^W(II)$	
-	-	-	543 ?	$T^W(II)$	543 ?
-	-	-	495 ?	$R^W(III)$	495 ?
obscured by ν_2^S mode ?				$W^W(III), T^W(III)$	

(iv) Quasi-Internal Modes of $(NiO_6^W)^{2+}$ Complex

374	378	380	382	ν_1^c	378
			349 ?	$\nu_6^c + \nu_4^c ?$	349 ?
297		298		$2\nu_6^c$	298
272	265	266	278	ν_2^c	270
	248	256	250		251
214	214	215	215	ν_5^c	215
				ν_3^c	(251)
				ν_4^c	(227)
				ν_6^c	(217)
					149

(v) Translatory Optical Modes

			175(LO)	
164	167		168(TO)	
	146	147		
	138		137(LO)	
122	121	122**	118(TO)	
	107		100(LO)	$t_o (2A_1+4B_1+2B_2+5E)$
85**			86(TO)	
	69**	71**	75(LO)	
		62**	64(TO)	
45**	47**	50	53(LO)	
			42(TO)	

contd.

Table 5.5 contd.

1	2	3	4	5	6
(vi) Librations of SO_4^{2-} and $(\text{NiO}_6^{\text{w}})^{2+}$					
?	?	?	?	1^{s} and 1^{c}	?

^x Measured from Raman spectra (cf Figs. 5.5 and 5.6) recorded in geometries (indicated under heads of columns 1-4 or their equivalents); frequency positions where no band is observed for an allowed mode are shown by dashes. Doubtful interpretations and existence of bands have been questioned (?) marked. Bands arising due to spillover of strong bands in other polarization have been starred (*). Bands which may also arise due to reasons other than the spillover of strong bands but not due to allowed modes have been marked by double stars (**).

^y Superscripts w, s and c refer to the modes of H_2O , SO_4^{2-} and $(\text{NiO}_6^{\text{w}})^{2+}$ respectively. Notations, other than t_o for translatory optical modes and l for librational modes, are after Herzberg Ref. 89.

^z ν_{av} represents the average of frequencies given in columns (1-4); frequencies in parentheses given under this head are from the IR data reported by Jager and Schaack Ref. 83; frequency of ν_6^{c} mode (149 cm^{-1}) has been deduced from $2\nu_6^{\text{c}}$ (298 cm^{-1}).

TABLE 5.6

Frequencies (cm^{-1}) of IR active phonons observed in ATR spectra^x of single crystal of $\alpha\text{-NiSO}_4 \cdot 6\text{H}_2\text{O}$ recorded at angles of incidence $\theta_i = 37.5, 45$ & 50° .

$\theta_i = 37.5^\circ$	$\theta_i = 45^\circ$	$\theta_i = 50^\circ$	Assignments
3470	3420		$\nu_3^w(\text{III})$
3310 ?	3280		$\nu_3^w(\text{II})$
	3180		$\nu_1^w(\text{II})$
3100 ?			$\nu_1^w(\text{I})$
	3000		$\nu_3^w(\text{I})$
1625	1625	1625	ν_2^w
1120	1102	1105	ν_3^s
?	1065	1070	$\nu_4^s + \nu_2^s$
830	832	832 sh	$R^w(\text{I})$
772	783	783	$W^w(\text{I})$
650	660	665	$R^w(\text{II})$
?	622	625 sh	$W^w(\text{II})$ and ν_4^s
582	592	595	$T^w(\text{II})$
540	540	540 sh	$R^w(\text{III})$
		445	$W^w(\text{III})$
400	400	400	$T^w(\text{III})$

^x Shown in Fig. 5.7 and recorded by keeping (001) plane of crystal in contact with ATR element (KRS-5 crystal). sh = shoulder

TABLE 5.7

Phonon frequencies (in cm^{-1}) observed in IR spectra^x of microcrystalline samples of $\alpha\text{-Ni}(\text{C}_2\text{O}_4)_2 \cdot 6\text{H}_2\text{O}$ (NSH) and $\alpha\text{-NiSO}_4 \cdot 6\text{D}_2\text{O}$ (NSD).

1	NSH		Assignments	NSD (RT)	$\nu_{\text{H}}/\nu_{\text{D}}^{\text{y}}$	HFMP ^z
	(RT)	(LT)				
1	2	3	4	5	6	7
Group a	3460	3480	ν_3^{w} (III)	2560	1.35	
		3410	ν_1^{w} (III)			
	3290	3310	ν_3^{w} (II), ν_1^{w} (II)	2420	1.36	
		3240	2 ν_2^{w} (II)			3284
	3045	3095	ν_3^{w} (I)	2250 ?	1.35	
	2400	2400	ν_2^{w} (I) + W^{w} (I)			2427
	2260	2265	ν_2^{w} (II) + W^{w} (II)			2267
	2095	2120	ν_2^{w} (III) + W^{w} (III)			2095
	1635	1642	ν_2^{w}	1208	1.35	
	1240	1240	2 ν_4^{s}			1220
	1148	1148	ν_3^{s}	1092		1060
	1102	1095				
	1065	1065	ν_4^{s} + ν_2^{s}			
	983	985	ν_1^{s}	983		
	845	864	R^{w} (I)			
Group b	780	792	W^{w} (I)	576	1.38	
	735	750	T^{w} (I)			
	660	675	R^{w} (II)			
	626	632	W^{w} (II)	490	1.27	
	575	584	T^{w} (II)			

contd.

Table 5.7 contd.

1	2	3	4	5	6	7
	610	610	ν_4^s	620		
	507	515	$R^w(\text{III})$			
Group c	460	473	$W^w(\text{III})$	382	1.25	
	110	124	$T^w(\text{III})$			
		375	ν_1^c			

^x Shown in Figs. 5.8(c), 5.9(c) and 5.9(d).

^y Ratio of frequencies of a mode of H_2O observed in RT spectra of NSH and of D_2O in NSD.

^z HFMP = harmonic frequency of multiphonon process.

TABLE 5.8

Force field constants^a for librational modes of H_2O

Molecule	$k_{\text{C}} = k'_{\text{C}}$	k'_{H}	k_{H}^b	k_{H}^c	k_{H}^d	Δk_{H}^e
(i) <u>RT spectra</u>						
$\text{H}_2\text{O}(\text{I})$	0.42	0.88	0.81	0.64	0.73	± 0.09
$\text{H}_2\text{O}(\text{II})$	0.42	0.54	0.52	0.39	0.46	± 0.07
$\text{H}_2\text{O}(\text{III})$	0.42	0.32	0.28	0.20	0.24	± 0.04
(ii) <u>LT spectra</u>						
$\text{H}_2\text{O}(\text{I})$	0.42	0.92	0.84	0.67	0.75	± 0.09
$\text{H}_2\text{O}(\text{II})$	0.42	0.56	0.53	0.41	0.47	± 0.07
$\text{H}_2\text{O}(\text{III})$	0.42	0.34	0.31	0.21	0.26	± 0.05

^a in mdyne/Å. ^b computed from Eqn. 5.7e. ^c computed from Eqn. 5.7f. ^d mean of the values given in columns 4 and 5. ^e deviations in k_{H} values.

TABLE 5.9

Symmetry classification of 288 phonon modes in α -NiSO₄·6H₂O crystal

Phonon originating from ^a	Present study ^b	Jager and Schaack ^c
$\nu(\text{H}_2\text{O})$	$9A_1+9A_2+9B_1+9B_2+18E$	$10A_1+8A_2+8B_1+10B_2+18E$
Librational (H_2O)	$9A_1+9A_2+9B_1+9B_2+18E$	$8A_1+10A_2+10B_1+8B_2+18E$
$\nu(\text{SO}_4^{2-})$	$5A_1+4A_2+4B_1+5B_2+9E$	$5A_1+4A_2+4B_1+5B_2+9E$
$\nu(\text{Complex})$	$8A_1+7A_2+7B_1+8B_2+15E$	$7A_1+8A_2+8B_1+7B_2+15E$
External Rotations	$2A_1+4A_2+4B_1+2B_2+6E$	$A_1+5A_2+3B_1+3B_2+6E$
External Translations	$2A_1+4A_2+4B_1+2B_2+6E$	$A_1+5A_2+3B_1+3B_2+6E$
Total	$35A_1+37A_2+37B_1+35B_2+72E$	$32A_1+40A_2+36B_1+36B_2+72E$

^a ν denotes the internal modes.^b Results of the unit cell approach and the site symmetry approach considering $(\text{H}_2\text{O}^w)_6^{2+}$ part of the complex as a molecular unit of O_h symmetry and each H₂O molecule as separate entity for its librational and internal modes.^c Results of the site symmetry approach considering T_h symmetry for $[\text{Ni}(\text{OH}_2)_6]^{2+}$. Detailed classification is given in Ref. 81.

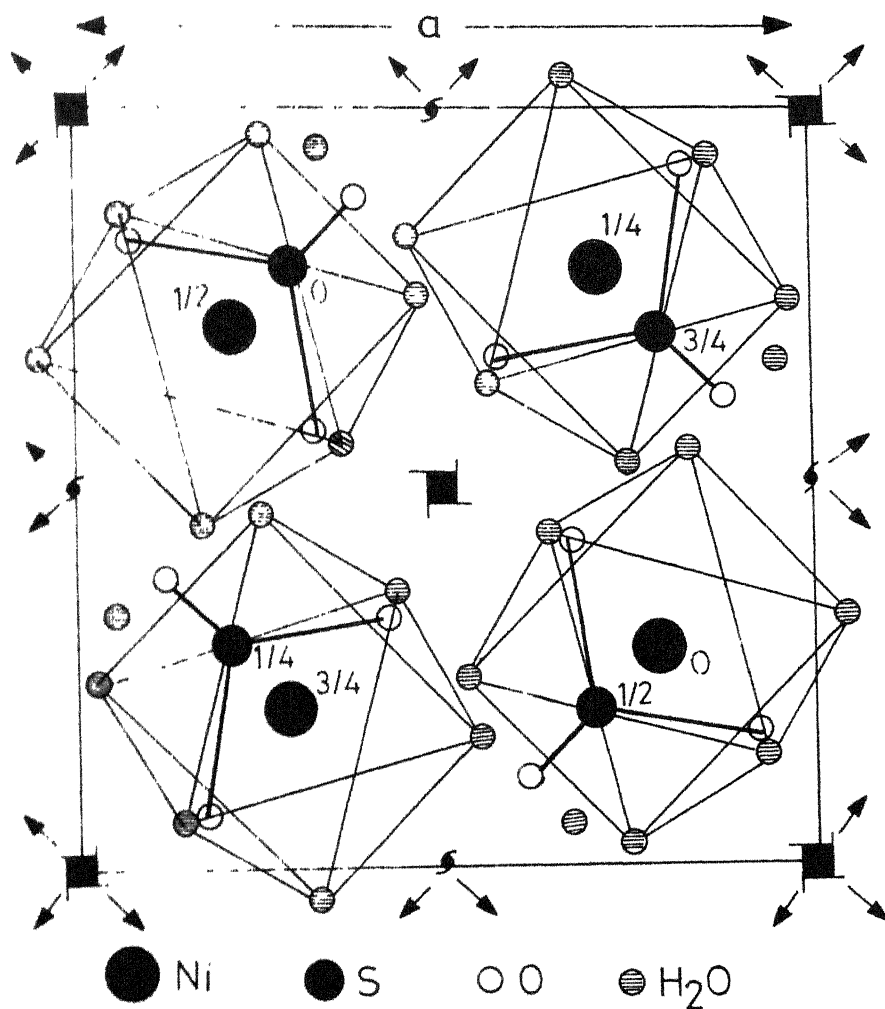


Fig. 5.1 Crystal structure of α - $\text{NiSO}_4 \cdot 6\text{H}_2\text{O}$; numbers 0, $1/4$, etc. represent heights of central atoms Ni and S respectively of $[\text{Ni}(\text{OH}_2)_6]^{2+}$ and SO_4^{2-} .

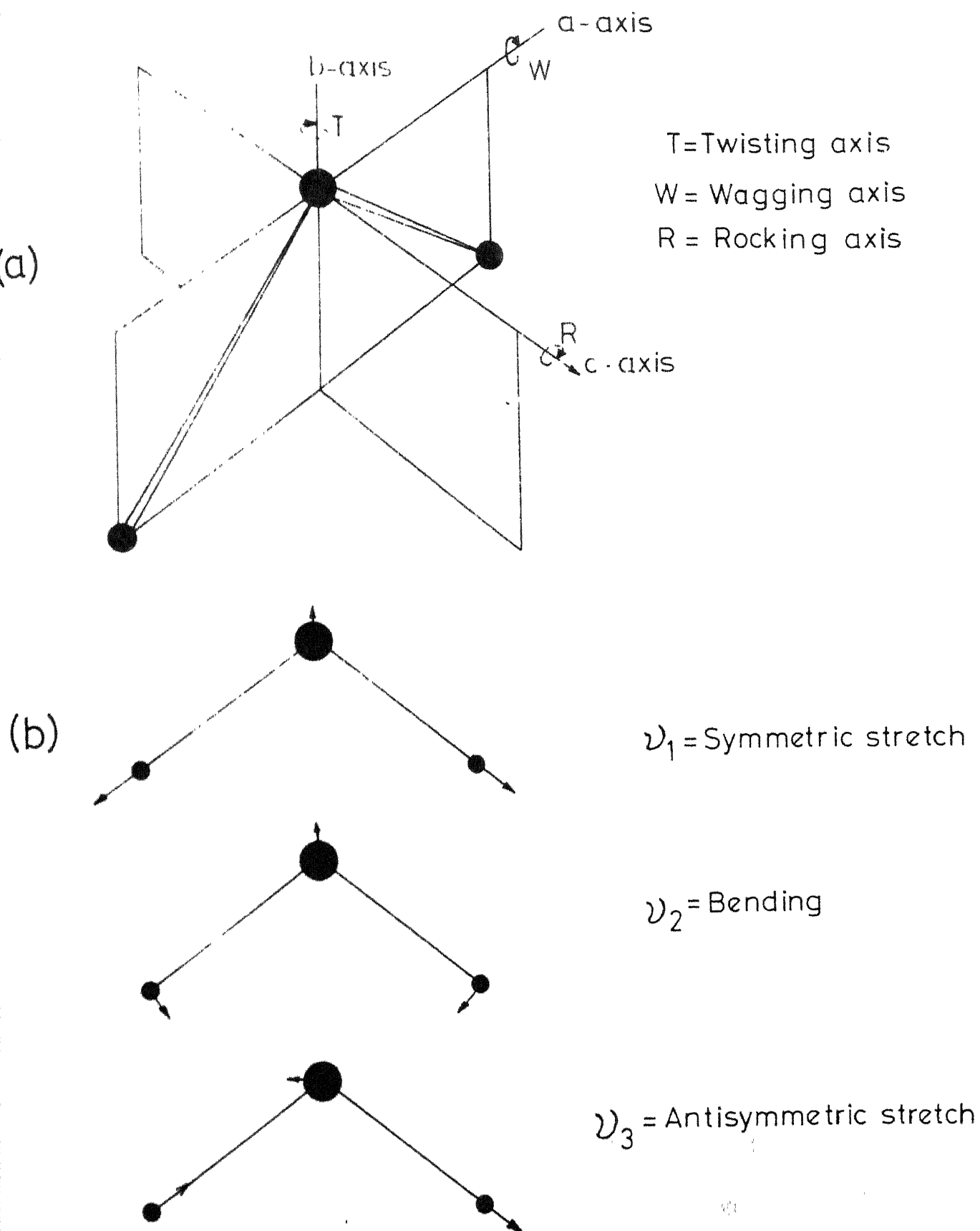


FIG 5.2 DIAGRAMMATICAL REPRESENTATION OF (a) LIBRATIONAL
(b) INTERNAL MODES OF WATER.

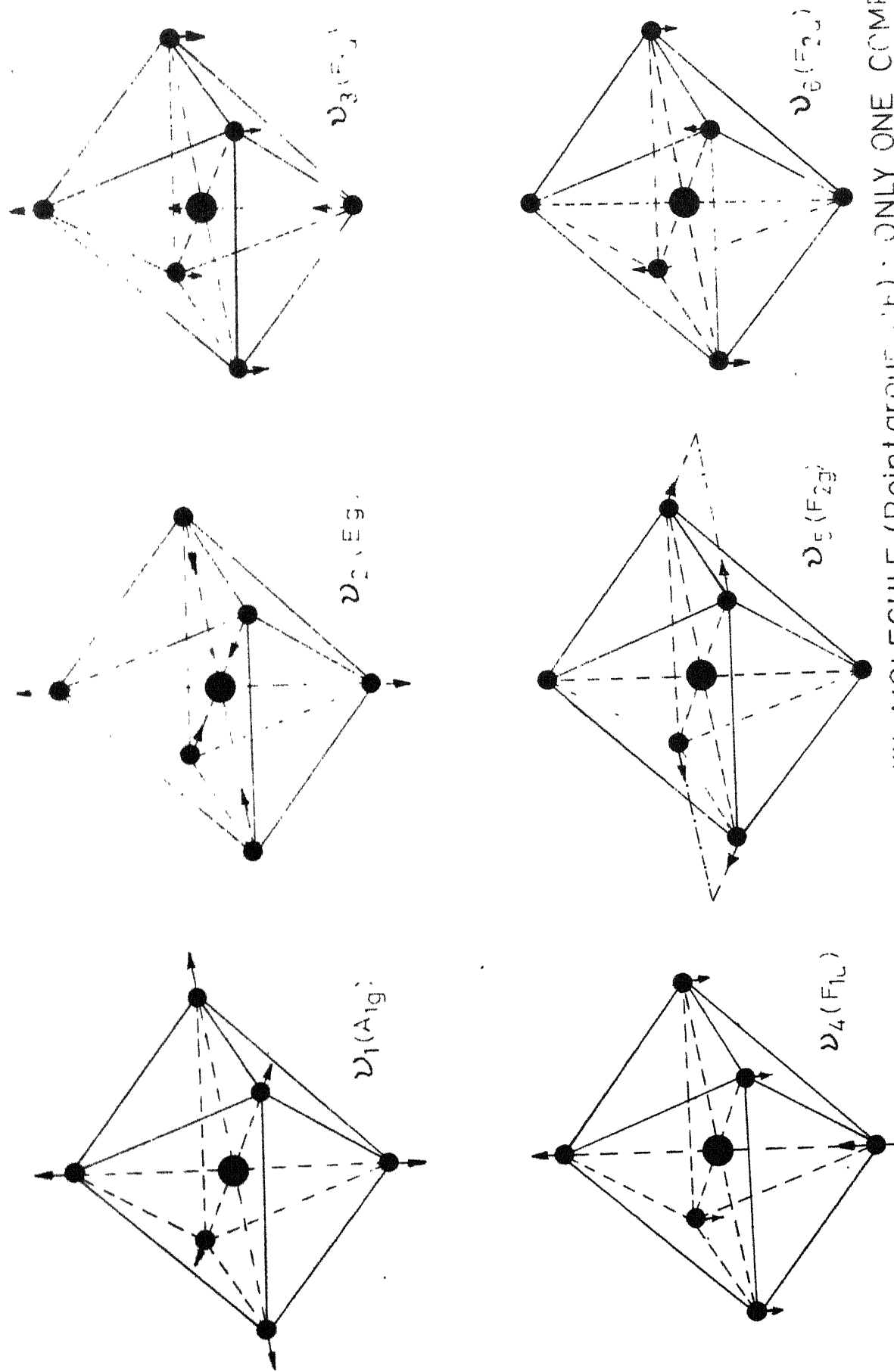


FIG.53 NORMAL VIBRATIONS OF XY_6 MOLECULE (Point group O_h): ONLY ONE COMPONENT OF EACH DEGENERATE VIBRATION IS SHOWN

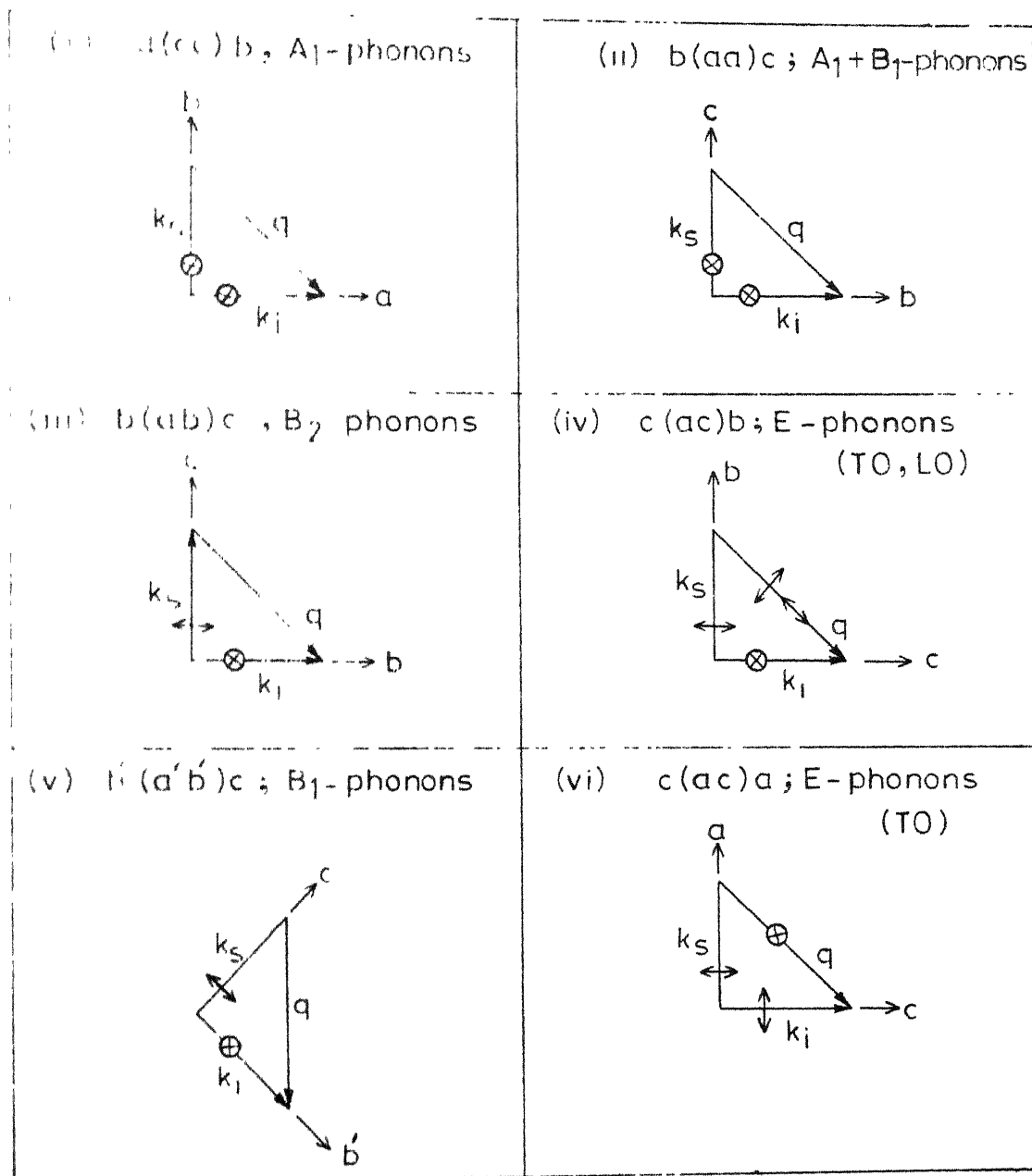


Fig.5.4 Scattering diagrams for all arrangements discussed in this chapter.

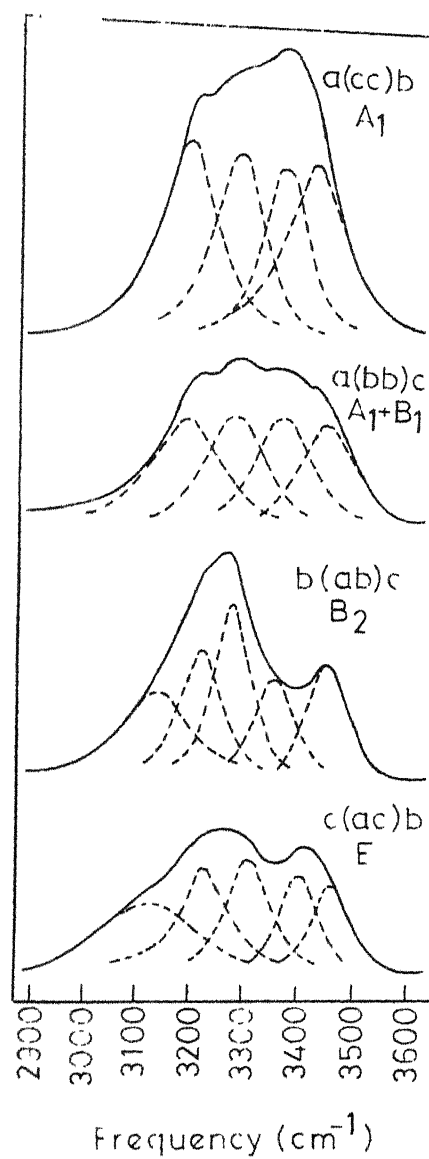


Fig. 5.5 Raman spectra in O-H stretching region of α -NiSO₄·6H₂O single crystal.

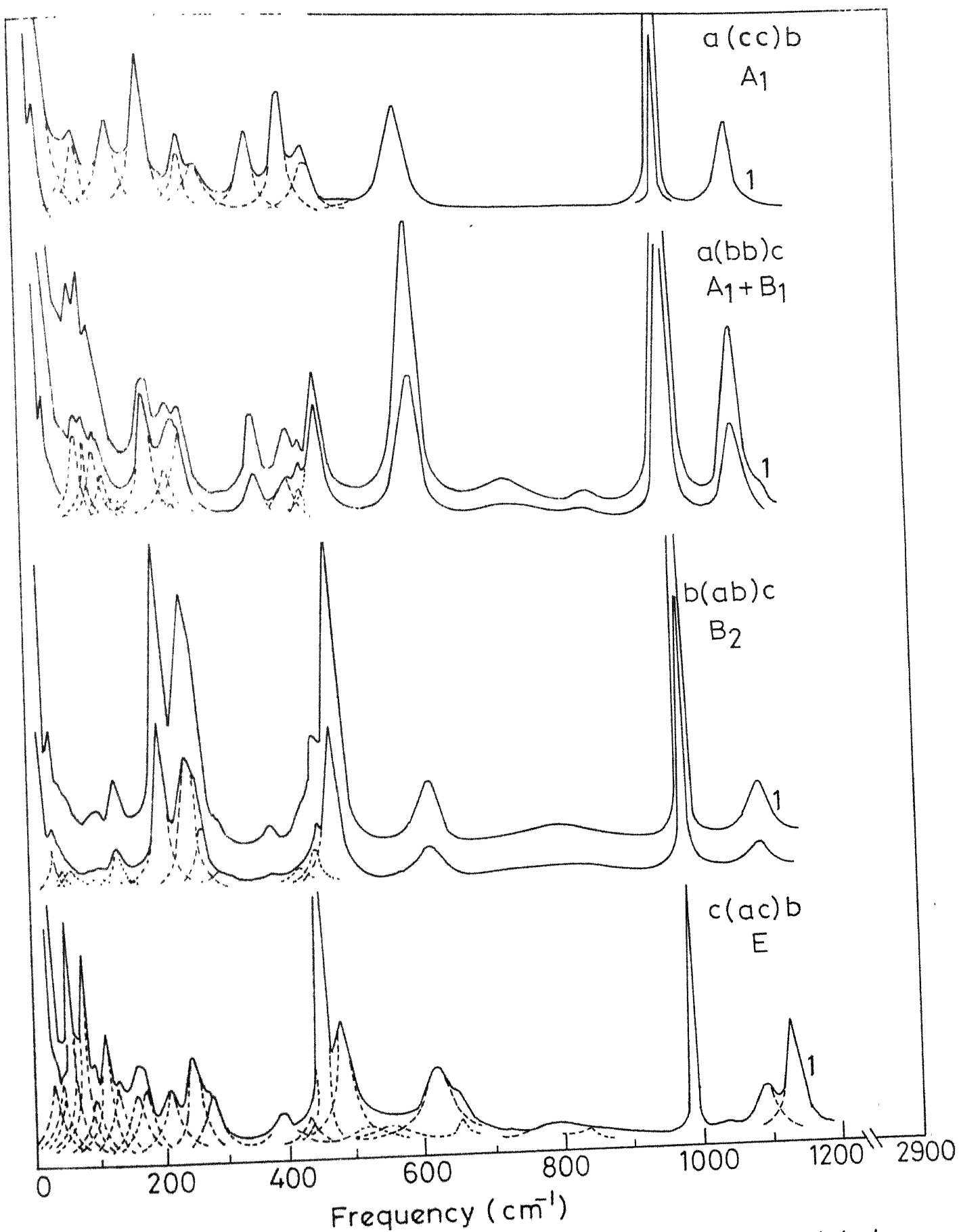


Fig.5.6 Raman spectra of $\alpha\text{-NiSO}_4 \cdot 6\text{H}_2\text{O}$ single crystal below 2900 cm^{-1} (1 recorded in similar conditions).

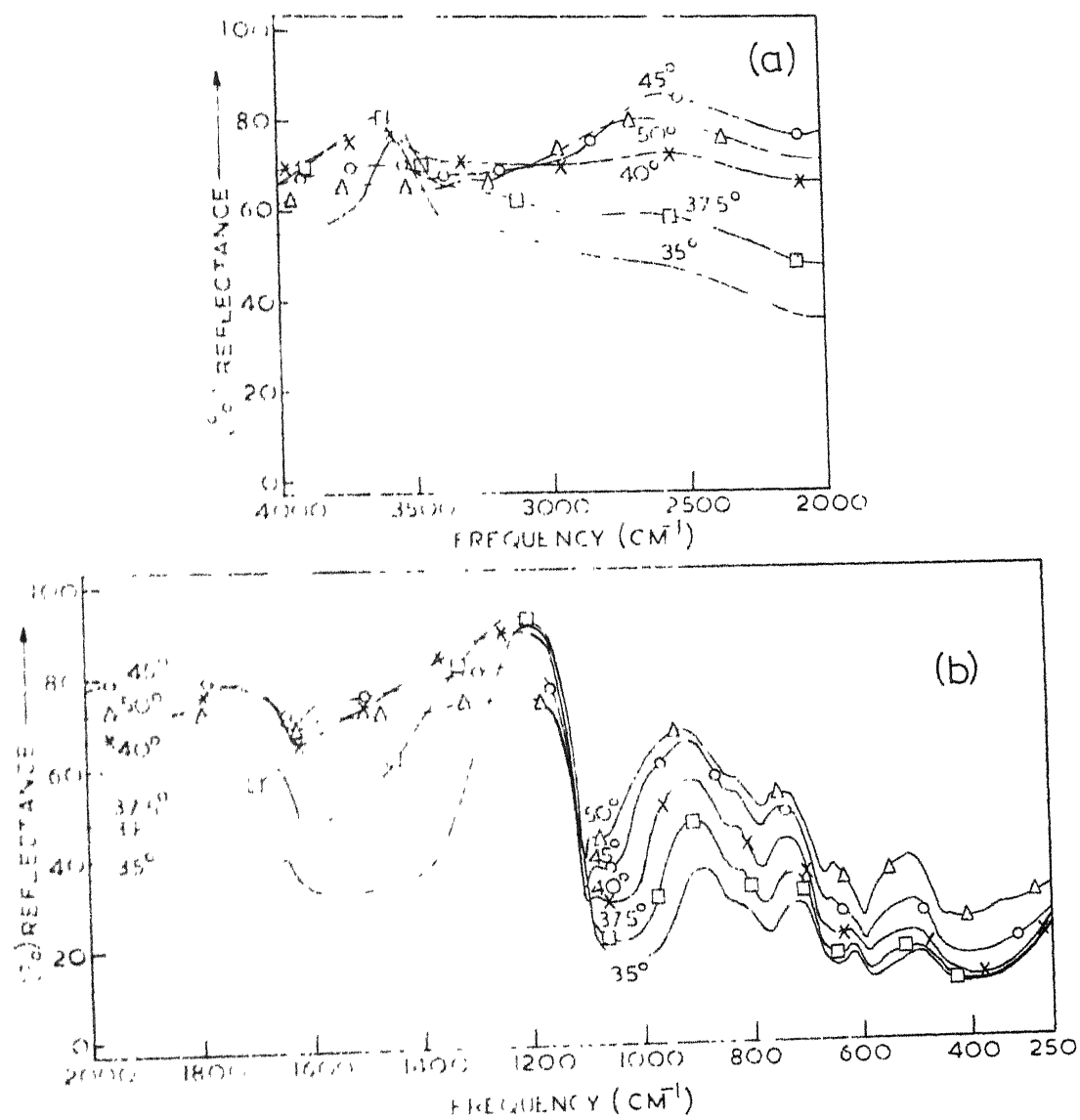


Fig 5.7 IR (ATR) spectra of single crystal of α - $\text{NiSO}_4 \cdot 6\text{H}_2\text{O}$ in (a) 4000–2000 cm^{-1} (b) 2000–250 cm^{-1} range recorded by keeping its (001) plane in contact with ZnTe crystal.

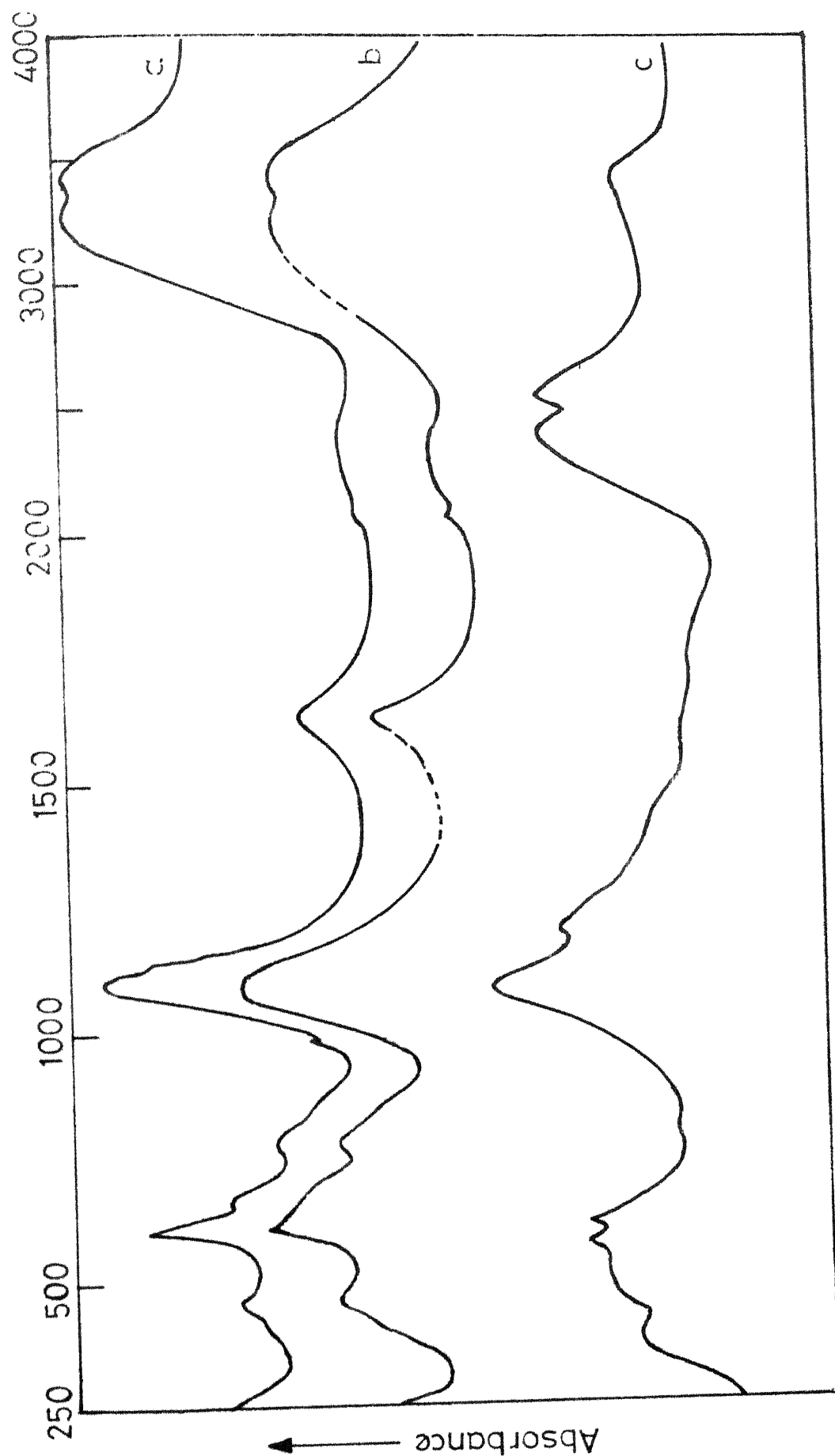


Fig.5.8 IR spectra of microcrystalline α -NiSO₄·6H₂O (a & b) and α -NiSO₄·6D₂O (c); (a) & (c) in KBr pellet and (b) in nujol mull (nujol bands compensated).

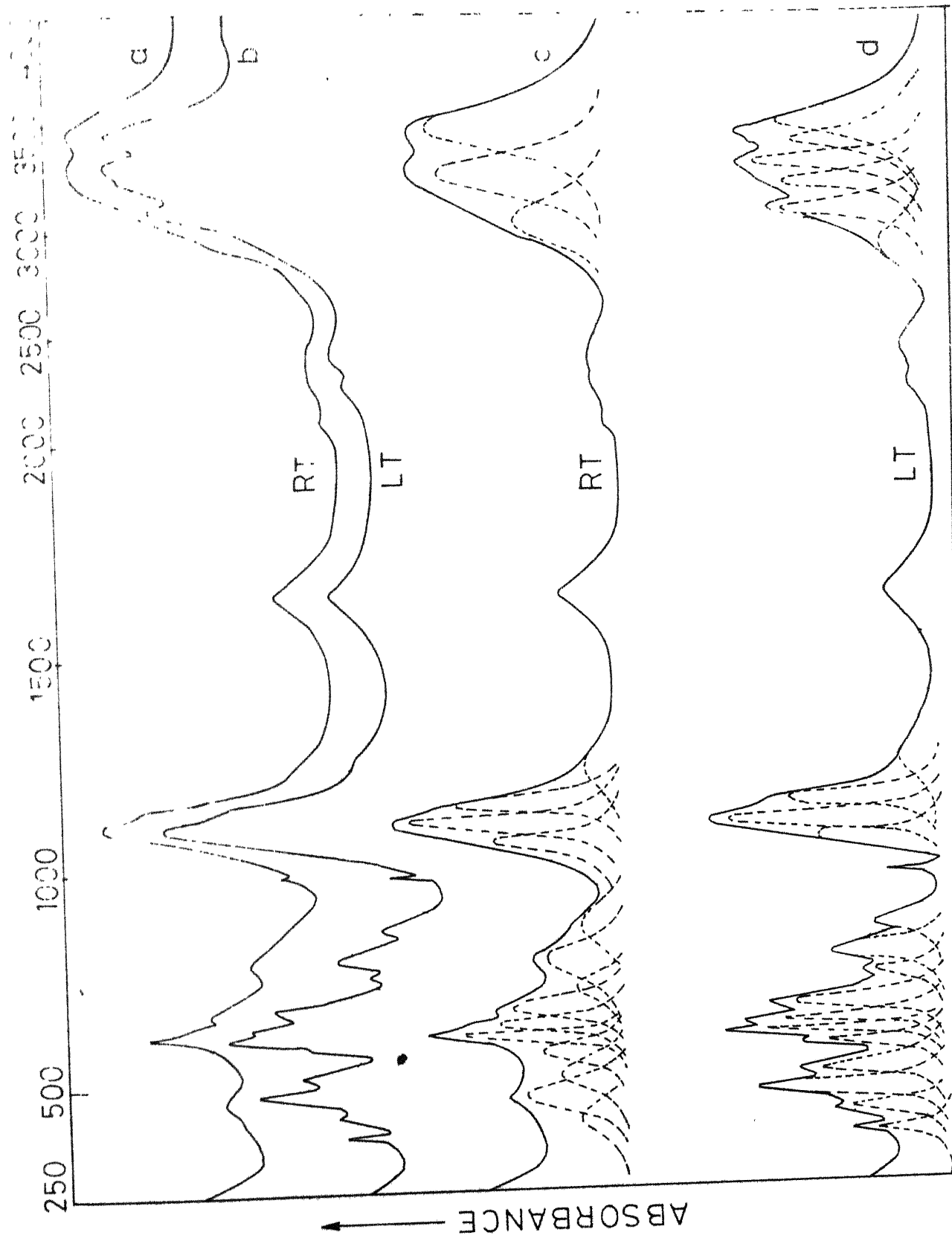


Fig.5.9 IR spectra of microcrystalline α - $\text{NiSO}_4 \cdot 6\text{H}_2\text{O}$; (a) & (b) reproduced as such as recorded, (c) & (d) retraced after neglecting scattering effects.

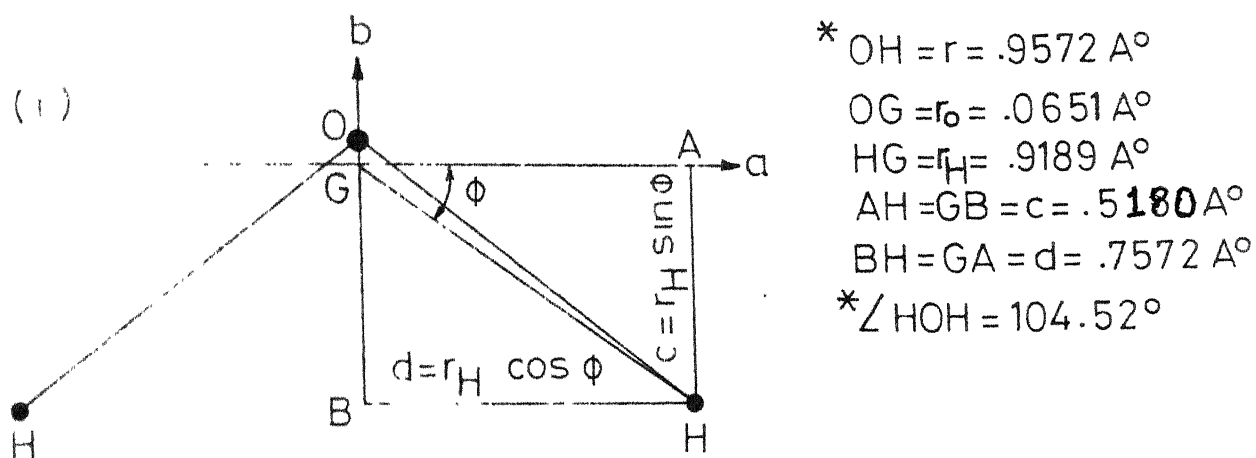
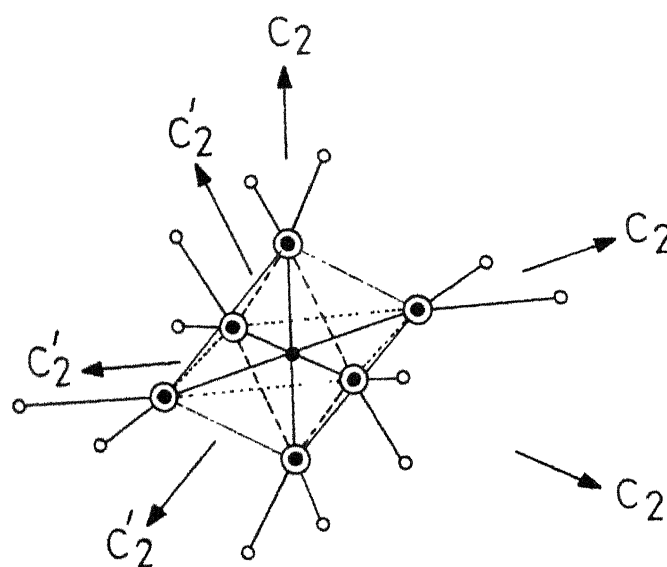


Fig 5.10. Geometry of H_2O molecule in vapour (*from ref.85).
 c-axis passes through G \perp to H_2O plane



- Ni
- ⊙ Oxygen
- Hydrogen

Fig. 5.11 Model structure of $[Ni(OH_2)_6]^{2+}$ complex ion.

ON THE SYMMETRY BEHAVIOUR OF METAL-AQUO-COMPLEX $[M(OH_2)_6]^{2+}$
 AN ANALYSIS FOR $[Ni(OH_2)_6]^{2+}$ IN α -NiSC₄·6H₂O

The metal-aquo-complex $[M(OH_2)_6]^{2+}$ occupies lattice positions like a single molecular unit in several crystal hydrates⁸⁶ and thus can statically be regarded as a quasi-molecule. The complex has been considered some times^{81,87} as a system of symmetry T_h while at others⁸⁸ that of O_h in order to discuss its dynamics. The question, whether both of these point groups are equally appropriate or one of them should be preferred, has not been answered. Herewith we discuss the symmetry behaviour of $[Ni(OH_2)_6]^{2+}$ in NSH crystal as a special case.

A hypothetically symmetric structure of $[Ni(OH_2)_6]^{2+}$ (in which all Ni—O distances are equal and all H₂O molecules have C_{2v} symmetry with H atom configuration compatible with T_h symmetry) is shown in Fig. 5.11. The T_h point group has⁸⁹ only one class of two fold axes ($3C_2$), each of which would pass through the Ni atom and the oppositely situated pair of oxygen atoms as shown in the figure by unprimed C_2 axes.

Crystallographically it is known⁶⁶ that NSH crystal belongs to D_4^4 space group with 4 formula units per unit cell. In the crystal the $[Ni(OH_2)_6]^{2+}$ complex occupies C_2 site the two fold axis of which passes only through Ni atom (not through the oxygen atoms) and all the H₂O molecules of the complex occupy C_1 sites. Thus H₂O positions in the crystal are incompatible with the site symmetry C_2 of Ni atom under T_h symmetry of the complex; hence a correct correlation between C_2 axes of the point groups T_h of the complex and C_2 of the site, — necessary to

find out the symmetry species of 288 phonon branches describing the dynamics of NSH crystal — can not be established.

Evidently, the modes of $[\text{Ni}(\text{CH}_2)_6]^{2+}$ for this crystal can not be considered as the bases of different irreducible representations of T_h point group. The appropriateness of O_h symmetry, which could be the only other choice neglecting the positions of H atoms and under assumptions specified before, may now be examined.

The O_h point group has two classes of C_2 operations⁸⁹; one of them contains $3C_2$ passing through Ni atom and the two O atoms identical to that of T_h point group, but the other contains $6C'_2$ passing through the Ni atom and bisecting two parallel sides joining nearest O atoms (corresponding to the primed axes in Fig. 5.11). The C_2 axis of the site of $[\text{Ni}(\text{CH}_2)_6]^{2+}$ complex in the crystal belongs to this latter class of C'_2 operations. A consistent correlation between C'_2 (i.e. C_2 of the site) and O_h point groups can, therefore, be established.

It is important to note that no configuration of H atoms in the complex can be consistent with O_h symmetry but this is a better choice since under it the positions of O atoms (nearest neighbours of Ni atom) are compatible with C_2 site of the complex. Consequently, it has to be conceived that positions of H atoms do not affect the dynamics and symmetry behaviour of the complex. It implies that the intermolecular interactions in the complex involving H atoms are insignificant to influence its motion. The H atoms can, therefore, be neglected. Thus the interactions mainly responsible to associate Ni atom with six H_2O molecules to form $[\text{Ni}(\text{OH}_2)_6]^{2+}$ complex are; (i) the metal-oxygen co-ordination and (ii) the oxygen - oxygen interaction. Effectively, therefore, $[\text{NiO}_6]^w$ part of the complex behaves as a molecular unit of O_h symmetry

where C^W represents H_2C as a single particle having mass equal to 18 amu.

The dynamics of $(NiC_6^W)^{2+}$ molecular unit accounts only for those modes which involve translatory degrees of freedom, i.e. relative displacements of centres of mass of each of the six H_2C molecules and the Ni atom; the librational and the internal modes of H_2C are left aside revealing that each of the six H_2C molecules behaves as a separate entity for these modes. For such a differential behaviour, the distinction, that the translatory modes involve displacement of centre of mass of a molecule while the librational and internal modes keep it fixed, appears to be a responsible factor. Following these inferences we worked out the classification of 288 phonon modes in NSH under C_h symmetry for $(NiC_6^W)^{2+}$ using the site symmetry approach (cf Table 5.4). A brief summary of this classification is given in column 2 of Table 5.9. It is found to be identical with that obtained by unit cell approach as evident from the comparison of results obtained in Tables 5.2 and 5.4. This supports the validity of C_h symmetry consideration.

It may not be out of place to mention that Jager and Schaack⁸¹ have also obtained the symmetry species of 288 phonons in NSH crystal on the basis of the site symmetry approach, and on the assumption of T_h symmetry for $[Ni(OH_2)_6]^{2+}$ group. Their results are summarised in column 3 of Table 5.9. A detailed comparison of various modes obtained by Jager and Schaack⁸¹ with those obtained during present investigation (cf columns 3 and 2 in Table 5.9) reveals that for Sc_4^{2-} modes, the symmetry break-up is identical but not for the modes involving H_2C and $[Ni(OH_2)_6]^{2+}$; obviously because of the wrong assumption of T_h group and incorrect correlation between the C_2 axes of T_h of the complex and C_2 of the site.

Although we have not examined the symmetry behaviour of $[\text{Ni}(\text{OH}_2)_6]^{2+}$ type metal-aquo-complex in other crystals, the O_h symmetry may be generalized for it as discussed in the following. The observed $\text{M} \cdots \text{O}^{\text{W}}$ distances in large number of complexes lie within $2.0 - 2.8 \text{ \AA}^{86}$ and are therefore not shorter than $\text{Ni} \cdots \text{O}^{\text{W}} (2.02 \text{ \AA})$ in NSH. Thus the distances between different water molecules within a complex would also not be shorter than those in $[\text{Ni}(\text{OH}_2)_6]^{2+}$. Since the strength of intermolecular interactions decreases with increasing separation between the molecules, such interactions involving H atoms in other complexes are expected to be as weak (may be even weaker) as in $[\text{Ni}(\text{OH}_2)_6]^{2+}$. Thus, as has been shown in case of NSH, the positions of H atoms should not decide the symmetry behaviour of metal aquo-complex in other crystals also which supports our generalization; cases like $[\text{Al}(\text{OH}_2)_6]^{2+} (\text{Al} \cdots \text{O}^{\text{W}} = 1.87 \text{ \AA})^{86}$ where $\text{M} \cdots \text{O}^{\text{W}}$ distances are shorter than $\text{Ni} \cdots \text{O}^{\text{W}}$ may act as exceptions to it.

APPENDIX 5.2

The frequency (ν , in cm^{-1}), integrated intensity (I^x in parenthesis) and the width (FWHMI, cm^{-1}) of Raman bands in the spectra of single crystal of $\alpha\text{-NiSO}_4 \cdot 6\text{H}_2\text{O}$.

$A_1(\text{cc})$		$A_1 + B_1(\text{aa/bb})$		$B_2(\text{ab})$		$E(\text{ac/bc})$	
ν	(I) FWHMI	ν	(I) FWHMI	ν	(I) FWHMI	ν	(I) FWHMI
1	2	3	4	5	6	7	8
3428	(12.5) 125	3455	(7.5) 145	3455	(8.2) 85	3460	(5.5) 82
3375	(7.5) 110	3375	(7.6) 138	3360	(7.0) 82	3404	(6.0) 82
3290	(7.1) 95	3285	(8.1) 145	3282	(12.1) 78	3310	(8.0) 85
				3230	(6.3) 85	3223	(8.0) 100
3190*	(10.0) 125	3198*	(10.0) 185	3144*	(10.0) 135	3134*	(10.0) 200
		1123	sh			1130	(21.0) 22
1083**	(10.0) 22	1087**	(10.0) 32	1095**	(10.0) 38	1089**	(10.0) 30
983	(?) 5	985	(?) 5	985	(12.0) 5	987	(16.0) 7
		867	df			860?	df
		753	df	806	df	796	df

contd.

Appendix 5.2 contd.

1	2	3	4	5	6	7	8
						645	(1.0) 14
603	(20.0) 39	618	(16.0) 34	619	(12.0) 36	616	(25.0) 50
						543?	df
						495?	df
461	(7.5) 30	472	(7.5) 24	475	(44.0) 24	475	(25.0) 30
		445	(1.0) 10	446	(4.0) 15	446?	(?)
426	(12.0) 20	428	(3.1) 27	428	(2.5) 23	426	(3.0) 15
374	(9.5) 24	378	(4.0) 24	380	(2.3) 25	382	(5.0) 28
297	(10.0) 44			298	sh	349?	sh
272	(4.5) 16	265	(6.5) 26	266	sh	278	(9.5) 22
		248	(3.5) 23	256	(35.0) 32	250	(11.5) 17
214	(16.0) 21	214	(8.0) 21	215	(23.0) 17	215	(8.0) 25
						175	(7.8) 17
164	(10.0) 24	167	(1.8) 28			168	(6.4) 16
		146	(2.0) 14	147	(6.0) 17		
		138	(4.0) 17			137	(7.0) 15

contd.

Appendix 5.2 contd.

1	2	3	4	5	6	7	8
122	(6.5) 19	121	(2.8) 11	122	(1.0) 22	118	(12.0) 15
		107	(4.5) 20			100	(4.0) 10
85	(1.5) 12					86	(14.0) 9
		69	sh	71	(4.0) 21	75	(2.2) 9
				62	(2.0) 11	64	(17.0) 10
				50	(4.2) 9	53	(5.0) 8
45	sh	47	sh			42	sh

^x For the relativeness of these value see the text, sh = shoulder,
df = diffuse.

APPENDIX 5.3

Frequency (ν), width (FWHMI, $\Delta\nu$) and relative integrated intensity (I) of IR bands observed in spectra of microcrystalline α -NiSO₄·6H₂O

RT (300°K) spectra			LT (120°K) spectra		
$\nu(\text{cm}^{-1})$	$\Delta\nu(\text{cm}^{-1})$	I^x	$\nu(\text{cm}^{-1})$	$\Delta\nu(\text{cm}^{-1})$	I^y
3460	220	39.0	3480	160	23.0
			3410	130	16.0
3290	220	37.0	3310	120	21.0
			3240	120	16.0
3045	260	19.0	3095	120	16.0
2400	?	df	2400	?	df
2260	?	df	2265	?	df
2095	?	df	2120	?	df
1635	130	5.0	1642	130	5.0
1240	120	3.1	1240	120	3.4
1148	45	6.7	1148	45	7.1
1102	40	10.0	1095	40	10.0
1065	42	4.5	1065	40	4.5
983	8	?	985	8	0.3
845	120	3.2	864	45	2.6
780	105	5.8	792	45	4.9
735	80	2.4	750	40	1.8
660	55	4.7	675	35	5.6
626	40	4.1	632	25	4.2
610	20	3.0	610	20	3.2
575	60	3.5	584	30	2.8
507	90	4.0	515	40	4.5
460	80	6.0	478	40	8.5
410	105	3.2	424	40	2.7
			375	20	1.0

^xRelative to the arbitrarily chosen intensity 10.0 for 1102 cm⁻¹ band,
df = deffuse.

^yRelative to the arbitrarily chosen intensity 10.0 for 1095 cm⁻¹ band.

CHAPTER VI

SUMMARY

The present spectroscopic investigations using IR absorption and Raman scattering techniques were undertaken with a view to understand the lattice dynamics and related phenomenon (e.g. the ferroelectric phase transition) in $(\text{NH}_4)_2\text{SO}_4$, $(\text{NH}_4)_2\text{BeF}_4$ and $\alpha\text{-NiSO}_4 \cdot 6\text{H}_2\text{O}$ crystals. The resulting inferences have been summarized in this chapter alongwith the other important informations available on these solids in literature.

$(\text{NH}_4)_2\text{SO}_4$ undergoes a ferroelectric phase transition at T_c (223°K). Above and below this temperature, the crystal belongs to D_{2h}^{16} and C_{2v}^9 space groups respectively. In paraelectric phase ($T < T_c$), both NH_4^+ and SO_4^{2-} ions occupy $C_s(\sigma_{ab})$ sites while C_1 sites in the ferroelectric. The crystal contains crystallographically inequivalent $\text{NH}_4^+(\text{I})$ and $\text{NH}_4^+(\text{II})$ ions. The SO_4^{2-} ion has almost a tetrahedral structure in paraelectric phase but relatively large distortions in ferroelectric phase. On the other hand, NH_4^+ ions possess more distortions in the former phase than in the latter phase. The H-bonds are relatively weaker in paraelectric but on the average they are strong in both phases. All these informations based on crystallographic studies agree well with our spectroscopic observations which also add that (i) the force fields governing the dynamics of $\text{NH}_4^+(\text{I})$ and $\text{NH}_4^+(\text{II})$ are almost identical and (ii) the phenomenon of proton tunneling occurs (as also proposed by others) in the double minimum

potential possibly exhibited by some of the stronger H-bonds (N-H...O) in the crystal. Although, latter inference is corroborated by few other studies, however a more direct evidence is still needed.

The ferroelectric phase transition in $(\text{NH}_4)_2\text{SO}_4$, is an abruptly occurring; first order transition accompanied by a latent heat of about 0.93 kcal/mole. The volume and dimensions of the unit cell exhibit significant and sudden change at the transition temperature. This temperature is neither affected by deuteration nor by electrostatic biasing field applied along the ferroelectric c-axis. The hysteresis curve just above T_c exhibits a line shape. The change in birefringence at T_c is mainly accounted for by elasto-optic effect. The line width and the second moment of PMR spectra are not affected by the transition.

Alongwith the above inferences drawn out from earlier studies, we note from our experiments that (i) on cooling the crystal, the SO_4^{2-} ion gets considerably distorted in a narrow range of temperature around T_c and (ii) the NH_4^+ ions follow a relatively slow change. In addition, the computations based on a point charge model assumed for the electrostatic charge distribution in a tetrahedral AB_4^{n+} ion show that (i) SO_4^{2-} ion contributes about 50% of the total spontaneous polarization at 180°K and (ii) the array of dipoles, with respect to their c-components, defines a ferroelectric structure, while an anti-ferroelectric structure with respect to their a- and b- components.

In view of all these observations, it has been inferred that (i) the driving interactions of the transition in $(\text{NH}_4)_2\text{SO}_4$ arise due to covalency effects in S-O bonds of SO_4^{2-} ion which triggers the transition; the NH_4^+ ions acquire an appropriate change, (ii) the order parameter, needed for phenomenological description of the transition, may have several

components but the spontaneous strain at SO_4^{2-} sites appears to be the major one, (iii) the soft mode may be considered to be a mixed mode having major contributions from the internal modes of SO_4^{2-} ion, (iv) the mechanism of the transition involves change in internal structure of SO_4^{2-} ion; it is neither as simple as order-disorder of permanent dipole moments of NH_4^+ ions nor is displacive type involving relative displacements of NH_4^+ and SO_4^{2-} ions, (v) the transition appears to be an ordinary molecular phase transition resulting ferroelectricity as its secondary effect; thus $(\text{NH}_4)_2\text{SO}_4$ has been correctly put among the improper ferroelectrics, (vi) the spontaneous polarization most likely depends on the temperature of the crystal, hence such results reported by Unruh and coworkers are more realistic in comparison to those reported by Hoshino et al and Ikeda et al and (vii) the observation, showing dependence of T_c on the strength of electrostatic biasing field reported by Kamiyoshi and Miyamoto seems to be unrealistic; the correct observations are perhaps those reported by Hoshino et al and Unruh.

Our other investigated crystal $(\text{NH}_4)_2\text{BeF}_4$, is isostructural with $(\text{NH}_4)_2\text{SO}_4$ in the paraelectric phase. Although in the ferroelectric phase both crystals belong to C_{2v}^9 space group, the axis of symmetry (C_2) is observed along b-axis in the former crystal while along c-axis in the latter. The observed Raman spectra of single crystal and the IR spectra of microcrystalline $(\text{NH}_4)_2\text{BeF}_4$ can be consistently analysed in view of the above mentioned knowledge of the structure of this crystal. This analysis indicates that (i) the H-bonds on the average are weaker (not very significantly) in $(\text{NH}_4)_2\text{BeF}_4$ than in $(\text{NH}_4)_2\text{SO}_4$, (ii) the force fields describing the dynamics of crystallographically inequivalent $\text{NH}_4^+(\text{I})$ and $\text{NH}_4^+(\text{II})$ are almost similar and (iii) the phenomenon of proton tunneling

perhaps occurs in the double minimum potential which may possibly be shown by H-bonds (N-H...F) becoming enough strong in ferroelectric phase of $(\text{NH}_4)_2\text{BeF}_4$.

Although, the ferroelectric phase transition in $(\text{NH}_4)_2\text{BeF}_4$ is a first order transition, it is close to being a second order. The value of T_c (176°K) goes up by 3° on deuteration. The biasing electrostatic field promotes the transition and a double loop is exhibited by the hysteresis curve just above T_c . The change in the birefringence can be accounted for by electro-optic effect. The line width and the second moment of PMR spectra of $(\text{NH}_4)_2\text{BeF}_4$ are not affected by the transition. The spontaneous polarization increases with decreasing temperature. Alongwith these facts known from earlier studies, the present investigations add that (i) BeF_4^{2-} ion has enough distortions to contribute significantly to the spontaneous polarization of $(\text{NH}_4)_2\text{BeF}_4$, and (ii) the changes in dynamics and structure of BeF_4^{2-} and NH_4^+ ions occur in a wide range of temperature around T_c .

Above mentioned observations can be simultaneously rationalized if the following model is considered. Accordingly (i) the driving interactions of the transition in $(\text{NH}_4)_2\text{BeF}_4$ are of electrostatic type and seem to be centred in BeF_4^{2-} ion whose Be-F bonds have 72% ionic character, (ii) the crystal is a proper ferroelectric in which the spontaneous polarization acts as the major component of order parameter needed to develop the phenomenological theory of the transition, (iii) the transition can also be described in terms of a soft mode (mixed mode) having major contributions from modes involving displacements of F^- ions; minor contribution from the translatory modes of NH_4^+ can explain the shift of T_c on deuteration and (iv) the mechanism of the transition is not as simple as order-disorder

phenomenon involving permanent dipole moments of NH_4^+ ions; it rather involves the relative displacements of constituting ions.

Although, $(\text{NH}_4)_2\text{SO}_4$ and $(\text{NH}_4)_2\text{BeF}_4$ are isostructural with each other and the cation triggers the transition in both crystals, however the former behaves as an improper ferroelectric showing spontaneous polarization along c-axis, while the latter is a proper ferroelectric showing spontaneous polarization along b-axis. Such a differential behaviour may be attributed to the fact that Be-F bonds are highly ionic while the S-O bonds are highly covalent.

The tetramolecular unit cell of the remaining $\alpha\text{-NiSO}_4 \cdot 6\text{H}_2\text{O}$ belongs to D_4^4 space group. The crystal appears to be the stacking of equal number of $[\text{Ni}(\text{OH}_2)_6]^{2+}$ and SO_4^{2-} polyhedra assuming almost the O_h and the T_d structures respectively; both occupy C_2 sites with only central atoms on the axis of symmetry. Six H_2O molecules of the metal-aquo-complex $[\text{Ni}(\text{OH}_2)_6]^{2+}$ are equally distributed over three inequivalent sites of C_1 symmetry. All these structural informations can be consistently correlated with the observed Raman and IR spectra. On the basis of a group theoretical analysis, it has been shown that the $[\text{Ni}(\text{OH}_2)_6]^{2+}$ exhibits O_h symmetry behaviour for its quasi-internal modes which account for all translatory degrees of freedom of one Ni^{2+} ion and six H_2O molecules; each H_2O molecule behaves as a separate entity for its internal and librational modes. Such a differential behaviour may be rationalised in terms of the fact that translatory vibrations result in the displacements of centre of mass of a molecule while the internal and librational modes keep it fixed. It has been argued that intermolecular interactions in $[\text{Ni}(\text{OH}_2)_6]^{2+}$ complex involving H atoms are negligibly weak. This inference may be

applied to most of the complexes of $[\text{Ni}(\text{OH}_2)_6]^{2+}$ type. A simple model developed to compute the force field constants involved in the librational modes of H_2O , reveals that: (i) these modes are mainly governed by the force fields provided by the displacements of H atoms and (ii) the wagging frequency must be lower than the rocking frequency for a H_2O molecule showing in-plane bent H-bonds while the reverse is expected for the one showing bifurcated H-bonds. In certain cases experiments may show observations diversing from the latter inference within the errors arising due to the simplicity of the model used.

As such the present investigations on $(\text{NH}_4)_2\text{SO}_4$, $(\text{NH}_4)_2\text{BeF}_4$ and $\alpha\text{-NiSO}_4 \cdot 6\text{H}_2\text{O}$ provide fairly accurate spectroscopic (Raman and IR) data. The detailed analysis of these data has helped in understanding the lattice dynamics of these solids and also the phenomenon of ferroelectric phase transition in the isomorphous $(\text{NH}_4)_2\text{SO}_4$ and $(\text{NH}_4)_2\text{BeF}_4$. It also deals fairly, with the dynamics of H_2O molecule in a large crystal, the $\alpha\text{-NiSO}_4 \cdot 6\text{H}_2\text{O}$. Finally it is hoped, that these investigations may prove to be the assets to unravel the lattice dynamics and related phenomena in crystals similar to those studied here.

LIST OF ATTACHED PUBLICATIONS

1. Optical Phonons in Molecular Crystals of Halogens, Proc. Nucl. Phys. Solid State Phys. Symposium (BARC), Madurai, Vol. 3, 485 (1970).
2. The Out-of-Plane Vibrational Modes of Chlorobenzene in its Ground and First Singlet ~~Excited~~ States, J. Mol. Spectrosc. 47, 126 (1973).
3. The 2699 Å Band System of Chlorobenzene, Indian Institute of Technology, Kanpur, Phys. Tech. Rep. No. 36/70.

**Pre-print from the proceedings of
Nuclear Physics & Solid States Physics Symposium
Madurai, 1970
Vol. 3**

OPTICAL PHONONS IN MOLECULAR CRYSTALS OF HALOGENS

Y.S. Jain and H.D. Sisti

Department of Physics

Indian Institute of Technology, Kanpur-16

I. INTRODUCTION

In this paper we suggest a model to explain the observed infrared (ir) absorption and Raman scattering by the optical phonons in halogen crystals which can not be understood satisfactorily considering only two coplanar molecules in a unit cell⁽¹⁻³⁾.

II. DISCUSSION

X-ray diffraction studies in the polycrystalline films of halogens indicate that all of them exhibit a molecular layer structure and belong to $\sqrt{2}$ space group with four molecules per unit cell⁽⁴⁻⁶⁾. This structure in which each molecule is located at the site C_{2h} is shown schematically in the left half of Fig. 1 and is hereafter referred to as model I. An analysis based on this model does not explain the invariably observed internal modes of halogens in the ir spectra of all these crystals. A better comprehension of the optical phonons could be achieved if our suggestion regarding a model having 4 molecules in a unit cell and belonging to space group $\sqrt{2}$ is valid for the crystal structure. A schematic diagram for the suggested model (referred to as model II) is shown in the right half of Fig. 1.

In model II the halogen molecules are constrained to have C_s site symmetry by displacing them with respect to their positions in model I by a small but finite amount in the bc plane; thus destroying the centre of inversion falling on their inter atomic axis. Model II maintains close consistency with the structure assigned from X-ray techniques in the sense that the dimensions of the unit cell and the separations bet-

The displacements required

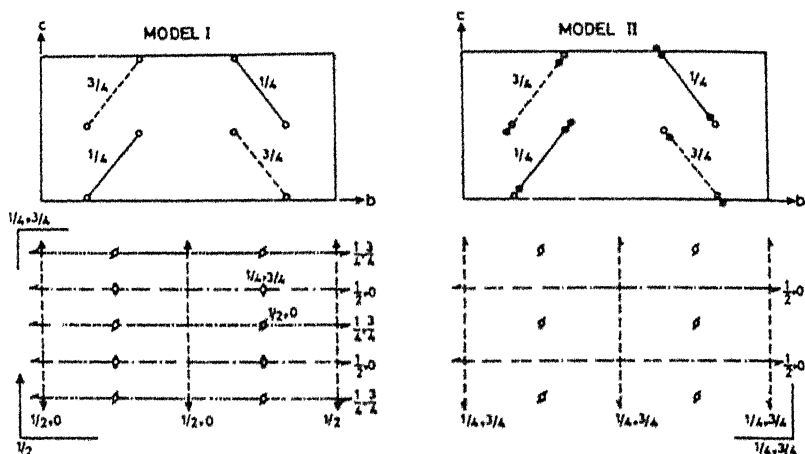


FIG. 1. Projection of crystal structure of halogens in bc plane in models I and II with existing symmetries shown underneath. The original halogen positions denoted by open circles (\circ) have been displaced to take positions of filled circles (\bullet) in model II. Standard notations are used to denote: the mirror (σ), the glide (σ_g), the diagonal glide (σ_d) planes; the two fold (C_2), the two fold screw (C_2h) axes and inversion centres (i). The fractional numbers denote the height in terms of lattice constant a .

to convert model I to model II may possibly be undetectable by X-ray techniques.

Taking 4 molecules per unit cell, the spectral activity and polarizations of fundamental optical phonons and acoustic modes have been summarized in Table 1 for both model I (column 4) and model II (column 6).

Table 1: Symmetry species of fundamental phonons in halogen crystals

Types of motion	Iso-lated	Symmetry			
		Crystalline state			
		Model I		Model II	
		Site	Crystall	Site	Crystall
	$D_{\infty h}$	C_{2h}	D_{2h}^+	C_s	D_{2h}
Translation	Σ_u^+	B_u	$2B_{2u}+B_{1u}+B_{1u}^*$	A'	$A_g+B_{2g}+B_{2u}+B_{1u}^*$
	Π_u	A_u	$2A_u+B_{3u}+B_{3u}^*$	A''	$B_{1g}+B_{2g}+A_u+B_{3u}^*$
		B_u	$2B_{1u}+B_{2u}+B_{2u}^*$	A'	$A_g+B_{2g}+B_{1u}+B_{2u}^*$
Rotation	Π_g	A_g	$2A_g+2B_{3g}$	A'	$A_g+B_{2g}+B_{1u}+B_{2u}$
		B_g	$2B_{1g}+2B_{2g}$	A''	$B_{1g}+B_{2g}+A_u+B_{3u}$
Vibration	Σ_g^+	A_g	$2A_g+2B_{3g}$	A'	$A_g+B_{2g}+B_{1u}+B_{2u}$

† In these columns B_{1u} , B_{2u} and B_{3u} denote the infrared (ir) active modes polarized along x, y and z-axis, respectively. All the modes with g subscript are Raman active. The u species (except A_u) are ir active.

* Indicates the acoustic modes.

The available ir and Raman data have been summarized in Table II where our tentative assignments (column 5) based on model II have been given along with those of earlier workers⁽²⁻³⁾ (column 4).

Model II explains the occurrence of the internal modes in the ir spectra of all these crystals (Of. Table II). The intensity distribution in the Raman spectra also supports the model in the sense that the two most intense bands could be attributed to the librational modes⁽⁷⁾. The splittings observed in Raman scattering in the internal phonon region and the occurrence of only two prominent bands in ir in

Table II : Observed optical phonons and their assignments in halogen crystals

Band positions* (in cm ⁻¹)			Proposed Assignments*	
Cl ₂	Br ₂	I ₂	Earlier†	Model II
Raman				
533 (s)	294 (s)		A _g (I _u)	A _g (Im)
520 (w)	256 (w)		Iso(Im)	Iso (Im)
522(vw)			Iso(Im)	Iso (Im)
	501(vw)		B _{3g} (Im)	B _{3g} (Im)
130(vw)	110(vw)		B _{3g} (L)	B _{1g} +B _{2g} (T)
113 (s)	56 (s)		A _g (L)	A _g +B _{3g} (L)
94 (s)	32 (s)		A _g (L)	B _{1g} +B _{2g} (L)
77(vw)	70(vw)		B _{1g} (L)	A _g +B _{3g} (T)
	53(vw)		?	A _g +B _{3g} (T)
Infrared				
	231 (w)	211 (v) 210**	?	B _{1u} +B _{2u} (Im)
60 (s)	74 (s)	55 (s) 61**	B _{2u} (T)	B _{2u} (T)
62 (s)	40 (s)	41 (s) 41**	B _{3u} (T)	B _{3u} (T)
	?	?		B _{1u} +B _{2u} (L) +B _{3u}

*The Raman data are from references (2) and (3); and ir data are from reference (1) (and ir absorption data for solid iodine taken at RT using nujol mull technique have been shown in the table with double asterisk. Symbols (s), (w) and (vw) have been used to denote strong, weak and very weak intensities.

†The translational, librational, and internal modes have been denote by (T), (L) and (Im) respectively. 'Iso' represents A_g type mode corresponding to the isotopic species.

‡The assignments of Raman lines are from references (2) and (3) and those of ir bands are from reference (1).

The absence of a few additional expected librational bands in the ir spectra for model II may be due to very small change in dipole moment for these modes. Single crystal work on iodine would be necessary to unequivocally support the above model.

The authors are grateful to Professor F. Venkateswarlu for helpful discussions during the course of work. Thanks are due to the CSIR

REFERENCES

1. S.T. Walmsley, and A. Anderson, Mol. Phys. 7, 411 (1964).
2. M. Suzuki, T. Yokoyama and M. Ito, J. Chem. Phys. 50, 5392 (1969).
3. M. Suzuki, T. Yokoyama and M. Ito, J. Chem. Phys. 51, 1929 (1969).
4. R.L. Collin, Acta, Cryst., 5 431 (1952); 9, 537 (1956).
5. R. Vonnegut, and B.E. Warren, J. Amer. Chem. Soc. 58, 2459 (1936).
6. A.I. Kitaigorodski, T.L. Khotsyanova, and Y.T. Struchov, J. Phys. Chem., Moscow, 27, 780 (1951).
7. S. Bhagavantam, and T. Venkatarayadu, Proc. Ind. Acad. Sci. A9, 224 (1939).

DISCUSSION

K.S. Chandrasekaran

X-ray diffraction gives straight forward information about the symmetry elements of the unit cell. Centre of symmetry is also unambiguously found by statistical methods as well as by anomalous scattering techniques for non-centrosymmetric cases. After finding the structure (i.e., the positions of the atoms in the unit cell) by comparing calculated and observed diffraction intensities, information on local symmetry is also obtained.

The Out-of-Plane Vibrational Modes of Chlorobenzene in Its Ground and First Singlet Excited States

Y. S. JAIN AND H. D. BIST¹

Spectroscopy Laboratory, Department of Physics, Indian Institute of Technology, Kanpur 16, India

The study of 2699 Å electronic band system of chlorobenzene has been extended to extract out all the six b_1 and three a_2 modes in both the ground state (1A_1) and the electronically excited first singlet state (1B_2). The procedure of the extraction of these modes on the basis of observed sequences, cross-sequences, and overtones has especially been elaborated. Strong Fermi interaction has been observed between the vibrational level ν'_{6b} and combination level $\nu'_{16a} + \nu'_{16b}$ in 1B_2 state. The uniqueness of the assignments of the modes has been critically discussed.

INTRODUCTION

The planar fundamentals of chlorobenzene in both the ground (1A_1) and excited (1B_2) states have already been discussed before (1, 2) following a method developed earlier for the gyrovibronic analysis of phenol (3-5). Verma and Bist (6) have also reported the most probable molecular geometry of chlorobenzene in its 1B_2 state on the basis of the excited state inertial constants obtained by Cvitas and Hollas (7) by fitting the observed electronic band contour with the envelopes computed for trial sets of rotational constants. However, no comprehensive data are available for the non-totally-symmetric out-of-plane modes of the molecule. In this paper we report the out-of-plane fundamentals of chlorobenzene deduced by following a method used earlier by Bist *et al.* (4) for the three isotopic species of phenol.

EXPERIMENTAL

The survey scan of the electronic absorption was recorded with the help of a half meter Jarrell-Ash Spectrometer fitted with a Beckman recorder. A 125 W hydrogen lamp served as the source of continuous radiations. The pressure inside a 10 cm path length quartz cell was varied using dry ice for cooling the reservoir of the sample. The details for recording the high resolution electronic and infrared spectra have been described earlier (1).

RESULTS AND DISCUSSION

Computation of Fundamental Frequencies

Chlorobenzene has 30 normal modes of vibration. On the basis of the analysis of high resolution rovibronic spectrum eleven a_1 and ten b_2 planar modes of the molecule could

¹ Present Address: Chemistry Department, University of Western Ontario, London, Canada (on leave)

be easily identified as B- and A-type contours, respectively (1). The nonplanar vibrations, however, do not appear in the spectrum as 1-0 or 0-1 transitions since the selection rules for them are given by

$$\Delta v'' + \Delta v' = 0, 2, 4, \dots$$

Although chance coincidences in a spectrum (so rich in bands) are apt to lead to erroneous assignment, the fact that 1-1 transitions give rise to the most intense bands is helpful in making reliable assignment of the out of plane vibrational fundamentals, all of which fortunately fall below 1000 cm^{-1} for the molecule under discussion. This ensures that there are sufficient molecules in the corresponding v'' levels to give rise to strong bands for sequences and cross-sequences.

The survey scan of electronic ${}^e\text{B}_2 \rightarrow {}^e\text{A}_1$ transition of chlorobenzene, as shown in Fig. 1, has been used to estimate the intensities of the main bands in the region $2800\text{--}2350\text{ \AA}$. The assignment of some of the prominent peaks are also marked in the figure.

The observed prominent sequence-intervals are listed in Table I in order of decreasing intensity. Sequences and cross-sequences connecting a_2 fundamentals are shown in Fig. 2 while those connecting b_1 fundamentals are shown in Fig. 3. In the middle portion of each figure the numbers denote the approximate intensity of the transitions with respect to arbitrarily chosen intensity of the origin (0-0) band as 100. Notations suggested by Wilson (8) have been used to denote the vibrational modes of the molecule.

The combination differences between the pairs of levels have been computed from the observed sequences and cross-sequences using ν''_{16a} , ν'_{16a} , ν''_{16b} , and ν'_{16b} frequency levels as base levels. To fix ν''_{16a} and ν''_{16b} frequencies, the use has been made of the observed overtone transitions $16a_2^0$ (-806.78 cm^{-1}) and $16b_2^0$ (-934.12 cm^{-1}). These data lead to $\nu'_{16a} = 403.39\text{ cm}^{-1}$ and $\nu'_{16b} = 467.06\text{ cm}^{-1}$ with the assumption that in ${}^e\text{A}_1$ state $16a$ and $16b$ modes behave as harmonic modes of vibration. The reliability of the assumption lies in the fact that ν'_{16a} (403.0 cm^{-1}) and ν'_{16b} (466.9 cm^{-1}) frequencies obtained from other studies (9) are almost equal to those obtained in present. The base frequencies ν'_{16a} and ν'_{16b} could now be easily deduced by using sequence transitions $16a_1^1$ and $16b_1^1$ which are reasonably assigned to the intense bands at -200.33 cm^{-1} and -146.57 cm^{-1} , respectively. The frequencies ν'_{16a} (203.07 cm^{-1}) and ν'_{16b} (320.49 cm^{-1}) calculated in this way are confirmed by their overtones observed at 408.58 cm^{-1} and 639.88 cm^{-1} , respectively. Finally the frequency of each of the fundamentals could be calculated by adding the base frequency and the mean value of the related combination difference.

Cvitas and Hollas (7) have discussed the assignment of some prominent sequence bands (cf. Table I). However, we disagree with them in a few cases for obvious reasons. The authors (7), however, misinterpreted the sequence band observed at -37.25 cm^{-1} as $16a_1^1$ and could not find any reliable assignment for one of the strong sequence bands observed at -200.33 cm^{-1} . The former band is undoubtedly $6a_1^1$ arising due to the abundance of ${}^{37}\text{Cl-C}_6\text{H}_5$ molecules. This is evident first from the apparent ratio (1:3) of the intensity of this band to that of the band observed at -38.56 cm^{-1} which corresponds to $6a_1^1$ transition in ${}^{35}\text{Cl-C}_6\text{H}_5$ molecule (1), and secondly by its calculated value (-37.23 cm^{-1}) from ν''_{6a} (410.39 cm^{-1}) and ν'_{6a} (373.16 cm^{-1}) frequencies of $6a$ mode of ${}^{37}\text{Cl-C}_6\text{H}_5$ molecule (1, 2). The sequence band observed at -200.33 cm^{-1} should involve an a -type vibration according to Cvitas and Hollas (7) and should cor-

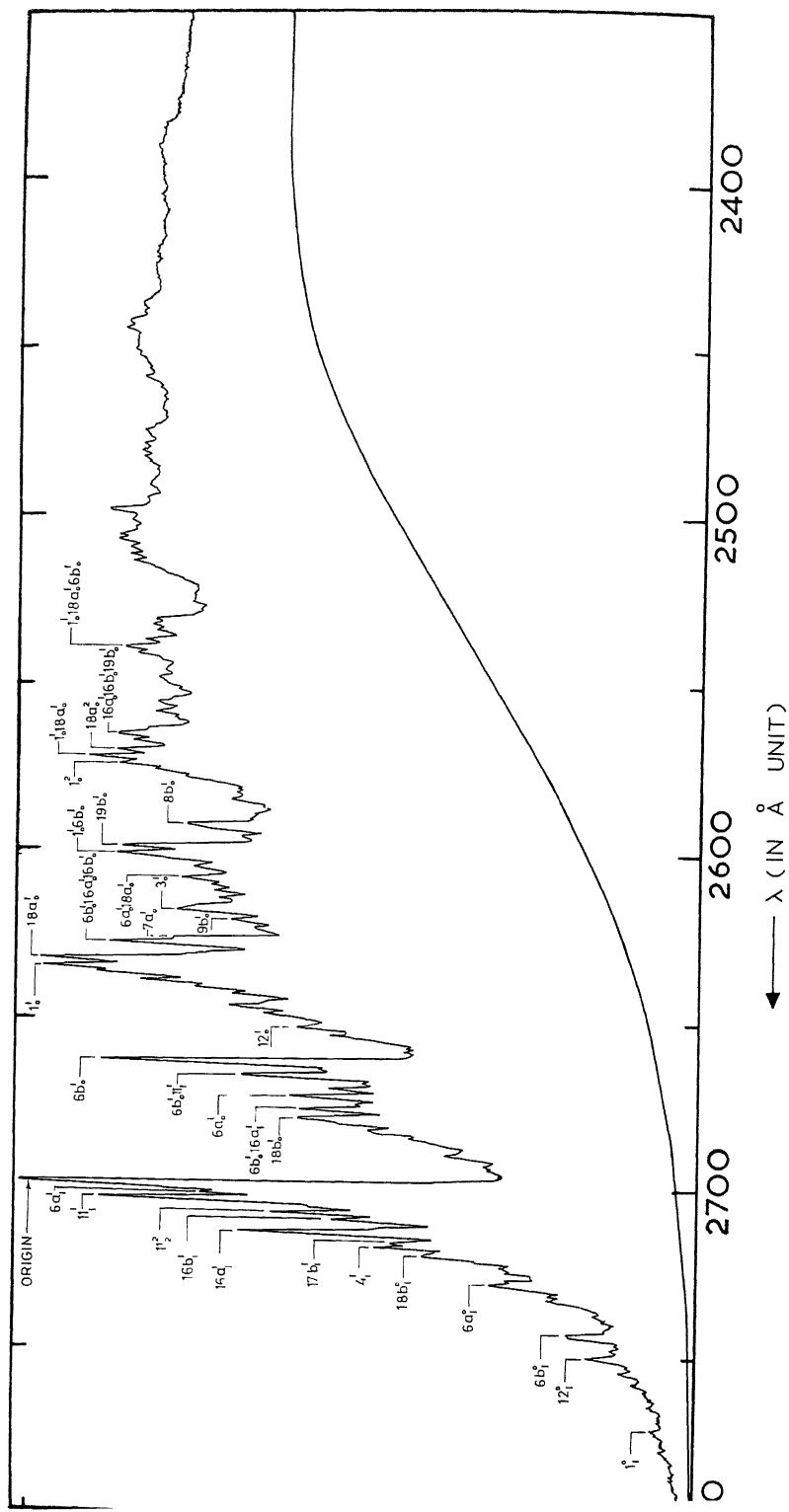


FIG. 1 Vapor phase electronic spectrum of chlorobenzene recorded with a half meter Jarrell-Ash grating using 10 cm path length cell at 22°C

TABLE I
 PROMINENT SEQUENCE BANDS ARRANGED IN ORDER OF DECREASING INTENSITY

Sequence band positions (in cm^{-1})	Assignments	
	Cvitas and Hollas (7) ^a	Present study ^b
- 60 02	20_1^1 (11_1^1)	11_1^1
- 7 43	30_1^1 ($18b_1^1$)	$18b_1^1$
-200 33	?	$16a_1^1$
- 38 56	11_1^1 ($6a_1^1$)	$6a_1^1$
-146 57	19_1^1 ($16b_1^1$) ²	$16b_1^1$
- 37 25	14_1^1 ($16a_1^1$) ²	$6a_1^1$
- 93 80	29_1^1 ($6b_1^1$)	$6b_1^1$
- 89 85	$20_0^1 14_0^1 29_1^0$ ($11_0^1 16a_0^1 6b_1^0$)	$16a_0^1 16b_0^1 6b_1^0$

^a Assignments expressed in parentheses are in the notations used in the present study

^b ₂ denotes transition in $^{37}\text{Cl}-\text{C}_6\text{H}_5$ molecules

respond to a lower frequency mode as indicated by its appreciable intensity. The band could, therefore, be only assigned as $16a_1^1$ transition.

The computed frequencies (accurate to $\pm 1 \text{ cm}^{-1}$) of the vibrations have been summarized in Table II along with those of phenol. The correctness of the frequencies lies in the facts. (1) that these frequencies have been sought as the best fit to the observed

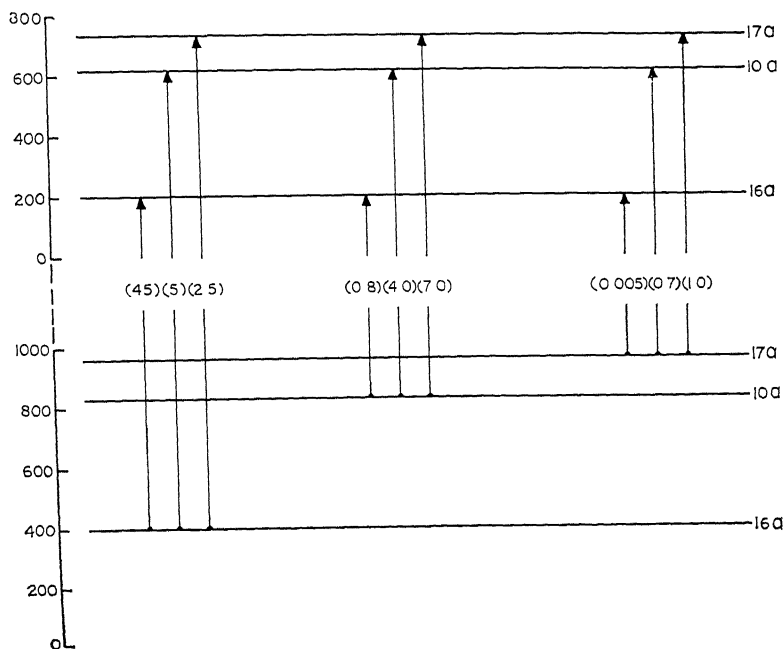


FIG 2 Sequences and cross-sequences connecting a_2 fundamentals of chlorobenzene. The sequences are strong while the cross-sequences except $10a_1^0$ $17a_0^1$ are weak. Transitions shown exhibit B-type

sequence and cross-sequence transitions corroborated by observed overtone transitions and (ii) that there exists an excellent agreement between the vibrations of chlorobenzene and phenol except for two X -sensitive modes $16b$ and 11 . All the b_1 modes in the excited state show a general diminution in their magnitude with respect to those of phenol in the corresponding electronic state, the maximum change being 50% for the mode 11 (cf. Table II). The lowest frequency ν'_{16a} of $16a$ mode is, however, higher in magnitude as compared to the corresponding mode of phenol. These differential changes in a_2 and b_1

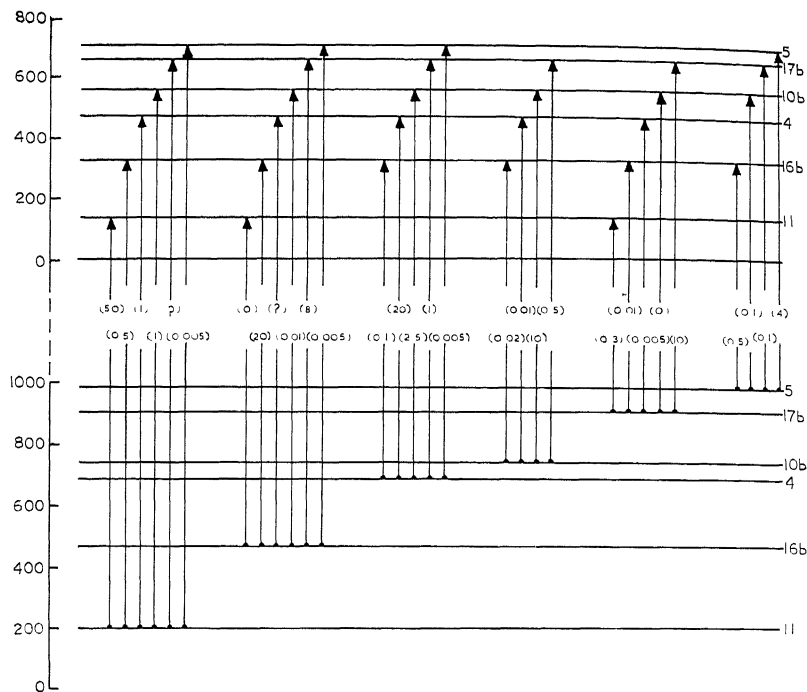


FIG. 3 Sequences and cross-sequences connecting b_1 fundamentals of chlorobenzene. Sequences are intense, while cross-sequences are weak. The transitions shown exhibit B-type band contour. An interrogation mark (?) denotes a transition overlapped by strong bands in the spectrum.

species may be indicative of a pronounced mixing between some of the modes belonging to the two species in the excited state, probably more so in the case of phenol which, in fact, does not belong to C_{2v} symmetry.

Fermi Resonance

Strong Fermi interaction has been observed between fundamental level ν'_{6b} and a combination level of the same symmetry b_2 giving rise to strong bands at 521.03 and 524.98 cm^{-1} . This is indicated by the fact that the intensity varies considerably in sequences associated with these two bands. The combination level can only be comprised of ν'_{16a} and ν'_{16b} fundamental levels since they exactly fit into the requirements of Fermi resonance. Cvitas and Hollar (7) reported that the combination level of ν'_{16a} and ν'_{16b}

$\nu'_{16a} = 384 \text{ cm}^{-1}$ and $\nu'_{11} = 136 \text{ cm}^{-1}$ fundamental levels. On the basis of this assignment and the misinterpretation of -37.25 cm^{-1} sequence band as $16a_1^1$, they computed $\nu''_{16a} = 421 \text{ cm}^{-1}$ which is unlikely because it is far off from its value of 400 cm^{-1} observed in the Raman spectrum of liquid $\text{Cl-C}_6\text{H}_5$ (10) and from 403.0 cm^{-1} deduced from difference bands observed in high resolution infrared spectra of vapor phase $\text{Cl-C}_6\text{H}_5$.

(9) The fundamental level ν'_{6b} , therefore, undergoes Fermi interaction with $\nu'_{16a} + \nu'_{16b}$ combination level rather than $\nu'_{16a} + \nu'_{11}$ combination level

Notations in the Excited State

It may be remarked at the outset that the notations in the excited state are just for the sake of convenience. The primary consideration to denote an excited state level has been the most intense sequence from the group of transitions emanating from the corresponding ground state level, where the notations are more established (1). However, even in the ground state, the normal coordinate analysis of monosubstituted ben-

TABLE II
OUT-OF-PLANE VIBRATIONAL FREQUENCIES IN CHLOROBENZENE AND PHENOL- d_6

Species	Mode	Approximate description	³⁵ ClC ₆ H ₅		C ₆ H ₅ OH ^b		A ^d
			u v	1 r ^a	u v	1 r	
^e A ₁ -State							
a ₂	17a	CH bend	962	961 1	995 2	962 ^c	3 5
	10a	CH bend	831	832 1	817 2	828 ^c	1 7
	16a	CC twist	403	403 0	408 5	415 ^c	-1 3
b ₁	5	CH bend	981	981 0	972 5	—	-0 9
	17b	CH bend	903	902 3	881.0	881	2 3
	10b	CH bend	741	740 5	750 6	751	-1 2
	4	CC twist	684	684 6	685 9	686	-0 3
	16b	X-sensitive	467	466 9	502 8	503	-7 6
	11	X-sensitive	197	(198 0)*	244 5	242	-23 8
^e B ₂ -State							
a ₂	17a	CH bend	729		734 1		-0 6
	10a	CH bend	616		615 9		0 0
	16a	CC twist	203		187 0		7 9
b ₁	5	CH bend	699		725 6		-3 8
	17b	CH bend	655		700 1		-6 8
	10b	CH bend	556		579 8		-4.3
	4	CC twist	422		441 3		-3.5
	16b	X-sensitive	320		358 3		-11 7
	11	X-sensitive	138		206 4		-49 6

^a See reference (9), * the data in parentheses denotes the Raman value in liquid sample

^b H D BIST, J C D BRAND, AND D R WILLIAMS, *J. Mol. Spectrosc.* 24, 413 (1967)

^c J C EVANS, *Spectrochim. Acta* 16, 382 (1960)

^d $A = \frac{(\nu\text{C}_6\text{H}_5\text{Cl} - \nu\text{C}_6\text{H}_5\text{OH})}{100}$, taking more accurate u v data alone

TABLE III
POSITIONS OF BANDS (IN TERMS OF $\Delta\nu$)^a USED IN DEDUCING THE
OUT-OF-PLANE VIBRATIONS

Assign- ments	$\Delta\nu$ (cm ⁻¹)		I ^b	Assign- ments	$\Delta\nu$ (cm ⁻¹)		I ^b
	Observed	Calcu- lated			Observed	Calcu- lated	
17a ₂ ⁰	-1917 79	-1924	0 02	10b ₁ ¹	-185 62	-185	10 0
17b ₂ ⁰	-1803 94	-1806	0 4	16b ₁ ¹	-146 57	-147	20 0
10a ₂ ⁰	-1659 16	-1662	0 01	10b ₀ ¹ 4 ₁ ⁰	-128 38	-128	2 5
10b ₂ ⁰	-1480 53	-1482	0 02	17a ₀ ¹ 10a ₁ ⁰	-101 56	-102	7 0
4 ₂ ⁰	-1369 30	-1368	0 1	17b ₀ ¹ 10b ₁ ⁰	- 85 80	- 86	0 5
16b ₂ ⁰	- 934 12	- 934	0 5	11 ₁ ¹	- 60 02	- 59	50 0
16a ₂ ⁰	- 806 78	- 806	1 9	17b ₀ ¹ 4 ₁ ⁰	- 29 20	- 29	1 0
11 ₀ ¹ 17b ₁ ⁰	- 764 03	- 765	0 3	0,0 (origin)	0 0	—	100 0
16a ₀ ¹ 17a ₁ ⁰	- 758 38	- 759	0 005	5 ₀ ¹ 4 ₁ ⁰	15 20	15	0 005
16b ₀ ¹ 5 ₁ ⁰	- 660 66	- 661	0 5	10b ₀ ¹ 16b ₁ ⁰	88 50	89	0 01
16a ₀ ¹ 10a ₁ ⁰	- 628 05	- 628	0 8	16b ₀ ¹ 11 ₁ ⁰	122 97	123	0 5
16b ₀ ¹ 17b ₁ ⁰	- 581 84	- 583	0.01	17b ₀ ¹ 16b ₁ ⁰	187 62	188	8 0
4 ₀ ¹ 17b ₁ ⁰	- 480 68	- 481	0 005	10a ₀ ¹ 16a ₁ ⁰	212 45	213	5 0
10b ₀ ¹ 5 ₁ ⁰	- 426 76	- 425	0 1	4 ₀ ¹ 11 ₁ ⁰	224 76	225	1 0
16b ₀ ¹ 10b ₁ ⁰	- 421 30	- 421	0 02	5 ₀ ¹ 16b ₁ ⁰	231 40	232	0 005
16b ₀ ¹ 4 ₁ ⁰	- 363 73	- 364	0 1	11 ₀ ²	274 15	276	2 0
10a ₀ ¹ 17a ₁ ⁰	- 345 35	- 346	0 7	17a ₀ ¹ 16a ₁ ⁰	326 45	326	2 5
17b ₀ ¹ 5 ₁ ⁰	- 326 24	- 326	0 1	10b ₀ ¹ 11 ₁ ⁰	358 59	359	1 0
4 ₀ ¹ 10b ₁ ⁰	- 318 76	- 319	0 01	16a ₀ ²	408 58	406	6 0
5 ₁ ¹	- 282 56	- 282	4 0	5 ₀ ¹ 11 ₁ ⁰	501 41	502	0 005
4 ₁ ¹	- 261 67	- 262	20 0	16b ₀ ²	639 88	640	4 0
17b ₁ ¹	- 247 70	- 248	10 0	4 ₀ ²	839 60	844	1 5
17a ₁ ¹	- 232 68	- 233	1 0	10b ₀ ²	1112 89	1112	1 0
10a ₁ ¹	- 215 28	- 215	4.0	10a ₀ ²	1228 19	1232	2 0
16a ₁ ¹	- 200 33	- 200	45 0	17b ₀ ²	1309 32	1310	0 5

^a $\Delta\nu$ = (term value of a band - term value of origin band 37050 92 cm⁻¹)

^b Intensity relative to that of origin taken as 100 (arbitrarily)

zenes shows that the out-of-plane modes exhibit considerable amount of mixing with each other, and, hence, non of the modes could be described as pure unmixed vibration (11). Thus, it should be remembered that a one-to-one correlation between modes of different electronic states may be still more difficult to establish. However, the notations are useful for brevity and we prefer to use them, likewise, to describe the vibrations of the molecule in its excited state.

Conclusion

In ²B₂ state of the molecule, the force fields governing the planar modes exhibit small changes (in comparison to those in ²A₁ state) except in cases of ring-breathing (1) and ring-deformation (6b) modes. The latter two modes and all the nonplanar ones seem to exhibit appreciable decrease in the strength of their governing force fields. It appears that the molecule retains C_{2v} symmetry in its excited state.

APPENDIX

The compilation of the frequencies of about 800 bands observed in the 2699 Å band system of the molecule has been made in the form of a technical report (12). From this report we tabulate here (cf. Table III) the assignment, observed positions, and relative intensity (I) of only those bands which have been used in deducing the frequencies of the nonplanar modes. The positions of the bands, calculated by using the frequencies of nonplanar modes found in the present study, have also been included in Table III. The relative intensity of the bands has been estimated approximately by taking the intensity of origin band as 100 (arbitrarily)

ACKNOWLEDGMENTS

Thanks are due to Council of Scientific and Industrial Research for financial assistance. One of us (H D B) is grateful to Professor J C D Brand (London, Canada) for kind hospitality during the course of experimental work, and (Y S J) wishes to thank Dr Kamal Kumar for useful suggestions and discussions

RECEIVED October 12, 1972

REFERENCES

- 1 H D BIST, V N SARIN, A OJHA, AND Y S JAIN, *Spectrochim Acta* **26A**, 841 (1970)
- 2 H D BIST, V N SARIN, A OJHA, AND Y S JAIN, *Appl Spectrosc* **24**, 292 (1970)
- 3 H D BIST, J C D BRAND, AND D R WILLIAMS, *J Mol Spectrosc* **21**, 76 (1966)
- 4 H D BIST, J C D BRAND, AND D R WILLIAMS, *J Mol Spectrosc* **24**, 402, 413 (1967)
- 5 J C D BRAND AND H D BIST, *Proc Int Conf Spectrosc* **1**, 261 (1967)
- 6 A L VERMA AND H D BIST, *Chem Phys Lett* **4**, 15 (1970)
- 7 T CVITAS AND J M HOLLAS, *J Mol Phys* **18**, 101 (1970)
- 8 E. B WILSON, JR, *Phys Rev* **45**, 706 (1934)
- 9 V N SARIN, Ph D THESIS, Indian Institute of Technology Kanpur, India, 1970)
- 10 D H WHIFFEN, *J Chem Soc* 1350 (1956)
- 11 V S TOMAR, H D BIST, AND V D GUPTA, unpublished data
- 12 Y S JAIN AND H D BIST, unpublished data

see the attached technical
report No 36/70

Technical Report No. 36/70

THE 2699 Å BAND SYSTEM OF CHLOROBENZENE

Y.S. Jain and H.D. Bist

DEPARTMENT OF PHYSICS
INDIAN INSTITUTE OF TECHNOLOGY KANPUR

APPENDIX I

In this section, the frequencies, relative intensities and assignments for a majority of the vibronic bands observed in $\underline{B}_2^e - \underline{A}_1^e$ electronic band system of chlorobenzene have been tabulated.

The bands observed are either \underline{A}_e - or \underline{B}_e -type^{1,2} in the usual asymmetric top notation. No band was found to have hybrid band character or \underline{C}_e -type contour. The (0,0) origin band, all the totally symmetric a_1 fundamentals, and even combinations or overtones of all the modes have \underline{B}_e -type contour, showing a prominent relatively sharper peak in the middle, with weak hump on its high frequency side, and a comparatively weak broader component on its low frequency side. The inplane non-totally symmetric b_2 vibrations or the combinations having b_2 symmetry show \underline{A}_e -type contour with only one sharp peak. The middle peak for \underline{B}_e -type contour and single peak for \underline{A}_e -type contour have been measured. In either case the rovibronic origin lies approximately 2.6 cm⁻¹ to low wave number side of intense peak³. The estimation of relative intensity of the bands is based on the intensities of the peak instead of the integrated absorptions which would involve large and uncertain corrections for overlapping of the bands etc. The band type is not stated in the tables though it is implied in the vibrational assignments.

The $v' - v''$ transitions in the mode \underline{k} have been conventionally represented by $\underline{k}_{v''}^{v'}$ and multiple quantum changes by $\underline{k}_{v''}^{v'} \underline{l}_{v''}^{v'}$ $\underline{m}_{v''}^{v'}$ etc⁴. The Wilson's notation⁵ for the benzene ring have been used to denote the different modes. The superscript "i" before each notation has been used to identify

transitions involving $C_6H_5Cl^{37}$ molecule¹.

The positions of the bands i.e. the frequencies of corresponding transitions have been tabulated in column 2 and assignments in the column 1. The difference $\Delta\nu$ between the frequency of a particular band and the (0,0) origin band has been noted down in column 3, and the corresponding calculated value from the fundamentals and prominent sequences in column 4. The difference between the values given in the column 3 and 4 gives $2x$ shown in the column 5. $2x$, in case of overtone is $2x\omega_e$ under diatomic approximation⁶, while for other combination bands shows the effect of combined anharmonicities. The positions of some very weak bands which could not be assigned are also tabulated putting question mark (?) in assignment column.

REFERENCES

1. H.D. Bist, V.N. Sarin, A. Ojha and Y.S. Jain, *Spectrochim. Acta*, 26A, 841 (1970).
2. H.D. Bist, V.N. Sarin, A. Ojha and Y.S. Jain, *Appl. Spectry.*, 24, 292 (1970).
3. T. Cvitas and J.M. Hollas, *J. Mol. Phys.*, 18, 101 (1970).
4. H.D. Bist, J.C.D. Brand, and D.R. Williams, *J. Mol. Spectry*, 24, 413-467 (1967).
5. E.B. Wilson, Jr., *Phys. Rev.*, 45, 706 (1934).
6. G. Herzberg, "Infrared and Raman Spectra", D. Van Nostrand Company Inc. New York, 1945.

Band positions and relative intensities. The intensities (in parantheses) are relative to origin band = 100.

Assignment	Band position	$\Delta V(\text{cm}^{-1})$		2X
		Observed	Calculated	
1	2	3	4	5
$1_1^0 18a_1^0$	35020.62(.03)	- 2030.30	- 2029.46	- 0.8
$1_1^0 6b_1^0 16a_2^2$	029.80(.01)	- 2021.12	- 2020.42	- 0.7
1_2^0	044.42(.5)	- 2006.50	- 2007.56	0.6
$6a_1^0 8a_1^0$	049.89(.01)	- 2001.03	- 2003.25	2.2
$17a_2^0$	133.13(.02)	- 1917.79	- 1923.46	5.7
?	140.66(.01)	- 1910.26		
$8a_1^0 18b_1^0$	168.69(.05)	- 1882.23	- 1881.15	- 1.1
$6a_1^0 19b_1^0$	184.73(.03)	- 1866.15	- 1864.64	- 1.5
$9a_1^0 12_1^0$	192.30(.02)	- 1856.62	- 1859.50	2.9
$1_1^0 6b_1^0 16a_1^1 6a_1^1$	193.86(.02)	- 1857.06	- 1857.57	0.5
$6b_1^0 16a_1^1 18a_1^0$	209.73(.02)	- 1841.19	- 1840.91	- 0.3
$1_1^0 6b_1^0 16a_1^1 18b_1^1$	221.97(.02)	- 1828.95	- 1826.44	- 2.5
$1_1^0 6b_1^0 16a_1^1$	230.16(.1)	- 1820.76	- 1819.01	- 1.8
$17b_2^0$	246.98(.4)	- 1803.94	- 1805.02	- 1.1
$7a_1^0 12_1^0$	250.11(.03)	- 1800.81	- 1799.08	- 1.7
$10a_1^0 17a_1^0$	256.10(.04)	- 1794.82	- 1792.95	- 1.9
$12_1^0 18a_1^0 11_1^1$	258.97(.01)	- 1791.95	- 1792.18	0.2
$6b_1^0 9b_1^0$	265.95(.01)	- 1784.97	- 1781.99	- 3.0
$12_1^0 15_1^0$	276.10(.04)	- 1774.82	- 1774.11	- 0.7
$1_1^0 12_1^0 11_1^1$	281.09(.05)	- 1769.83	- 1770.28	- 0.5

contd.

1	2	3	4	5
$6b_1^0 9a_1^0$	35283.59(.05)	- 1767.33	- 1767.92	0.6
?	300.05(.05)	- 1750.87		
$12_1^0 18a_1^0 18b_1^1$	312.61(.01)	- 1738.31	- 1739.59	1.3
$10a_1^0 17b_1^0$	315.41(.01)	- 1735.51	- 1733.73	- 1.0
$12_1^0 18a_1^0$	319.76(.03)	- 1731.16	- 1732.16	1.0
$5_1^0 10b_1^0$	330.65(.05)	- 1720.27	- 1722.90	2.6
$1_1^0 12_1^0$	340.96(.1)	- 1709.96	- 1710.26	0.3
$6b_1^0 7a_1^0$	343.84(.1)	- 1707.08	- 1707.50	0.4
$10b_1^0 17a_1^0$	345.73(.005)	- 1705.19	- 1703.16	- 2.0
$6b_1^0 11_1^1 18a_1^0$	351.62(.02)	- 1699.30	- 1700.60	1.3
$3_1^0 6a_1^0$	362.98(.05)	- 1687.94	- 1688.61	0.7
$1_1^0 6b_1^0 11_1^1$	371.30(.05)	- 1679.62	- 1678.70	0.9
$4_1^0 5_1^0$	386.16(.01)	- 1664.76	- 1665.38	0.6
$10a_2^0$	391.76(.01)	- 1659.16	- 1662.44	3.3
$1_1^0 6b_1^0 6a_1^1$	393.08(.01)	- 1657.84	- 1657.24	- 0.6
$6b_1^0 18a_1^0 18b_1^1$	403.02(.02)	- 1647.90	- 1648.01	0.1
$10b_1^0 17b_1^0$	409.36(.08)	- 1641.56	- 1643.94	2.4
$6b_1^0 18a_1^0$	410.48(.05)	- 1640.44	- 1640.58	0.1
$1_1^0 6b_1^0 18b_1^1$	423.39(.06)	- 1627.03	- 1626.11	- 0.9
$1_1^0 6b_1^0$	431.21(.2)	- 1619.71	- 1618.68	- 1.0
$8b_1^0$	452.73(.05)	- 1598.19	- 1598.19	-
$8a_1^0$	464.48(.02)	- 1586.44	- 1586.44	-
$10a_1^0 10b_1^0 18b_1^1$	473.35(.01)	- 1577.57	- 1580.08	2.5
$10a_1^0 10b_1^0$	481.31(.01)	- 1569.61	- 1572.65	3.0

1	2	3	4	5
$4_1^{\circ}10a_1^{\circ}$	35536.03(.02)	- 1514.89	- 1515.13	0.2
?	546.19(.02)	- 1504.73		
$7a_1^{\circ}16a_2^2$	561.63(.15)	- 1489.29	- 1490.86	1.6
$6a_1^{\circ}15_1^{\circ}$	565.44(.03)	- 1485.48	- 1484.44	- 1.0
$19a_1^{\circ}$	568.64(.1)	- 1482.28	-	-
$10b_2^{\circ}$	570.39(.02)	- 1480.53	- 1482.86	2.3
?	578.66(.01)	- 1472.26		
$6b_1^{\circ}12_1^{\circ}16b_1^1$	585.24(.10)	- 1465.68	- 1467.95	2.3
$9b_1^{\circ}18b_1^{\circ}$	592.38(.08)	- 1458.54	- 1461.80	3.3
$19b_1^{\circ}$	603.09(.03)	- 1447.83	-	-
$5_1^{\circ}16b_1^{\circ}$	604.18(.03)	- 1446.74	- 1448.53	1.8
$6a_1^{\circ}18a_1^{\circ}$	609.13(.05)	- 1441.79	- 1442.49	0.7
$4_1^{\circ}10b_1^{\circ}18b_1^1$	617.88(.01)	- 1433.04	- 1432.77	- 0.3
$16a_2^218a_1^{\circ}18b_1^1$	620.90(.01)	- 1430.02	- 1431.37	1.4
$1_1^{\circ}6a_1^{\circ}18b_1^1$	622.83(.01)	- 1428.09	- 1428.02	- 0.1
$4_1^{\circ}10b_1^{\circ}$	624.75(.08)	- 1426.17	- 1425.34	- 0.8
$16a_2^218a_1^{\circ}$	628.27(.1)	- 1422.65	- 1423.94	1.3
$1_1^{\circ}6a_1^{\circ}$	630.54(.2)	- 1420.33	- 1420.59	0.2
12_2°	633.48(.3)	- 1412.44	- 1412.96	- 0.5
$1_1^{\circ}16a_2^218b_1^1$	642.41(.05)	- 1408.51	- 1409.47	1.0
$1_1^{\circ}16a_2^2$	648.61(.2)	- 1402.31	- 1402.04	- 0.3
?	660.12(.05)	- 1390.80		
$6b_1^17a_1^{\circ}16a_1^1$	663.35(.05)	- 1387.57	- 1386.73	0.8
$7a_1^{\circ}18b_1^{\circ}$	664.79(.1)	- 1386.13	- 1387.31	1.2

contd.

1	2	3	4	5
$5_1^{\circ}16a_1^{\circ}$	35669.40(.2)	- 1381.52	- 1384.87	3.4
$5_1^17a_1^{\circ}$	676.70(.1)	- 1374.22	- 1375.16	0.9
4_2°	681.62(.1)	- 1369.30	- 1369.57	0.3
$16b_1^{\circ}17b_1^{\circ}$	683.19(.1)	- 1367.73	- 1367.82	0.1
$15_1^{\circ}18b_1^{\circ}$	689.59(.01)	- 1361.33	- 1361.80	0.5
$4_1^17a_1^{\circ}$	697.45(.2)	- 1353.47	- 1354.34	0.9
$9a_1^{\circ}16a_1^1$	699.49(.3)	- 1351.43	- 1353.35	1.9
$7a_1^{\circ}17b_1^1$	711.76(.1)	- 1339.16	- 1340.30	1.1
$6a_1^17a_1^{\circ}16a_1^1$	718.47(.1)	- 1332.45	- 1331.49	1.0
14_1°	724.36(.2)	- 1326.56	-	-
$6b_1^{\circ}12_1^{\circ}$	729.23(.5)	- 1321.69	- 1321.33	- 0.2
$5_1^118a_1^{\circ}$	745.01(.1)	- 1305.91	- 1308.24	2.3
$1_1^{\circ}18b_1^{\circ}$	751.99(.5)	- 1298.93	- 1298.49	0.4
$7a_1^{\circ}16a_1^1$	759.08(.5)	- 1291.84	- 1292.93	1.1
$1_1^17a_1^{\circ}16a_1^1$	761.08(.1)	- 1289.86	- 1290.87	1.0
$4_1^118a_1^{\circ}$	763.77(.1)	- 1287.15	- 1287.35	0.2
$1_1^{\circ}5_1^1$	765.35(.05)	- 1285.57	- 1286.34	0.8
$7a_1^{\circ}10b_1^1$	771.64(.01)	- 1279.28	- 1278.22	- 1.0
$17b_1^118a_1^{\circ}$	776.66(.05)	- 1274.26	- 1273.38	- 0.9
3_1°	779.14(.2)	- 1271.78	-	-
$7a_1^{\circ}11_3^3$	781.31(.05)	- 1269.50	- 1271.92	2.4
$1_1^{\circ}4_1^1$	785.31(.3)	- 1265.61	- 1265.45	- 0.2
$1_1^{\circ}17b_1^1$	800.62(.1)	- 1250.30	- 1251.48	1.2
$7a_1^{\circ}16b_1^118b_1^1$	803.75(.05)	- 1247.17	- 1246.60	- 0.6

contd.

1	2	3	4	5
$1_1^0 6a_1^1 16a_1^1$	35808.70(.25)	- 1242.22	- 1242.67	0.5
$7a_1^0 16b_1^1$	312.64(.15)	- 1233.23	- 1239.17	0.9
$10a_1^0 16a_1^0$	316.58(.2)	- 1234.34	- 1234.62	0.3
$6b_2^0$	324.95(.5)	- 1225.97	- 1229.30	3.3
$9a_1^0 11_1^1 18b_1^1$	327.44(.05)	- 1223.43	- 1220.47	- 3.0
$7a_1^0 4_1^0 10b_1^1$	329.12(.05)	- 1221.80	- 1220.98	- 0.8
$9a_1^0 11_1^1$	337.90(.15)	- 1213.02	- 1213.04	0.0
$7a_1^0 11_2^2$	338.73(.10)	- 1212.19	- 1212.32	0.1
$10b_1^1 18a_1^0$	339.34(.10)	- 1211.08	- 1211.30	0.2
$1_1^0 16a_1^1$	346.74(.5)	- 1204.18	- 1204.11	- 0.1
$7a_1^0 10a_1^0 17a_1^1$	353.03(.005)	- 1192.39	- 1194.16	1.3
$6a_1^1 9a_1^0$	360.21(.005)	- 1190.71	- 1191.58	0.9
$1_1^0 10b_1^1$	362.33(.05)	- 1183.54	- 1189.40	0.9
$6b_1^1 17a_1^0$	365.36(.05)	- 1185.56	- 1186.40	0.8
$1_1^0 11_3^3$	368.35(.03)	- 1182.57	- 1183.10	0.5
$7a_1^0 6b_1^0 16a_1^1 16b_1^1$	369.44(.05)	- 1181.43	- 1182.45	1.0
$5_1^0 11_1^0$	372.16(.01)	- 1178.76	- 1178.96	0.2
$16b_1^1 18a_1^0$	380.57(.05)	- 1170.35	- 1172.25	1.9
$9b_1^0$	383.33(.05)	- 1167.09	-	-
$9a_1^0 18b_1^1$	390.39(.1)	- 1160.03	- 1160.45	0.4
$7a_1^0 11_1^1 18b_1^1$	392.25(.01)	- 1158.67	- 1160.05	1.4
$9a_1^0$	397.90(.1)	- 1153.02	-	-
$7a_1^0 11_1^1$	399.56(.3)	- 1151.36	- 1152.62	1.3
$11_2^2 18a_1^0$	906.09(.1)	- 1144.83	- 1145.40	0.6

contd.

1	2	3	4	5
$6a_1^1 7a_1^0$	35918.31(.2)	- 1132.61	- 1131.16	- 1.5
$18a_1^0 10a_1^0 17a_0^1$	922.75(.1)	- 1128.17	- 1127.24	- 0.9
$6a_1^0 12_1^0$	927.54(.3)	- 1123.33	- 1123.29	- 0.1
$1_1^0 11_2^2$	923.35(.3)	- 1122.57	- 1123.50	0.9
$6b_1^1 18a_1^0$	931.53(.05)	- 1119.58	- 1119.48	- 0.1
$1_1^0 10a_1^0 17a_0^1$	945.72(.05)	- 1105.20	- 1105.34	0.1
$6a_0^1 19a_1^0$	947.34(.05)	- 1103.58	- 1104.04	0.5
$7a_1^0 18b_1^1$	951.87(.4)	- 1099.05	- 1100.03	1.0
$11_1^0 17b_1^0$	954.97(.1)	- 1095.95	- 1100.00	4.1
$7a_1^0$	958.32(1.5)	- 1092.60	-	-
$i_7 a_1^0$	960.38(.4)	- 1090.54	-	-
$11_1^1 18a_1^0$	965.31(.5)	- 1085.61	- 1085.70	0.1
$6b_0^1 8b_1^0$	973.25(.1)	- 1077.67	- 1077.16	- 0.5
$15_1^0 18b_1^1$	976.11(.05)	- 1074.81	- 1075.06	0.3
$1_1^0 11_1^1 18b_1^1$	978.85(.3)	- 1072.07	- 1071.23	- 0.3
15_1^0	933.29(.3)	- 1067.63	-	-
$1_1^0 11_1^1$	987.20(1)	- 1063.72	- 1063.80	0.1
$1_1^0 6a_1^1 18b_1^1$	36001.51(.01)	- 1049.41	- 1049.77	0.4
$1_1^0 6a_1^1$	008.86(.8)	- 1042.06	- 1042.34	0.3
$18a_1^0 13b_1^1$	017.50(.8)	- 1033.42	- 1033.11	- 0.3
$13a_1^0$	025.24(2.5)	- 1025.68	-	-
$1_1^0 18b_1^1$	039.66(1)	- 1011.26	- 1011.21	- 0.1
$16a_3^1$	0.43.64(.4)	- 1007.23	- 1007.11	- 0.2

contd.

1	2	3	4	5
1_1^0	36047.14(3)	- 1003.73	-	-
?	056.52(.2)	- 994.40		
$5_1^{12^0}$	061.70(.1)	- 989.22	- 989.04	- 0.2
?	069.35(.05)	- 981.57		
$4_1^{12^0}18b_1^1$	075.27(.05)	- 975.65	- 975.58	- 0.1
?	078.94(.01)	- 971.93		
$4_1^{12^0}$	083.30(1)	- 967.62	- 968.15	0.5
$i_4^{12^0}$	085.56(.05)	- 965.36	- 966.27	0.8
$12_1^{17b_1^1}$	097.07(.05)	- 953.85	- 954.18	0.3
$6a_1^{12^0}16a_1^1$	103.29(.2)	- 947.63	- 945.37	- 2.3
$i_6a_1^{12^0}16a_1^1$	107.45(.05)	- 943.47	- 942.18	- 1.3
$10b_1^{11^0}$	112.82(.8)	- 938.10	- 938.92	0.8
$16b_2^0$	116.32(.1)	- 934.12	- 934.12	0.0
$6b_1^{11^0}17b_1^1$	123.99(.08)	- 921.93	- 922.62	0.7
$6b_1^{16a_1^1}10a_1^{17a_1^1}$	133.03(.01)	- 917.89	- 916.79	- 1.1
$12_1^{16a_1^1}13b_1^1$	137.61(.01)	- 913.31	- 914.24	0.9
$12_1^{16a_1^1}$	144.54(1)	- 906.33	- 906.81	0.4
$i_1^{12^0}16a_1^1$	146.41(.2)	- 904.51	- 904.93	0.4
$5_1^{16b_1^0}$	153.84(.05)	- 897.08	- 897.46	0.4
$10b_1^{12^0}$	159.13(.01)	- 891.79	- 892.10	0.3
$4_1^{16b_1^0}18b_1^1$	165.26(.01)	- 885.66	- 884.00	- 1.7
$11_1^{14^0}$	168.30(.01)	- 880.62	- 881.40	0.8
$4_1^{16b_1^0}$	173.84(.1)	- 877.08	- 876.57	- 0.5
$6b_1^{17b_1^1}18b_1^1$	181.09(.005)	- 869.83	- 870.03	0.2

contd.

1	2	3	4	5
$11_1^1 16a_2^0$	36 184.74(.02)	- 866.13	- 366.80	0.6
$6b_1^0 17b_1^1$	183.51(.1)	- 862.41	- 862.60	0.1
$12_1^0 16b_1^1$	198.26(.6)	- 852.66	- 853.05	0.4
$11_2^2 12_1^0 13b_1^1$	216.94(.05)	- 833.98	- 833.63	- 0.4
$6a_2^0$	220.98(.2)	- 829.94	- 833.62	3.7
$11_2^2 12_1^0$	225.23(1)	- 825.69	- 826.20	0.5
$6b_1^0 16a_1^1 13b_1^1$	227.03(.5)	- 823.39	- 822.66	- 1.2
$6b_1^0 11_1^1 16b_1^1$	229.71(.3)	- 821.21	- 821.49	0.3
$6b_1^0 16a_1^1$	235.10(2.5)	- 815.82	- 815.23	- 0.6
$6a_1^0 16a_2^2$	237.68(.05)	- 813.24	- 815.07	1.7
$12_1^0 10a_1^0 17a_0^1$	240.58(.2)	- 810.34	- 808.04	- 2.3
$16a_2^0$	244.14(1)	- 806.78	- 806.80	0.0
$7a_1^0 13b_0^1$	246.77(.01)	- 804.15	- 805.21	1.1
$6b_1^0 10b_1^1$	250.58(.3)	- 800.34	- 800.52	0.2
$12_1^0 6b_1^0 16a_0^1 10b_0^1$	253.04(.01)	- 797.83	- 796.33	- 1.6
$6b_1^0 11_3^3$	256.99(.4)	- 793.93	- 794.22	0.3
$6b_1^0 9a_1^1$	262.50(.05)	- 788.42	- 787.33	- 1.1
$6b_1^0 11_1^1 10a_1^0 17a_0^1$	272.50(.1)	- 778.42	- 776.48	- 1.9
$11_1^1 12_1^0 13b_1^1$	277.29(.3)	- 773.63	- 773.93	0.6
$6b_1^0 16b_1^1 13b_1^1$	282.73(.2)	- 768.14	- 768.90	0.8
$11_1^1 12_1^0$	285.49(1)	- 765.43	- 766.50	1.1
$11_0^1 17b_1^0$	286.89(.3)	- 764.03	- 764.57	0.5
$6b_1^0 16b_1^1$	289.36(.5)	- 761.56	- 761.47	- 0.1

contd.

1	2	3	4	5
$16a_1^1 17a_1^0$	36292.54(.005)	- 753.33	- 758.66	0.3
$6a_1^1 12_1^0 18b_1^1$	296.77(.005)	- 754.15	- 752.47	- 1.7
$6a_1^1 12_1^0$	302.93(.2)	- 747.99	- 745.04	- 3.0
$6b_1^0 4_1^0 10b_1^1$	303.11(.05)	- 742.81)	- 743.28	0.5
$6b_1^0 11_2^2 18b_1^1$	309.76(.01)	- 741.16	- 741.05	- 0.1
$6b_1^0 11_2^2$	316.49(.3)	- 734.43	- 734.62	0.2
$12_1^0 18b_2^2$	331.68(.2)	- 719.24	- 721.34	2.1
$6b_1^0 10a_1^0 17a_1^1$	334.79(1)	- 716.13	- 716.46	0.3
$12_1^0 18b_1^1$	333.66(2.5)	- 712.86	- 713.91	1.1
$6b_2^1$	342.72(1)	- 708.20	- 708.70	0.5
12_1^0	344.44(3)	- 706.43	-	-
$i_1 12_1^0$	346.32(1.5)	- 704.60	-	-
$5_1^1 6a_1^0$	351.96(.01)	- 698.96	- 699.37	0.4
$6b_1^0 11_1^1 18b_2^2$	359.56(.005)	- 691.36	- 639.78	- 1.6
$6b_1^0 11_1^1 18b_1^1$	367.71(.5)	- 683.21	- 682.35	- 0.9
$4_1^1 6a_1^0$	370.75(.04)	- 680.17	- 678.48	- 1.7
$6b_1^0 11_1^1$	376.07(2)	- 674.35	- 674.92	0.1
$6a_1^0 17b_1^1$	386.57(.05)	- 664.35	- 664.51	0.2
$5_1^0 16b_1^1$	390.26(.5)	- 660.66	- 660.98	0.3
$6a_2^1 16a_1^1$	396.13(.05)	- 654.79	- 655.70	0.9
$6a_1^1 6b_1^0$	397.59(.8)	- 653.33	- 653.46	0.1
$i_1 6a_1^1 6b_1^0$	393.93(.3)	- 651.99	- 652.15	0.2
$16a_2^2 17b_1^1$	404.23(.4)	- 646.64	- 645.96	- 0.7
$6b_1^0 18b_2^2$	421.03(.8)	- 629.84	- 629.36	- 0.5

contd.

1	2	3	4	5
$10a_1^o 16a_1^1$	36422.37(.3)	- 628.05	- 628.15	0.1
$6a_1^o 16a_1^1 18b_1^1$	426.00(.1)	- 624.92	- 624.57	- 0.4
$6b_1^o 18b_1^1$	428.59(2)	- 622.33	- 622.33	0.0
$6a_1^o 16a_1^1$	434.13(1)	- 616.74	- 617.14	0.4
$6b_1^o$	436.02(9)	- 614.90	-	-
$i 6a_1^o 16a_1^1$	440.43(.01)	- 610.49	- 610.72	0.2
?	444.73(.05)	- 606.19		
$10b_1^o 11_1^1$	446.77(.05)	- 604.15	- 603.49	0.3
$6a_1^o 10b_1^1$	448.60(.05)	- 602.32	- 602.43	0.1
$11_1^o 16a_1^o$	450.36(.05)	- 600.56	- 600.89	0.3
$6a_1^o 11_3^3$	456.59(.02)	- 594.33	- 596.13	1.8
$18b_2^o$	462.85(.05)	- 588.07	- 589.42	1.4
$16b_1^1 17b_1^o$	469.63(.01)	- 581.24	- 582.02	0.8
$5_1^1 18b_1^o$	474.24(.005)	- 576.63	- 577.27	0.6
$6a_1^o 16b_1^1 18b_1^1$	479.86(.05)	- 571.06	- 570.81	- 0.3
$6a_1^o 16b_1^1$	494.31(.05)	- 563.11	- 563.38	0.3
$16a_2^2 16b_1^1$	505.67(.4)	- 545.25	- 544.83	- 0.4
$17b_1^1 18b_1^o$	508.47(.2)	- 542.45	- 542.41	0.0
$10b_1^o 16a_1^1$	510.70(.2)	- 540.22	- 538.36	- 1.9
$6a_1^o 11_2^2$	526.14(.1)	- 535.88	- 536.53	0.7
4_2^2	530.68(.1)	- 524.78	- 523.34	- 1.4
$6a_1^o 10a_1^o 17a_1^1$	532.86(.1)	- 520.24	- 518.37	- 1.9
$16a_1^1 18b_1^o$	556.24(1.5)	- 494.68	- 495.04	0.4
$6a_1^o 11_1^1 18b_1^1$	563.96(.05)	- 486.96	- 484.26	- 2.7

contd.

1	2	3	4	5
$5_1^{11}16a_1^1$	36560.30(.1)	- 482.54	- 482.89	0.4
$4_1^{11}17b_1^0$	570.24(.005)	- 480.68	- 480.09	- 0.6
$6a_1^{11}11_1^1$	572.05(1)	- 478.87	- 476.83	- 2.0
$i_1^{11}6a_1^{11}11_1^1$	578.55(.2)	- 472.37	- 470.41	- 2.0
$4_1^{11}16a_1^{11}18b_1^1$	580.90(.2)	- 470.02	- 469.43	- 0.6
$4_1^{11}16a_1^1$	589.17(2)	- 461.75	- 462.00	0.3
$6a_2^1$	595.84(1)	- 455.03	- 455.37	0.3
$i_1^{11}6a_2^1$	603.30(.1)	- 447.62	- 447.64	0.0
$16a_1^{11}17b_1^1$	605.60(.2)	- 445.32	- 448.03	2.7
$16b_1^{11}18b_1^0$	608.90(.1)	- 442.02	- 441.23	- 0.7
$6a_1^{11}16a_2^2$	614.80(.2)	- 436.12	- 436.82	0.7
$6a_1^{11}18b_2^2$	618.58(.05)	- 432.34	- 431.67	- 0.7
$5_1^{11}16b_1^1$	622.62(.05)	- 428.30	- 429.13	0.8
$5_1^{11}10b_1^0$	624.16(.1)	- 426.76	- 425.68	- 1.1
$6a_1^{11}18b_1^1$	626.53(2)	- 424.39	- 424.24	- 0.2
$10b_1^{11}16b_1^0$	629.62(.02)	- 421.30	- 420.94	- 0.4
$6a_1^0$	634.11(8)	- 416.81	-	-
$i_1^{11}6a_1^0$	640.53(2)	- 410.39	-	-
$16a_2^{11}18b_1^1$	644.04(1)	- 406.83	- 405.69	- 1.2
$16a_2^2$	652.66(10)	- 398.26	- 400.66	2.4
$11_2^{11}2_1^{11}$	668.48(1)	- 382.44	- 381.39	- 1.0
$i_1^{11}11_2^{11}2_1^{11}$	669.77(.8)	- 381.15	- 380.50	- 0.7
$5_1^{11}10a_1^1$	683.95(.3)	- 366.97	- 365.54	- 1.4
$4_1^{11}10a_1^017a_1^1$	686.00(.4)	- 364.92	- 363.23	- 1.7

contd.

1	2	3	4	5
$4_1^0 16b_0^1$	36637.19(.1)	- 363.73	- 363.42	- 0.3
$11_1^1 18b_1^0$	695.98(.5)	- 354.94	- 354.73	- 0.2
$16a_1^1 16b_1^1$	701.64(.2)	- 349.23	- 346.90	- 2.4
$10a_0^1 17a_1^0$	705.57(.7)	- 345.35	- 345.80	0.5
$6b_1^1 17b_1^1$	710.62(.5)	- 340.30	- 341.50	1.2
$6a_1^1 18b_1^0$	713.33(.2)	- 332.59	- 333.27	0.7
$10b_1^1 16b_1^1$	713.65(.1)	- 332.27	- 332.29	0.0
$5_1^0 17b_0^1$	724.68(.1)	- 326.24	- 326.39	0.2
$4_1^1 11_1^1$	728.13(2)	- 322.74	- 321.71	- 1.0
$4_0^1 10b_1^0$	732.16(.01)	- 318.76	- 319.01	0.3
$11_1^1 17b_1^1$	743.49(1)	- 307.43	- 307.72	0.3
$18b_2^1$	748.21(2)	- 302.71	- 302.14	- 0.6
$4_1^1 6a_1^1$	752.71(1.5)	- 298.21	- 300.23	2.0
$18b_1^0$	753.21(6)	- 294.71	-	-
$i_1 18b_1^0$	760.15(1.5)	- 290.77	-	-
5_1^1	768.36(4)	- 282.56	- 282.62	0.1
$4_1^1 18b_2^2$	771.33(.5)	- 279.59	- 276.53	- 3.1
$4_1^1 18b_1^1$	780.40(5)	- 270.52	- 269.10	- 1.4
$11_2^2 16b_1^1$	784.93(2)	- 265.99	- 266.29	0.3
4_1^1	789.25(20)	- 261.67	- 261.49	- 0.2
$17b_1^1 18b_1^1$	795.43(1)	- 255.49	- 255.13	- 0.4
$17b_1^1$	803.22(10)	- 247.70	- 247.43	- 0.3
$10b_1^1 11_1^1$	806.51(1)	- 244.41	- 245.64	1.2
$6a_1^1 16a_1^1$	812.28(8)	- 238.64	- 238.89	0.3

contd.

1	2	3	4	5
$i 6a_1^1 17a_1^1$	36813.68(3)	- 237.24	- 237.58	0.3
$17a_1^1$	818.24(1)	- 232.68	- 232.34	- 0.3
$10b_1^1 16a_1^1$	826.50(.5)	- 224.42	- 224.18	- 0.2
$10a_1^1$	835.64(4)	- 215.28	- 215.29	0.0
$16a_1^1 18b_1^1$	842.56(15)	- 208.36	- 207.76	- 0.6
$11_1^1 16b_1^1$	844.45(5)	- 206.47	- 206.59	0.1
$16a_1^1$	850.59(45)	- 200.33	- 200.33	0.0
$10b_1^1 18b_1^1$	857.66(1)	- 193.26	- 193.05	- 0.2
$6b_1^0 16a_1^1 16b_1^1 10a_1^0 17a_1^1$	861.26(1.5)	- 189.66	- 191.41	1.8
$10b_1^1$	865.30(10)	- 185.62	- 185.82	0.2
11_3^3	871.60(8)	- 179.32	- 180.06	0.7
$i 11_3^3$	872.89(2.5)	- 178.03		
$9a_1^1$	877.54(.2)	- 173.38	- 172.43	- 0.9
$6a_2^2 6b_1^0 16a_1^1 16b_1^1$	883.43(.2)	- 167.49	- 166.64	- 0.9
$11_1^1 10a_1^0 17a_1^1$	886.97(1.5)	- 163.95	- 161.58	- 2.4
$6a_1^1 11_2^2$	892.24(.5)	- 158.68	- 158.28	- 0.4
$16b_1^1 18b_1^1$	896.40(5)	- 154.52	- 154.00	- 0.5
$11_1^1 6b_1^0 16a_1^1 16b_1^1$	902.69(2)	- 148.23	- 149.87	1.6
$16b_1^1$	904.35(15)	- 146.57	- 146.57	0.0
$6a_1^1 10a_1^0 17a_1^1$	912.29(.5)	- 138.63	- 140.12	1.5
$4_1^0 10b_1^1$	922.54(5)	- 128.33	- 128.30	- 0.1
11_2^2	931.20(10)	- 119.72	- 120.04	0.2
$i 11_2^2$	932.09(3)	- 118.83		
$10a_1^0 17a_1^1 18b_1^1$	942.59(2)	- 108.33	- 108.99	0.7

contd.

1	2	3	4	5
$10a_1^o 17a_1^1$	36949.36(7)	- 101.56	- 101.83	0.3
$6b_1^1 18b_1^1$	950.98(2)	- 99.94	- 101.23	1.3
$6a_1^1 11_1^1$	953.05(2)	- 97.87	- 98.58	0.7
$6b_1^1$	957.12(6)	- 93.80	- 93.87	0.1
$6b_1^o 16a_1^1 16b_1^1$	961.07(5)	- 89.35	- 89.92	0.1
$10b_1^o 17b_1^1$	965.12(.05)	- 85.80	- 86.35	0.6
$6a_2^2$	974.13(5)	- 76.79	- 77.32	0.5
$i_6a_2^2$	978.26(.01)	- 72.66	- 74.50	1.8
$11_1^1 18b_1^1$	981.96(6)	- 68.96	- 67.45	- 1.5
11_1^1	990.90(25)	- 60.02	- 59.55	- 0.5
$6a_1^1 18b_2^2$	996.35(1)	- 54.57	- 53.42	- 1.2
$6a_1^1 18b_1^1$	37004.90(3)	- 46.02	- 45.99	0.0
$6a_1^1$	012.36(3)	- 38.56	- 38.57	0.0
$i_6a_1^1$	013.67(3)	- 37.25	- 37.23	0.0
$4_1^o 17b_1^1$	021.72(1)	- 29.20	- 28.83	- 0.4
$18b_2^2$	036.06(10)	- 14.86	- 14.86	0.0
$18b_1^1$	043.49(30)	- 7.43	- 7.44	0.0
O-O Origin	37050.92(100)			
$4_1^1 6b_1^1 17b_1^1$	060.27(.2)	9.35	11.66	2.3
$4_1^1 16a_1^o$	039.03(.1)	18.11	19.02	0.9
15_1^1	073.24(.05)	22.32	22.11	- 0.2
$4_1^1 18b_1^1$	075.15(.05)	24.23	25.72	1.5
$1_1^o 6b_2^2$	082.40(.05)	31.58	32.54	1.0
$7a_1^1 18a_1^o$	090.47(.01)	39.55	39.42	- 0.1

contd.

1	2	3	4	5
$17b_1^1 18b_0^1$	37091.29(.01)	40.37	39.69	- 0.7
$4_1^0 17a_0^1$	095.46(.1)	45.54	45.43	- 0.1
$6a_1^1 16a_1^1 18b_0^1$	102.05(.005)	51.13	48.50	- 2.6
$12_0^1 6b_1^0$	107.23(.01)	56.36	56.40	0.0
$1_1^0 7a_0^1$	112.64(.5)	61.72	61.32	- 0.4
$4_1^1 16a_1^2 16b_0^1$	116.06(2)	65.14	63.04	- 2.1
$16a_1^1 18b_1^2$	128.99(.7)	73.07	79.63	1.6
$11_1^1 16b_1^1 18b_0^1$	130.54(.2)	79.62	80.80	1.2
$1_1^1 16a_1^1 18b_0^1$	135.14(.2)	84.22	84.94	0.7
$16a_1^1 18b_0^1$	137.02(2)	86.10	87.06	1.0
$10b_0^1 16b_1^0$	139.42(.01)	88.50	88.55	0.1
$5_1^1 6a_0^1$	146.54(.05)	95.62	95.68	0.1
$6a_1^0 6b_0^1 18_1^1$	143.73(.05)	97.81	96.79	- 1.0
$1_1^1 10b_1^1 18b_0^1$	150.82(.01)	99.90	99.65	- 0.3
$10b_1^1 18b_0^1$	152.33(.05)	101.46	101.77	0.3
$6a_1^0 6b_0^1$	156.47(.1)	105.55	104.22	- 1.4
$6a_1^0 16a_0^1 16b_0^1$	160.49(.01)	109.57	108.17	- 1.4
?	163.63(.01)	112.71		
$4_1^1 6a_0^1$	167.17(.01)	115.31	116.57	1.3
$11_1^0 16b_0^1$	173.39(.5)	122.97	123.00	0.0
$16a_2^3 16b_0^1$	176.93(5)	126.06	126.72	0.6
$6a_0^1 17b_1^1$	182.08(.01)	131.16	130.54	- 0.7
$16b_1^1 18b_1^2$	183.69(.05)	132.77	133.39	0.6
$6b_1^1 10b_1^1 16a_1^1$	186.17(.005)	135.25	135.08	- 0.2

contd.

1	2	3	4	5
$i_{16b_1^1 18b_1^1}$	37189.18(.02)	138.26	138.70	0.4
$16b_1^1 18b_1^1$	191.36(.1)	140.44	140.82	0.4
$1_1^o 9b_1^1$	196.54(.1)	145.62	145.62	0.0
?	193.50(.05)	147.58		
$10a_1^1 16b_1^o$	199.81(.02)	148.89	148.87	0.0
$10b_1^1 16a_1^o$	203.13(.2)	152.21	152.21	0.0
$i_{4_1^o 10b_1^1 18b_1^1}$	205.75(.1)	154.83	156.89	2.1
$4_1^o 10b_1^1 18b_1^1$	207.84(.2)	156.92	159.01	2.1
$i_{11_2^2 18b_1^2}$	209.47(.005)	158.55	159.01	0.4
$11_2^2 18b_1^2$	210.88(.01)	159.96	160.24	0.3
$i_{11_2^2 18b_1^1}$	215.40(.2)	164.48	166.44	1.9
$11_2^2 18b_1^1$	216.93(.6)	166.01	167.67	1.7
$3_1^1 18a_1^o$	219.29(.01)	168.37	168.62	0.2
$6a_1^1 16a_1^1 18b_1^1$	220.89(.05)	169.97	170.48	0.6
$6a_1^1 16a_1^1$	229.33(.5)	178.91	177.91	- 1.0
$16b_1^o 17b_1^1$	233.54(3)	187.62	188.02	0.4
$1_1^o 3_1^1$	241.73(.005)	190.81	190.52	- 0.3
$6b_1^1 18b_1^1$	243.98(.005)	193.06	193.59	0.5
$i_{6a_1^1 11_3^3}$	247.06(.02)	196.14	195.13	- 1.0
$6a_1^1 11_3^3$	252.67(2)	201.75	193.92	- 2.8
$16a_1^3$	259.72(1)	208.80	208.25	- 0.5
$10a_1^1 16a_1^o$	263.37(5)	212.45	212.53	0.1
?	265.01(.01)	214.09		
$11_1^1 18b_1^2$	269.32(2)	218.40	219.94	1.5

contd.

1	2	3	4	5
$4_1^{111} 1_1^0$	37275.68(1)	224.76	224.93'	0.1
$11_1^{11} 16b_1^1$	277.45(5)	226.53	227.37	0.9
$5_1^{11} 16b_1^0$	282.32(.005)	231.40	231.79	0.4
$5_1^{11} 16b_1^1$	287.84(.01)	236.92	233.47	1.6
$5_1^{11} 16a_1^{11} 16b_1^1$	290.89(.01)	239.07	242.42	3.4
$6a_1^{11} 18b_1^2$	292.08(.05)	241.88	241.40	- 0.5
$i_1^{11} 6a_1^{11} 18b_1^1$	297.54(.1)	246.62	248.02	1.4
$6a_1^{11} 18b_1^1$	299.26(5)	248.34	248.83	0.5
$6a_1^{11} 12_1^1$	304.90(2)	253.98	254.49	0.5
$4_1^{11} 16b_1^1$	307.60(3)	256.68	259.36	2.7
$6a_1^{11} 11_2^2$	310.08(3)	259.16	258.52	- 0.6
$4_1^{11} 16a_1^{11} 16b_1^1$	313.55(6)	262.63	263.31	0.7
$11_1^{11} 16a_1^{11} 16b_1^1$	314.83(4)	263.91	264.63	0.7
$6b_1^{11} 17b_1^1$	321.46(2)	270.54	273.33	2.8
$18b_2^3$	323.78(5)	272.86	272.53	- 0.3
11_1^2	325.07(2)	274.15	275.88	1.7
$16a_1^{11} 16b_1^{11} 17b_1^1$	327.17(1.5)	276.25	277.28	1.1
$i_1^{11} 18b_1^2$	329.16(3)	278.15	277.84	- 0.3
$18b_1^2$	331.16(10)	280.24	279.96	- 0.3
$6b_1^{11} 6a_1^{11} 16a_1^1$	333.44(.2)	282.52	282.14	- 0.4
$i_1^{11} 18b_1^1$	336.19(6)	285.27	-	-
$18b_1^1$	338.31(20)	287.39	-	-
$6a_2^3$	352.32(.05)	301.40	301.45	0.1
$6b_1^{11} 10a_1^1$	355.75(.05)	304.83	306.00	1.2

contd.

$6a_0^{111}18b_1^1$	37360.04(.3)	309.12	310.79	1.7
$6b_0^{116}18b_1^1$	163.66(12)	312.74	313.27	0.5
$16a_1^216b_0^118b_1^1$	367.13(.1)	316.26	317.22	1.0
$6a_0^{111}11_1^1$	366.33(3)	317.41	318.22	0.8
$11_1^{116}16b_1^216a_0^1$	370.23(2)	319.31	318.39	- 0.9
$6b_0^{116}16a_1^1$	372.23(25)	321.31	320.70	0.6
$16a_1^216b_0^1$	375.95(8)	325.03	324.65	0.4
$16a_1^017a_0^1$	377.37(2.5)	326.45	325.99	- 0.5
$12_1^016b_0^2$	382.67(.01)	331.75	329.84	- 1.9
$6a_1^218b_1^1$	333.67(3)	332.75	332.25	- 0.5
$i_1^26a_1^2$	336.26(.5)	335.34	335.91	0.6
$6a_1^2$	390.79(2)	339.37	339.68	- 0.2
$11_1^{116}16a_0^2$	395.39(1)	344.47	346.12	1.7
$11_3^{116}16a_0^116b_0^1$	396.63(2)	345.71	345.66	- 0.2
$i_1^{113}16a_0^116b_0^1$	397.73(.01)	346.81	346.95	- 0.1
?	400.59(.2)	349.67		
$6b_1^018a_0^1$	401.73(.5)	350.81	350.75	- 0.1
$6b_0^{110}17a_0^111_1^1$	406.91(.05)	355.99	359.45	3.5
$10b_0^{111}11_1^0$	409.51(.5)	358.59	358.12	0.5
$10a_1^017a_0^111_1^{116}16a_0^116b_0^1$	411.53(.5)	360.61	363.40	2.8
$6a_0^{118}18b_2^2$	414.94(.1)	363.02	363.38	0.4
$6b_0^{116}16b_1^118b_1^1$	416.36(1)	365.94	367.03	1.1
$6a_0^{118}18b_1^1$	421.94(6)	370.98	370.31	- 0.2
$i_1^26a_0^1$	424.03(25)	373.16	374.46	1.3

contd.

1	2	3	4	5
$6a_0^1$	37429.16(15)	378.24	—	—
$16a_0^1 16b_1^2$	430.41(8)	379.49	378.41	— 1.1
$4_1^0 10b_0^1 16a_0^1 16b_0^1$	446.49(4)	395.57	396.60	1.0
$6b_0^1 11_2^2$	450.49(3)	399.57	401.31	1.7
$11_2^2 16a_0^1 16b_0^1$	453.50(20)	405.58	405.26	— 0.3
$16a_0^2$	459.50(12)	408.53	406.14	— 2.4
$6b_1^2 18b_1^1$	465.35(.02)	414.43	419.80	5.4
$15_1^0 19b_0^1$	466.73(.01)	415.81	415.58	— 0.2
$6b_0^1 10a_1^0 17a_0^1$	468.77(.5)	417.85	419.47	1.6
$6b_1^1 16a_0^1 16b_0^1 18b_1^1$	470.61(.01)	419.69	423.75	4.1
$15_1^0 19a_0^1$	472.27(.01)	421.35	421.40	0.1
$6b_1^2$	473.87(4)	422.95	427.23	4.3
$6b_1^0 16a_0^2 16b_0^2 18b_1^1$	475.59(.1)	424.67	427.70	3.0
$6b_1^1 16a_0^1 16b_0^1$	477.55(4)	426.63	431.18	4.6
$6b_1^0 16a_0^2 16b_0^2$	482.59(6)	431.67	435.13	3.5
?	485.57(.5)	434.65		
$16b_0^2 16a_1^1$	489.44(.01)	438.52	440.65	2.1
$12_1^0 9b_0^1$	492.49(1)	441.57	442.92	1.4
$6b_0^1 11_1^1 18b_2^2$	494.16(.05)	443.24	446.15	2.9
$11_1^1 16a_0^1 16b_0^1 18b_2^2$	499.14(5)	448.22	450.10	1.9
$6b_1^0 7a_0^1$	501.09(1)	450.17	450.20	0.0
$6b_0^1 11_1^1 18b_1^1$	502.13(2)	451.26	453.58	2.3
$11_1^1 16a_0^1 16b_0^1 18b_1^1$	506.96(1)	456.04	457.53	1.5
$6b_0^1 11_1^1$	511.98(20)	461.06	461.01	— 0.1

contd.

1	2	3	4	5
$11_1^{11}16a_0^{11}16b_0^{11}$	37515.67(25)	464.75	464.96	0.2
$12_0^{11}16a_1^{11}$	521.14(.01)	470.22	470.97	0.8
$6b_1^0 15_0^{11}$	524.30(.2)	473.33	474.84	1.0
$6b_0^{11}6a_1^{11}18b_1^{11}$	526.58(.2)	475.56	475.04	- 0.5
$6a_1^{11}16a_0^{11}16b_0^{11}18b_1^{11}$	529.01(4)	473.09	473.99	0.9
$1_1^0 19b_0^{11}$	530.41(.5)	479.49	479.43	- 0.1
$6b_0^{11}6a_1^{11}$	532.97(12)	482.05	482.47	0.4
$i 6b_0^{11}6a_1^{11}$	534.07(.5)	483.15	483.78	0.6
$6a_1^{11}16a_0^{11}16b_0^{11}$	537.05(2)	486.13	486.42	0.3
$i 6a_1^{11}16a_0^{11}16b_0^{11}$	538.23(.5)	487.36	487.73	0.4
$16b_1^3$	543.34(.1)	492.42	494.41	2.0
$10b_0^2 6b_1^0$	548.96(.01)	498.04	496.32	1.7
?	550.65(.01)	499.73		
$5_0^{11}11_1^0$	552.33(.005)	501.41	501.36	- 0.1
$16a_0^{11}16b_0^{11}18b_2^2$	560.02(10)	509.10	510.12	1.0
$6b_0^{11}18b_1^{11}$	563.99(15)	513.07	513.60	0.5
$1_0^{11}6a_1^0$	564.93(1)	514.06	514.51	0.5
$16a_0^{11}16b_0^{11}18b_1^{11}$	567.90(25)	516.98	517.55	0.6
$6b_0^{11}$	571.95(45)	521.03	-	-
$16a_0^{11}16b_0^{11}$	575.90(40)	524.98	523.56	- 1.4
$1_0^{11}16a_2^2$	585.77(.02)	534.35	533.06	- 1.8
$6a_1^0 18a_0^{11}$	600.13(.02)	549.26	548.84	- 1.4
$4_0^{11}11_0^{11}$	609.51(.05)	558.59	560.36	1.3
$16a_2^2 18a_0^{11}$	613.83(.8)	567.91	567.39	- 0.5

contd.

1	2	3	4	5
$11_1^1 16b_0^2 18b_1^1$	37622.22(.05)	571.30	573.53	2.2
$18b_0^2$	627.37(.02)	576.95	574.78	2.2
$16b_0^2 11_1^1$	631.26(1)	580.34	580.96	0.6
$12_0^1 6b_1^0 16b_0^1 16a_0^1$	632.39(.05)	581.47	581.45	0.0
$9a_0^1 16a_2^2$	633.24(.05)	582.32	582.33	0.0
$1_0^1 5_1^1 11_1^1$	641.99(.1)	591.07	588.74	- 2.3
$11_1^1 12_0^1$	660.93(.02)	610.06	611.28	1.2
$6a_1^0 6b_0^2$	669.96(.02)	619.04	619.51	0.3
$16a_1^1 16b_1^1 18a_0^1$	673.07(.1)	622.15	618.75	- 3.4
$4_0^1 16a_0^1$	675.05(.02)	624.13	625.49	1.4
$16b_0^2 18b_2^2$	676.74(.02)	625.82	626.12	0.3
$16b_0^2 18b_1^1$	682.96(.4)	632.04	633.55	1.5
$1_0^1 18b_1^0$	687.76(.2)	636.34	636.61	- 0.2
$16b_0^2$	690.80(4)	639.38	640.98	1.1
$11_1^1 4_1^1 18a_0^1$	693.13(.3)	642.21	643.96	1.8
$6a_1^0 7a_0^1$	699.91(.2)	648.99	648.29	- 0.7
$1_0^1 5_1^1$	702.47(.3)	651.55	648.76	- 2.8
$7a_0^1 16a_2^2 18b_1^1$	703.38(.2)	657.46	659.41	2.0
$1_0^1 1_1^1 18b_1^1$	712.90(.4)	661.98	662.22	0.2
$12_0^1 18b_1^1$	713.74(.5)	662.82	663.87	1.1
$7a_0^1 16a_2^2$	716.14(.01)	665.22	666.84	1.6
$1_0^1 4_1^1$	721.33(.5)	670.46	669.65	0.8
12_0^1	722.22(5)	671.30	-	-
$5_1^1 18a_0^1$	732.28(2)	681.36	683.09	1.7

contd.

1	2	3	4	5
$1_{\text{O}}^{117b_1^1}$	37734.94(.05)	684.02	683.62	0.4
$9a_{\text{O}}^{118b_1^0}$	737.54(.05)	686.62	685.88	0.7
$1_{\text{O}}^{16a_1^1}1_{\text{O}}^{16a_1^1}$	741.60(.05)	690.63	692.43	1.8
$10b_{\text{O}}^{111_{\text{O}}^1}$	744.54(.01)	693.62	693.55	- 0.1
$4_{\text{O}}^{118a_1^1}1_{\text{O}}^{18b_1^1}$	748.55(.1)	697.63	696.55	- 1.1
$4_{\text{O}}^{118a_1^1}$	754.51(.01)	703.59	703.98	0.4
$17b_{\text{O}}^{118a_1^1}1_{\text{O}}^{18b_1^1}$	763.59(.05)	712.65	710.52	- 2.1
$10b_{\text{O}}^21_{\text{O}}^{16a_2^2}$	765.91(.5)	714.99	712.96	- 2.0
$17b_{\text{O}}^{118a_1^1}$	769.00(.1)	718.08	717.95	- 0.1
$4_{\text{O}}^{19a_1^1}$	770.84(1)	719.92	718.92	- 1.0
$1_{\text{O}}^{16a_1^1}1_{\text{O}}^{18b_1^1}$	775.94(.1)	725.02	723.56	- 1.5
$6a_{\text{O}}^{116a_1^1}1_{\text{O}}^{18a_1^1}$	777.62(.2)	726.70	726.76	0.1
$1_{\text{O}}^{16a_1^1}$	782.78(3)	731.86	730.99	- 0.9
$9a_{\text{O}}^{117b_1^1}$	784.35(.5)	733.43	732.89	0.5
$4_{\text{O}}^{116b_1^1}$	795.73(.05)	744.81	742.91	- 1.9
$1_{\text{O}}^{110b_1^1}$	798.63(.1)	747.71	745.70	- 2.0
$1_{\text{O}}^{111_3^3}$	804.13(.5)	753.21	752.00	- 1.2
$6a_{\text{O}}^2$	807.60(.5)	756.68	756.48	0.2
$16a_{\text{O}}^{113a_1^1}$	815.21(5)	764.29	765.32	1.0
$5_{\text{O}}^{116a_1^2}1_{\text{O}}^{16b_1^2}$	816.65(4)	765.73	767.40	1.7
$7a_{\text{O}}^{118b_1^0}$	820.79(.05)	769.87	770.39	0.5
$4_{\text{O}}^{116b_1^2}$	825.07(.5)	774.15	780.39	6.2
$1_{\text{O}}^{116b_1^1}1_{\text{O}}^{18b_1^1}$	827.33(.8)	776.91	777.32	0.4
$10b_{\text{O}}^{118a_1^1}$	828.95(.5)	778.03	780.03	2.0

contd.

1	2	3	4	5
$1_0^{11}16b_1^1$	37835.35(2)	784.43	784.75	0.3
$11_3^{31}18a_0^1$	836.31(1)	785.39	786.33	0.9
$11_0^{11}17b_0^1$	841.00(.05)	790.08	793.02	2.9
$6b_0^{21}17b_1^1$	843.35(.05)	792.43	794.36	1.9
$16a_0^{21}16b_0^{21}17b_1^1$	851.12(1)	800.20	802.26	2.1
$1_0^{14}1_1^{10}b_0^1$	853.31(.1)	802.39	802.94	0.6
$4_1^{17}a_0^1$	854.77(.5)	803.85	803.43	- 0.4
$6b_0^{11}18b_0^1$	860.34(.05)	809.42	808.42	- 1.0
$1_0^{11}1_2^{12}$	863.33(4)	812.41	811.60	- 0.8
$16a_0^{11}16b_0^{11}18b_0^1$	864.44(.01)	813.52	812.37	- 1.2
$16b_1^{11}18a_0^1$	867.99(1)	817.07	819.08	2.0
$10a_0^{11}16a_0^1$	869.72(.05)	818.80	819.00	0.2
$6a_1^{17}a_0^{11}16a_1^1$	876.16(.5)	825.24	826.21	1.0
$1_0^{11}10a_1^{10}17a_0^1$	880.87(2)	829.95	829.76	- 0.2
$9a_0^{11}16b_1^1$	884.32(.05)	833.40	834.02	0.6
$1_0^{16}b_1^1$	888.19(1)	837.27	837.52	0.3
4_0^2	890.52(2)	839.60	844.84	5.2
$11_2^{21}18a_0^1$	895.71(6)	844.79	845.93	1.1
$7a_0^{11}16a_1^{11}18b_1^1$	905.10(1.5)	854.18	857.34	3.2
$16a_0^{11}17b_0^1$	906.88(1)	855.96	858.15	2.2
$7a_0^{11}16a_1^1$	913.60(5)	862.63	864.77	2.1
$1_0^{11}11_1^{11}18b_1^1$	915.22(.5)	864.30	863.87	- 0.4
$1_0^{11}11_1^1$	922.98(8)	872.06	871.30	- 0.7
$10b_0^{11}16b_0^1$	924.62(2)	873.71	876.10	2.4

contd.

1	2	3	4	5
$7a_0^{11}11_3^3$	37935.78(.1)	884.86	885.78	0.9
$1_0^{16}a_1^{11}18b_1^1$	936.92(.05)	886.00	887.33	1.3
$11_1^{11}18a_0^{11}18b_2^2$	937.92(.05)	887.00	890.77	3.8
$1_0^{16}a_1^1$	943.43(1.5)	892.51	894.76	2.3
$11_1^{11}18a_0^{11}18b_1^1$	946.83(2.5)	895.96	898.20	2.2
$6b_0^{16}a_0^1$	948.96(.05)	898.04	899.27	1.2
$16a_0^{21}16b_1^3$	949.85(.2)	898.93	903.39	4.5
$6a_0^{11}16a_0^{11}16b_0^1$	951.04(.01)	900.12	903.22	3.1
$11_1^{11}18a_0^1$	955.78(10)	904.86	905.63	0.8
$7a_0^{11}16b_1^1$	970.66(1)	919.74	918.53	- 1.2
$1_0^{11}18b_1^1$	975.32(10)	924.40	923.89	- 0.5
$6a_1^{11}18a_0^1$	977.32(5)	926.40	927.09	0.7
1_0^1	982.24(43)	931.32	-	-
$7a_0^{14}11_1^{10}b_0^1$	937.72(.05)	936.80	936.72	- 0.1
$18a_0^{11}18b_3^3$	991.17(.05)	940.25	943.36	3.1
$6a_1^{19}a_0^1$	993.18(.05)	942.26	942.03	- 0.2
$13a_0^{11}18b_2^2$	33000.12(4)	949.20	950.79	- 1.6
$6b_1^{11}16a_0^{22}16b_0^2$	005.17(.5)	954.25	956.16	1.9
$18a_0^{11}13b_1^1$	008.19(15)	957.27	958.22	1.0
$12_0^{11}13b_0^1$	010.04(.01)	959.12	958.69	- 0.4
$18a_0^1$	0.16.57(50)	965.65	-	-
$6b_1^{17}a_0^1$	021.77(1)	970.85	971.30	0.5
$9a_0^{11}13b_1^1$	023.53(1)	972.61	973.16	0.6
$6b_0^{21}11_1^1$	026.30(2)	975.38	982.04	6.6

contd.

1	2	3	4	5
$9a_0^1$	38031.51(5)	980.59	—	—
$11_1^1 16_0^2 16b_0^2$	036.29(.5)	985.37	989.94	4.6
$6b_0^2 6a_1^1 18b_1^1$	041.65(.2)	990.37	996.07	5.7
$3_0^1 16a_1^1$	042.99(1)	992.07	993.97	1.9
$6b_1^1 15_0^1$	045.83(2)	994.91	995.94	1.0
$6b_0^2 6a_1^1$	049.35(2)	998.43	1003.50	5.1
$9b_0^1 16b_1^1$	052.20(.5)	1001.28	1002.83	1.6
$7a_0^1 11_1^1$	055.29(2)	1004.37	1005.08	0.7
$6a_1^1 16a_0^2 16b_0^2$	059.34(.01)	1008.92	1011.40	2.5
$6a_1^1 7a_0^1$	076.80(.5)	1025.88	1026.54	0.7
$6b_0^2 18b_1^1$	079.25(.5)	1028.23	1034.63	6.4
$11_1^1 15_0^1$	080.70(.05)	1029.78	1029.72	— 0.1
$3b_0^1 16a_0^1 16b_0^1 18b_1^1$	083.71(6)	1032.79	1033.58	5.8
$6b_0^2$	087.24(3)	1036.32	1042.06	5.9
$6a_1^0 1_0^1 16a_0^1 16b_0^1$	092.45(.05)	1041.53	1039.49	— 2.0
$6b_0^1 16a_0^1 16b_0^1$	093.14(25)	1042.22	1046.01	3.8
$16a_0^2 16b_0^2$	097.52(3)	1046.60	1049.96	3.4
$6a_0^1 12_0^1$	098.94(.05)	1048.02	1049.54	1.5
$1_0^1 7a_0^1 18b_1^1$	107.10(.2)	1056.18	1054.73	— 1.5
$7a_0^1 18b_1^1$	108.06(1)	1057.14	1057.67	0.5
$1_0^1 7a_0^1$	113.08(3)	1062.16	—	—
$7a_0^1$	116.02(8)	1065.10	—	—
$19b_0^1 16a_1^0$	117.99(.05)	1067.07	1066.40	— 0.7
$4_0^1 17b_0^1$	126.46(.5)	1075.54	1077.50	2.0

contd.

1	2	3	4	5
15_0^1	30 140.66(1)	1089.74	-	-
$9b_0^1 11_1^1$	142.91(.2)	1091.99	1089.38	- 3.6
?	147.92(.5)	1097.00		
$1_0^1 6b_0^1 16a_1^1 16b_1^1$	155.14(.5)	1104.22	1105.45	1.2
$10b_0^2 18b_1^1$	155.90(.2)	1104.98	1103.79	- 1.2
$10b_0^2$	163.81(2)	1112.89	1111.22	- 1.7
$4_0^1 5_0^1$	171.11(.05)	1120.19	1121.27	1.1
$6a_2^2 14_0^1$	183.71(.1)	1132.79	1133.33	0.5
$3_0^1 11_1^1$	185.39(.1)	1134.47	1134.28	- 0.2
$9b_0^1 18b_1^1$	192.44(.2)	1141.52	1141.97	0.5
$11_1^1 14_0^1 18b_1^1$	193.28(.3)	1142.36	1142.67	0.3
$9b_0^1$	200.32(3)	1149.40	-	-
$11_1^1 14_0^1$	201.77(1)	1150.85	1150.10	- 0.8
$10a_0^1 10b_0^1$	220.80(.01)	1169.88	1171.54	1.7
$6a_1^1 14_0^1$	222.81(.01)	1171.89	1171.56	- 0.3
$18b_2^1 19b_0^1$	232.93(.01)	1182.06	1181.07	- 1.0
$3_0^1 18b_1^1$	237.93(.05)	1187.06	1186.87	- 0.2
$18b_1^1 19b_0^1$	240.79(.1)	1189.87	1188.50	- 1.4
$1_0^1 4_1^1 6b_0^1$	242.22(.2)	1191.30	1190.63	- 0.9
$6b_0^1 12_0^1$	242.62(.5)	1191.68	1192.33	0.7
3_0^1	245.22(10)	1194.30	-	-
$12_0^1 16a_0^1 16b_0^1$	247.67(.2)	1196.75	1196.28	- 0.5
$14_0^1 18b_1^1$	253.01(1)	1202.09	1202.69	0.6
$1_0^1 6b_0^1 17b_1^1$	253.42(.2)	1202.50	1204.65	2.2

contd.

1	2	3	4	5
14_0^1	38261.04(10)	1210.12	-	-
$10b_0^1 17b_0^1$	263.53(.05)	1212.61	1210.69	- 1.9
$1_0^1 18b_0^1$	270.18(1)	1219.26	1218.71	- 0.6
$10a_0^2 18b_1^1$	272.05(.05)	1221.13	1220.76	- 0.4
$10a_0^2$	279.11(2)	1223.19	1231.86	3.7
$17b_1^1 19a_0^1$	282.54(.2)	1231.62	1232.44	0.8
$8b_0^1 16a_1^1 16b_1^1$	287.46(.2)	1236.54	1237.52	1.8
$1_0^1 6b_0^1 16a_1^1 18b_1^1$	295.15(.5)	1244.27	1244.59	0.3
$1_0^1 6b_0^1 16a_1^1$	300.09(.05)	1249.07	1252.02	3.0
$5_0^1 10b_0^1$	301.36(.05)	1250.44	1254.46	4.0
$1_0^1 6b_0^1 16a_1^1$	302.94(2)	1252.02	1252.02	0.0
$11_1^1 16b_1^1 19b_0^1$	326.60(.5)	1275.68	1276.62	0.9
$1_0^1 11_3^3 16a_0^1 16b_0^1$	328.36(.1)	1277.44	1276.98	0.5
$16a_1^1 19a_0^1$	330.39(.05)	1279.47	1279.81	0.3
$16a_1^1 19b_0^1$	332.57(.8)	1281.65	1282.88	1.2
$10b_0^1 17a_0^1$	335.82(.01)	1284.90	1285.00	0.1
$8b_0^1 13b_1^0$	339.65(.01)	1288.73	1289.71	1.0
$10b_1^1 19b_0^1$	346.98(.05)	1296.06	1297.59	1.5
$1_0^1 6b_0^1 16b_1^1$	354.97(.8)	1304.05	1305.78	1.7
$17b_0^2$	360.24(.5)	1309.32	1310.16	0.8
$6b_0^2 18b_0^1$	375.19(.5)	1324.27	1329.45	5.2
$6b_0^1 16a_0^1 16b_0^1 13b_0^1$	378.31(.8)	1327.39	1333.40	6.0
$16a_0^2 16b_0^2 18b_0^1$	381.49(.8)	1330.57	1337.35	6.7
$1_0^1 6b_0^1 11_2^2$	382.67(1)	1331.75	1332.63	0.9

contd.

1	2	3	4	5
$1_0^1 1_2^2 16a_0^1 16b_0^1$	38303.02(.5)	1335.10	1336.58	1.6
$3b_0^1 17b_1^1$	337.40(2)	1336.48	1336.72	0.2
12_0^2	392.18(.5)	1341.26	1342.60	1.3
$6a_0^1 13a_0^1$	393.93(5)	1343.01	1343.89	0.9
$10a_0^1 17a_0^1$	397.16(.05)	1346.24	1345.32	- 0.9
$5_0^1 17b_0^1$	400.37(.5)	1349.95	1353.93	4.0
$7a_0^1 18b_0^1$	401.32(.8)	1350.90	1352.49	2.6
$6a_0^1 9a_0^1$	407.36(.5)	1356.94	1358.33	1.9
$11_2^2 19b_0^1$	413.14(1)	1362.22	1363.49	1.3
$6b_0^1 11_2^2 18a_0^1$	413.41(2)	1367.49	1366.96	- 0.5
$11_2^2 16a_0^1 16b_0^1 18a_0^1$	422.55(.05)	1371.63	1370.91	- 0.7
$16a_0^2 13a_0^1$	425.20(1)	1374.23	1371.79	- 2.5
$15_0^1 13b_0^1$	429.06(.05)	1373.14	1377.13	- 1.0
$17a_0^1 17b_0^1$	431.25(1)	1380.33	1334.47	4.1
$3b_1^1 16a_1^1$	434.34(1)	1333.92	1334.09	0.2
$1_0^1 11_1^1 16a_0^1 16b_0^1 13b_1^1$	430.65(.5)	1387.73	1338.35	1.1
$1_0^1 6b_0^1 11_1^1$	442.90(2.5)	1391.90	1392.33	0.4
$1_0^1 11_1^1 16a_0^1 16b_0^1$	446.35(2.5)	1395.93	1396.28	0.4
$1_0^1 6b_0^1 6a_1^1$	460.17(.2)	1415.25	1413.79	- 1.5
$11_1^1 19b_0^1 13b_1^1$	467.39(.2)	1416.47	1415.76	- 0.7
$1_0^1 16a_0^1 16b_0^1 6a_1^1$	467.94(.2)	1417.02	1417.74	0.7
$11_1^1 19a_0^1$	469.25(.2)	1418.33	1420.12	1.8
$11_1^1 19b_0^1$	474.40(4)	1423.43	1423.19	- 0.3
$6b_0^1 13a_0^1 11_1^1$	473.30(2)	1427.38	1426.66	- 1.2

contd.

1	2	3	4	5
$9b_o^1 13b_1^2$	38481.30(.05)	1430.53	1429.36	- 1.0
$9b_o^1 13b_o^1$	488.43(.5)	1437.51	1436.79	- 0.7
$1_o^1 6b_o^1 13b_2^2$	489.32(1)	1433.40	1437.49	- 0.9
$1_o^1 16a_o^1 16b_o^1 13b_2^2$	491.57(.8)	1440.65	1441.44	0.8
$1_o^1 6b_o^1 13b_1^1$	495.78(8)	1444.36	1444.92	0.1
$1_o^1 16a_o^1 16b_o^1 13b_1^1$	499.27(3)	1448.35	1443.87	0.5
$1_o^1 6b_o^1$	501.02(15)	1450.10	1452.35	2.3
$1_o^1 16a_o^1 16b_o^1$	507.20(6)	1456.23	1456.30	0.0
$6a_o^1 15_o^1$	513.53(.05)	1467.61	1467.98	0.4
$13b_2^2 19b_o^1$	520.62(.2)	1469.70	1468.35	- 1.4
$7a_o^1 16a_o^2$	522.48(1)	1471.56	1471.24	- 0.3
$19a_o^1 13b_1^1$	525.31(.1)	1474.39	1472.71	- 1.7
$19b_o^1 13b_1^1$	526.94(3)	1476.02	1475.78	- 0.2
$19a_o^1$	531.06(5)	1480.14	-	-
$3_o^1 13b_o^1$	531.94(2)	1481.02	1481.69	0.7
$19b_o^1$	534.13(15)	1483.21	-	-
$6b_o^1 13a_o^1$	535.21(12)	1484.29	1486.68	2.4
?	536.62(.05)	1487.70		
$16a_o^1 16b_o^1 16a_o^1$	539.95(.5)	1489.03	1490.63	1.6
$6a_o^1 10b_o^2$	542.60(.01)	1491.68	1489.46	- 2.2
$8a_o^1 6a_1^1$	544.99(.01)	1494.07	1493.20	- 0.9
$14_o^1 13b_o^1$	546.32(.01)	1495.40	1497.51	2.1
$6b_o^1 9a_o^1$	551.62(.01)	1500.70	1501.62	0.9
$9a_o^1 16a_o^1 16b_o^1$	557.65(.1)	1506.73	1505.57	- 1.2

contd.

1	2	3	4	5
?	33572.47(.05)	1521.55		
$11\frac{1}{1}18b\frac{1}{0}$	575.24(.2)	1524.32	1524.40	0.1
$6a\frac{1}{0}9b\frac{1}{0}$	577.63(.2)	1526.76	1527.64	0.9
$8a\frac{1}{0}$	532.63(.5)	1531.76	-	-
$6b\frac{3}{0}18b\frac{1}{1}$	601.83(1)	1550.96	1555.66	4.7
$6b\frac{2}{0}16a\frac{1}{0}16b\frac{1}{0}18b\frac{1}{1}$	606.16(.5)	1555.24	1559.61	4.2
$6b\frac{3}{0}$	609.96(2.5)	1559.04	1563.09	4.1
$6b\frac{2}{0}16a\frac{1}{0}16b\frac{1}{0}$	615.24(2)	1564.32	1567.04	2.7
$6b\frac{1}{0}16a\frac{2}{0}16b\frac{2}{0}$	613.78(2)	1567.36	1570.99	3.1
$16b\frac{3}{0}16a\frac{3}{0}$	621.63(.2)	1570.71	1574.94	4.2
$3\frac{1}{0}6a\frac{1}{0}$	623.69(.1)	1572.77	1572.69	- 0.1
$6a\frac{1}{0}14\frac{1}{0}18b\frac{2}{2}$	625.65(.5)	1574.73	1573.50	- 1.2
$8b\frac{1}{0}18b\frac{1}{1}$	629.35(1.5)	1573.43	1576.99	- 1.4
$6a\frac{1}{0}14\frac{1}{0}18b\frac{1}{1}$	631.57(1.5)	1580.65	1580.93	0.3
$8b\frac{1}{0}$	635.34(10)	1584.42	-	-
$7a\frac{1}{0}6b\frac{1}{0}$	635.91(6)	1584.99	1586.13	1.1
$6a\frac{1}{0}14\frac{1}{0}$	636.64(8)	1587.72	1588.36	0.6
$7a\frac{1}{0}16a\frac{1}{0}16b\frac{1}{0}$	639.48(6)	1588.56	1590.08	2.5
$1\frac{1}{0}12\frac{1}{0}$	651.35(.05)	1600.43	1602.62	2.2
$15\frac{1}{0}16a\frac{1}{0}16b\frac{1}{0}$	665.09(.5)	1614.17	1614.72	0.6
$14\frac{1}{0}16a\frac{2}{0}$	666.64(.05)	1615.72	1618.73	3.0
$6b\frac{1}{0}10b\frac{2}{0}$	680.44(.5)	1629.52	1633.92	4.4
$1\frac{1}{0}14\frac{1}{1}18a\frac{1}{0}$	682.09(.1)	1631.17	1635.30	4.1
$1\frac{1}{0}16a\frac{1}{0}10a\frac{1}{1}$	747.09(4)	1696.17	1696.64	0.5

contd.

1	2	3	4	5
	38753.37(.05)	1702.45		
$7a_0^1 16b_0^2$	757.37(.5)	1706.91	1706.08	- 0.8
$3_0^1 6b_0^1$	763.15(.01)	1712.23	1715.33	3.1
$3_0^1 16a_0^1 16b_0^1$	767.59(.5)	1716.67	1719.28	2.6
$16a_1^1 18a_0^2$	779.57(.2)	1723.65	1730.97	2.3
$6b_0^1 14_0^1$	782.36(.2)	1731.44	1731.15	- 0.3
$14_0^1 16a_0^1 16b_0^1$	785.46(.05)	1734.54	1735.10	0.6
$7a_0^1 12_0^1$	786.94(.05)	1736.02	1736.40	0.4
$18b_0^1 19b_0^1$	820.91(.2)	1769.99	1770.60	0.6
$6b_0^1 18a_0^1 18b_0^1$	825.56(1)	1774.64	1774.07	- 0.6
$1_0^2 11_1^1$	852.65(2)	1801.64	1802.62	1.0
$11_2^2 18a_0^2$	859.25(.05)	1808.33	1811.58	3.3
?	864.51(.1)	1813.59		
$9b_0^1 12_0^1$	871.57(.02)	1820.65	1820.70	0.1
?	874.37(.5)	1823.45		
?	875.84(.1)	1824.92		
$1_0^1 11_1^1 18a_0^1 18b_1^1$	878.20(.5)	1827.28	1829.52	2.2
$1_0^1 11_1^1 18a_0^1$	883.91(3)	1835.99	1836.95	1.0
?	890.12(.01)	1839.20		
$1_0^1 18a_0^1 6a_1^1$	907.93(.02)	1857.04	1858.41	1.4
1_0^2	911.95(5)	1861.03	1862.44	1.4
$6a_0^1 19b_0^1$	913.09(.1)	1862.17	1861.45	- 0.7
$3_0^1 12_0^1$	916.04(.05)	1865.12	1865.60	0.5
$11_1^1 18a_0^2$	919.83(2)	1868.91	1871.28	2.4

contd.

1	2	3	4	5
$8b_o^1 18b_o^1$	38 921.32(.5)	1870.90	1871.81	0.9
$12_o^1 14_o^1$	932.16(.5)	1881.24	1881.42	0.2
$16a_o^2 19a_o^1$	937.57(.05)	1886.65	1886.28	0.4
$1_o^1 18a_o^1 18b_1^1$	938.71(1)	1887.79	1889.54	1.8
$6a_1^1 18a_o^2$	939.56(.5)	1888.64	1892.74	4.1
$16a_o^2 19b_o^1$	941.31(.5)	1890.39	1889.35	- 1.0
$1_o^1 18a_o^1$	946.45(15)	1895.53	1896.97	1.4
$1_o^1 9a_o^1 18b_1^1$	952.51(.5)	1901.59	1904.48	2.9
$6a_o^1 8a_o^1$	956.32(.1)	1905.90	1910.00	4.1
$1_o^1 9a_o^1$	961.95(2)	1911.03	1911.91	0.9
$18a_o^2 18b_1^1$	972.17(1)	1921.25	1923.87	2.6
?	973.62(.5)	1922.70		
?	975.36(.05)	1924.44		
$18a_o^2$	978.82(3)	1927.90	1931.30	2.4
$9a_o^1 18a_o^1 18b_1^1$	985.21(.1)	1934.29	1938.81	4.5
$9a_o^1 18a_o^1$	994.77(1)	1943.85	1946.24	2.4
$9a_o^2$	39007.94(.5)	1957.02	1961.18	4.2
$6a_o^1 19b_o^1$	013.07(1)	1962.15	1962.66	0.5
$6a_1^1 16a_o^1 16b_o^1 19b_o^1$	015.46(.5)	1964.54	1965.68	1.1
$1_o^1 16b_o^1 16a_o^1 16b_o^1$	022.66(2.5)	1971.74	1977.33	5.6
?	0.23.97(.5)	1973.05		
$1_o^1 16a_o^2 16b_o^2$	027.99(.1)	1977.07	1981.28	4.2
$6b_o^1 19a_o^1 18b_1^1$	043.20(.1)	1992.28	1993.74	1.5
$1_o^1 7a_o^1$	046.05(6)	1995.13	1996.62	1.5

contd.

1	2	3	4	5
$6b_{\text{O}}^1 19a_{\text{O}}^1$	39051.44(2)	2000.52	2001.17	0.7
$6b_{\text{O}}^1 19b_{\text{O}}^1$	056.66(8)	2005.74	2004.24	- 1.5
$16a_{\text{O}}^1 16b_{\text{O}}^1 19b_{\text{O}}^1$	058.55(1)	2007.63	2008.19	0.6
$1_{\text{O}}^1 15_{\text{O}}^1$	070.31(.2)	2019.39	2021.06	1.2
$7a_{\text{O}}^1 18a_{\text{O}}^1 18b_{\text{O}}^1$	071.99(.1)	2021.07	2023.32	2.3
$7a_{\text{O}}^1 18a_{\text{O}}^1$	076.93(1.5)	2026.01	2027.31	1.8
$7a_{\text{O}}^1 18a_{\text{O}}^1$	078.65(4)	2027.73	2030.75	3.0
?	081.01(.05)	2030.09		
?	083.14(.02)	2032.22		
$7a_{\text{O}}^1 9a_{\text{O}}^1 18b_{\text{O}}^1$	085.20(.02)	2034.28	2038.26	4.0
$7a_{\text{O}}^1 9a_{\text{O}}^1$	093.15(1)	2042.23	2045.69	3.5
$6b_{\text{O}}^1 8a_{\text{O}}^1$	103.41(.5)	2052.49	2052.79	0.3
$15_{\text{O}}^1 18a_{\text{O}}^1$	105.00(.8)	2054.08	2055.39	1.3
$3_{\text{O}}^1 7a_{\text{O}}^1 16a_{\text{O}}^1$	111.19(.05)	2060.27	2059.07	- 1.2
$6b_{\text{O}}^1 16a_{\text{O}}^1 16b_{\text{O}}^1$	126.11(.05)	2075.19	2083.07	12.9
$6b_{\text{O}}^2 16a_{\text{O}}^2 16b_{\text{O}}^2$	131.62(1)	2080.70	2092.02	11.3
?	147.57(.02)	2096.65		
?	153.43(.05)	2102.56		
$6b_{\text{O}}^1 8b_{\text{O}}^1$	156.26(.05)	2105.34	2105.45	0.1
$8b_{\text{O}}^1 16a_{\text{O}}^1 16b_{\text{O}}^1$	160.54(.1)	2109.62	2109.40	- 0.2
$9b_{\text{O}}^1 18a_{\text{O}}^1$	165.33(2)	2114.41	2115.05	0.6
$1_{\text{O}}^1 3_{\text{O}}^1$	173.34(1.5)	2122.42	2125.62	3.2
$1_{\text{O}}^1 12_{\text{O}}^1 16a_{\text{O}}^1 16b_{\text{O}}^1$	175.46(.5)	2124.54	2127.60	3.1
$7a_{\text{O}}^2$	177.92(.05)	2127.00	2130.20	3.2

contd.

1	2	3	4	5
1_{014}^1	39191.73(2)	2140.31	2141.44	1.4
1_{018b}^1	202.56(.1)	2151.64	2150.03	- 1.6
12_{019b}^1	204.27(.2)	2153.35	2154.51	1.2
15_{017a}^1	205.12(.2)	2154.20	2154.84	0.6
3_{018a}^1	207.68(.?)	2156.76	2159.95	3.2
3_{019a}^1	221.62(1)	2170.70	2174.89	4.2
14_{018a}^1	224.20(.1)	2173.23	2175.77	2.5
$1_{018a}^1 1_{018b}^1$	233.60(.2)	2182.63	2184.36	1.7
$9a_{014}^1$	243.00(1)	2192.08	2190.71	- 1.4
$7a_{019b}^1$	265.46(.3)	2214.54	2214.50	0.0
?	279.69(.05)	2223.77		
$3_{017a}^1 1_{018b}^1$	303.11(.01)	2252.19	2251.97	- 0.2
$3b_{012}^1$	304.41(.02)	2253.49	2255.72	2.2
3_{017a}^1	309.53(1)	2258.61	2259.40	0.8
$7a_{014}^1$	320.52(.5)	2269.60	2275.22	5.6
$1_{016a}^1 1_{018a}^1$	324.38(.3)	2273.46	2273.85	0.4
$1_{017a}^1 1_{018b}^1$	330.31(.5)	2279.89	2283.81	3.9
$6b_{018b}^1 1_{019b}^1$	344.70(.5)	2293.73	2291.63	- 2.2
$9b_{01}^2$	348.92(.5)	2298.00	2298.80	0.8
14_{015}^1	350.59(.05)	2299.67	2299.86	0.2
$6a_{018a}^1 1_{018a}^2$	354.62(.05)	2303.70	2309.54	5.8
$1_{016a}^1 1_{017a}^1$	425.46(.5)	2374.54	2374.66	0.1
1_{016b}^2	432.45(2)	2381.53	2383.67	2.1
$1_{016a}^2 1_{016b}^1$	439.02(1)	2388.10	2387.62	- 0.5

contd.

1	2	3	4	5
3_0^2	39441.16(.2)	2390.24	2388.60	- 1.4
$3_0^1 14_0^1 18b_1^1$	444.64(.05)	2393.72	2396.99	3.3
$3_0^1 14_0^1$	453.49(1.5)	2402.57	2404.42	1.9
$1_0^1 19b_0^1 18b_1^1$	457.56(1)	2406.64	2407.10	0.5
$1_0^1 19b_0^1$	464.95(5)	2414.03	2414.53	0.5
$1_0^1 6b_0^1 18a_0^1$	470.03(.3)	2419.11	2418.00	- 1.1
$1_0^1 14_0^1 18b_0^1$	475.16(.5)	2424.24	2428.83	4.6
$1_0^1 6b_0^1 9a_0^1$	483.68(.05)	2432.76	2432.94	0.2
$1_0^1 9a_0^1 16a_0^1 16b_0^1$	488.87(.05)	2437.95	2436.89	- 1.1
$6b_0^1 18a_0^2$	493.99(1)	2443.07	2452.33	8.3
$16a_0^1 16b_0^1 18a_0^2$	497.14(.5)	2446.22	2456.28	10.1
$18a_0^1 19b_0^1$	498.43(.05)	2447.51	2448.86	1.4
$6a_0^1 6b_0^1 8b_0^1$	533.59(2)	2482.67	2483.69	1.0
$1_0^1 6b_0^2 16a_0^1 16b_0^1$	546.84(1)	2495.92	2498.36	3.4
$1_0^1 8b_0^1$	561.43(.1)	2510.50	2515.74	5.2
$1_0^1 6b_0^1 7a_0^1$	565.86(.5)	2514.94	1517.45	2.5
$1_0^1 6a_0^1 14_0^1$	568.89(.5)	2517.97	2519.68	1.7
$1_0^1 7a_0^1 16a_0^1 16b_0^1$	570.04(.1)	2519.12	2521.40	2.3
$6b_0^1 16a_0^1 16b_0^1 19a_0^1$	576.76(.1)	2525.84	2526.15	1.3
$16a_0^2 16b_0^2 19a_0^1$	579.56(.5)	2528.64	2530.10	1.5
$1_0^2 12_0^1$	584.50(.5)	2533.58	2533.94	0.4
$1_0^1 6b_0^1 15_0^1$	591.79(.02)	2540.87	2542.09	1.2
$1_0^1 15_0^1 16a_0^1 16b_0^1$	593.92(.5)	2543.00	2546.04	3.0
$6b_0^1 7a_0^1 18a_0^1$	595.97(.2)	2545.05	2551.78	6.7

contd.

1	2	3	4	5
$7a_o^1 19b_o^1$	39597.80(.05)	2546.88	2548.31	2.4
$8b_o^1 18a_o^1$	600.78(.1)	2549.86	2550.07	0.2
$15_o^1 19a_o^1$	620.95(.1)	2570.03	2569.88	- 0.2
$15_o^1 19b_o^1$	624.99(.1)	2574.07	2572.95	- 1.1.
$9b_o^1 19a_o^1$	675.06(.1)	2624.14	2629.50	5.4
$1_o^1 18a_o^2$	909.77(.3)	2858.85	2862.62	4.8
$1_o^1 9a_o^1 18a_o^1$	925.26(.01)	2874.34	2877.56	3.2
$13_o^1 16a_1^1$	933.46(.05)	2882.54	2883.32	1.8
$13a_o^3$	943.60(.05)	2892.68	2896.95	4.3
$1_o^1 6b_o^1 19b_o^1$	986.60(.3)	2935.68	2935.56	- 0.1
$1_o^1 7a_o^1 18a_o^1$	40013.39(.3)	2962.47	2962.07	- 0.4
$19b_o^2$	019.65(.05)	2968.73	2966.42	- 2.3
$1_o^1 15_o^1 13a_o^1$	035.51(.1)	2984.59	2986.74	2.2
$7a_o^1 18a_o^2$	039.84(.01)	2988.92	2996.40	7.5
$1_o^1 6b_o^3 16a_o^1 16b_o^1$	066.43(.05)	3015.51	3019.39	3.9
$15_o^1 18a_o^2$	072.27(.1)	3021.35	3021.04	- 0.3
$13_o^1 11_1^1$	074.32(.2)	3023.40	3023.63	0.2
$1_o^1 18a_o^1 9b_o^1$	096.01(.05)	3045.09	3046.37	1.3
?	102.90(.2)	3051.98		
$1_o^2 3_o^1$	104.82(.2)	3053.90	3056.94	3.0
$7b_o^1$	106.93(.2)	3056.01	-	-
$1_o^2 14_o^1$	124.04(.05)	3073.12	3072.76	- 0.4
$9b_o^1 18a_o^2$	127.73(.3)	3076.86	3080.70	3.8
$1_o^1 7a_o^1 15_o^1$	131.53(.1)	3080.61	3086.16	5.6

contd.

1	2	3	4	5
13_{O}^1	40134.67(.8)	3083.65	-	-
$7a_{\text{O}}^2 18a_{\text{O}}^1$	146.36(.08)	3095.94	3095.85	- 0.1
$1_{\text{O}}^1 14_{\text{O}}^1 18a_{\text{O}}^1$	159.53(.04)	3108.61	3107.09	- 1.5
$3_{\text{O}}^1 13a_{\text{O}}^2$	171.80(.01)	3120.88	3125.70	4.8
$14_{\text{O}}^1 13a_{\text{O}}^2$	190.07(.2)	3139.75	3141.42	2.3
$20a_{\text{O}}^1$	209.09(.1)	3150.17	-	-
$1_{\text{O}}^1 7a_{\text{O}}^1 13a_{\text{O}}^1 13b_{\text{O}}^1$	297.13(.05)	3246.26	3249.46	3.2
$1_{\text{O}}^2 19b_{\text{O}}^1$	393.33(.5)	3342.41	3345.85	3.4
$1_{\text{O}}^2 18a_{\text{O}}^1 6b_{\text{O}}^1$	393.78(.2)	3347.06	3349.32	1.5
?	401.14(.05)	3350.22		
$1_{\text{O}}^2 16a_{\text{O}}^1 16b_{\text{O}}^1 18a_{\text{O}}^1$	403.22(.2)	3352.30	3353.27	1.0
$1_{\text{O}}^1 18a_{\text{O}}^1 19b_{\text{O}}^1$	426.21(.3)	3375.29	3380.18	4.9
$1_{\text{O}}^1 6b_{\text{O}}^1 9a_{\text{O}}^1 18a_{\text{O}}^1$	444.31(.2)	3393.39	3398.59	5.2
$18a_{\text{O}}^2 19b_{\text{O}}^1$	455.80(.5)	3404.88	3414.51	9.6
$18a_{\text{O}}^2 8b_{\text{O}}^1$	563.24(.01)	3512.32	3515.72	3.4
$6b_{\text{O}}^1 7a_{\text{O}}^2 9b_{\text{O}}^1$	851.86(.2)	3800.94	3800.63	- 0.3